ČESKÉ VYSOKÉ UČENÍ TECHNICKÉ V PRAZE
FAKULTA JADERNÁ A FYZIKÁLNĚ INŽENÝRSKÁ

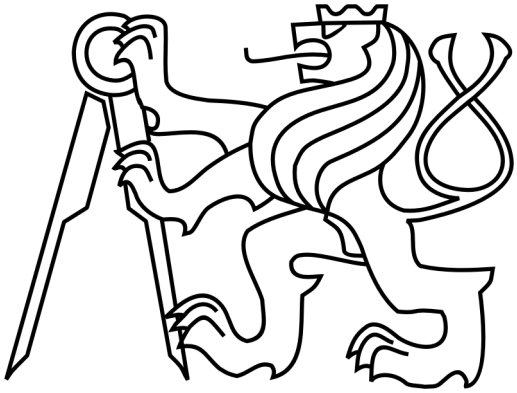

HABILITAČNÍ PRÁCE

Fyzika kvarkov ťažkých vôní

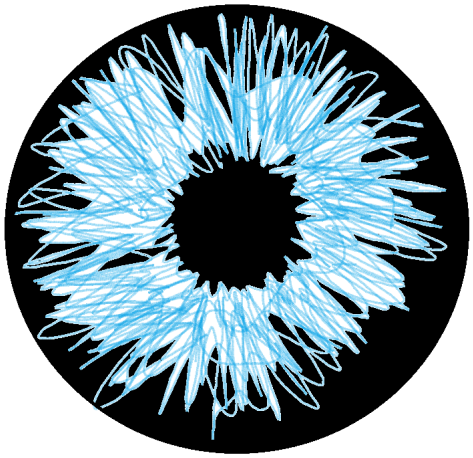

Praha, 2018 **Dr.rer.nat., Mgr. Jaroslav Bielčík, MSc.**

Fyzika kvarkov ťažkých vôní

Dr.rer.nat., Mgr. Jaroslav Bielčík, MSc.

Abstrakt

Hlavnou témou tejto práce je fyzika kvarkov ťažkých vôní vytvorených v ultra - relativistických jadro-jadrových zrážkach. Urýchľovač RHIC (Relativistic Heavy Ion Collider) v Brookhavenskom národnom laboratóriu umožnil experimentálne skúmať vlastnosti jadrovej hmoty v podmienkach vysokej teploty a energetickej hustoty, za ktorých sa teoreticky predpovedal fazový prechod do nového stavu hmoty, kvarkovo-gluónovej plazmy. Je niekoľko exprimentálnych pozorovateľných, ktoré na popis tejto hmoty môžeme využiť. V tejto práci sa budeme sústrediť na pozorovatelné, ktoré súvisia s pôvabnými a krásnymi kvarkami. Tieto kvarky sa tvoria v skorých fázach jadro-jadrovej zrážky a sú preto citlivé na jednotlivé fázy vývoja systému. Meranie tvorby ťažkých kvarkov v protón-protónových zrážkach je dôležitým testom výpočtov kvantovej chromodynamiky v poruchovom režime a taktiež ako referencia pre merania v jadro-jadrových zrážkach. Pôvabné kvarkónium hrá dôležitú úlohu, keďže jeho tvorba v jadro-jadrových zrážkach má byť podľa očakávaní potlačená z dôvodu tepelne závislého Debyového farebného tienenia. Kým jadrový modifikačný faktor je zásadný pre pochopenie energetických strát ťažkých kvarkov v horúcej a hustej hmote, merania hydrodynamického toku prinášajú ďalšiu informáciu a je ich možné interpretovať v súvislosti s rýchlosťou celkovej termalizácie systému. Z prezentovaných výsledkov v tejto práci plynie, že výpočty kvantovej chromodynamiky v poruchovom režime dobre popisujú produkciu pôvabných kvarkov v p+p zrážkach a z meraní jadrového modifikačného faktora vyplýva, že pôvabné kvarky strácajú energiu možno podobne ako kvarky ľahké. Prekvapivo meranie toku J/ψ je zhodné s nulou a polarizácia v helicitnej sústave má tendenciu byť pozdĺžna s rastúcou hodnotou p_T. Ostatné merania z experimentu STAR, ktoré využívajú signály z detektora Heavy Flavor Tracker, potvrdzujú naše predošlé výsledky a umožnujú dalšie typy analýz. V blízkej budúcnosti sa experiment STAR, v rámci programu energetickej prehliadky Beam Energy Scan, zameria na hľadanie kritického bodu fázového diagramu jadrovej hmoty a hraničné prejavy kvarkovo-gluónovej plazmy.

Heavy flavor physics

Dr.rer.nat., Mgr. Jaroslav Bielčík, MSc.

Abstract

In this work heavy flavor production in ultrarelativistic heavy ion collisions is discussed. The experiments at the Relativistic Heavy Ion Collider in Brookhaven National Laboratory enabled to study the properties of nuclear matter under conditions of high temperature and energy density, where the phase transition to a new state of matter, Quark Gluon Plasma was theoretically predicted. There are several experimental tools to uncover the characteristics of this matter. Here we focus on observables related to charm and bottom quarks. These quarks are produced in early phase of the collisions and therefore are sensitive to all phases of system evolution. The measurement of heavy quark production in p+p collisions is an important test of perturbative Quantum Chromodynamics calculations and also a baseline for heavy ion measurements. The charmonium plays very special role in the heavy ion collisions while suppression of its production in heavy ion collisions is expected due to temperature sensitive Debye color screening. While nuclear modification factor is essential to understand the energy loss of heavy quarks in hot and dense matter the measurements of hydrodynamic flow are an additional constraint and can be related to speed of system thermalization. Results discussed here from the STAR experiment show that perturbative Quantum Chromodynamics is well describing charm production in p+p collisions and nuclear modification of charm mesons indicate that energy loss might be similar to tha of light quarks. Surprisingly the flow of J/ψ is consistent with no flow at low transverse momentum and J/ψ polarization in helicity frame indicates a trend towards longitudinal polarization as p_T increases. Recent preliminary measurements using information from the STAR Heavy Flavor Tracker confirm the previous results and in addition provide access to new type of studies. In near future, the Beam energy scan program of STAR will focus on determination of the critical point of phase diagram of nuclear matter and the onset of Quark Gluon Plasma signals.

Prehlásenie

Predložená habilitačná práca je založená na odborných publikáciach, ktoré boli vytvorené v rámci veľkých medzinárodných kolaborácií a tímov, preto by som rád na úvod špecifikoval podiel autora na predloženom súbore prác. Súhrnne je spoluautorstvo všetkých publikácií uvedených v zozname publikácií na konci práce v časti *Zoznam autorových publikácií* oprávnené a založené na publikačných pravidlách experimentálnych kolaborácií STAR, ALICE a HADES. Podieľal som sa na nich rôznym spôsobom, jednak aktívnou účasťou pri zbere experimentálnych údajov, podporou prevádzky a údržby detektorov, kontrolou kvality a kalibráciou meraných údajov, prípravou fyzikálnych meraní, fyzikálnou analýzou dát, interpretáciou výsledkov, ale aj písaním samotných odborných textov, vedením užších autorských tímov v rámci kolaborácie alebo účasťou v týchto tímoch. Do úzkeho výberu publikácií, ktoré komentujem v tejto práci, som vybral tie, u ktorých považujem svoj podiel za zásadný a obsahovo dobre demonštrujú môj hlavný vedecký záujem v rokoch 2004 až 2016. Z dôvodu kompaktnosti dokumentu som do výberu zámerne nezaradil publikácie z tohto obdobia Ref. [145, 171, 197, 215, 222, 266, 287, 300, 345, 361], na ktorých mám tiež zásadný podiel, z dôvodu, že sú tematicky vzdialené hlavnej téme tejto práce. Taktiež som do výberu nezaradil odborné texty Ref. [13, 37, 50, 53, 72, 85, 179, 220, 225, 236, 316, 334], ktoré síce vyšli i v referovaných časopisoch, ale obsahujú predbežné výsledky, ktoré boli upresnené v ďalších textoch, alebo majú charakter súhrnných kompilácií výsledkov.

Autorský podiel na vybranom súbore siedmych publikácií v tejto práci je nasledovný. U článku B. I. Abelev *et al.*, Phys. Rev. Lett. **98**, 192301 (2007) som previedol hlavnú analýzu dát so zrážok Au+Au a podieľal som sa na príprave textu publikácie a taktiež na následnej oprave výsledkov, ktorá nastala na základe korekcií, ktoré boli mimo moju úlohu v analýze dát. U článku L. Adamczyk *et al.* Phys. Rev. D **86**, 072013 (2012) som bol hlavným autorom textu publikácie, interpretácie výsledkov. Fyzikálna analýza bola prevedená v tíme spolu so svojim doktorandom Dr. Davidom Tlustým [T1]. U článku J. Crkovska *et al.* Phys. Rev. C **95** no.1, 014910 (2017) som bol členom malého autorského tímu s kolegami z Univerzity v Oslo. Môj hlavný podiel bol pri formulácii fyzikálneho obsahu projektu, kontrole výpočtov, ktoré boli vykonané v tíme so svojou diplomantkou Ing. Janou Crkovskou [D5], pri príprave textu publikácie a formulácii fyzikálnej interpretácie výsledkov. U ďalších článkov L. Adamczyk *et al.* Phys. Rev. Lett. **111**, no. 5, 052301 (2013), H. Agakishiev *et al.*, Phys. Rev. D

83, 052006 (2011) som bol zodpovedný za kontrolu analýzy dát a simulácií, odbornú prípravu textu a formuláciu fyzikálnych záverov. U L. Adamczyk *et al.*, Phys. Lett. B **739**, 180 (2014) a L. Adamczyk *et al.*, Phys. Lett. B **771**, 13 (2017) som tento proces prípravy článkov navyše viedol. Samotná analýza experimentálnych údajov bola prevedená v tíme s členmi mojej fyzikálnej skupiny ťažkých kvarkov experimentu STAR, ktorú som viedol v rokoch 2010-2012.

Poďakovanie

Predložená práca je založená na výsledkoch, ktoré som dosiahol hlavne v rámci kolaborácií STAR a ALICE. Rád by som poďakoval svojim najbližším spolupracovníkom a členom môjho výskumného týmu.

V prvom rade by som poďakoval svojej manželke a kolegyni dr. Jane Bielčíkovej za porozumenie a vytvorenie inšpiratívneho partnerstva a skvelú vedeckú spoluprácu.

Rád by som poďakoval prof. Johnovi Harrisovi a prof. Thomasovi Ullrichovi za mentorstvo a podporu v prvých rokoch mojej práce na experimente STAR na Yalovej Univerzite v rokoch 2004-2007. Chcem poďakovať doc. Vojtěchovi Petráčkovi a doc. Michalovi Šumberovi za iniciovanie a podporu pri založení skupiny experimentu STAR na FJFI ČVUT a za podporu pri práci pre experiment ALICE. Ďakujem dr. Michalovi Brozovi a dr. Janovi Nemčíkovi za príjemnú odbornú spoluprácu. Špeciálne chcem tiež poďakovať dr. Petrovi Chaloupkovi za spoluprácu a nasadenie bez ktorého by naša výzkumná skupina nemohla fungovať. Rád by som poďakoval zahraničným kolegom prof. Larise Bravina, prof. Sonie Kabana, dr. Danielovi Kikolovi, dr. Xin Dongovi a dr. Elene Bruna za cenné diskusie a tvorivú spoluprácu.

Rád by som poďakoval za podporu českého týmu v experimente STAR prof. Nu Xu (bývalému hovorcovi experimentu STAR), prof. Zhangbu Xu (hovorcovi experimentu STAR) a prof. Helen Caines (hovorkyni experimentu STAR).

V rokoch 2012-2015 som spolupracoval s dr. Gyulnarou Eyyubovou a dr. Barbarou Trzeciak počas ich postdoktorandského pobytu v mojom tíme v Prahe, za skvelú spoluprácu im ďakujem.

Za najdôležitejších partnerov vo vedeckej práci považujem svoje študentky a svojich študentov, s ktorými som mal možnosť spolupracovať pri ich doktorských, magisterských, či bakalárskych prácach. Rád by som týmto mladým kolegyniam a kolegom menovite poďakoval dr. Olge Rusňákovej [B4, D4, T2], dr. Davidovi Tlustému [T1], dr. Michalovi Vajzerovi [B2, D3, T3], Ing. Miroslavovi Šimkovi, Ing. Lukášovi Kramárikovi [B11,D7], Ing. Jane Crkovskej [B6,D5] , Ing. Kataríne Gajdošovej [B9,D6], dr. Michalovi Tesařovi [B1, D2], dr. Miroslavovi Krusovi [D1], Ing. Jakubovi Kvapilovi [B13, D9], Ing. Janovi Vaňkovi [B14, D8], Ing. Miroslavovi Šaurovi [B12], Ing. Vojtěchovi Pacíkovi [B10], Ing. Otovi Kukralovi [B7], Ing. Kamile Vysokej [B8], Bc. Jitke Brabcovej [B5], Ing. Michalovi Slobodovi [B3], Bc. Zuzane Moravcovej [B15], Tomášovi Truhlářovi, Bc. Róbertovi Líčenikovi a Ing. Michalovi Kocanovi.

V neposlednej rade by som rád poďakoval prof. Igorovi Jexovi (dekanovi FJFI ČVUT) a prof. Gocemu Chadzitaskosovi (vedúcemu katedry fyziky FJFI ČVUT) za všestrannú podporu.

Táto práca je napísaná slovensky ako poďakovanie mojim drahým rodičom: *Ó, mojej matky reč je krásota, je milota, je rozkoš, láska svätá; je, vidím, cítim, celok života, môj pokrm dobrý, moja čaša zlatá a moja odev, ktorej neviem ceny... Buď požehnaný, kto sa pohodil v tom so mnou, trvá pritom nepremenný; buď kliaty, kto sa zaprel, odrodil...* (Pavol Országh-Hviezdoslav: Letorosty III, Mňa kedys' zvádzal svet)

Obsah

Kapitola 1

Kvarkovo-gluónová plazma

Od nepamäti ľudia využívajú svoj rozum na pochopenie sveta v ktorom žijú. Tieto znalosti, založené na pozorovaní prírodných javov, umožnili človeku lepšie využiť prírodné zdroje k svojim potrebám, prírodné javy s dobrou mierou úspechu predpovedať a prispôsobiť sa im. Dospeli k presvedčeniu, že svet je poznateľný, riadi sa univerzálnymi pravidlami, ktoré môžu byť overiteľné. Veda je proces poznávania sveta, založený na pozorovaní prírodných javov a experimentoch, ktoré tieto prírodné procesy môžu opakovať v zjednodušených a kontrolovateľných podmienkach. Veda je založená na pozorovaných faktoch, na tvorbe hypotéz a teórií, ich upresňovaní, testovaní či vyvracaní. Je to neustály dynamický proces, ktorý pokračuje s rôznymi odbočkami dopredu k hlbšiemu pochopeniu prírody, ktorej sme sami zároveň súčasťou. Fyzika sa oddelila z prírodných vied v 19. storočí. Jej úlohou je pochopiť prírodu na tej úplne najzákladnejšej, najhlbšej úrovni. Hoci sa mnohokrát opakovalo, že sa nám podarilo objaviť a následne vysvetliť pôvodne neočakávané a nepredstaviteľné javy, zdá sa, že sme v poznávaní sveta ešte ďaleko od úplnosti. Pohľad na ostatné storočie, ktoré si najviac spájam so vznikom jadrovej fyziky, kvantovej mechaniky a teórie relativity ukazuje, že cesta od nových základných objavov k nesmierne významným aplikáciam je prekvapivo krátka. Od objavu radioaktivity v roku 1896 Henrim Becquerelom do prvej jadrovej elektrárne v roku 1954 v Obninsku uplynulo 60 rokov, od prvých krokov ku kvantovej mechanike Maxa Plancka v roku 1900 ku konštrukcii tranzistorov Johnom Bardeenom a Walterom Brattainom v roku 1947 uplynulo necelých 50 rokov, alebo od konštrukcie laseru v roku 1960 Theodorom H. Maimanom do klinických uplatnení v laserových operáciách v roku 1983 Dongom R. Choiom a Robertom N. Ginsburgom v roku 1983 len niečo cez 20 rokov. Napriek tomu, že vedkyne a vedcov v základnom výskume vo fyzike poháňa dopredu práve snaha pochopiť zákony prírody, uplatnenia týchto poznatkov sú rýchle a rozsiahle. Spoločnosti, ktoré dlhodobo pestujú vedu a investujú prostriedky do vzdelávania (Izrael, Južná Kórea, Japonsko, škandinávske krajiny, západná Európa a USA) dosahujú vyšší stupeň rozvoja a blahobytu.

Z pohľadu súčasnej modernej fyziky sa celý poznaný svet na základnej úrovni skladá z elementárnych častíc, ktoré medzi sebou pôsobia štyrmi silami. Prvá elementárna

častica - elektrón bola objavená už v roku 1897 Josephom J. Thomsonom, avšak až pozorovania Ernsta Rutherforda viedli k poznaniu, že atóm sa skladá z malého kladne nabitého a hmotného jadra a elektróny okolo neho obiehajú. V prvej polovici dvadsiateho storočia sa po objavení protónov a neutrónov objavili ďalšie častice: mióny, pióny, kaóny a lambda baryóny. Tieto častice boli objavené v meraniach kozmického žiarenia. Toto žiarenie je zložené z primárnej zložky, z častíc, ktoré prilietajú do zemskej atmosféry z vesmíru, kde vznikajú a urýchľujú sa v astrofyzikálnych procesoch. To sú hlavne elektróny, protóny, hélium, uhlík, kyslík, železo a ďalšie jadrá syntetizované vo hviezdach. Tieto častice reagujú s medzihviezdnym plynom a vznikajú ďalšie častice, ktoré nie sú časté v jadrovej syntéze vo hviezdach, ako lítium, berýlium, bór, ale aj antiprotóny a pozitróny. V hustej zemskej atmosfére potom toto primárne kozmické žiarenie interaguje a na zem dopadajú hlavne elektróny, pozitróny a mióny. Avšak práve pozorovaním kozmického žiarenia v rôznych výškach atmosféry sa podarilo zistiť, že jadrová hmota je komplikovanejšia ako tá, ktorú poznáme zo zloženia jadier atómov. Prvý protónový synchrotron, ktorý svojou urýchľovacou energiou nad hranicou GeV (eV je jednotka energie používaná v časticovej fyzike, 1 eV $\approx 1,6 \times 10^{-19}$ J) umožnil pozorovať mezóny známe dovtedy z kozmického žiarenia a objavovať nové častice, bol Cosmotron v Brookhavenskom národnom laboratóriu (BNL) v USA. Plnú energiu 3.3 GeV dosiahol v roku 1953 a zahájil obdobie, keď sa podarilo nájsť záplavu nových častíc. Na chvíľu sa mohlo zdať, že svet je zložitejší a zložitejší. Fyzici Murray Gell-Mann a George Zweig navrhli, nezávisle od seba, v roku 1964 kvarkový model. Kvarky majú zlomkový elektrický náboj $\pm 1/3e$ alebo $\pm 2/3e$. Pozorované častice sa skladajú z kvarkov, ktoré sú spolu s leptónmi (elektrón, mión, tauón) úplne základnými čiastočkami hmoty. Ku každému leptónu existuje príslušný typ neutrína s veľmi malou hmotnosťou. Na popis bežnej hmoty si vystačíme s dvoma najľahšími kvarkami u (up - hore, $m_u = 2,2^{+0,6}_{-0,4}$ MeV [R1]) a d (down - dolu, $m_d = 4,7^{+0,5}_{-0,4}$ MeV) a elektrónom. Z týchtov kvarkov sa skladajú protóny (uud) a neutróny (ddu). Postupne sa zistilo, že existujú aj ďalšie typy kvarkov s (strange - podivný, $m_s = 96^{+8}_{-4}$ MeV), c (charm – pôvabný, $m_c = 1,28 \pm 0,03$ GeV), b (beauty - krásny alebo bottom - spodný, $m_b = 4,18^{+0,04}_{-0,03}$ GeV) a t (top - vrchný alebo true - pravdivý, $m_t = 173,1 \pm 0,6$ GeV). Hovoríme o šiestich rôznych vôňach kvarkov. Ťažké kvarky majú hmotnosť väčšiu ako sú hmotnosti nukleónov. Z kvarkov sa skladajú všetky pozorované hadróny. Buď sa jedná o trojkvarkové kombinácie - baryóny alebo o kombinácie kvarku a antikvarku - mezóny. V roku 2015 sa experimentu LHCb v CERN podarilo preukázať existenciu pentakvarkov $P_c^+(4450)$ a $P_c^+(4380)$ [R2], hadrónov skladajúcich sa zo štyroch kvarkov a jedného antikvarku. Všetky častice majú svoje antičastice. Častice a antičastice môžu navzájom anihilovať a uvoľniť energiu odpovedajúcu ich kľudovej hmotnosti. Analogicky je možné z energie páry častica-antičastica vytvoriť. Tieto elementárne častice v rámci súčasného teoretického popisu v štandardnom modeli časticovej fyziky interagujú elektromagnetickou, silnou a slabou silou. Tieto interakcie nastávajú pomocou

výmeny bozónov: gluónov u silnej interakcie, W^+, W^-, Z^0 u slabej interakcie, γ u elektromagnetickej interakcie. V rámci štandardného modelu hrá dôležitú úlohu Higgsov bozón, objavený v roku 2012 v CERN [R3,R4] a ktorý objasňuje relatívne veľkú hmotnosť W a Z bozónov oproti nehmotnému fotónu. Gravitačná sila, ktorá pôsobí medzi časticami s hmotnosťou, nie je súčasťou štandardného modelu. Silná sila, ktorá je zodpovedná za väzbu kvarkov v hadrónoch, je spojená s existenciou farebného náboja. Kvarky existujú v troch farebných stavoch. Gluóny nesú farbu a antifarbu a môžu na rozdiel od fotónov interagovať silne medzi sebou. Teória silných interakcií je kvantová chromodynamika, neabelovská kalibračná teória založená na lokálnej kalibračnej grupe symetrií SU(3). V jej rámci má silná interakcia neobvyklé vlastnosti, ako je asymptotická sloboda a farebné uväznenie. Pri malej vzdialenosti a vysokej energii je sila interakcie malá, avšak pri odďaľovaní kvarkov sila interakcie zostáva rovnaká a kvarky nie je možné z hadrónu uvoľniť. Tomu hovoríme farebné uväznenie. Od istej chvíle je pri oddeľovaní energeticky výhodné vytvoriť kvark-atikvark pár a tieto kvarky sa môžu pospájať opäť do hadrónov. Výsledkom je, že kvark nemôžeme nikdy pozorovať priamo a pri vytvorení vysokoenergetického kvarku či gluónu napokon v experimente pozorujeme výtrysk častíc jedným smerom.

V prvých okamihoch po Veľkom tresku pred 14 miliardami rokov bola hustota a teplota jadrovej hmoty tak veľká, že sa usudzuje, že existovala vo forme prapolievky voľných kvarkov a gluónov, kvarkovo-gluónovej plazmy (QGP). Postupným rozpínaním teplota klesla a nastal fázový prechod do stavu, keď sa kvarky a gluóny uväznili do hadrónov. Je fascinujúce, že experimenty s využitím ultrarelativistických jadro-jadrových zrážok dokážu v laboratóriu tieto podmienky nastoliť a skúmať fázové stavy jadrovej hmoty, vrátane kvarkovo-gluónovej plazmy. Výpočty poruchovej kvantovej chromodynamiky (pQCD) na mriežke ukazujú, že fázový prechod hadrónového plynu do QGP by mal nastať pri teplote okolo $T_c \approx 160$ MeV (pri baryónovom chemickom potenciáli $\mu_b = 0$ GeV). Na Obr.1.1 je schematicky zobrazený časopriestorový priebeh jadro-jadrovej zrážky. Pri zrážke sa kinetická energia urýchlených jadier premení na hmotu, kvarky a gluóny. Prvá fáza zrážky je predrovnovážna, v nej sa z virtuálnych kvánt vytvoria reálne partóny a tie navzájom interagujú, až nastane rovnovážny stav kvarkovo-gluónovej plazmy. Vyjadrené vlastným časom systému sa odhaduje, že predrovnovážny stav trvá $\tau_0 \approx 1$ fm/c . Ďalej sa systém v stave QGP rozpína a chladne. V tejto fáze, ktorá može trvať okolo 10 fm/c (t.j. 3×10^{-23}s), prebiehajú fyzikálne procesy, ktorých prejavy sa snažíme experimentálne identifikovať a interpretovať. Na ich základe sa pokúšame QGP charakterizovať a opísať. Teplota jadrovej hmoty po zrážke pri energiách na urýchľovači RHIC sa z meraní priamych fotónov odhaduje na viac než 500 MeV. Keď QGP ochladne na T_c, nastane fázový prechod do hadrónového plynu, kde sú kvarky viazané do hadrónov. I v tejto fáze môžu hadróny interagovať v pružných a nepružných zrážkach až nastane moment chemického vymrznutia pri T_{ch} a potom sa už pomery hadrónov nemenia, i keď až do tepelného vymrznutia pri T_{fo}

môžu interagovať pružne. Následne prestanú interagovať a pokračujú v lete od bodu zrážky. Keďže, až na protón, sú hadróny nestabilné, v detektoroch detegujeme prevažne dcérske častice hadrónových rozpadov, typicky protóny, pióny, kaóny a elektróny a ich antičastice.

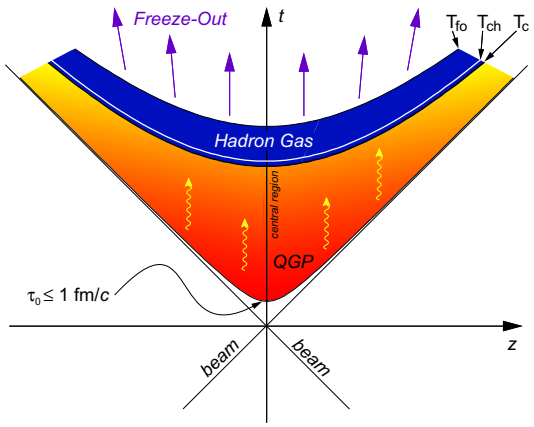

Obr. 1.1: Schematické zobrazenie časopriestorového priebehu jadro-jadrovej zrážky. Jadrová hmota prejde po sformovaní QGP rozpínaním a následne fázovým prechodom do hadrónového plynu pri T_c. Hadróny ešte navzájom interagujú a systém prejde chemickým a tepelným vymrznutím pri T_{ch} a T_{fo}. Prevzaté z Ref. [R5]

Program ultrarelativistických jadro-jadrových zrážok začal v roku 1986 zrážkami kyslíku ^{16}O na olove ^{208}Pb na urýchľovači SPS v CERN a zrážkami kyslíku ^{16}O na zlate ^{197}Au na urýchľovači AGS v BNL. Aj v súčasnosti hrajú tieto dve laboratória vedúcu úlohu v skúmaní vlastností QGP. V BNL na urýchľovači RHIC je aktívny experiment STAR, ktorý plánuje svoj experimentálny program až do roku 2022. V CERN sa na urýchľovači LHC týmto stavom hmoty zaoberá hlavne experiment ALICE spolu s experimentmi ATLAS, CMS a od roku 2013 aj experiment LHCb. Výsledky experimentov na SPS naznačili, že hmota vytvorená v centrálnych ultrarelativistických jadro-jadrových zrážkach má prejavy, ktoré sú v súlade s produkciou QGP [R6]. Centrálne zrážky sú zrážky s malým zrážkovým parametrom, obvykle sa vyjadrujeme v percentách najcentrálnejších zrážok. V centrálnych zrážkach je napríklad produkcia podivných baryónov zosilnená vzhľadom k protón-protónovým zrážkam v dôsledku interakcií medzi kvarkami a gluónmi pri vysokých gluónových hustotách. Taktiež sa pozorovalo potlačenie produkcie J/ψ nad rámec prejavov studenej jadrovej hmoty v súlade s farebným tienením dikvarkového väzbového potenciálu pri vysokých teplotách a hustotách energie. Experimenty na RHIC objavili ďalšie úplne nové javy. Hmota vytvorená v zrážkach Au+Au pri energii $\sqrt{s_{NN}} = 200$ GeV je nepriehľadná pre vysokoenergetické partóny vyprodukované v počiatočných fázach jadrovej zrážky v tvrdých procesoch. Táto vlastnosť sa prejavuje ako zhášanie výtryskov častíc v dôsledku strát energie partónov interagujúcich s kvarkami a gluónmi v QGP. Pozorovaná hmota má kolektívne chovanie s kvarkami a gluónmi ako základnými stupňami voľnosti. Dá sa popísať hydro-

dynamickými modelmi ideálnej kvapaliny s najmenšou doteraz pozorovanou hodnotou $\frac{\eta}{s}$, pomeru šmykovej viskozity a entropie. Na Obr. 1.2 je kompilácia merania závislosti jadrového modifikačného faktora (R_{AA}) rôznych druhov častíc na priečnej hybnosti z experimentu PHENIX pre centrálne zrážky Au+Au pri $\sqrt{s_{NN}} = 200$ GeV [R7]. R_{AA} je pomer výťažku produkcie častíc nameraného v jadro-jadrovej zrážke a v referenčnej protón-protónovej zrážke vynásobenej priemerným počtom binárnych zrážok v jadro-jadrovej zrážke ($\langle N_{bin} \rangle$). Používa sa na kvantifikáciu vplyvu jadrovej hmoty na produkciu častíc. Produkcia častíc, ktoré vznikajú v tvrdých procesoch, je škálovaná s $\langle N_{bin} \rangle$. V prípade, že by v jadrovej hmote nebola ďalej ovplyvnená, hodnota R_{AA} by mala byť 1. Toto vidíme na Obr. 1.2 pre priame fotóny γ, avšak produkcia ostatných častíc je potlačená pri vysokých hodnotách p_T. Produkcia častíc z tvrdých procesov prevažuje pri hodnotách p_T väčších než 2 - 4 GeV/c . Napríklad produkcia π^0 je v oblasti nad 4 GeV/c potlačená faktorom 5, čo odpovedá hodnote $R_{AA} \approx 0{,}2$. Toto sa interpretuje ako dôsledok zhášania výtryskov častíc, pretože z dôvodu strát energie vyprodukovaných vysokoenergetických partónov v QGP toto vedie k následnej produkcii častíc s menšou hodnotou p_T. Keďže priame fotóny s QGP neinteragujú silne, nie sú vzhľadom k p+p potlačené.

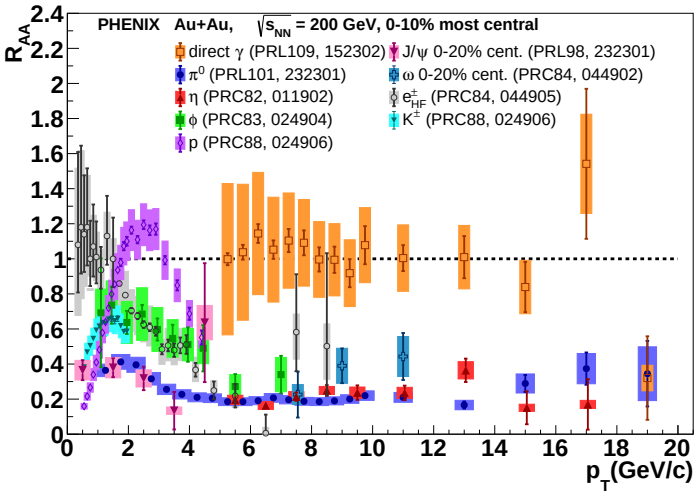

Obr. 1.2: Závislosť jadrového modifikačného faktora na priečnej hybnosti pre priame $\gamma, \pi^0, \eta, \phi, \omega, K^{\pm}, e^{\pm}$ z rozpadov hadrónov ťažkých vôní, J/ψ a protónov, nameraná experimentom PHENIX pre centrálne zrážky Au+Au pri $\sqrt{s_{NN}} = 200$ GeV. Prevzaté z Ref. [R7].

Kritický rozbor prvých meraní na urýchľovači RHIC jednotlivé experimentálne kolaborácie publikovali ako tzv. biele knihy jednotlivých experimentov: STAR [13], PHENIX [R8], BRAHMS [R9], PHOBOS [R10]. V ostatných rokoch sa podarilo experimentu STAR previesť aj niekoľko neočakávaných meraní a objavov. Podarilo sa previesť prvé experimentálne meranie produkcie antihypertrícia [102] (Science 328 (2010) 58), viazaného stavu antineutrónu, antiprotónu a častice antilambda. Taktiež sme priamo

pozorovali produkciu antihélia [127] (Nature 473 (2011) 353), najťažšieho doposiaľ vyprodukovaného antijadra. Zmerali sme tiež, že interakcia medzi antiprotónmi je príťažlivá [300] (Nature 527 (2015) 345). Meraním globálnej polarizácie Λ hyperónu sme nepriamo zistili, že jadrová hmota produkovaná v jadro-jadrových zrážkach má aj extrémnu hodnotu vírivosti $\omega \approx (9 \pm 1) \times 10^{21} s^{-1}$, očakávanú z dôvodu veľkého momentu hybnosti (až $1000\hbar$) v necentrálnych zrážkach [361] (Nature 548 (2017) 62).

V ďalšej časti tejto kapitoly sa zameráme na teoretické skúmanie vplyvu výtryskov častíc na kvantifikáciu trojuholníkového toku. V ďalších kapitolách budeme diskutovať merania spojené s produkciou ťažkých kvarkov z experimentu STAR.

1.1 Vplyv výtryskov častíc a interakcií v konečnom strave na trojuholníkový tok

Doterajšie experimentálne výsledky z ultra-relativistických zrážok ukazujú, že vývoj horúcej a hustej jadrovej hmoty prebieha podľa pravidiel hydrodynamiky s malou viskozitou, ako ideálna jadrová kvapalina. Toto kolektívne chovanie je možné kvantifikovať napríklad parametrizovaním uhlového rozdelenia vytvorených častíc vzhľadom k rovine zrážky (vzťah (1) v priloženom článku). Avšak je niekoľko možných ďalších fyzikálnych javov, ktoré túto parametrizáciu narušujú, pretože efektívne spôsobujú korelácie medzi vzniknutými hadrónmi. Parameter v_2, eliptický tok, súvisí s deformáciou tvaru jadrovej hmoty na počiatku zrážky. Z dôvodu symetrického rozdelenia energie v zrážke sa očakávalo, že všetky nepárne členy n>1 Fourierovho rozvoja definujúceho koeficienty kolektívneho toku budú nulové a až v nedávnej dobe sa rozvinulo štúdium parametra v_3, takzvaného trojúholníkového toku [R11]. Fluktuácie tvaru oblasti prekryvu jadier pri zrážke vedú k jeho nenulovým hodnotám. V článku J. Crkovska *et al., Influence of jets and decays of resonances on the triangular flow in ultrarelativistic heavy-ion collisions* Phys. Rev. C **95** no.1, 014910 (2017) sme skúmali vplyv produkcie výtryskov častíc a rozpadov rezonancií na trojúholníkový tok rôznych hadrónov pri energiách zrážok na urýchľovači LHC v CERN. Túto štúdiu sme previedli pomocou výpočtov a simulácií v rámci generátora zrážok HYDJET++ [R12]. V rámci tohto Monte Carlo generátora sú jadro-jadrové zrážky simulované ako superpozícia dvoch fáz: mäkkej a tvrdej. Obe časti sú simulované osobitne. Častice v mäkkej fáze sú modelované na hyperploche chemického a termálneho vymrznutia pomocou parametrizovanej relativistickej hydrodynamiky. Z javov vo finálnom stave zrážky sú zahrnuté dvojčasticové a trojčasticové rozpady viac než 360 mezónových a baryónových rezonancií. Častice z tvrdej fázy sú simulované pomocou modelu PYQUEN [R13]. Ten vychádza z rozdelenia výtryskov častíc generovaných pomocou PYTHIA [R14] a vzniknuté partóny sú modifikované v jadrovej hmote v dôsledku radiačných a zrážkových strát energie. Následne sú partóny hadronizované v rámci Lundského strunového modelu (Lund string model). Partóny vyprodukované s menšími hybnosťami ako p_T^{min} sú pridané do mäkkej zložky.

Ako je vysvetlené v článku (vzťahy (3) a (4)), anizotropický tok je v modeli jednak dôsledkom priestorovej excentricity reakčnej zóny prekrývajúcich sa jadier v priečnej rovine zrážky (parameter $\epsilon(b)$) a jednak dôsledkom dodatočnej anizotropie jadrovej tekutiny, keď azimutálny uhol rýchlosti tekutiny je nelineárne korelovaný (parameter $\theta(b)$) s priestorovým azimutálnym uhlom. Hodnoty oboch parametrov sa získali fitovaním experimentálnych meraní eliptického toku. Trojúholníkový tok je zavedený ďalším parametrom (parameter $\epsilon_3(b)$) v popise priečneho polomeru hyperplochy vymrznutia. V článku sme študovali rôzne fyzikálne príspevky do trojuholníkového toku. Ukázali sme, že pri energiách na LHC (Pb+Pb 2.76 TeV a centralita 20-30%) rozpady rezonancií majú významný vplyv na veľkosť v_3, zosilňujú ho, pre nabité hadróny s p_T viac než 1 GeV/c (viz. Fig.1). (V ďalšom texte budem rozlišovať odkazovanie sa na obrázky v komentári (Obr.) a odkazovanie sa na obrázky v priložených článkoch. U druhého prípadu budem citovať obrázky tak, ako sa objavujú v článkoch (Fig., FIG., atd.).) Pri pohľade na rôzne druhy hadrónov, začína vplyv rozpadov rezonancií u piónov už od 1 GeV/c, avšak pri ťažších hadrónoch ako kaón, lambda a protón je vplyv výrazný až od $p_T \approx 2$ GeV/c (viz. Fig.4). Produkcia výtryskov častíc - tvrdá časť spektra sa prejavuje poklesom v_3 pri vyšších p_T. U ťažších častíc sa pokles prejavuje u relatívne vyšších p_T, ako u ľahších častíc (viz. Fig.1 a Fig.2). Výpočty modelu HYDJET++ dobre popisujú integrované merania v_3 pre rôzne centrality zrážok Pb+Pb 2.76 TeV merané experimentom ATLAS. Niektoré rezonancie zvyšujú a niektoré znižujú v_3 piónov. Celkovo rozpady rezonancií len málo ovplyvňujú integrované hodnoty v_3 nabitých hadrónov (viz. Fig.7). Výrazný je vplyv tvrdej zložky z výtryskov častíc, ktorá redukuje v_3. Ďalej sme skúmali škálovanie toku. Na experimentoch na urýchľovači RHIC sa experimentálne ukázalo, že závislosť eliptického toku v_2 na priečnej kinetickej energii K$E_T \equiv m_T$-m_0 sa škáluje pre rôzne hadróny v prípade, keď sa obe veličiny vydelia počtom valenčných kvarkov n_q do hodnoty K$E_T/n_q \approx 1$ GeV [R15]. V prípade hadrónov produkovaných v mäkkých procesoch bez zahrnutia následných rozpadov rezonancií HYDJET++ predpovedá škálovanie v intervale KE_T/n_q 0,5 až 1,2 GeV. Zahrnutie rozpadov rezonancií rozširuje toto škálovanie až k hodnote 1,7 GeV. Naopak zahrnutie produkcie častíc z tvrdej zložky - výtryskov častíc spôsobí rozmazanie škálovania (viz Fig. 11). S J. Crkovskou sme previedli podobnú štúdiu aj pre energie na urýchľovači RHIC [D5]. Ukázalo sa, že po zahrnutí rezonancií nastáva škálovanie a následný vplyv výtryskov má naň malý vplyv.

V poslednej dobe veľkú pozornosť získalo štúdium kolektívneho toku a dvojčasticových korelácií v malých systémoch, v protón-protónových a protón-jadrových zrážkach. Tieto zrážky sa dlho považovali za referenčné merania a tvorba QGP alebo kolektívne prejavy sa u nich neočakávali. Avšak merania z experimentov napr. CMS [R16, R17] alebo ALICE [183, 208, 250] ukázali, že korelácie medzi časticami v týchto zrážkach sú podobné ako v jadro-jadrových zrážkach pri rovnakej početnosti častíc. Tieto pozorovania viedli k čiastočnému prehodnoteniu interpretácie meraní toku a taktiež k vývoju

ďalších veličín, ktoré kolektívne chovanie lepšie charakterizujú [R18]. Javí sa, že aj v protón-jadrových zrážkach nastáva kolektívne hydrodynamické rozpínanie [R19].

Article reprint

PHYSICAL REVIEW C **95**, 014910 (2017)

Influence of jets and decays of resonances on the triangular flow in ultrarelativistic heavy-ion collisions

J. Crkovská,[1,2] J. Bielčík,[1] L. Bravina,[3,4,5] B. H. Brusheim Johansson,[3,4] E. Zabrodin,[3,4,5,6] G. Eyyubova,[6] V. L. Korotkikh,[6] I. P. Lokhtin,[6] L. V. Malinina,[6,7] S. V. Petrushanko,[6] and A. M. Snigirev[6]

[1]*Faculty of Nuclear Sciences and Physical Engineering, Czech Technical University in Prague, CR-11519 Prague, Czech Republic*
[2]*Institut de Physique Nucléaire, CNRS-IN2P3, Université Paris-Sud, Université Paris-Saclay, F-91406 Orsay Cedex, France*
[3]*Department of Physics, University of Oslo, Postboks 1048 Blindern, N-0316 Oslo, Norway*
[4]*Frankfurt Institute for Advanced Studies, Ruth-Moufang-Straße 1, D-60438 Frankfurt am Main, Germany*
[5]*National Research Nuclear University "MEPhI" (Moscow Engineering Physics Institute), RU-115409 Moscow, Russia*
[6]*Skobeltsyn Institute of Nuclear Physics, Moscow State University, RU-119991 Moscow, Russia*
[7]*Joint Institute for Nuclear Researches, RU-141980 Dubna, Russia*

(Received 31 March 2016; revised manuscript received 19 August 2016; published 23 January 2017)

Triangular flow v_3 of identified and inclusive particles in Pb + Pb collisions at $\sqrt{s_{NN}} = 2.76$ TeV is studied as a function of centrality and transverse momentum within the HYDJET++ model. The model enables one to investigate the influence of both hard processes and final-state interactions on the harmonics of particle anisotropic flow. Decays of resonances are found to increase the magnitude of the $v_3(p_T)$ distributions at $p_T \geqslant 2$ GeV/c and shift their maxima to higher transverse momenta. The p_T-integrated triangular flow, however, becomes slightly weakened for all centralities studied. The resonance decays also modify the spectra towards the number-of-constituent-quark scaling fulfillment for the triangular flow, whereas jets are the main source of the scaling violation at the energies available at the CERN Large Hadron Collider (LHC). Comparison with the corresponding spectra of elliptic flow reveals that resonance decays and jets act in a similar manner on both $v_3(p_T)$ and $v_2(p_T)$ behavior. Obtained results are also confronted with the experimental data on differential triangular flow of identified hadrons, ratio $v_3^{1/3}(p_T)/v_2^{1/2}(p_T)$, and p_T-integrated triangular flow of charged hadrons.

DOI: 10.1103/PhysRevC.95.014910

I. INTRODUCTION

Collective flow of hadrons produced in ultrarelativistic heavy-ion collisions is one of the signals especially sensitive to the creation of even a small amount of quark-gluon plasma (QGP) [1–3]. To quantify this phenomenon an expansion of the azimuthal distribution of hadrons in a Fourier series was proposed in Refs. [4,5]:

$$\frac{dN}{d\phi} \propto 1 + 2\sum_{n=1}^{\infty} v_n \cos\left[n(\phi - \Psi_n)\right]. \tag{1}$$

Here ϕ denotes the azimuthal angle between the particle transverse momentum and the participant event plane, and Ψ_n is the azimuth of the event plane of the nth flow component. The coefficients v_n are the flow harmonics that can be found after the averaging of cosines in Eq. (1) over all particles in an event and all events in the data sample:

$$v_n = \langle\langle \cos\left[n(\phi - \Psi_n)\right]\rangle\rangle. \tag{2}$$

Modifications of the proposed analysis are possible [6], but we keep the traditional scheme to compare our results to the experimental data. For almost 20 years experimentalists and theorists have intensively investigated mainly the two lowest-order coefficients, called directed v_1 and elliptic v_2 flow, see, e.g., Refs. [7,8] and references therein, whereas the study of triangular v_3 flow and higher harmonics started not long ago [9–12].

In collisions of similar nuclei, such as gold-gold or lead-lead, the higher-order odd-flow harmonics measured with respect to the reaction plane are expected to vanish under the assumption of a symmetric energy distribution. Experiments confirm that $v_3(\Psi_2) = 0$. However, initial-state fluctuations can lead to a nonvanishing participant triangularity [9], which is approximately linear to the triangular flow in its own participant plane Ψ_3 [13,14]. In many theoretical works devoted to the investigation of the signal in heavy-ion collisions, topics such as the response of v_3 to the initial triangularity ε_3 of the collision zone and sensitivity to initial-state fluctuations and to viscosity of hot QCD matter have been treated [9,13–15]. Our study focuses mainly on the influence of jets and decays of resonances on the formation of v_3, which to our best knowledge has not been explored extensively yet (see Refs. [16] and [17]). The event generator HYDJET++ [18] is employed for the simulation of Pb + Pb collisions at $\sqrt{s_{NN}} = 2.76$ TeV.

HYDJET++ suits very well for these purposes because the model includes the treatment of both soft and hard processes and has an extensive table of hadronic resonances, including the charmed ones, with more than 400 baryonic and mesonic states. The properties of the model and the generation of the anisotropic flow in it are discussed in Sec. II. Section III presents the results on differential and integrated triangular flow of charged hadrons produced from central to (semi)peripheral Pb + Pb collisions at $\sqrt{s_{NN}} = 2.76$ TeV. Here the partial contributions of hydrodynamic processes, jets, and decays of resonances to the formation of the final v_3 are studied. Ratios $v_3^{1/3}/v_2^{1/2}$ and fulfillment of the number-of-constituent-quark (NCQ) scaling are investigated as well. Finally, conclusions are drawn in Sec. IV.

Article reprint

J. CRKOVSKÁ *et al.* PHYSICAL REVIEW C **95**, 014910 (2017)

II. GENERATION OF TRIANGULAR FLOW IN HYDJET++

The Monte Carlo event generator HYDJET++ (hydrodynamics with jets) treats a relativistic heavy-ion collision as a superposition of a soft, hydrolike state, hadronized as a result of a sudden thermal freeze-out, and a hard multiparton state, where energetic partons experience collisional and radiative energy losses in an expanding quark-gluon fluid [18]. The simulation of both states proceeds independently. In the soft sector the thermalized system of hadrons is generated on the hypersurfaces of chemical and thermal freeze-out given by the parametrized relativistic hydrodynamics with preset freeze-out conditions [19,20]. This approach is similar to the THERMINATOR model [21]. The effective thermal volume of the fireball is used to calculate the mean multiplicities of hadrons produced at the freeze-out hypersurface. The volume is generated on an event-by-event basis. It is proportional to the number of wounded nucleons at a given centrality provided by the Glauber model of multiparticle scattering. The only final-state interactions taken into account are the two- and three-body decays of resonances. The table of resonances is quite extensive and contains more than 360 meson and baryon (anti)states including the charmed ones.

The next part of HYDJET++, which describes the hard partonic interactions, employs the generator PYQUEN [22] for simulation of single hard nucleon-nucleon collisions. It starts with the PYTHIA-generated initial parton distributions and generation of the spatial vertexes of jet production, proceeds with the rescattering-by-rescattering propagation of partons through the hot and dense medium, determines the partons' mean free path as well as radiative and collisional energy loss, and, finally, hadronizes the hard partons and in-medium emitted gluons according to the Lund string model. Thus for each symmetric heavy-ion collision at a given impact parameter, the mean number of jets is a product of binary NN collisions and the integral cross section of the hard process with the certain minimum momentum transfer, $p_T^{\min}$. Partons produced in initial hard scatterings with a transverse momentum transfer lower than $p_T^{\min}$ are excluded from the hard component. Their products of hadronization are added to the thermalized component of the particle spectrum. These hadrons, however, can carry only weak anisotropic flow arising because of the well-known jet-quenching effect. Details of the model can be found in Refs. [18–20,23]. It is worth noting that the combination of parametrized hydrodynamics with jets was able to explain the falloff of the elliptic flow, v_2, at high transverse momenta and violation of the mass ordering of $v_2(p_T)$ distributions for mesons and baryons at $p_T \approx 2$ GeV/c [24], to predict the violation of the number-of-constituent-quark scaling for v_2 at the energies available at the LHC [24,25], and to describe the rise of the high-p_T tail of the v_4/v_2^2 ratio at the energies available at the BNL Relativistic Heavy Ion Collider (RHIC) and the LHC [26,27]. The extension of HYDJET++ to the triangular flow was done in Ref. [28]. The interplay of v_2 and v_3 in the model describes the nonlinear contributions of elliptic and triangular flow to higher flow harmonics including the hexagonal one [28,29], as well as the long-range dihadron correlations, known as ridge [30]. Triangular flow is a very important ingredient of the model and it is thus worth discussing the features of its generation.

Anisotropic flow emerges in HYDJET++ because of the following reasons. The profile of the nuclear overlap zone in the transverse plane can be approximated by an ellipse with the spatial eccentricity $\varepsilon(b) = (R_y^2 - R_x^2)/(R_y^2 + R_x^2)$, where b is the impact parameter, and R_y and R_x are the long- and short-ellipse radii, respectively. Then, the transverse radius of the fireball reads

$$R_{\rm ell}(b,\phi) = R_{\rm fo}(b)\frac{\sqrt{1-\varepsilon^2(b)}}{\sqrt{1+\varepsilon(b)\cos 2\phi}}, \tag{3}$$

where

$$R_{\rm fo}(b) \equiv \sqrt{\left(R_x^2 + R_y^2\right)/2} = R_0\sqrt{1-\varepsilon(b)}, \tag{4}$$

with R_0 being the freeze-out transverse radius in a perfectly central collision with $b = 0$. Because every fluid cell is carrying a certain momentum, the spatial anisotropy at the freeze-out will be transformed into the momentum anisotropy. Unlike several other models, HYDJET++ does not rely on isotropic parametrization, where the azimuthal angle of the fluid velocity, $\phi_{\rm fluid}$, coincides with the azimuthal angle ϕ. Instead, these two angles are correlated via the nonlinear function [20]

$$\tan\phi_{\rm fluid} = \sqrt{\frac{1-\delta(b)}{1+\delta(b)}}\tan\phi, \tag{5}$$

where the new anisotropy parameter, $\delta(b)$, is introduced. Both spatial and flow anisotropy parameters, $\varepsilon(b)$ and $\delta(b)$, are proportional to the initial spatial anisotropy $\varepsilon_0 = b/(2R_A)$. Their values are fixed after fitting the HYDJET++ calculations to the measured elliptic flow.

To extend the model to the triangular flow the transverse radius of the freeze-out hypersurface was modified accordingly [28]:

$$R_{\rm trian}(b,\phi) = R_{\rm ell}(b,\phi)\{1 + \varepsilon_3(b)\cos[3(\phi - \Psi_3)]\}. \tag{6}$$

Because experiments show no correlation between the event planes of the second and third harmonics, i.e., $v_2(\Psi_3) = v_3(\Psi_2) = 0$, these planes are also uncorrelated in HYDJET++. The new parameter $\varepsilon_3(b)$ entering Eq. (6) is responsible for the creation of triangularity in the system. Similarly to $\varepsilon(b)$, it can also be proportional to the initial eccentricity $\varepsilon_0(b)$ or considered as a free parameter.

Note, that the model possesses event-by-event (EbyE) fluctuations even when the values of the anisotropy parameters, $\varepsilon(b)$, $\delta(b)$, and $\varepsilon_3(b)$, are fixed at the fixed impact parameter b. The sources of the EbyE fluctuations are fluctuations in particle multiplicities, coordinates, and momenta, as well as production of minijets and decays of resonances. Recently, HYDJET++ was extended [31] to match the measured EbyE fluctuations quantitatively. For this purpose the three parameters were not fixed anymore but rather smeared normally around their most probable values. The smearing procedure, however, does not change the distributions of either differential $v_{2(3)}(p_T,b)$ or p_T-integrated $v_{2(3)}(b)$ characteristics, because these results are obtained after the averaging over quite substantial amounts of generated events.

Article reprint

INFLUENCE OF JETS AND DECAYS OF RESONANCES ON ... PHYSICAL REVIEW C **95**, 014910 (2017)

III. TRIANGULAR FLOW IN Pb + Pb COLLISIONS AT LHC

The transverse momentum dependence and the centrality dependence of the triangular flow of hadrons were studied in Pb + Pb collisions at center-of-mass energy $\sqrt{s_{NN}} = 2.76$ TeV. The considered p_T interval was $0 \leqslant p_T \leqslant 8\,\mathrm{GeV}/c$, whereas the centrality range $0 \leqslant \sigma/\sigma_{\mathrm{geo}} \leqslant 50\%$ was subdivided into five bins, namely, 0–10%, 10–20%, 20–30%, 30–40%, and 40–50%. Because the yields of hadrons with transverse momenta larger than 1 GeV/c rapidly drop, the generated event statistics was about 1 000 000 events for each centrality bin to provide reliable values for v_3 at $p_T \geqslant 4$ GeV/c. A detailed comparison of the HYDJET++ calculations of v_3 to the corresponding data by the ATLAS Collaboration [32] and the CMS Collaboration [33] was done in Ref. [28]. In the present article our primary goal is to reveal the contributions of different processes to the formation of triangular flow. We start from the interplay of soft processes and jets.

A. Interplay of soft and hard processes

In what follows, we distinguish between the spectra of particles

(i) directly frozen at the freeze-out hypersurface in hydro calculations (direct hydro),
(ii) direct hydro + resonance decays (soft processes only),
(iii) directly produced in jet fragmentation,
(iv) directly produced from jets + resonance decays (hard processes only),
(v) directly produced from hydro and jets, and
(vi) produced in all processes, i.e., hydro + jets + resonance decays.

Figure 1 shows the $v_3(p_T)$ spectrum of charged hadrons produced in collisions with centrality $20\% \leqslant \sigma/\sigma_{\mathrm{geo}} \leqslant 30\%$.

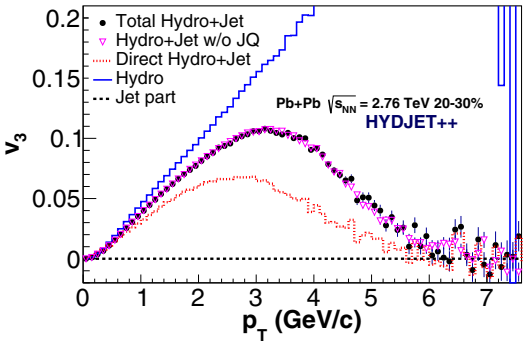

FIG. 1. The p_T dependence of different components of the triangular flow of charged particles produced in the HYDJET++ model for Pb + Pb collisions at $\sqrt{s_{NN}} = 2.76$ TeV at centrality 20–30%. The shown distributions are the $v_3(p_T)$ of particles coming from the hydro part (ii) (solid line), from the jets (iii) (dashed line), and of directly produced particles in both soft and hard (v) interactions (dotted line). Final triangular flow (vi) is presented by the solid circles, and triangles indicate the v_3 calculated without the jet quenching.

In addition to the resulting triangular flow (vi), the partial contributions coming from the hydrodynamic part with resonances (ii), the jet fragmentation (iii), and particles produced either at the freeze-out hypersurface or decoupled from jets (v) are displayed as well. To study the influence of the jet-medium interaction on the triangular flow, we plot in Fig. 1 also the calculations without the jet quenching. Note that the triangular flow of hadrons originated from the jets both with and without the jet quenching is consistent with zero in the model. Hadrons coming from soft hydrodynamic processes demonstrate an almost linear rise of triangular flow with increasing transverse momentum at $0.3 \leqslant p_T \leqslant 4$ GeV/c. Hydrodynamics, however, dominates the particle production at $p_T \lesssim 2.5$ GeV/c only, whereas at higher transverse momenta the particle spectrum is dominated by the jet hadrons. These circumstances cause the falloff of the $v_3(p_T)$ at $p_T \geqslant 3.5$ GeV/c. The jet quenching enhances the yield of hadrons with low and intermediate transverse momenta. These particles should reduce the triangular flow in low- and intermediate-p_T ranges. However, their admixture is very small compared to hadrons produced in soft processes. As one can see in Fig. 1, the impact of the jet quenching on the development of the p_T-differential v_3 is insignificantly small. Decays of resonances increase the triangular flow of charged hadrons at $p_T \geqslant 1$ GeV/c. This follows from the comparison of $v_3(p_T)$ of hadrons directly frozen at the freeze-out hypersurface or produced in the course of the jet fragmentation (dotted curve) with the total signal (solid circles), which includes also the hadrons coming from the decays of resonances. The detailed discussion of the influence of resonance decays on the triangular flow is given in Sec. III B.

Transverse momentum distributions of the triangular flow (vi) of most abundant charged hadrons, such as pions, kaons, (anti)protons, and (anti)Λ's are depicted in Fig. 2(a) together with the hydrodynamic parts (ii) of their spectra, shown separately in Fig. 2(b). Several things are worth mentioning here. In hydrodynamic calculations both meson and baryon branches show a linear rise at $0.5 \leqslant p_T \leqslant 5$ GeV/c. Mesonic flow is stronger than that of (anti)protons, whereas for full hydro+jets calculations this is true only for $p_T \leqslant 2.5$ GeV/c. At higher transverse momenta the triangular flow of protons and antiprotons, $v_3^{\bar{p}+p}(p_T)$, continues to rise, while the triangular flow of charged pions, $v_3^{\pi^{\pm}}(p_T)$, and kaons, $v_3^{K^{\pm}}(p_T)$, drops. This effect is also caused by the jet hadrons. The heavier the particle, the harder its p_T-spectrum in hydrodynamics is. Thus, jets start to reduce the $v_3(p_T)$ distribution of heavy hadrons at larger transverse momenta compared to light hadrons, as seen in Fig. 2(a).

Recently, the triangular flow of identified hadrons in Pb + Pb collisions at $\sqrt{s} = 2.76$ TeV was measured at different centralities by the ALICE Collaboration [34]. The results of HYDJET++ calculations for charged pions, kaons, and protons with antiprotons are plotted onto the experimental data in Fig. 3 for four centrality bins, 10–20%, 20–30%, 30–40%, and 40–50%. It follows from the comparison that the model provides a fair description of the data. It reproduces correctly the mass ordering of hadron v_3 at $p_T \leqslant 2$ GeV/c and its violation at higher transverse momenta.

Article reprint

J. CRKOVSKÁ *et al.* PHYSICAL REVIEW C **95**, 014910 (2017)

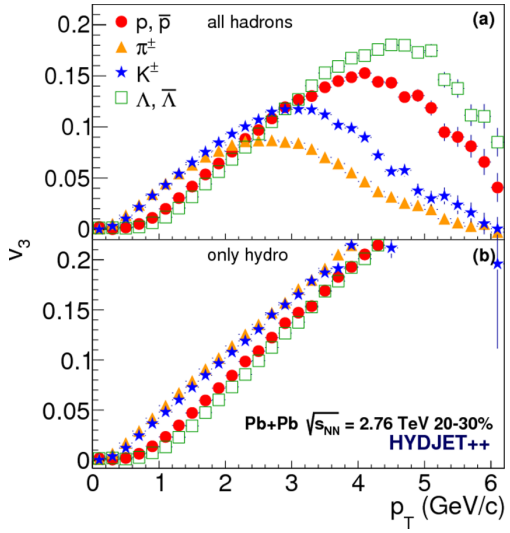

FIG. 2. The p_T dependence of (a) total triangular flow (vi) and (b) its hydro component (ii) in the HYDJET++ model for Pb + Pb collisions at $\sqrt{s_{NN}} = 2.76$ TeV at centrality 20–30%. The hadron species are $p + \bar{p}$ (solid circles), charged pions (solid triangles), charged kaons (solid stars), and $\Lambda + \overline{\Lambda}$ (open squares).

B. Influence of resonances

The differential spectra $v_3(p_T)$ of $\pi^{\pm}$, $K^{\pm}$, $p + \bar{p}$, and $\Lambda + \overline{\Lambda}$ are displayed in Fig. 4 for (semi)central (0–10%) collisions and in Fig. 5 for semiperipheral (30–40%) collisions. Here the spectra of hadrons directly produced either on the freeze-out hypersurface or in the course of jet fragmentation (v) are compared to the final distributions (vi), where decays of resonances are taken into account. For both centrality intervals the physical picture is qualitatively similar. Namely, decays of resonances do not vary significantly the triangular flow of hadronic species at transverse momenta below 1 GeV/c for pions and below 2 GeV/c for heavier particles. At higher transverse momenta the situation is changed. Hadrons coming from the resonance decays enhance the differential v_3 of all species and shift the maxima of the distributions by 0.5–1.0 GeV/c towards higher p_T. The maxima of $v_3(p_T)$ demonstrate the rise of about 25% with shifting centrality from 0–10% to 30–40% (cf. Figs. 4 and 5).

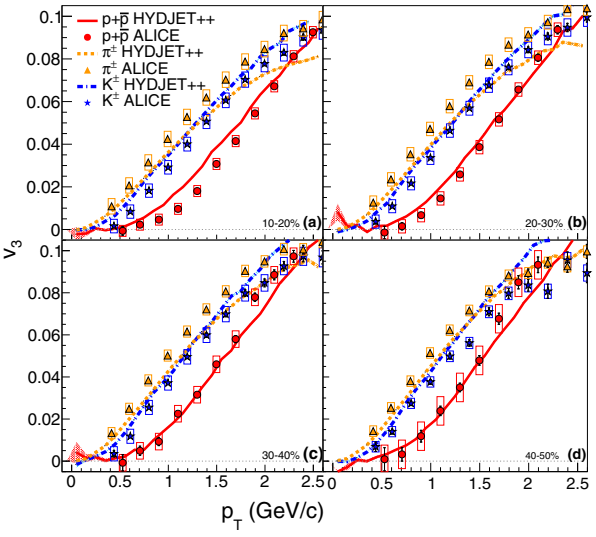

FIG. 3. The p_T dependence of triangular flow of $\pi^{\pm}$ (dashed lines), $K^{\pm}$ (dash-dotted lines), and $p + \bar{p}$ (solid lines) in HYDJET++ calculations of Pb + Pb collisions at 2.76 TeV at centrality (a) 10–20%, (b) 20–30%, (c) 30–40%, and (d) 40–50%. Corresponding experimental data from Ref. [34] are shown by solid triangles ($\pi^{\pm}$), stars ($K^{\pm}$), and circles ($p + \bar{p}$), respectively.

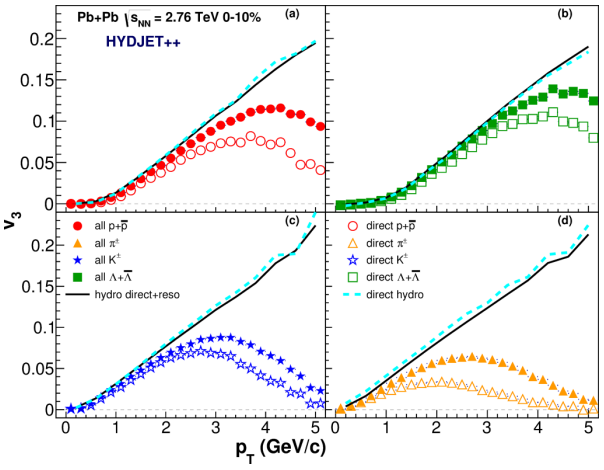

FIG. 4. The p_T dependence of triangular flow of (i) direct hadrons in hydro (dashed lines), (ii) all hadrons in hydro (solid lines), (v) direct hadrons in soft and hard processes (open symbols), and (vi) all hadrons (solid symbols) produced in the HYDJET++ model for Pb + Pb collisions at $\sqrt{s_{NN}} = 2.76$ TeV with centrality 0–10% for (a) $p + \bar{p}$, (b) $\Lambda + \overline{\Lambda}$, (c) charged kaons, and (d) charged pions.

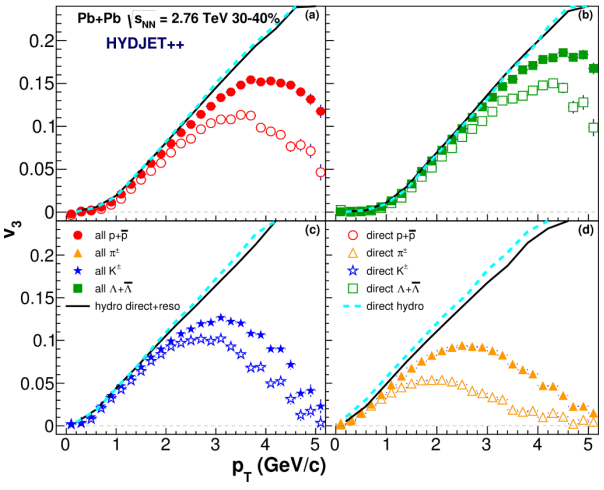

FIG. 5. The same as Fig. 4 but for centrality 30–40%.

In addition to these two distributions representing processes (v) and (vi), we plot in Figs. 4 and 5 two curves showing the $v_3(p_T)$ of particles directly produced from hydro (i) and its modification after the resonance decays (ii). For $p + \bar{p}$ and $\Lambda + \overline{\Lambda}$ both curves are very close to each other, whereas the $v_3(p_T)$ of charged kaons and, especially, of charged pions after the decays of resonances is a bit lower than that of directly produced particles. This result does not contradict the opposite behavior of the final spectra. The resonances are more abundantly produced in soft processes compared to the hard ones. Decays of resonances significantly increase the particle yields in the soft part of the spectrum; therefore fractions of hydroparticles dominate the particle spectra to larger transverse momenta. Consequently, the rise of the p_T-differential triangular flow will persist to larger values of p_T. Recall that not all resonances are equally important. As was shown in Ref. [17], the set of resonances needed for the description of the flow harmonics v_n of pions and protons can be reduced to 20–30 species only.

On the other side, the main part of particle spectrum consists of hadrons with transverse momenta lower than 1 GeV/c and pions are the dominant fraction of the spectrum, and for them the softest part of the $v_3(p_T)$ distribution seems to carry a bit weaker triangular flow after the decays of resonances compared to that of directly produced pions, as shown in Fig. 5. Therefore, the problem is twofold. First, it is necessary to scrutinize how the decays of resonances alter the pion triangular flow. After that we should get the integrated values of v_3 at different centralities.

At the energies available at the LHC of $\sqrt{s_{NN}} = 2.76$ TeV or higher only about 20% of pions are produced in HYDJET++ directly at the freeze-out hypersurface. The rest comes out as a result of decays of various resonances, both mesonic and baryonic. If we consider an isotropic decay of a baryon resonance on a pion and a lighter baryon, then, because of the decay kinematics, the daughter baryon should carry almost the same transverse momentum as the decaying resonance, whereas the pion p_T is much softer. This type of reaction will boost the triangular flow of the soft part of the pionic spectrum because the averaged triangular flow of heavy resonances is larger than that of pions. For meson resonances the softening or hardening of the pion triangular flow depends on the number of pions in the final state. To illustrate this let us consider three decays: $\rho \to \pi\pi$ (26% of pion yield), $\omega \to \pi\pi\pi$ (11%), and $\Delta \to p + p/\bar{p}$ (less than 2%). The differential $v_3(p_T)$ of these resonances and their decay products are compared in Fig. 6 to the triangular flow of directly produced pions and (anti)protons. The triangular flow of pions from ρ decays is just a bit softer than the v_3 of ρ mesons. Consequently, it is harder than the triangular flow of direct pions at $p_T \leqslant 1.5$ GeV/c [see Fig. 6(a)]. The spectrum of pions from ω decays, in contrast, is much softer than that of ω's. Thus, their triangular flow at $p_T \leqslant 1.5$ GeV/c is even stronger than that of the direct pions. A similar tendency is revealed by pions from the Δ decays. Therefore, some resonances will enhance the pion triangular flow in the soft p_T region, whereas other will reduce it.

The result of this interplay is seen in Fig. 7, which shows the integrated values of the triangular flow of charged hadrons calculated in five centrality bins. The triangular flow of direct particles and that of direct particles together with products of resonance decays obtained in the hydro part of the model are shown separately. To compare the model results to the experimental data, the integration over the transverse momentum was done in two intervals: $1 \leqslant p_T \leqslant 2$ GeV/c, displayed in Fig. 7(a), and $2 < p_T \leqslant 3$ GeV/c, displayed in Fig. 7(b). Experimental data from the ATLAS Collaboration [32] are plotted onto the HYDJET++ calculations. We see that decays of resonances just slightly reduce the integrated v_3. The triangular flow at $2 < p_T \leqslant 3$ GeV/c in the hydrodynamic part is almost twice as strong as the v_3 at $1 \leqslant p_T \leqslant 2$ GeV/c. Jets significantly diminish the triangular flow in both p_T intervals.

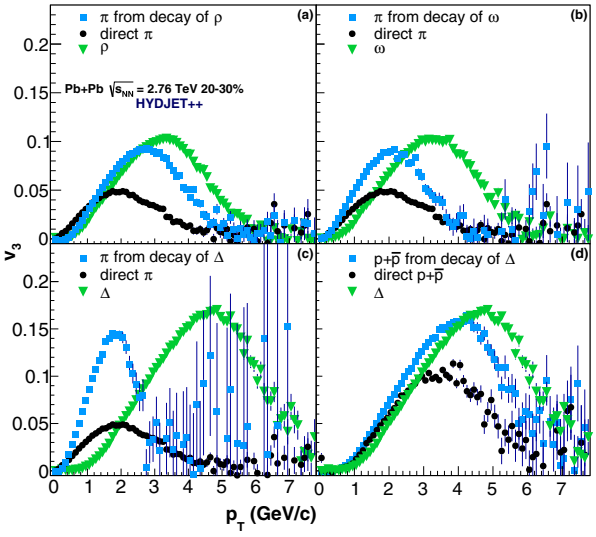

FIG. 6. The p_T dependence of triangular flow of charged pions produced both directly (circles) and in decays (squares) of (a) ρ and (b) ω, respectively, in the HYDJET++ model for Pb + Pb collisions at $\sqrt{s_{NN}} = 2.76$ TeV with centrality 20–30%. (c) and (d) The same as panels (a) and (b) but for (c) charged pions and (d) $p + \bar{p}$ produced in decays of Δ's. The flow of resonances is shown in each window by triangles.

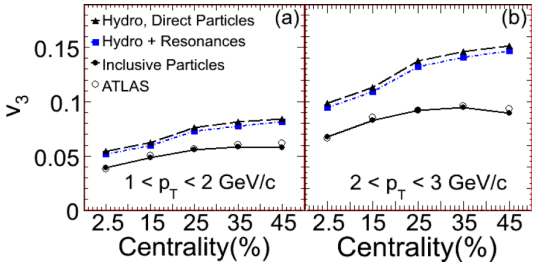

FIG. 7. p_T-integrated triangular flow of inclusive charged hadrons with (a) $1 \leqslant p_T \leqslant 2$ GeV/c and (b) $2 < p_T \leqslant 3$ GeV/c as a function of centrality in Pb + Pb collisions at $\sqrt{s_{NN}} = 2.76$ TeV. Triangles and squares present the calculations for direct particles (i) and direct plus decays of resonances (ii), respectively, only in the hydro part of the model. Final results are shown by solid circles, and open circles are the experimental data from Ref. [32]. Lines are drawn to guide the eye.

Article reprint
J. CRKOVSKÁ *et al.* PHYSICAL REVIEW C **95**, 014910 (2017)

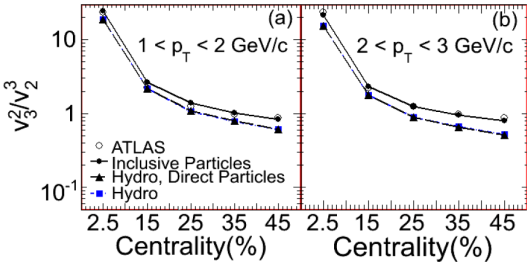

FIG. 8. The same as Fig. 7 but for the ratio v_3^2/v_2^3 of p_T-integrated triangular and elliptic flow.

C. Ratio $v_3^{1/3}/v_2^{1/2}$

The ratios $v_n^{1/n}/v_2^{1/2}$ were suggested in Ref. [32] as a probe to study the possible scaling properties of the flow harmonics. The ratio of triangular and elliptic flow, where both harmonics are integrated over the transverse momentum range, reveals no indication of the scaling trend. The results are presented in Fig. 8. As in the previous figure, two groups of hadrons are selected, one with $1 \leqslant p_T \leqslant 2$ GeV/c and another with $2 < pT \leqslant 3$ GeV/c to compare the HYDJET++ calculations to the experimental data. To see the changing of the ratio with increasing impact parameter more distinctly, the ratio v_3^2/v_2^3 is used. Again, the decays of resonances make no impact on the ratio, which clearly drops as the reaction becomes more peripheral. Note that jets increase the final ratio compared to the pure hydro part. We should come back to this point later.

If the ratio $v_3^{1/3}/v_2^{1/2}$ is plotted as a function of transverse momentum in various centrality bins, as shown in Fig. 9, then the considered distributions are remarkably flat. The ratios $v_3^{1/3}(p_T)/v_2^{1/2}(p_T)$ do not depend on p_T in a quite broad range of transverse momentum from 1 GeV/c up to 6 GeV/c. This p_T independence, however, is not predefined in HYDJET++,

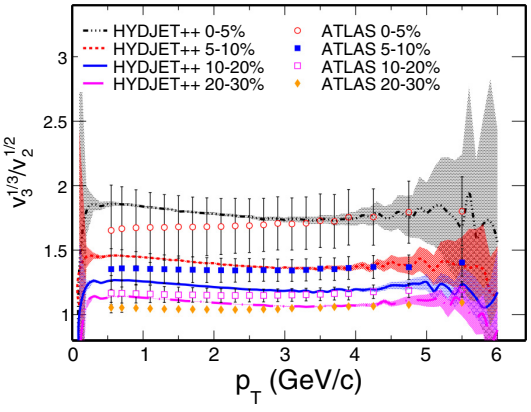

FIG. 9. Ratio $v_3^{1/3}/v_2^{1/2}$ as a function of p_T in centrality bins 0-5% (dotted line), 5–10% (dashed line), 10–20% (solid line), and 20–30% (dash-dotted line). Shaded areas indicate the statistical error bands in the model. The corresponding ATLAS data from Ref. [32] are shown by open circles, filled squares, open squares, and diamonds, respectively.

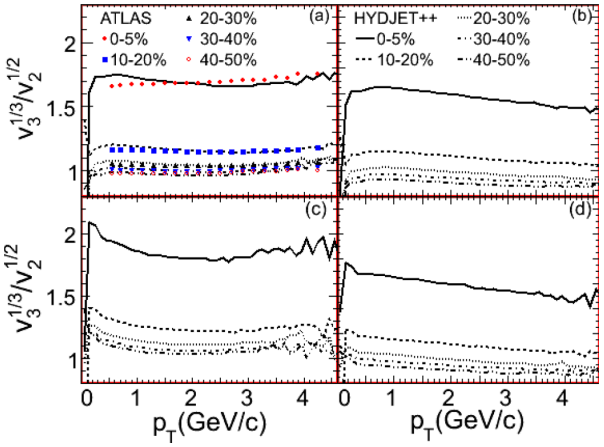

FIG. 10. The same as Fig. 9 but for (a) ratios of total signals in 0–5% (solid curve), 10–20% (dashed curve), 20–30% (dotted curve), 30–40% (dash-dotted curve), and 40–50% (dash-dot-dotted curve) centrality bins; (b) ratios of only hydrodynamic parts (ii) of both flows; (c) ratios of the flow harmonics for only directly produced particles (v); and (d) ratios of the flow harmonics for only directly produced particles in the hydrodynamic part of the model (i).

but arises as a result of nontrivial interplay between soft and hard processes.

To study this effect we selected from the particle spectrum the following types of hadrons: directly produced hadrons (v), hadrons directly produced in the soft processes only (i), and hadrons from direct hydro plus the hadrons from resonance decays (ii). The calculated ratios $v_3^{1/3}(p_T)/v_2^{1/2}(p_T)$ are depicted in Fig. 10. In Fig. 10(d) one can see that this ratio decreases with rising p_T for directly produced hadrons in the hydromodulus of the model for all centrality intervals. Decays of resonances make the slopes of the ratios less steep [see Fig. 10(b)]. Finally, the rise of the tails at $p_T \geqslant 2$ GeV/c is provided by the jet particles, as shown in Fig. 10(c). Here the jets and the final-state interactions are working together towards the formation of a plateau at $1 \leqslant p_T \leqslant 6$ GeV/c. At higher transverse momenta jets may cause the rise of the ratio, similar to that of $v^{1/4}/v_2^{1/2}$, observed both experimentally [35] and in HYDJET++ [27]. The lack of statistics and large error bars, however, does not permit us to make more definite conclusions.

D. NCQ scaling

The NCQ scaling was first observed for the elliptic flow of hadron species in Au + Au collisions at the energy available at the RHIC of $\sqrt{s_{NN}} = 200$ GeV [36,37]. It was found that if one plots the v_2 as a function of the transverse kinetic energy of the hadron, $KE_T \equiv m_T - m_0$, and divides both v_2 and KE_T by the number of constituent quarks in the hadron, n_q, then the excitation functions $v_2^{\rm hadr}(KE_T/n_q)/n_q$ of different hadrons sit on the top of each other up to $KE_T/n_q \approx 0.8$–1.0 GeV [38]. It was pointed out in Refs. [24,25] that, because of the stronger jet influence, the fulfillment of the NCQ scaling at the LHC should be worsened compared to that at the RHIC. The worsening of

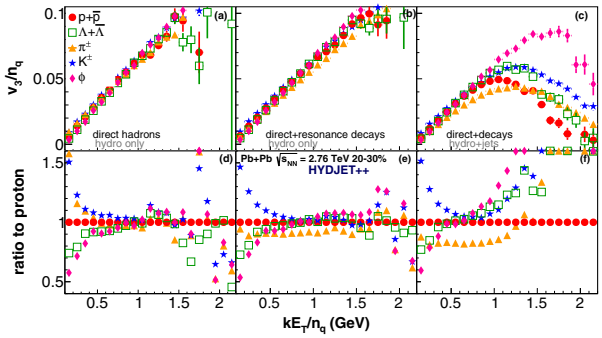

FIG. 11. Upper row: The KE_T/n_q dependence of the triangular flow for (a) direct hadrons (i), (b) hadrons produced in soft processes only (ii), and (c) hadrons produced both in soft and hard processes (vi) in the HYDJET++ model in Pb + Pb collisions at $\sqrt{s_{NN}} = 2.76$ TeV with centrality 20–30%. The considered hadron species are: $p + \bar{p}$ (solid circles), $\Lambda + \overline{\Lambda}$ (open squares), $\pi^{\pm}$ (solid triangles), $K^{\pm}$ (stars), and ϕ (diamonds). Bottom row: The KE_T/n_q dependence of the distributions in the upper row normalized to the triangular flow of $p + \bar{p}$, $(v_3/n_q)/(v_3^{p+\bar{p}}/3)$.

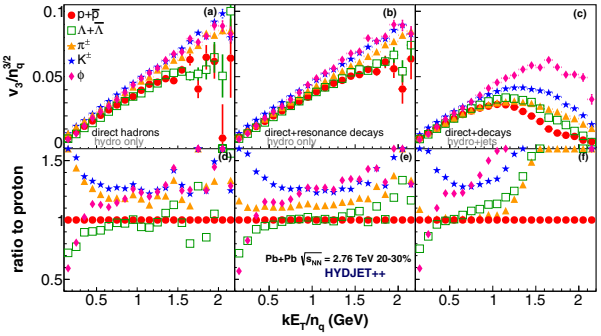

FIG. 12. The same as Fig. 11 but for $v_3(KE_T/n_q)/n_q^{3/2}$ distributions.

the NCQ scaling conditions for the elliptic flow at the LHC was later observed by the ALICE Collaboration [39,40].

It is instructive, therefore, to check the NCQ scaling for the triangular flow of hadronic species at $\sqrt{s_{NN}} = 2.76$ TeV. To elaborate on the role of final-state interactions and the hard processes, we plot in Fig. 11 separately (a) the triangular flow of the main hadron species produced directly on the freeze-out hypersurface (i), (b) then added to their spectra the flow of particles produced after the decays of resonances (ii), and finally (c) the resulting v_3 of hadrons produced in both soft and hard processes (vi). For clarity, all distribution functions $v_3^{\rm hadr}(KE_T/n_q)/n_q$ were also normalized to that of (anti)protons, shown in the bottom row of Fig. 11. One can see in Fig. 11(a) that the NCQ scaling is fulfilled in HYDJET++ within the 10% accuracy limit for the v_3 of main hadron species, frozen already at the freeze-out hypersurface, in the range $0.5 \leqslant KE_T \leqslant 1.2$ GeV. This occurs because, as we already saw in Figs. 4 and 5, resonances increase the triangular flow of lighter hadrons at intermediate p_T and shift the maxima of their differential distributions to higher p_T values. Some hadrons, such as ϕ mesons, do not get the feed-down from resonances, thus their distributions become closer to those of light mesons at intermediate transverse momenta. However, at $p_T \gtrsim 3$ GeV/c the particle spectra are dominated by the jet hadrons, for which the scaling conditions are not relevant. The hadrons fragmenting from jets lead to only approximate fulfillment of the NCQ scaling for the hadron triangular flow in the interval $0.15 \leqslant KE_T \leqslant 1.1$ GeV.

It was suggested in Ref. [41] to use the ratio $v_n^{\rm hadr}/(n_q)^{n/2}$ instead of the standard $v_n^{\rm hadr}/n_q$ to search for the NCQ scaling of the nth flow harmonic. The modified scaling for 0–50% central Au + Au collisions at the highest energy available at the RHIC was observed for v_2, v_3, and v_4 [42]. The HYDJET++ distributions $v_3^{\rm hadr}/n_q^{3/2}$ are shown in Fig. 12. Only approximate scaling within ±15% margins is seen for hadrons with $0.5 \leqslant KE_T \leqslant 1.5$ GeV produced in soft processes. When jets are taken into account, the interval of approximate scaling fulfillment for all but ϕ mesons shrinks to $0.5 \leqslant KE_T \leqslant 1.0$ GeV.

IV. CONCLUSIONS

The triangular flow v_3 of charged inclusive and identified hadrons was studied within the HYDJET++ model in Pb + Pb collisions at $\sqrt{s_{NN}} = 2.76$ TeV and centralities $0\% \leqslant \sigma/\sigma_{\rm geo} \leqslant 50\%$. The model couples soft hydrolike states to hard processes and contains an extended table of resonances, thus allowing for investigation of the interplay between soft processes, jets, and resonance decays on the formation of particle v_3. The results can be summarized as follows.

The triangular flows of identified hadrons produced in soft processes display an almost linear rise at $0.3 \leqslant p_T \leqslant 5$ GeV/c. The mass ordering effect is achieved, i.e., the flow of mesons is stronger than that of baryons. The fraction of hadrons produced in jet fragmentation is the most abundant in particle spectra at $p_T \geqslant 2.5$ GeV/c. Since these hadrons carry almost no v_3, the distribution functions $v_3(p_T)$ experience a falloff at intermediate transverse momenta. The interplay of hard and soft processes leads also to breaking of the mass ordering of the triangular flow, because jet particles start to dominate spectra of heavy hadrons at larger p_T compared to those of light hadrons. It appears that switching off the jet quenching does not influence the final differential triangular flow $v_3(p_T)$. Model calculations agree well with recent experimental data.

Decays of resonances distinctly modify the differential distributions of hadrons $v_3(p_T)$ at $p_T \geqslant 2$ GeV/c. The maxima of the spectra become about 25% higher. Simultaneously, they are shifted by 0.5–1.0 GeV/c towards higher transverse momenta. In contrast, the influence of resonance decays on the p_T-integrated triangular flow is extremely small.

The flatness of the ratios $v_3^{1/3}(p_T)/v_2^{1/2}(p_T)$ at different centralities emerges in HYDJET++ as a result of interplay of final-state interactions and jets. These ratios decrease with rising transverse momenta for particles directly frozen at the freeze-out hypersurface. Decays of resonances reduce the

values of $v_3^{1/3}/v_2^{1/2}$ at low p_T, whereas the jet hadrons boost their high-p_T tails, thus leading to independence of the ratios on transverse momentum in a broad range of $0.5 \leqslant p_T \leqslant 5$ GeV/c.

The two mechanisms, however, work in opposite directions when we consider the fulfillment of the NCQ scaling for the triangular flow. In this case decays of resonances enhance the high-p_T parts of the $v_3^{\rm hadr}(KE_T/n_q)/n_q$ spectra of light hadrons, thus extending the upper KE_T limit of the NCQ scaling performance. Jet particles, in their turn, carry very weak flow and wash out the signal. We verified also the NCQ scaling conditions for $v_3^{\rm hadr}(KE_T/n_q)/n_q^{3/2}$ distributions. The result stays put; i.e., hadrons decoupling from jets are worsening the scaling, while the final-state interactions act toward its fulfillment.

ACKNOWLEDGMENTS

Fruitful discussions with M. Bleicher, L. Csernai, I. Mishustin, and H. Stöcker are gratefully acknowledged. We thank also our colleagues from the CMS, ALICE, and ATLAS Collaborations for the extended cooperation. This work was supported in part by Grant No. INGO II LG15001 of the Ministry of Education, Youth and Sports of the Czech Republic; the Grant Agency of Czech Republic under Grant No. 13-20841S; the Department of Physics, University of Oslo; the Frankfurt Institute for Advanced Studies (FIAS); and a grant from the President of Russian Federation for Scientific Schools (Grant No. 7989.2016.2). L.B. acknowledges the financial support of the Alexander von Humboldt Foundation. B.H.B.J. acknowledges the financial support of the Norwegian Research Council (NFR).

[1] H. Stöcker and W. Greiner, Phys. Rep. **137**, 277 (1986).
[2] W. Reisdorf and H. G. Ritter, Annu. Rev. Nucl. Part. Sci. **47**, 663 (1997).
[3] L. V. Bravina, L. P. Csernai, P. Levai, and D. Strottman, Phys. Rev. C **50**, 2161 (1994).
[4] S. Voloshin and Y. Zhang, Z. Phys. C **70**, 665 (1996).
[5] A. M. Poskanzer and S. A. Voloshin, Phys. Rev. C **58**, 1671 (1998).
[6] L. P. Csernai and H. Stöcker, J. Phys. G **41**, 124001 (2014).
[7] S. A. Voloshin, A. M. Poskanzer, and R. Snellings, in *Relativistic Heavy Ion Physics*, Landolt-Börnstein Database Vol. 23, edited by R. Stock (Springer, Berlin, 2010), pp. 5–54.
[8] U. Heinz and R. Snellings, Annu. Rev. Nucl. Part. Sci. **63**, 123 (2013).
[9] B. Alver and G. Roland, Phys. Rev. C **81**, 054905 (2010).
[10] J. Velkovska *et al.* (CMS Collaboration), J. Phys. G **38**, 124011 (2011).
[11] J. Jia *et al.* (ATLAS Collaboration), J. Phys. G **38**, 124012 (2011).
[12] R. Snellings *et al.* (ALICE Collaboration), J. Phys. G **38**, 124013 (2011).
[13] H. Petersen, G.-Y. Qin, S. A. Bass, and B. Müller, Phys. Rev. C **82**, 041901 (2010).
[14] Z. Qiu and U. Heinz, Phys. Rev. C **84**, 024911 (2011).
[15] B. H. Alver, C. Gombeaud, M. Luzum, and J.-Y. Ollitrault, Phys. Rev. C **82**, 034913 (2010).
[16] M. Schulc and B. Tomášik, Phys. Rev. C **90**, 064910 (2014); J. Phys. G: Nucl. Part. Phys. **43**, 125106 (2016).
[17] Z. Qiu, C. Shen, and U. Heinz, Phys. Rev. C **86**, 064906 (2012).
[18] I. P. Lokhtin, L. V. Malinina, S. V. Petrushanko, A. M. Snigirev, I. Arsene, and K. Tywoniuk, Comput. Phys. Commun. **180**, 779 (2009).
[19] N. S. Amelin, R. Lednicky, T. A. Pocheptsov, I. P. Lokhtin, L. V. Malinina, A. M. Snigirev, Iu. A. Karpenko, and Yu. M. Sinyukov, Phys. Rev. C **74**, 064901 (2006).
[20] N. S. Amelin, R. Lednicky, I. P. Lokhtin, L. V. Malinina, A. M. Snigirev, Iu. A. Karpenko, Yu. M. Sinyukov, I. Arsene, and L. Bravina, Phys. Rev. C **77**, 014903 (2008).
[21] M. Chojnacki, A. Kisiel, W. Florkowski, and W. Broniowski, Comput. Phys. Commun. **183**, 746 (2012).
[22] I. P. Lokhtin and A. M. Snigirev, Eur. Phys. J. C **45**, 211 (2006).
[23] I. P. Lokhtin, A. V. Belyaev, L. V. Malinina, S. V. Petrushanko, E. R. Rogochaya, and A. M. Snigirev, Eur. Phys. J. C **72**, 2045 (2012).
[24] G. Eyyubova, L. V. Bravina, E. E. Zabrodin, V. L. Korotkikh, I. P. Lokhtin, L. V. Malinina, S. V. Petrushanko, and A. M. Snigirev, Phys. Rev. C **80**, 064907 (2009).
[25] E. Zabrodin, G. Eyyubova, L. Bravina, I. P. Lokhtin, L. V. Malinina, S. V. Petrushanko, and A. M. Snigirev, J. Phys. G **37**, 094060 (2010).
[26] E. Zabrodin, G. Eyyubova, L. Malinina, and L. Bravina, Acta Phys. Pol. B Proc. Suppl. **5**, 349 (2012).
[27] L. Bravina, B. H. Brusheim Johansson, G. Eyyubova, and E. Zabrodin, Phys. Rev. C **87**, 034901 (2013).
[28] L. V. Bravina, B. H. Brusheim Johansson, G. Kh. Eyyubova, V. L. Korotkikh, I. P. Lokhtin, L. V. Malinina, S. V. Petrushanko, A. M. Snigirev, and E. E. Zabrodin, Eur. Phys. J. C **74**, 2807 (2014).
[29] L. Bravina, B. H. Brusheim Johansson, E. E. Zabrodin, G. Eyyubova, V. L. Korotkikh, I. P. Lokhtin, L. V. Malinina, S. V. Petrushanko, and A. M. Snigirev, Phys. Rev. C **89**, 024909 (2014).
[30] G. Eyyubova, V. L. Korotkikh, I. P. Lokhtin, S. V. Petrushanko, A. M. Snigirev, L. Bravina, and E. E. Zabrodin, Phys. Rev. C **91**, 064907 (2015).
[31] L. V. Bravina, E. S. Fotina, V. L. Korotkikh, I. P. Lokhtin, L. V. Malinina, E. N. Nazarova, S. V. Petrushanko, A. M. Snigirev, and E. E. Zabrodin, Eur. Phys. J. C **75**, 588 (2015).
[32] G. Aad *et al.* (ATLAS Collaboration), Phys. Rev. C **86**, 014907 (2012).
[33] S. Chatrchyan *et al.* (CMS Collaboration), Phys. Rev. C **87**, 014902 (2013).
[34] J. Adam *et al.* (ALICE Collaboration), J. High Energy Phys. 09 (2016) 164.
[35] B. Abelev *et al.* (ALICE Collaboration), Phys. Lett. B **719**, 18 (2013).
[36] J. Adams *et al.* (STAR Collaboration), Phys. Rev. Lett. **92**, 052302 (2004).

Article reprint

[37] S. S. Adler *et al.* (PHENIX Collaboration), Phys. Rev. Lett. **91**, 182301 (2003).
[38] A. Adare *et al.* (PHENIX Collaboration), Phys. Rev. Lett. **98**, 162301 (2007).
[39] M. Krzewicki *et al.* (ALICE Collaboration), J. Phys. G **38**, 124047 (2011).
[40] F. Noferini *et al.* (ALICE Collaboration), Nucl. Phys. A **904-905**, 483c (2013).
[41] R. Lacey *et al.* (PHENIX Collaboration), J. Phys. G **38**, 124048 (2011).
[42] A. Adare *et al.* (PHENIX Collaboration), Phys. Rev. C **93**, 051902(R) (2016).

Kapitola 2

Produkcia kvarkov ťažkých vôní v protón-protónových zrážkach

Väčšina vyprodukovaných častíc v protónových a jadrových zrážkach pri energiach urýchlenia na RHIC sa skladá z najľahších kvarkov u, d, s. Pri energetických zrážkach partónov je avšak možné v počiatočnej fáze zrážky vytvoriť kvarky ťažké, pôvabný kvark c a krásny kvark b. Vznikajú hlavne v gluón-gluónových zrážkach [R20]. Vďaka relatívne vysokej hmotnosti je možné vypočítať produkciu ťažkých kvarkov pomocov poruchovej QCD a preto je nesmierne zaujímavé konfrontovať tieto výpočty a ďalšie aspekty QCD pomocou experimentálnych meraní. Najpriamejšou možnosťou je premerať produkciu všetkých častíc, ktoré sa z týchto kvarkov skladajú. To sú prednostne D a B mezóny. Tieto mezóny sa rozpadajú slabou interakciou na ľahšie častice, keďže je nutné meniť v rozpade vôňu kvarkov. Rozpadajú sa rádovo stovky mikrometrov od zrážky a preto ich nie je možne pozorovať priamo v dráhovom detektore. S použitím detektora typu HFT, je možné použiť topologické výberové kritéria na potenciálne rozpadové produkty a potlačiť náhodné kombinácie častíc. Keďže hadrónové rozpady vedú na dvojice K a π alebo trojice častíc v prípade, že nie je možné využiť topologickú analýzu, je nutné hľadať správne kombinácie v obrovskom pozadí náhodných kombinácií. Ďalšou možnosťou je využiť semileptónové rozpady a identifikovať elektróny z týchto rozpadov. V tomto prípade je nevýhodou, že sa meria spojité kontinuum elektrónového spektra. Po odpočítaní pozadia z iných zdrojov je možné priamo iba pomocou topologickej analýzy oddeliť jednotlivé príspevky do spektra z rozpadov D a B mezónov. Na druhej strane výhodou merania pomocou elektrónov je možnosť zapojenia elektromagnetického kalorimetra v experimente STAR do nastavenia spúšťacieho systému pri zbere experimentálnych údajov a výberu udalostí s vyšším množstvom elektrónových kandidátov s vysokou hodnotou p_T. Experiment STAR publikoval prvé meranie ťažkých kvarkov v Ref. [R21] v p+p a d+Au zrážkach. Jednalo sa o kombinované meranie D mezónov a elektrónov pochádzajúcich zo semileptónových rozpadov ťažkých kvarkov, tzv. nefotónových elektrónov. V tomto článku sa použili dáta z roku 2003. Spektrá mali z dôvodu malého súboru vhodných dát, keďže bola v prevádzke

len časť TOF detektora, malý rozsah priečnych hybností $p_T < 4$ GeV/c. V roku 2004 STAR uviedol do prevádzky elektromagnetický kalorimeter EMC, to umožnilo využitie tohto detektora v spúšťacom systéme a tiež pre lepšiu identifikáciu elektrónov. Schematické zobrazenie experimentu STAR je na obrázku Obr. 2.1. Využitie EMC umožnilo výrazne rozšíriť rozsah merania, až do priečnych hybností, kde sa očakáva dominancia výťažku elektrónov z B rozpadov nad elektrónmi z D rozpadov. Tieto výsledky z protón-protónových zrážok boli publikované v článku [41], ktorý je súčasťou tejto práce v Kapitole 3. V článku sa spolu s p+p zrážkami publikovali aj spektrá zo zrážok d+Au a Au+Au pri energii zrážky $\sqrt{s_{NN}} = 200$ GeV. Výsledky boli po zverejnení revidované, keďže sa identifikovala zámena pri aplikácii účinnosti odpočítania pozadia z fotónových elektrónov, pochádzajúcich z konverzie gama kvánt z rozpadov π^0. Hlavným výsledkom z meraní z protón-protónových zrážok bolo porovnanie nameraného spektra priečnych hybností ($1,2 < p_T < 10$ GeV/c) s výpočtami FONLL (Fixed Order Next-to-Leading Log) pQCD [R22]. V rámci štatistických chýb meraní sú výpočty konzistentné s meranými spektrami. Podľa týchto výpočtov približne od $p_T \approx 5$ GeV/c začínajú v spektre dominovať príspevky z B rozpadov. Ďalšia analýza nefotónových elektrónov z experimentu STAR bola prevedená na súbore dát pochádzajúcich z rokov 2005 a 2008 [126]. Článok obsahujúci tieto merania je súčasťou tejto kapitoly H. Agakishiev *et al.*, *High p_T nonphotonic electron production in p+p collisions at $\sqrt{s_{NN}} = 200$ GeV*, Phys. Rev. D **83**, 052006 (2011). Pred meraním v roku 2008 sa z experimentu STAR vyňali kremíkové detektory, čo viedlo k významnému zníženiu pozadia z fotónových elektrónov, kvôli menšiemu množstvu konverzného materiálu. Napriek výrazne rozdielnemu pozadiu sú spektrá z oboch súborov dát vzájomne konzistentné (viz FIG.15). Výsledné spektrá sú v meranom intervale p_T = 2,5 - 10 GeV/c v zhode s horeuvedenými meraniami experimentu STAR a tiež s výsledkami experimentu PHENIX [R24].

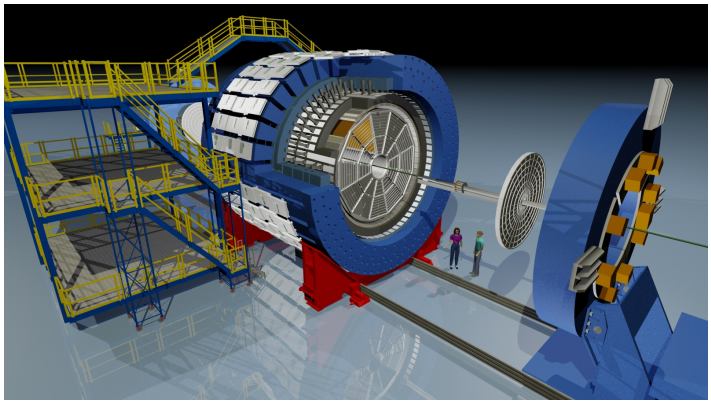

Obr. 2.1: Umelecké schematické zobrazenie experimentu STAR. Centrálnym detektorom je dráhový detektor časovo-projekčná komora TPC. Je obklopená detektorom doby letu TOF a elekromagnetickým kalorimetrom EMC. Tieto detektory sú umiestnené v magnetickom poli magnetu (na obrázku modrý).

Rozdiel v hmotnosti medzi D a B mezónom vedie k rozdielnemu vzájomnému uhlovému rozdeleniu dcérskych častíc v ich rozpadoch. U B mezónu je toto rozdelenie širšie. Na základe štúdia tohto rozdielu uhlových korelácií medzi nefotónovými elektrónmi a hadrónmi a prekladaní týchto korelácií očakávanými tvarmi pre D a B rozpad z generátora PYTHIA [R25] sa podarilo experimentu STAR oddeliť príspevok elektrónov z rozpadov častíc pochádzajúcich z b a c kvarkov [112]. V tomto článku se nám podarilo ukázať, že príspevok rozpadov častíc z b kvarkov v spektre priečnych hybností nefotónových elektrónov je menší ako príspevok rozpadov častíc z c kvarkov pri hybnostiach do $p_T \approx 5$ GeV/c, potom sa oba príspevky vyrovnajú. Toto meranie je v súlade s výpočtami z FONLL pQCD [R22]. Tieto výpočty síce predpovedajú tiež rast b príspevku, avšak štatistická presnosť merania nebola dostatočná, aby sa rast pri hybnostiach nad $p_T \approx 5$ GeV/c mohol preukázať. Pomocou zmeraného pomeru elektrónov z rozpadu mezónu B k elektrónom z D a B rozpadov, $\frac{e_B}{e_B+e_D}$ z článku Ref. [112] sme rozdelili výťažok nefotónových elektrónov v protón-protónových zrážkach na b a c časti. V porovnaní s výpočtami FONLL pQCD [R22] sú merania a výpočty konzistentné v rámci uvedenej presnosti.

V ďalšom priloženom článku v tejto kapitole, L. Adamczyk *et al.*, *Measurements of D^0 and D^* production in p+p collisions at $\sqrt{s}$ = 200 GeV*, Phys. Rev. D **86**, 072013 (2012), sa diskutuje prvé meranie produkcie pôvabných kvarkov v p+p zrážkach na urýchľovači RHIC pomocou priamej rekonštrukcie hadrónových rozpadov D mezónov. Na túto analýzu sa použili experimentálne údaje z experimentu STAR namerané v roku 2009. Pred týmto meraním došlo k výraznému nárastu počtu inštalovaných modulov detektora doby letu TOF. K dispozícii bolo 84 z celkových 120 sektorov. Aplikácia výberových kritérií zahrňujúcich informácie z tohto detektora významne vylepšila rozlíšenie kaónov od piónov do hybností okolo $p \approx 1{,}5$ GeV/c. Študovali sme rozpadové kanály dvoch mezónov: D^0 a $D^{*\pm}$. V prvom prípade šlo o rozpad $D^0(\overline{D^0}) \to K^{\mp}\pi^{\pm}$ s rozpadovým pomerom BR = 3,89 %. V druhom prípade šlo o rozpad $D^{*+} \to D^0\pi^+$ s rozpadovým pomerom BR = 67,7 %, kde sa D^0 ďalej rozpadlo na $D^0 \to K^-\pi^+$. Taktiež sme študovali nábojovo združený rozpad D^{*-}. Vďaka výbornému azimutálnemu pokrytiu a rozlíšeniu typu častíc v detektore STAR bolo možné určiť výťažok týchto mezónov i bez topologickej rekonštrukcie. V analýze D^0 sme skombinovali všetky nábojovo vhodné dvojice predvybraných kaónov a piónov a vykreslili sme invariantnú hmotnosť týchto dvojíc. Potom sme pomocou dvoch metód určili príspevok náhodných kombinácií, tzv. kombinatorického pozadia. V prvej metóde označenej *like-sign* (rovnaké znamienko) sme urobili dvojice v kombinácii s nesprávnym nábojom. V druhej metóde označenej *track-rotation* (otočenie dráhy) sme vytvárali kombinácie tak, že sme vždy príslušnú dráhu kaónu pootočili o 180° a až potom určili invariantnú hmotnosť. Obe metódy viedli k podobnému výťažku finálneho signálu (viz. FIG.3 a FIG.4) a rozdiel sa zahrnul do systematických chýb. Po odčítaní kombinatorického pozadia sa nám podarilo rozdeliť D^0 výťažok v intervale p_T = 0,6 - 2 GeV/c na dva

biny (viz. FIG.5). Pri analýze $D^{*\pm}$ sme využili skutočnosť, že rozpad $D^{*\pm}$ má malú hodnotu Q-faktoru, z dôvodu malého rozdielu hmotnosti $D^{*\pm}$ a D^0 . Keďže D^0 odnesie väčšinu hybnosti má zvyšný pión hybnosť veľmi malú. Preto sme stanovili výťažok pomocou hmotnostného rozdielu $\Delta M = M(K\pi\pi) - M(K\pi)$. Požadovali sme správnu nábojovú kombináciu a dvojice v druhom člene sme vyberali tak, aby mali správnu invariantnú hmotnosť pre D^0 . Kombinatorické pozadie sme opäť určili pomocou dvoch metód. V jednej sme vyberali chybnú nábojovú kombináciu v prvom člene a v druhej sme vyberali hmotnosť pre druhý člen mimo vhodný interval (viz. FIG.7). Podarilo sa nám určiť výťažok $D^{*\pm}$ v intervale p_T = 2 - 6 GeV/c a rozdeliť ho na 4 biny (viz. FIG.8). Po všetkých príslušných korekciách signálu na účinnosť a pokrytie detektorov a výberu signálu, sme spektrá $D^{*\pm}$ a D^0 vykreslili spolu ako diferenciálny účinný prierez $c\bar{c}$ produkcie, s tým, že sa výťažok vydelil príslušným fragmentačným pomerom. Výsledné spektrum sme preložili mocninnou funkciou a určili účinný prierez $c\bar{c}$ produkcie v strednej rapidite: $\frac{d\sigma}{dy}|^{c\bar{c}}_{y=0} = 170 \pm 45$ (stat.) $^{+38}_{-59}$ (sys.) μb (viz. FIG.15). Výpočty FONLL pQCD [R22] použité na porovnanie s nefotónovými elektrónmi sú tiež v rámci neurčitostí výpočtov v súlade s nameranými hodnotami, aj keď experimentálne body ležia na hornej hranici neurčitostí výpočtov. Na základe simulácii s PYTHIA 6 [R25] sme stanovili koeficient 4,7 ± 0,7 na extrapoláciu účinného prierezu do plnej rapidity. Totálny účinný prierez pôvabnej produkcie v p + p pri $\sqrt{s}$= 200 GeV sme stanovili na $\sigma_{c\bar{c}} = 797 \pm 210$ (stat.)$^{+208}_{-295}$ (sys.) μb.

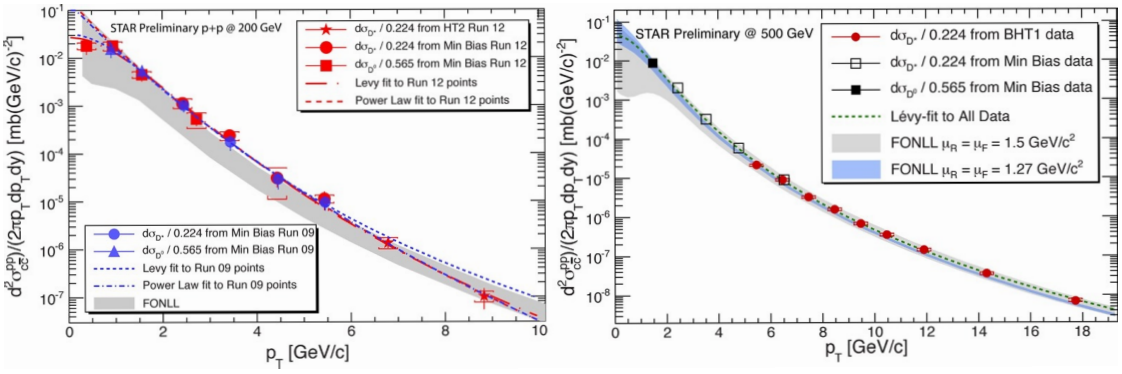

Obr. 2.2: Závislosť diferenciálneho účinného prierezu $c\bar{c}$ na priečnej hybnosti získaného z meraní $D^{*\pm}$ a D^0 v p + p zrážkach pri energii $\sqrt{s}$= 200 GeV (vľavo) a $\sqrt{s}$= 500 GeV. Farebné plochy ukazujú výpočty FONLL pQCD [R22]. Prevzaté z Ref. [R23].

Kolaborácia STAR merala p + p zrážky aj pri energii $\sqrt{s}$ = 500 GeV. Podarilo sa nám previesť analýzu $D^{*\pm}$ a D^0 nielen v zrážkach s najmenším zaujatím, ale aj použiť experimentálne údaje, ktoré boli merané pomocou spúšťača nastaveného tak, aby signál aspoň v jednej veži kalorimetra bol nad nastavenú hodnotu, ďalej označované ako HT (high-tower) dáta. Na základe výsledkov sme pripravili publikáciu, ktorá je v súčasnosti v internom schvalovacom procese v kolaborácii STAR. Hlavný výsledok je na obrázku Obr. 2.2 (vpravo). Aj pre túto energiu je popis produkcie v rámci FONLL

pQCD v zhode s experimentálnymi výsledkami. Detaily analýzy sú podrobne diskutované v doktorskej práci Davida Tlustého [T1], ktorú som viedol. Podobne i z p + p dát meraných v roku 2012 kolaborácia STAR previedla obdobnú analýzu pri energii $\sqrt{s} = 200$ GeV a výsledky sú v zhode s nami publikovanými výsledkami, ako je možné vidieť na obrázku Obr. 2.2 (vľavo).

Article reprint

PHYSICAL REVIEW D **83,** 052006 (2011)

High p_T nonphotonic electron production in $p + p$ collisions at $\sqrt{s} = 200$ GeV

H. Agakishiev,[17] M. M. Aggarwal,[29] Z. Ahammed,[21] A. V. Alakhverdyants,[17] I. Alekseev,[15] J. Alford,[18] B. D. Anderson,[18] C. D. Anson,[27] D. Arkhipkin,[2] G. S. Averichev,[17] J. Balewski,[22] D. R. Beavis,[2] N. K. Behera,[13] R. Bellwied,[43] M. J. Betancourt,[22] R. R. Betts,[7] A. Bhasin,[16] A. K. Bhati,[29] H. Bichsel,[49] J. Bielcik,[9] J. Bielcikova,[10] B. Biritz,[5] L. C. Bland,[2] I. G. Bordyuzhin,[15] W. Borowski,[40] J. Bouchet,[18] E. Braidot,[26] A. V. Brandin,[25] A. Bridgeman,[1] S. G. Brovko,[4] E. Bruna,[52] S. Bueltmann,[28] I. Bunzarov,[17] T. P. Burton,[2] X. Z. Cai,[39] H. Caines,[52] M. Calderón de la Barca Sánchez,[4] D. Cebra,[4] R. Cendejas,[5] M. C. Cervantes,[41] Z. Chajecki,[27] P. Chaloupka,[10] S. Chattopadhyay,[47] H. F. Chen,[37] J. H. Chen,[39] J. Y. Chen,[51] L. Chen,[51] J. Cheng,[44] M. Cherney,[8] A. Chikanian,[52] K. E. Choi,[33] W. Christie,[2] P. Chung,[10] M. J. M. Codrington,[41] R. Corliss,[22] J. G. Cramer,[49] H. J. Crawford,[3] S. Dash,[12] A. Davila Leyva,[42] L. C. De Silva,[43] R. R. Debbe,[2] T. G. Dedovich,[17] A. A. Derevschikov,[31] R. Derradi de Souza,[6] L. Didenko,[2] P. Djawotho,[41] S. M. Dogra,[16] X. Dong,[21] J. L. Drachenberg,[41] J. E. Draper,[4] J. C. Dunlop,[2] L. G. Efimov,[17] M. Elnimr,[50] J. Engelage,[3] G. Eppley,[35] M. Estienne,[40] L. Eun,[30] O. Evdokimov,[7] R. Fatemi,[19] J. Fedorisin,[17] R. G. Fersch,[19] P. Filip,[17] E. Finch,[52] V. Fine,[2] Y. Fisyak,[2] C. A. Gagliardi,[41] D. R. Gangadharan,[5] A. Geromitsos,[40] F. Geurts,[35] P. Ghosh,[47] Y. N. Gorbunov,[8] A. Gordon,[2] O. G. Grebenyuk,[21] D. Grosnick,[46] S. M. Guertin,[5] A. Gupta,[16] W. Guryn,[2] B. Haag,[4] O. Hajkova,[9] A. Hamed,[41] L-X. Han,[39] J. W. Harris,[52] J. P. Hays-Wehle,[22] M. Heinz,[52] S. Heppelmann,[30] A. Hirsch,[32] E. Hjort,[21] G. W. Hoffmann,[42] D. J. Hofman,[7] B. Huang,[37] H. Z. Huang,[5] T. J. Humanic,[27] L. Huo,[41] G. Igo,[5] P. Jacobs,[21] W. W. Jacobs,[14] C. Jena,[12] F. Jin,[39] J. Joseph,[18] E. G. Judd,[3] S. Kabana,[40] K. Kang,[44] J. Kapitan,[10] K. Kauder,[7] H. W. Ke,[51] D. Keane,[18] A. Kechechyan,[17] D. Kettler,[49] D. P. Kikola,[21] J. Kiryluk,[21] A. Kisiel,[48] V. Kizka,[17] S. R. Klein,[21] A. G. Knospe,[52] D. D. Koetke,[46] T. Kollegger,[11] J. Konzer,[32] I. Koralt,[28] L. Koroleva,[15] W. Korsch,[19] L. Kotchenda,[25] V. Kouchpil,[10] P. Kravtsov,[25] K. Krueger,[1] M. Krus,[9] L. Kumar,[18] P. Kurnadi,[5] M. A. C. Lamont,[2] J. M. Landgraf,[2] S. LaPointe,[50] J. Lauret,[2] A. Lebedev,[2] R. Lednicky,[17] J. H. Lee,[2] W. Leight,[22] M. J. LeVine,[2] C. Li,[37] L. Li,[42] N. Li,[51] W. Li,[39] X. Li,[32] X. Li,[38] Y. Li,[44] Z. M. Li,[51] M. A. Lisa,[27] F. Liu,[51] H. Liu,[4] J. Liu,[35] T. Ljubicic,[2] W. J. Llope,[35] R. S. Longacre,[2] W. A. Love,[2] Y. Lu,[37] E. V. Lukashov,[25] X. Luo,[37] G. L. Ma,[39] Y. G. Ma,[39] D. P. Mahapatra,[12] R. Majka,[52] O. I. Mall,[4] L. K. Mangotra,[16] R. Manweiler,[46] S. Margetis,[18] C. Markert,[42] H. Masui,[21] H. S. Matis,[21] Yu. A. Matulenko,[31] D. McDonald,[35] T. S. McShane,[8] A. Meschanin,[31] R. Milner,[22] N. G. Minaev,[31] S. Mioduszewski,[41] A. Mischke,[26] M. K. Mitrovski,[11] Y. Mohammed,[41] B. Mohanty,[47] M. M. Mondal,[47] B. Morozov,[15] D. A. Morozov,[31] M. G. Munhoz,[36] M. K. Mustafa,[32] M. Naglis,[21] B. K. Nandi,[13] T. K. Nayak,[47] P. K. Netrakanti,[32] L. V. Nogach,[31] S. B. Nurushev,[31] G. Odyniec,[21] A. Ogawa,[2] K. Oh,[33] A. Ohlson,[52] V. Okorokov,[25] E. W. Oldag,[42] D. Olson,[21] M. Pachr,[9] B. S. Page,[14] S. K. Pal,[47] Y. Pandit,[18] Y. Panebratsev,[17] T. Pawlak,[48] H. Pei,[7] T. Peitzmann,[26] C. Perkins,[3] W. Peryt,[48] S. C. Phatak,[12] P. Pile,[2] M. Planinic,[53] M. A. Ploskon,[21] J. Pluta,[48] D. Plyku,[28] N. Poljak,[53] A. M. Poskanzer,[21] B. V. K. S. Potukuchi,[16] C. B. Powell,[21] D. Prindle,[49] C. Pruneau,[50] N. K. Pruthi,[29] P. R. Pujahari,[13] J. Putschke,[52] H. Qiu,[20] R. Raniwala,[34] S. Raniwala,[34] R. L. Ray,[42] R. Redwine,[22] R. Reed,[4] H. G. Ritter,[21] J. B. Roberts,[35] O. V. Rogachevskiy,[17] J. L. Romero,[4] A. Rose,[21] L. Ruan,[2] J. Rusnak,[10] N. R. Sahoo,[47] S. Sakai,[21] I. Sakrejda,[21] S. Salur,[4] J. Sandweiss,[52] E. Sangaline,[4] A. Sarkar,[13] J. Schambach,[42] R. P. Scharenberg,[32] A. M. Schmah,[21] N. Schmitz,[23] T. R. Schuster,[11] J. Seele,[22] J. Seger,[8] I. Selyuzhenkov,[14] P. Seyboth,[23] E. Shahaliev,[17] M. Shao,[37] M. Sharma,[50] S. S. Shi,[51] Q. Y. Shou,[39] E. P. Sichtermann,[21] F. Simon,[23] R. N. Singaraju,[47] M. J. Skoby,[32] N. Smirnov,[52] P. Sorensen,[2] H. M. Spinka,[1] B. Srivastava,[32] T. D. S. Stanislaus,[46] D. Staszak,[5] S. G. Steadman,[22] J. R. Stevens,[14] R. Stock,[11] M. Strikhanov,[25] B. Stringfellow,[32] A. A. P. Suaide,[36] M. C. Suarez,[7] N. L. Subba,[18] M. Sumbera,[10] X. M. Sun,[21] Y. Sun,[37] Z. Sun,[20] B. Surrow,[22] D. N. Svirida,[15] T. J. M. Symons,[21] A. Szanto de Toledo,[36] J. Takahashi,[6] A. H. Tang,[2] Z. Tang,[37] L. H. Tarini,[50] T. Tarnowsky,[24] D. Thein,[42] J. H. Thomas,[21] J. Tian,[39] A. R. Timmins,[43] D. Tlusty,[10] M. Tokarev,[17] T. A. Trainor,[49] V. N. Tram,[21] S. Trentalange,[5] R. E. Tribble,[41] P. Tribedy,[47] O. D. Tsai,[5] T. Ullrich,[2] D. G. Underwood,[1] G. Van Buren,[2] G. van Nieuwenhuizen,[22] J. A. Vanfossen, Jr.,[18] R. Varma,[13] G. M. S. Vasconcelos,[6] A. N. Vasiliev,[31] F. Videbæk,[2] Y. P. Viyogi,[47] S. Vokal,[17] S. A. Voloshin,[50] M. Wada,[42] M. Walker,[22] F. Wang,[32] G. Wang,[5] H. Wang,[24] J. S. Wang,[20] Q. Wang,[32] X. L. Wang,[37] Y. Wang,[44] G. Webb,[19] J. C. Webb,[2] G. D. Westfall,[24] C. Whitten, Jr.,[5] H. Wieman,[21] S. W. Wissink,[14] R. Witt,[45] W. Witzke,[19] Y. F. Wu,[51] Z. Xiao,[44] W. Xie,[32] H. Xu,[20] N. Xu,[21] Q. H. Xu,[38] W. Xu,[5] Y. Xu,[37] Z. Xu,[2] L. Xue,[39] Y. Yang,[20] Y. Yang,[51] P. Yepes,[35] K. Yip,[2] I-K. Yoo,[33] M. Zawisza,[48] H. Zbroszczyk,[48] W. Zhan,[20] J. B. Zhang,[51] S. Zhang,[39] W. M. Zhang,[18] X. P. Zhang,[44] Y. Zhang,[21] Z. P. Zhang,[37] J. Zhao,[39] C. Zhong,[39] W. Zhou,[38] X. Zhu,[44] Y. H. Zhu,[39] R. Zoulkarneev,[17] and Y. Zoulkarneeva[17]

(STAR Collaboration)

Article reprint

[1]*Argonne National Laboratory, Argonne, Illinois 60439, USA*
[2]*Brookhaven National Laboratory, Upton, New York 11973, USA*
[3]*University of California, Berkeley, California 94720, USA*
[4]*University of California, Davis, California 95616, USA*
[5]*University of California, Los Angeles, California 90095, USA*
[6]*Universidade Estadual de Campinas, Sao Paulo, Brazil*
[7]*University of Illinois at Chicago, Chicago, Illinois 60607, USA*
[8]*Creighton University, Omaha, Nebraska 68178, USA*
[9]*Czech Technical University in Prague, FNSPE, Prague, 115 19, Czech Republic*
[10]*Nuclear Physics Institute AS CR, 250 68 Řež/Prague, Czech Republic*
[11]*University of Frankfurt, Frankfurt, Germany*
[12]*Institute of Physics, Bhubaneswar 751005, India*
[13]*Indian Institute of Technology, Mumbai, India*
[14]*Indiana University, Bloomington, Indiana 47408, USA*
[15]*Alikhanov Institute for Theoretical and Experimental Physics, Moscow, Russia*
[16]*University of Jammu, Jammu 180001, India*
[17]*Joint Institute for Nuclear Research, Dubna, 141 980, Russia*
[18]*Kent State University, Kent, Ohio 44242, USA*
[19]*University of Kentucky, Lexington, Kentucky 40506-0055, USA*
[20]*Institute of Modern Physics, Lanzhou, China*
[21]*Lawrence Berkeley National Laboratory, Berkeley, California 94720, USA*
[22]*Massachusetts Institute of Technology, Cambridge, Massachusetts 02139-4307, USA*
[23]*Max-Planck-Institut für Physik, Munich, Germany*
[24]*Michigan State University, East Lansing, Michigan 48824, USA*
[25]*Moscow Engineering Physics Institute, Moscow, Russia*
[26]*NIKHEF and Utrecht University, Amsterdam, The Netherlands*
[27]*Ohio State University, Columbus, Ohio 43210, USA*
[28]*Old Dominion University, Norfolk, Virginia 23529, USA*
[29]*Panjab University, Chandigarh 160014, India*
[30]*Pennsylvania State University, University Park, Pennsylvania 16802, USA*
[31]*Institute of High Energy Physics, Protvino, Russia*
[32]*Purdue University, West Lafayette, Indiana 47907, USA*
[33]*Pusan National University, Pusan, Republic of Korea*
[34]*University of Rajasthan, Jaipur 302004, India*
[35]*Rice University, Houston, Texas 77251, USA*
[36]*Universidade de Sao Paulo, Sao Paulo, Brazil*
[37]*University of Science & Technology of China, Hefei 230026, China*
[38]*Shandong University, Jinan, Shandong 250100, China*
[39]*Shanghai Institute of Applied Physics, Shanghai 201800, China*
[40]*SUBATECH, Nantes, France*
[41]*Texas A&M University, College Station, Texas 77843, USA*
[42]*University of Texas, Austin, Texas 78712, USA*
[43]*University of Houston, Houston, Texas 77204, USA*
[44]*Tsinghua University, Beijing 100084, China*
[45]*United States Naval Academy, Annapolis, Maryland 21402, USA*
[46]*Valparaiso University, Valparaiso, Indiana 46383, USA*
[47]*Variable Energy Cyclotron Centre, Kolkata 700064, India*
[48]*Warsaw University of Technology, Warsaw, Poland*
[49]*University of Washington, Seattle, Washington 98195, USA*
[50]*Wayne State University, Detroit, Michigan 48201, USA*
[51]*Institute of Particle Physics, CCNU (HZNU), Wuhan 430079, China*
[52]*Yale University, New Haven, Connecticut 06520, USA*
[53]*University of Zagreb, Zagreb, HR-10002, Croatia*

(Received 13 February 2011; published 22 March 2011)

We present the measurement of nonphotonic electron production at high transverse momentum ($p_T > 2.5$ GeV/c) in $p + p$ collisions at $\sqrt{s} = 200$ GeV using data recorded during 2005 and 2008 by the STAR experiment at the Relativistic Heavy Ion Collider (RHIC). The measured cross sections from the two runs are consistent with each other despite a large difference in photonic background levels due to different detector configurations. We compare the measured nonphotonic electron cross sections with previously published RHIC data and perturbative quantum chromodynamics

Article reprint

calculations. Using the relative contributions of B and D mesons to nonphotonic electrons, we determine the integrated cross sections of electrons ($\frac{e^+ + e^-}{2}$) at 3 GeV/c < p_T < 10 GeV/c from bottom and charm meson decays to be $[(d\sigma_{(B\to e)+(B\to D\to e)})/(dy_e)]_{y_e=0}$ = 4.0 ± 0.5(stat) ± 1.1(syst) nb and $[(d\sigma_{D\to e})/(dy_e)]_{y_e=0}$ = 6.2 ± 0.7(stat) ± 1.5(syst) nb, respectively.

DOI: 10.1103/PhysRevD.83.052006 PACS numbers: 13.20.Fc, 13.20.He, 25.75.Cj

I. INTRODUCTION

Heavy quark production in high-energy hadronic collisions has been a focus of interest for years. It is one of the few instances in which experimental measurements can be compared with QCD predictions over nearly the entire kinematical range [1–3]. Because of the large masses of charm and bottom quarks, they are produced almost exclusively during the initial high-Q parton-parton interactions and thus can be described by perturbative QCD calculations.

Measurement of heavy-flavor production in elementary collisions represents a crucial test of the validity of the current theoretical framework and its phenomenological inputs. It is also mandatory as a baseline for the interpretation of heavy-flavor production in nucleus-nucleus collisions [4]. In these heavy-ion collisions, one investigates the properties of the quark-gluon plasma (QGP), which is created at sufficiently high center-of-mass energies. Many effects on heavy-flavor production in heavy-ion collisions have been observed but are quantitatively not yet fully understood [4]. Of particular interest are effects which modify the transverse momentum spectra of heavy-flavor hadrons, including energy loss in the QGP (''jet quenching'') [5–9], as well as collective effects such as elliptic flow [10,11]. In addition, J/ψ might be regenerated in a dense plasma from the initial open charm yield [12], making precise measurements of the transverse momentum spectra in elementary $p + p$ collisions imperative.

Open heavy-flavor production in $p + p$, d + A, and A + A collisions at $\sqrt{s_{NN}}$ = 200 GeV has been studied at the Relativistic Heavy Ion Collider (RHIC) using a variety of final-state observables [4]. The STAR collaboration measured charm mesons directly through their hadronic decay channels [13–15]. Because of the lack of precise secondary vertex tracking and trigger capabilities, these measurements are restricted to low momenta (p_T < 3 GeV/c). Both STAR [15,16] and PHENIX [17,18] also measured heavy-flavor production through semileptonic decays of charm and bottom mesons ($D, B \to \ell \nu_\ell X$). While the measured decay leptons provide only limited information on the original kinematics of the heavy-flavor parton, these measurements are facilitated by fast online triggers and extend the kinematic range to high p_T.

In this paper, we report STAR results on nonphotonic electron production at midrapidity in $p + p$ collisions at $\sqrt{s}$ = 200 GeV using data recorded during the year 2005 (Run2005) and the year 2008 (Run2008) with a total integrated luminosity of 2.8 and 2.6 pb^{-1}, respectively. The present results are consistent with the next-to-leading logarithm (FONLL) calculation within its theoretical uncertainties. Utilizing the measured relative contributions of B and D mesons to nonphotonic electrons which were obtained from a study of electron-hadron correlations (e-h) [19], we determine the invariant cross section of electrons from bottom and charm meson decays separately at p_T > 3.0 GeV/c.

The article is organized as follows. In Sec. II we describe the STAR detectors and triggers relevant to this analysis. Section III describes the data analysis in detail, and in Sec. IV we present and discuss the results. Section V provides conclusions.

II. EXPERIMENT

A. Detectors

STAR is a large acceptance, multipurpose experiment composed of several individual detector subsystems with tracking inside a large solenoidal magnet generating a uniform field of 0.5 T [20]. The detector subsystems relevant for the present analysis are briefly described in the following.

1. Time projection chamber

The time projection chamber (TPC) [21] is the main charged particle tracking device in STAR. The TPC covers ±1.0 units in pseudorapidity (η) for tracks crossing all layers of pads, and the full azimuth. Particle momentum is determined from track curvature in the solenoidal field. In this analysis, TPC tracks are used for momentum determination, electron-hadron separation (using specific ionization dE/dx), to reconstruct the interaction vertex, and to project to the calorimeter for further hadron rejection.

2. Barrel electromagnetic calorimeter and barrel shower maximum detector

The barrel electromagnetic calorimeter (BEMC) measures the energy deposited by photons and electrons and provides a trigger signal. It is located inside the magnet coil outside the TPC, covering $|\eta| < 1.0$ and 2π in azimuth, matching the TPC acceptance. The BEMC is a lead-scintillator sampling electromagnetic calorimeter with a nominal energy resolution of $\delta E/E \sim 14\%/\sqrt{E/1\ \text{GeV}} \oplus 1.5\%$ [22]. The full calorimeter is segmented into 4800 projective towers. A tower covers 0.05 rad in ϕ and 0.05 units in η. Each tower consists of a stack of 20 layers of lead and 21 layers of scintillator with an active depth of

23.5 cm. The first two scintillator layers are read out separately providing the calorimeter preshower signal, which is not used in this analysis. A shower maximum detector (BSMD) is positioned behind the fifth scintillator layer. The BSMD is a double layer wire proportional counter with strip readout. The two layers of the BSMD, each containing 18 000 strips, provide precise spacial resolution in ϕ and η and improve the electron-hadron separation. The BEMC also provides a high-energy trigger based on the highest energy measured by a single tower in order to enrich the event samples with high-p_T electromagnetic energy deposition.

3. Trigger detectors

The beam-beam counters (BBC) [23] are two identical counters located on each side of the interaction region covering the full azimuth and $2.1 < |\eta| < 5.0$. Each detector consists of sets of small and large hexagonal scintillator tiles grouped into a ring and mounted around the beam pipe at a distance of 3.7 m from the interaction point. In both Run2008 and Run2005, the BBC served as a minimum-bias trigger to record the integrated luminosity by requiring a coincidence of signals in at least one of the small tiles ($3.3 < |\eta| < 5.0$) on each side of the interaction region. The cross section sampled with the BBC trigger is $26.1 \pm 0.2(\text{stat}) \pm 1.8(\text{syst})$ mb [24] for $p + p$ collisions. The timing signal recorded by the two BBC counters can be used to reconstruct the collision vertex along the beam direction with an accuracy of ~40 cm.

The data in d + Au collisions recorded during year 2008 is used as a crosscheck in this analysis (see Sec. III E). During this run, a pair of vertex position detectors (VPD) [25] was also used to select events. Each VPD consists of 19 lead converters plus plastic scintillators with photomultiplier-tube readout that are positioned very close to the beam pipe on each side of STAR. Each VPD is approximately 5.7 m from the interaction point and covers the pseudorapidity interval $4.24 < |\eta| < 5.1$. The VPD trigger condition is similar to that of the BBC trigger except that the VPD has much better timing resolution, enabling the selected events to be constrained to a smaller range ($\sim \pm 30$ cm in d + Au run) around the interaction point.

B. Material thickness in front of the TPC

Table I shows a rough estimate of material thickness between the interaction point and the inner field cage (IFC) of the TPC during Run2008 in the region relevant to the analysis. The amount of material is mostly from the beam pipe, the IFC, air, and a wrap around the beam pipe. In Run2005, the amount of material is estimated to be ~10 times larger in front of the TPC inner field cage [26] and is dominated by the silicon detectors which were removed before Run2008. The contribution from the TPC gas is not significant because we require the radial location of the first TPC point of reconstructed tracks to be less than 70 cm (see Sec. III B) in the Run2008 analysis; furthermore, conversion electrons originating from TPC gas have low probability to be reconstructed by the TPC tracking due to the short track length. While the Run2008 simulation describes the material distribution very well, the material budget for the support structure and electronics related to the silicon detectors is not reliably described in the Run2005 simulation [27]. This, however, has little effect on this analysis, as explained in Sec. III D.

TABLE I. Estimates of material thickness of the beam pipe, the wrap around the beam pipe, the TPC inner field cage, and air between the beam pipe and the inner field cage in Run2008.

Source	Thickness in radiation lengths
Beam pipe	0.29%
Beam pipe wrap	~0.14%
Air	~0.17%
Inner field cage	~0.45%

C. Triggers and data sets

The data reported in this paper were recorded during Run2005 and Run2008 at $\sqrt{s} = 200$ GeV. All events used in this analysis are required to satisfy a BEMC trigger and a BBC minimum-bias trigger. In addition, event samples using a VPD trigger in the 2008 d + Au collisions are used for systematic cross-checks as described in Sec. III E.

To enrich the data sample with high-p_T electromagnetic energy deposition, the BEMC trigger requires the energy deposition in at least one tower to exceed a preset threshold (high tower). Most of the energy from an electron or a photon will be deposited into a single tower since the tower size exceeds the radius of a typical electromagnetic shower. The Run2008 data sets used here were recorded using three high-tower triggers with different thresholds, corresponding to a sampled luminosity of ~2.6 pb^{-1}. Expressed in terms of transverse energy (E_T), the thresholds were approximately 2.6, 3.6, and 4.3 GeV. The Run2005 data sets used here are from two high-tower triggers with E_T thresholds of 2.6 GeV (HT1) and 3.5 GeV (HT2), corresponding to a sampled luminosity of ~2.8 pb^{-1}. In the Run2008 analysis, data sets from different high-tower triggers are treated together after being combined, with double counting avoided by removing duplicates in the corresponding high-tower analog-to-digital converter (ADC) spectra. Trigger efficiencies and prescale factors imposed by the data acquisition system are taken into account during the combination. In the analysis of the Run2005 data, HT1 and HT2 data are treated separately.

In Run2005 the integrated luminosity was monitored using the BBC minimum-bias trigger, while in Run2008, because of the large beam related background due to high luminosity, a high threshold high-tower trigger seeing a

Article reprint

total cross section of 1.49μb was used as luminosity monitor.

III. ANALYSIS

A. Photonic background removal

The main background in this analysis is the substantial flux of photonic electrons from photon conversion in the detector material and Dalitz decay of π^0 and η mesons. These contributions need to be subtracted in order to extract the nonphotonic electron yield, which is dominated by electrons from semileptonic decays of heavy-flavor mesons.

There are two distinct methods for evaluating contributions from photonic electrons. In the cocktail method, the estimated or measured invariant cross sections are used to calculate contributions from various sources (mostly π^0, η mesons), and to derive from those the photonic electron distributions. Given sufficient knowledge of the production yield of those mesons, this method allows one to determine directly the contributions from Dalitz decays. With this method, a detailed understanding of the material distribution in the detector is required in order to evaluate the contribution from photon conversion. Another method, used in this analysis, is less dependent on the exact knowledge of the amount of material. This method reconstructs the photonic electrons through the specific feature that photonic electron-positron pairs have very small invariant mass. Not all photonic electrons can be identified this way since one of the electrons may fall outside of the detector acceptance, or has a very low momentum, in which cases both electrons in the pair are not reconstructed. This inefficiency must be estimated through simulation.

Electron pairs are formed by combining an electron with $p_T > 2.5$ GeV/c, which we refer to as a primary electron, with all other electrons (partners) reconstructed in the same event, with opposite charge sign (unlike sign) or same charge sign (like sign). The upper two panels of Fig. 1 show the invariant mass spectra for primary electrons with 2.5 GeV/$c < p_T < 3.0$ GeV/c (left) and 8.0 GeV/$c < p_T < 10.0$ GeV/c. The unlike-sign spectrum includes pairs originating from photon conversion and Dalitz decay, as well as combinatorial background. The latter can be estimated using the like-sign pair spectrum. The photonic electron spectrum is obtained by subtracting like-sign from unlike-sign spectrum (unlike-minus-like). The broad shoulders extending toward higher masses in the spectra are caused by finite tracking resolution, which leads to a larger reconstructed opening angle when the reconstructed track helices of two conversion electrons intersect each other in the transverse plane. The overall width of the mass spectra depends on the primary electron p_T, but most photonic pairs are contained in range of $m_{ee} < 0.24$ GeV/c^2. The lower two panels of Fig. 1 show the simulated invariant mass spectra of the two dominant sources of photonic electrons, π^0 Dalitz and γ conversions,

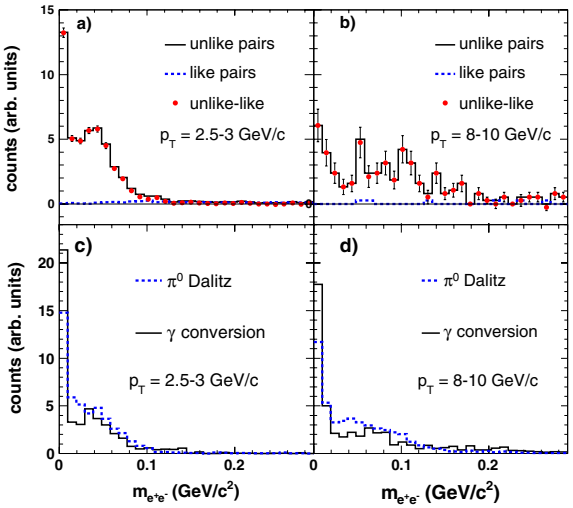

FIG. 1 (color online). The upper two panels show the electron pair invariant mass distributions for electrons at 2.5 GeV/$c <$ $p_T < 3.0$ GeV/c (a) and at 8.0 GeV/$c < p_T < 10.0$ GeV/c (b). Solid and dashed lines represent unlike-sign and like-sign pairs, respectively. Closed circles represent the difference of unlike and like. The lower two panels show the simulated invariant mass spectra with electrons at 2.5 GeV/$c < p_T < 3.0$ GeV/c (c) and at 8.0 GeV/$c < p_T < 10.0$ GeV/c (d). Solid and dashed lines represent results from γ conversions and π^0 Dalitz decay.

in the same two p_T regions, which are similar in shape due to similar decay kinematics. The electron spectrum obtained from the unlike-minus-like method is from pure photonic electrons because the combinatorial background is accurately described by the like-sign pair spectrum according to the simulation and the simulated mass spectra are in qualitative agreement with the data. This is also proved by the fact that the distribution of the normalized ionization energy loss (see Sec. III B) can be well described by a Gaussian function expected from electrons as shown in Fig. 4.

We calculate the yield of nonphotonic electrons according to

$$N(\text{npe}) = N(\text{inc}) \cdot \epsilon_{\text{purity}} - N(\text{pho})/\epsilon_{\text{pho}},$$

where N(npe) is the nonphotonic electron yield, N(inc) is the inclusive electron yield, N(pho) is the photonic electron yield, ϵ_{pho} is the photonic electron reconstruction efficiency defined as the fraction of the photonic electrons identified through invariant mass reconstruction, and ϵ_{purity} is the purity reflecting hadron contamination in the inclusive electron sample.

Electrons from open heavy-flavor decays dominate nonphotonic electrons. The contribution from semileptonic decay of kaons is negligible for $p_T > 2.5$ GeV/c [17]. Electrons from vector mesons (ρ, ω, ϕ, J/ψ, Υ) decays

Article reprint

H. AGAKISHIEV *et al.* PHYSICAL REVIEW D **83,** 052006 (2011)

and Drell-Yan processes are subtracted from the measurement (see Sec. III G for details).

B. Electron reconstruction and identification efficiency

In the analysis of the Run2008 data, we select only tracks with $p_T > 2.5$ GeV/c and $|\eta| < 0.5$. The event vertex position along the beam-axis (V_z) is required to be close to the center of the TPC, i.e. $|V_z| < 30$ cm. To avoid track reconstruction artifacts, such as track splitting, the selected tracks are required to have at least 52% of the maximum number of TPC points allowed in the TPC, a minimum of 20 TPC points and a distance-of-closest-approach (DCA) to the collision vertex less than 1.5 cm. For hadron rejection we apply a cut of $n\sigma_e > -1$ on the normalized ionization energy loss in the TPC [28], which is defined as

$$n\sigma_e = \log((dE/dx)/B_e)/\sigma_e,$$

where B_e is the expected mean dE/dx of an electron calculated from the Bichsel function [29] and σ_e is the TPC resolution of $\log((dE/dx)/B_e)$.

We reconstruct clusters in the BEMC and the BSMD by grouping adjacent hits that are likely to have originated from the same incident particle [27]. The selected tracks are extrapolated to the BEMC and the BSMD where they are associated with the closest clusters. The association windows for electrons are determined by measuring the distance between the track projection point at the BEMC (BSMD) and the closest BEMC (BSMD) cluster using photonic electrons from the unlike-minus-like pairs. Figure 2(a) shows the distribution of this distance at the BEMC along the beam direction for electrons from unlike-sign, like-sign, and unlike-minus-like pairs requiring $m_{e^+e^-} < 0.24$ GeV/c^2, a maximum 1.0 cm DCA between two helical-shaped electron tracks, and a 3.0 keV/cm $< dE/dx <$ 5.0 keV/cm cut on ionization energy loss for partner tracks. Most electrons are inside a window of ± 20 cm around the track projection point. The window in the azimuthal plane is determined to be ± 0.2 rad. Figure 2(b) shows the distribution of p/E_0 for electrons from unlike-sign, like-sign, and unlike-minus-like pairs, where E_0 is the energy of the most energetic tower in a BEMC cluster. The distribution is peaked around one due to the small mass of the electron and the fact that most electron energy is deposited into one tower. We apply a cut of $p/E_0 < 2.0$ to further reduce hadron contamination. Cuts on the association with BSMD clusters are kept loose to maintain high efficiency. Each track is required to have more than one associated BSMD strip in both ϕ and η planes.

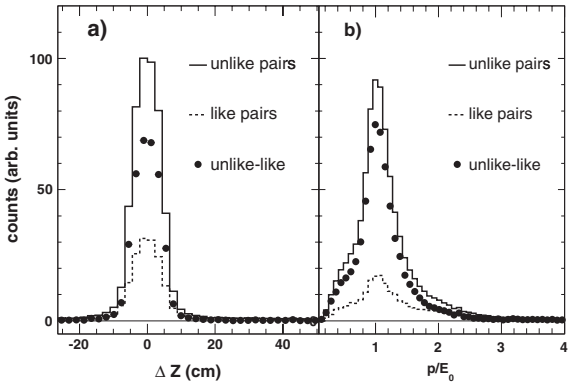

FIG. 2. (a) The distribution of the minimum distance between an electron track projection point at the BEMC and all BEMC clusters along the beam direction from unlike-sign electron candidate pairs (solid line), like-sign electron candidate pairs (dashed line), and unlike-minus-like (closed circles). (b) p/E_0 distribution from unlike-sign electron candidate pairs (solid line), like-sign electron candidate pairs (dashed line), and unlike-minus-like (closed circles).

The efficiencies of electron identification cuts are estimated directly from the data using pure photonic electrons obtained from the unlike-minus-like pairs requiring $m_{e^+e^-} < 0.24$ GeV/c^2, a maximum 1.0 cm DCA between two helical-shaped electron tracks, and a 3.0 keV/cm $<$ $dE/dx <$ 5.0 keV/cm cut on ionization energy loss for partner tracks. A cut of $p_T > 0.3$ GeV/c for partners is also applied, selecting a region where the simulation does a good job of describing the data. The efficiency for one specific cut is then calculated as the ratio of electron yield before the cut to that after the cut, while all the other electron identification cuts are applied. To avoid possible correlation among different cuts, efficiencies for all BEMC and BSMD cuts are calculated together. Figure 3(a) shows the breakdown of the electron identification efficiency as a function of p_T. The drop in the low p_T region comes mainly from BSMD inefficiency, while the drop in the

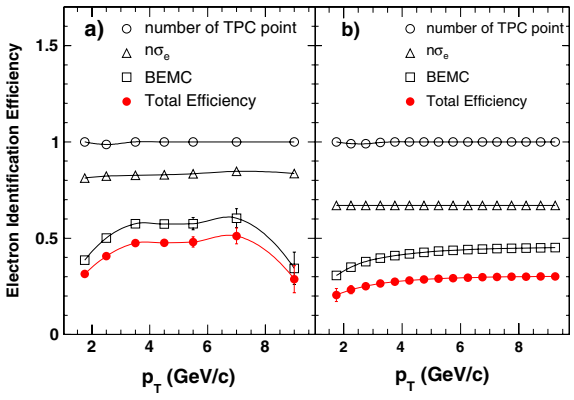

FIG. 3 (color online). Efficiencies of the cuts on number of TPC points (open circles), $n\sigma_e$ (open triangles), and BEMC (open squares) in (a) the Run2008 and (b) the Run2005 analyses. The closed circles represent the total efficiency which is the product of all individual ones.

Article reprint

high p_T region is caused by the p/E_0 cut. The uncertainties in the figure are purely statistical and are included as part of the systematic uncertainties for the cross-section calculation.

To maintain high track quality and suppress photonic electrons from conversion in the TPC gas, we require the radial location of the first TPC point to be less than 70 cm. This cut causes an inefficiency of $12.0 \pm 2.0\%$ for nonphotonic electrons according to the estimates from both simulation and data.

Through embedding simulated electrons into high-tower trigger events and processing them through the same software used for data production, single electron reconstruction efficiency in the TPC is found to be 0.84 ± 0.04 with little dependence on momentum for $p_T > 2.0$ GeV/c.

The analysis of the Run2005 data is slightly different from that of the Run2008 described above. Only half of the BEMC ($0 < \eta < 1.0$) was instrumented in 2005. Because of the presence of the silicon detectors, and their significant material budget, photonic backgrounds were substantially higher. We select only tracks with $0 < \eta < 0.5$ from -30 cm $< V_z < 20$ cm in order to avoid the supporting cone for the silicon detectors in the fiducial volume while keeping track quality cuts identical to those in the Run2008 analysis. However, we apply a tighter cut on the normalized ionization energy loss, i.e. $-0.7 < n\sigma_e < 3.0$, to improve hadron rejection. BEMC clusters are grouped with geometrically overlapping BSMD clusters to improve position resolution and electron-hadron discrimination through shower profile. The clustering algorithm is also modified to increase the efficiency of differentiating two overlapping BSMD clusters by lowering the energy threshold of the second cluster [30]. The minimum angle between track projection point at the BEMC and all BEMC clusters is required to be less than 0.05 rad. We also require each track to have more than one associated BSMD strip in both ϕ and η planes, and a tightened p/E cut of $0.3 < p/E < 1.5$, where E is the energy of the associated BEMC cluster. The efficiencies for the electron identification cuts are estimated by embedding simulated single electrons into minimum-bias PYTHIA [31] events. Figure 3(b) shows the breakdown of electron identification efficiency as a function of p_T in the Run2005 analysis. There is no drop at high p_T as in the Run2008 result because the energy of a whole BEMC cluster, instead of the highest tower, is used for the p/E cut. No cut on the first TPC point is applied in this analysis. To avoid the TPC tracking resolution effect that causes the broad shoulder extending toward higher masses in the invariant mass spectrum of the Run2008 analysis, we utilize a 2D invariant mass by ignoring the opening angle in the ϕ plane when reconstructing the e^+e^- invariant mass [30]. We require $-3 < n\sigma_e < 3$ for partner tracks, 2D $m_{e^+e^-} < 0.1$ GeV/c^2 for pairs, a maximum $0.1/0.05$ rad for the opening angle in the ϕ/θ plane, and a maximum 1.0 cm DCA between two electron helices. A cut of $p_T > 0.3$ GeV/c for partners is also applied so that the simulation can describe the data well.

By following independent analysis procedures from two RHIC runs where the amount of material for photonic background is significantly different, we will be able to validate our approach for measuring nonphotonic electron production.

C. Purity estimation

After applying all electron identification cuts, the inclusive sample of primary electrons is still contaminated with hadrons. To estimate the purity of electrons in the inclusive sample, we perform a constrained fit on the charged track $n\sigma_e$ distributions in different p_T regions with three Gaussian functions representing the expected distributions of $\pi^\pm$, $K^\pm + p^\pm$, and $e^\pm$. The purity is estimated from the fit.

Ideally the electron $n\sigma_e$ will follow the standard normal distribution. The actual distribution can be slightly different due to various effects in data calibrations. We can, however, determine its shape in different p_T regions directly from data using photonic electrons from the unlike-minus-like pairs. The left panel of Fig. 4 shows the $n\sigma_e$ distribution for tracks with (a) 2.5 GeV/$c < p_T < 3.0$ GeV/c and (b) 8.0 GeV/$c <$ $p_T < 10.0$ GeV/c from unlike-sign, like-sign pairs as well as for photonic electrons from the unlike-minus-like pairs. Here all electron identification cuts, except the $n\sigma_e$ cut, are applied. The $n\sigma_e$ of photonic electrons are well fitted with Gaussian functions. Figure 4(c) shows the mean

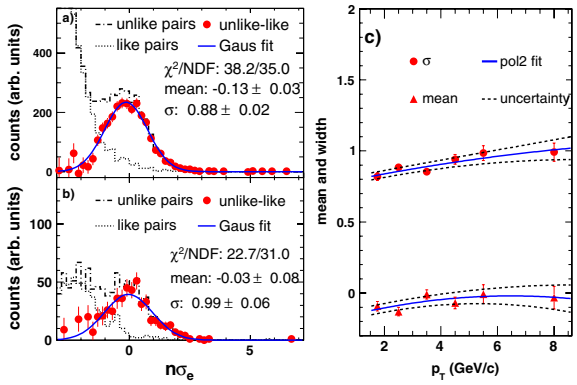

FIG. 4 (color online). Left two panels are $n\sigma_e$ distributions in the Run2008 analysis for unlike-sign (dot-dashed line), like-sign (dotted line), and unlike-minus-like (closed circles) pairs together with a Gaussian fit (solid lines) at (a) 2.5 GeV/$c < p_T < 3.0$ GeV/c and (b) 8.0 GeV/$c < p_T <$ 10.0 GeV/c after applying all the electron identification cuts except the $n\sigma_e$ cut. The right panel (c) shows the mean and width of the Gaussian fitting functions for pure photonic electron (unlike-minus-like) $n\sigma_e$ distribution as shown in the left panels for each p_T bin. See text for details.

Article reprint

H. AGAKISHIEV *et al.* PHYSICAL REVIEW D **83,** 052006 (2011)

and width of the Gaussian fit as a function of electron p_T, which, as discussed above, differ slightly from the ideal values. The solid lines in the figure are fits to the data using a second order polynomial function. The dotted lines are also second order polynomial fits to the data except that the data points are moved up and down simultaneously by 1 standard deviation. The region between the dotted lines represents a conservative estimate of the fit uncertainty since we assume that the points are fully correlated. The mean, width, and their corresponding uncertainties from the fits are used to define the shape of electron $n\sigma_e$ distribution in the following 3-Gaussian fit. The $n\sigma_e$ of $\pi^{\pm}$ and $K^{\pm} + p^{\pm}$ are also expected to follow Gaussian distributions [28]. Ideally their width is one and their means can be calculated through the Bichsel function [29]. These ideal values are used as the initial values of the fit parameters in the following 3-Gaussian fit.

Figure 5 shows the constrained 3-Gaussian fits to the $n\sigma_e$ distributions of inclusive electron candidates with 2.5 GeV/$c < p_T <$ 3.0 GeV/c in the Run2008 analysis (upper left), 2.5 GeV/$c < p_T <$ 3.5 GeV/c in the Run2005 analysis (lower left), and 8.0 GeV/$c < p_T <$ 10.0 GeV/c in the Run2008 analysis (right). Here we leave the $n\sigma_e$ cut open. The dotted, dot-dashed, and dashed lines represent, respectively, the fits for $K^{\pm} + p^{\pm}$, $\pi^{\pm}$, and $e^{\pm}$. Compared to the Run2008 analysis, the electron component in the Run2005 analysis at similar p_T is more prominent due to the larger conversion electron yield. The solid lines are the overall fits to the spectra. The purity is calculated as the ratio of the integral of the electron fit function to that of the overall fit function above the $n\sigma_e$ cut. No constraints are applied to the $K^{\pm} + p^{\pm}$ and $\pi^{\pm}$ functions unless the fits fail. To estimate the systematic uncertainty of the purity, the mean and width of the electron function are allowed to vary up to one, two, three, and four standard deviations from their central values. For each of the four constraints, we calculate one value of the purity. The final purity is taken as the mean and the systematic uncertainty is taken as the largest difference between the mean and the four values from the four constraints. To estimate the statistical uncertainty of the purity, we rely on a simple Monte-Carlo simulation. We first obtain a large sample of altered overall $n\sigma_e$ spectra by randomly shifting each data point in the original spectrum in Fig. 5 according to a Gaussian distribution with the mean and width set to be equal to the central value and the uncertainty of the original data point, respectively. We then obtain the purity distribution through calculating the purity from each of these altered spectra following the same procedure as discussed above. In the end, we fit the distribution with a Gaussian function and take its width as the statistical uncertainty. The total uncertainty of the purity is obtained as the quadratic sum of the statistical and systematic uncertainties.

We follow the same procedure in the Run2008 and the Run2005 analysis except that the overall $n\sigma_e$ distribution in the Run2008 analysis is the combined result from the data sets of all three high-tower triggers as described in Sec. II C, while in the Run2005 analysis, the purity are calculated separately for the two high-tower triggers. Figure 6 shows the purity as a function of electron p_T for the Run2008 (a) and the Run2005 (b) data. Tighter electron identification cuts and much higher photonic electron yield lead to much higher purity for the Run2005 inclusive electron sample.

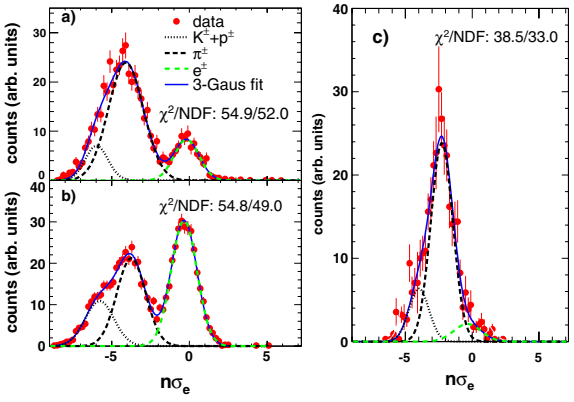

FIG. 5 (color online). $n\sigma_e$ distribution for inclusive electrons (closed circles) and fits from different components at (a) 2.5 GeV/$c < p_T <$ 3.0 GeV/c in the Run2008 analysis, (b) 2.5 GeV/$c < p_T <$ 3.5 GeV/c in the Run2005 analysis, and (c) 8.0 GeV/$c < p_T <$ 10.0 GeV/c in the Run2008 analysis after applying all electron identification cuts except the $n\sigma_e$ cut. Different curves represent $K^{\pm} + p^{\pm}$ (dotted line), $\pi^{\pm}$ (dot-dashed line), electrons (dashed line), and the overall fit (solid lines).

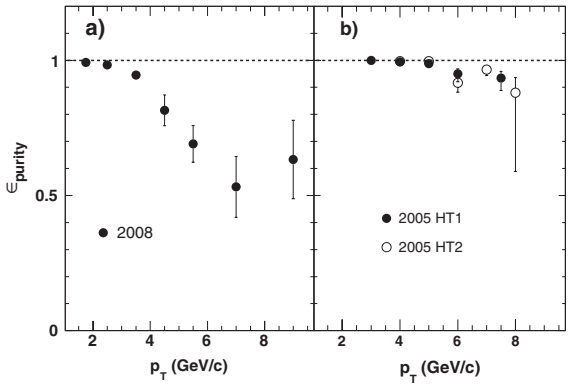

FIG. 6. Purity of the inclusive electron sample as a function of p_T in data from (a) Run2008 and (b) Run2005. The 2008 result is from combined data sets of all different high-tower triggers. The 2005 results for the two different high-tower triggers, i.e. HT1 (closed circles) and HT2 (open circles), are plotted separately.

Article reprint

D. Photonic electron reconstruction efficiency

Since photon conversions, π^0 and η meson Dalitz decays are the dominant sources of photonic electrons, they are the components that we used to calculate $\epsilon_{\rm pho}$, the photonic electron reconstruction efficiency, in the analysis of the Run2008 data. The $\epsilon_{\rm pho}$ for each individual component is calculated separately to account for its possible dependence on the decay kinematics of the parent particles. The final $\epsilon_{\rm pho}$ is obtained by combining results from all components according to their relative contribution to the photonic electron yield.

The determination of $\epsilon_{\rm pho}$ is done through reconstructing electrons from simulated γ conversion or Dalitz decay of π^0 and η with uniform p_T distributions that are embedded into high-tower trigger events. These events are then fully reconstructed using the same software chain as used for data analysis. To account for the efficiency dependence on the parent particle p_T, we use a fit function to the measured π^0 spectrum, the derived η and inclusive photon p_T spectra as weights. The fit function to the measured π^0 spectrum is provided by the PHENIX experiment in Ref. [32]. The η spectrum is derived from the π^0 measurement assuming m_T scaling, i.e. replacing p_T with $\sqrt{p_T^2 + m_h^2 - m_{\pi^0}^2}$ while keeping the function form unchanged. Figure 7(a) shows the derived inclusive γ p_T spectrum (solid line), and an estimate of its uncertainty represented by the region between the dotted and dot-dashed lines. Figure 7(b) shows the uncertainty in linear scale. The inclusive γ spectrum is obtained by adding the direct γ yield to the π^0 and η decay γ yield calculated using PYTHIA. The direct γ yield is obtained from the fit function to the direct γ measurement provided by the PHENIX experiment in Ref. [32]. The dot-dashed line represents the γ spectrum from π^0 and η decay alone. The dotted line is obtained by doubling the direct γ component in the inclusive photon spectrum. By comparing the ratio of the derived inclusive γ yield to that of π^0 and η decay photon with the double ratio measurement in Au + Au most peripheral collisions [33], we found the uncertainty covers the possible variations of the inclusive photon yield.

STAR simulations for γ conversion and Dalitz decay are based on GEANT3 [34] which incorrectly treats Dalitz decays as simple three-body decays in phase space. We therefore modified the GEANT decay routines using the correct Kroll-Wada decay formalism [35]. Their kinematics is strongly modified by the dynamic electromagnetic structure arising at the vertex of the transition which is formally described by a form factor. We included the most recent form factors using a linear approximation for the π^0 Dalitz decay [36], and a pole approximation for the decays of η [37].

Figure 8(a) shows the photonic electron reconstruction efficiency as a function of electron p_T for γ conversion, π^0 and η Dalitz decay electrons, which turn out to be very similar because of the similar decay kinematics. The increase towards larger electron p_T is due to the higher probability of reconstructing both electrons from high p_T (virtual) photons. The uncertainties shown in the plots are dominated by the statistics of the simulated events. The effect due to the variation of the inclusive photon spectrum shape is found to be negligible for this analysis. Figure 8(b) shows the combined photonic electron reconstruction efficiency for the Run2008 analysis, which is calculated as

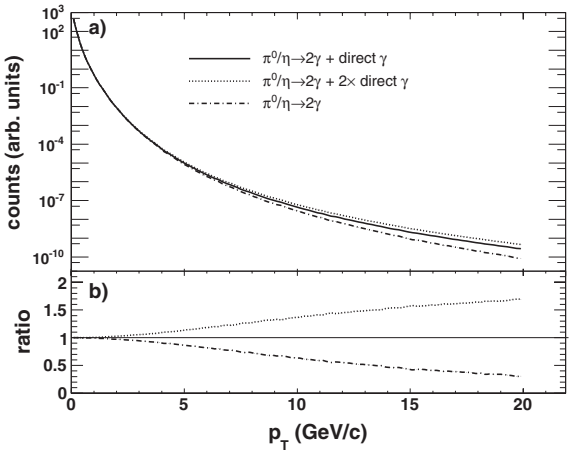

FIG. 7. (a) Derived p_T spectrum for inclusive photons (solid line) and the uncertainty represented by the region between the spectra of π^0 and η decay photons (dot-dashed line) and inclusive photon with doubled direct photon yield (dotted line) as well as their ratio to the inclusive photon as shown in (b).

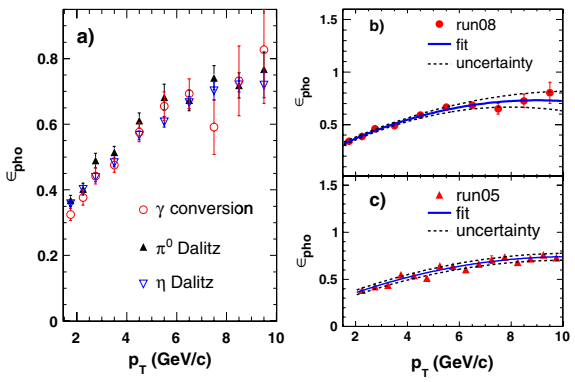

FIG. 8 (color online). Photonic electron reconstruction efficiency as a function of p_T for (a) γ conversion (open circles), π^0 (closed triangles), and η (open triangles) Dalitz decay for the Run2008 analysis, (b) combination of γ conversion, π^0 and η Dalitz decay for the Run2008 analysis, and (c) γ conversion for the Run2005 analysis. The solid line is a fit and the dashed lines represent the uncertainty. See text for details.

$$\epsilon_{\rm pho}(p_T) = \frac{N_e^{\gamma}(p_T)}{N_e^{\gamma}(p_T) + N_e^{\pi^0}(p_T) + N_e^{\eta}(p_T)} \cdot \epsilon_{\gamma}(p_T) + \frac{N_e^{\pi^0}(p_T)}{N_e^{\gamma}(p_T) + N_e^{\pi^0}(p_T) + N_e^{\eta}(p_T)} \cdot \epsilon_{\pi^0}(p_T) + \frac{N_e^{\eta}(p_T)}{N_e^{\gamma}(p_T) + N_e^{\pi^0}(p_T) + N_e^{\eta}(p_T)} \cdot \epsilon_{\eta}(p_T),$$

where N_e^{γ}, $N_e^{\pi^0}$, and N_e^{η} are, respectively, the yield of electrons from photon conversion, π^0 and η Dalitz decay; ϵ_{γ}, ϵ_{π^0}, and ϵ_{η} are the corresponding photonic electron reconstruction efficiencies. Based on Table I, approximately 36% of the photonic electrons are from π^0 Dalitz decay and about 10% are from η Dalitz decay. Their variations have a negligible effect on the results since ϵ_{γ}, ϵ_{π^0}, and ϵ_{η} are almost identical. The solid line is a second order polynomial fit to the data. The systematic uncertainty is represented by the region between the dotted lines, which are second order polynomial fits after moving all the data points simultaneously up and down by 1 standard deviation.

For the Run2005 analysis, the dominant source of photonic electrons is conversion in the silicon detectors. We therefore neglect contributions from Dalitz decays while following the same procedure as for the Run2008 analysis to calculate $\epsilon_{\rm pho}$. Figure 8(c) shows $\epsilon_{\rm pho}$ as a function of p_T for γ conversion for the Run2005 analysis. The solid line is a fit to the spectrum with a second order polynomial function and the region between dashed lines represents the uncertainty estimated in the same way as for the Run2008 analysis. The inclusion of the Dalitz decays is estimated to reduce the $\epsilon_{\rm pho}$ by less than 0.5% which is well within the systematic error. The uncertainty because of the inaccurate material distribution in the simulation as mentioned in Sec. II B is negligible since the majority of the material, dominated by our silicon detectors, is within a distance of 30 cm from beam pipe and the variation of $\epsilon_{\rm pho}$ of photonic electrons produced within this region is small.

E. Trigger efficiency

The trigger efficiency is the ratio of the electron yield from high-tower trigger events to that from minimum-bias trigger events after normalizing the two according to the integrated luminosity. To have a good understanding of trigger efficiency, one needs enough minimum-bias events for the baseline reference. However, for the Run2008 $p + p$ data, the number of minimum-bias events is too small to be used for this purpose. Fortunately, the Run2008 d + Au data were taken using the same sets of high-tower triggers as used for the $p + p$ run. Since the two data sets were taken serially, the high-tower trigger efficiency is expected to be the same. During the d + Au run, many events also were taken using the VPD trigger, which is essentially a less efficient minimum-bias trigger that can serve as the baseline reference for trigger efficiency analysis. As a cross-check, we also evaluate the trigger efficiency through the Run2008 $p + p$ simulation.

From the VPD trigger events, we first regenerate a high-tower trigger p_T spectrum by requiring $adc0$ of BEMC clusters to be larger than the threshold. The $adc0$ is the off-line ADC value of a BEMC cluster's most energetic tower which is one of the high towers responsible for firing a high-tower trigger. Figure 9(a) shows the $adc0$ distribution of photonic electrons from high-tower trigger events. The sharp cutoff around a value of 200 is the off-line ADC value of the trigger threshold setting. The smaller peak below the trigger threshold is due to electrons which happen to be in events triggered by something other than the electrons. By requiring $adc0$ to be larger than the threshold, we reject these electrons which did not trigger the event since the uncertainty of their yield is affected by many sources and is therefore hard to be evaluated reliably. When the threshold is correctly chosen, the regenerated spectrum shape should be very similar to that of the actual high-tower trigger. We therefore quantitatively determine the trigger threshold as the $adc0$ cut which minimizes the

$$\chi^2 = \sum_i \left(\frac{N_i(\text{VPD} + adc0)}{N_i(\text{HT})} - 1 \right)^2 \Big/ \sigma_i^2,$$

where $N_i(\text{VPD} + adc0)$ is the regenerated high-tower trigger electron yield from VPD events in the ith p_T bin, $N_i(\text{HT})$ is the electron yield at the same p_T bin from the actual high-tower trigger events, and σ_i is the uncertainty

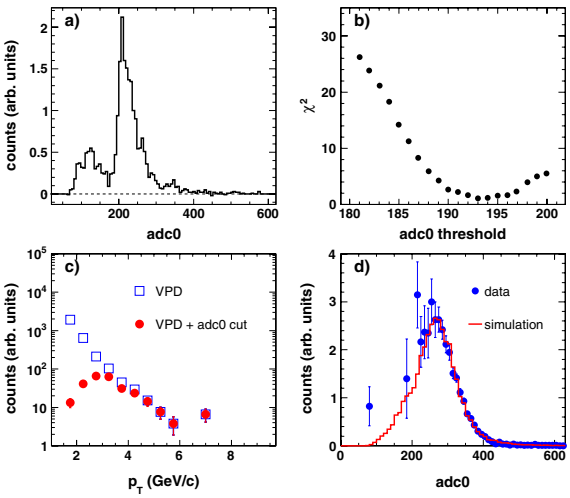

FIG. 9 (color online). (a) $adc0$ distribution for high-tower trigger events. (b) χ^2 as a function of the $adc0$ cut. (c) Raw inclusive electron p_T spectrum from VPD trigger in Run2008 d + Au collisions before (open squares) and after applying the $adc0 > 193$ cut (closed circles). (d) $adc0$ distribution for data (closed circles) and simulation (solid line) at $p_T = 4.0 - 5.0$ GeV/c. See text for details.

Article reprint

of $N_i(\mathrm{VPD} + adc0)$. Figure 9(b) shows the χ^2 as a function of the $adc0$ cut; the threshold is taken as 193. Figure 9(c) shows the p_T spectrum of raw inclusive electrons from the VPD trigger (open squares) and the regenerated high-tower spectrum (closed circles) after applying the $adc0 > 193$ cut used to calculate the trigger efficiency.

To estimate trigger efficiency through simulation, we tune the simulated single electron $adc0$ spectrum in each individual p_T bin to agree with the data in the region above the threshold. The data spectra are obtained from the unlike-minus-like pairs, i.e. pure photonic electrons. As a demonstration of the comparison, Fig. 9(d) shows the spectra from data (closed circles) and simulation (solid line) at $4.0\ \mathrm{GeV}/c < p_T < 5.0\ \mathrm{GeV}/c$. The efficiency is defined as the fraction of the simulated $adc0$ spectrum integral above the trigger threshold.

In the Run2008 analysis the raw p_T spectrum of nonphotonic electrons is obtained by combining the data sets of all three high-tower triggers. Since the shape of the combined spectrum is the same as that of the high-tower trigger with the lowest threshold, we only need to estimate the trigger efficiency of this lowest threshold trigger. Figure 10 shows the trigger efficiency as a function of p_T that is calculated using d + Au VPD events (closed circles) and simulated events (closed triangles) in the Run2008 analysis. At $p_T > 3.5\ \mathrm{GeV}/c$, they agree with each other reasonably well. At lower p_T, the simulated results are not reliable because the numerator in the efficiency calculation is only from a tail of the spectrum and a small mismatch between simulation and data can have a large impact on the results. On the other hand, the results from VPD events suffer from low statistics at high p_T. The final efficiency is therefore taken to be the combination of the two, i.e., at $p_T < 3.5\ \mathrm{GeV}/c$, the efficiency is equal to that from VPD events assigning a systematic uncertainty identical to the statistical uncertainty of the data point, while at high p_T, the efficiency is equal to the simulated results, and the systematic errors are from the tuning uncertainty.

In the Run2005 analysis, the efficiencies of the two high-tower triggers are estimated separately. While there are more minimum-bias events for Run2005 than for Run2008, the statistics are poor at $p_T > 2.0\ \mathrm{GeV}/c$. We thus rely on a fit to the spectrum, which consists of minimum-bias events at low p_T and high-tower trigger events at high p_T where the trigger is expected to be fully efficient, as the baseline reference for the trigger efficiency evaluation. Figure 11 shows the raw inclusive electron p_T spectrum from minimum-bias, HT1 and HT2 events. The fit uses a power-law function $A(1 + p_T/B)^{-n}$. The regions where we expect the HT1 and the HT2 trigger to be fully efficient are above 4.5 and 6.0 GeV/c, respectively. The dashed line shows the fit uncertainty, obtained from many fit trials. In a single fit trial, each data point is randomized with a Gaussian random number, with the mean to be the central value and the rms to be the statistical uncertainty of the data point. Additional systematic uncertainty coming from fits using different functions is included in the cross-section calculation and is not displayed in the figure. Figure 12 shows the efficiency of HT1 (a) and HT2 (b) triggers, defined as the ratio of the raw HT1 or HT2 inclusive electron spectrum to the baseline fit function. We used error functions to parametrize both efficiencies. The dashed lines represent the uncertainty, obtained in the same way as for the Fig. 11 fits.

High-tower trigger efficiency for photonic and nonphotonic electrons can be different. Unlike nonphotonic electrons, a photonic electron always has a partner. In case both share the same BEMC tower, the deposited energy will be higher than that for an isolated electron and will lead to a higher efficiency. The effect can be quantified by

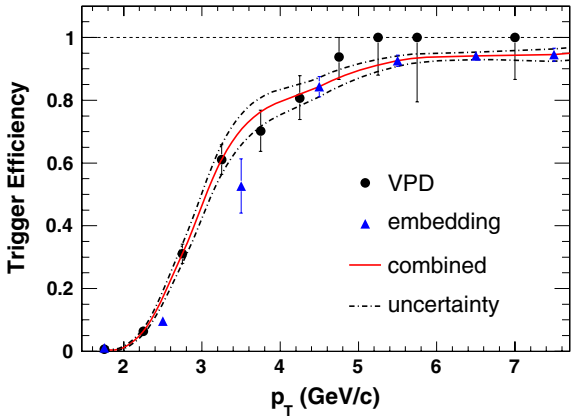

FIG. 10 (color online). p_T dependence of high-tower trigger efficiency from data (closed circles), simulation (closed triangles), and combined results (solid line) for Run2008 analysis. The dashed lines represent the uncertainty. See text for details.

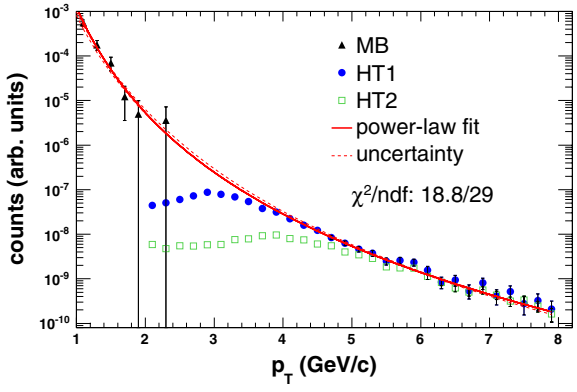

FIG. 11 (color online). Raw inclusive electron p_T spectrum for minimum-bias (closed triangles) and two high-tower triggers, i.e. HT1 (closed circles) and HT2 (open squares) together with a power-law fit (solid line) and fit uncertainty (dashed line) for Run2005 analysis.

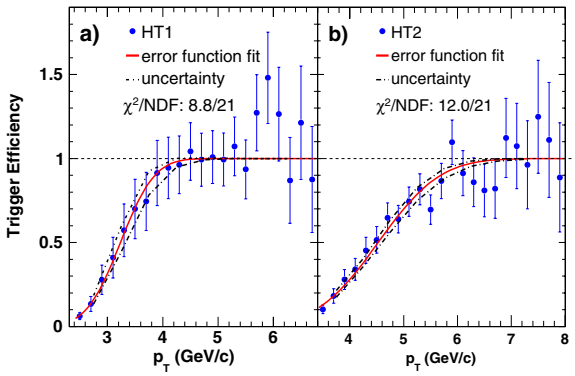

FIG. 12 (color online). p_T dependence of trigger efficiency for the two high-tower triggers, i.e. HT1 (a) and HT2 (b) including result from data (closed circles) for Run2005, an error function fit (solid lines), and the fit uncertainty (dot-dashed lines).

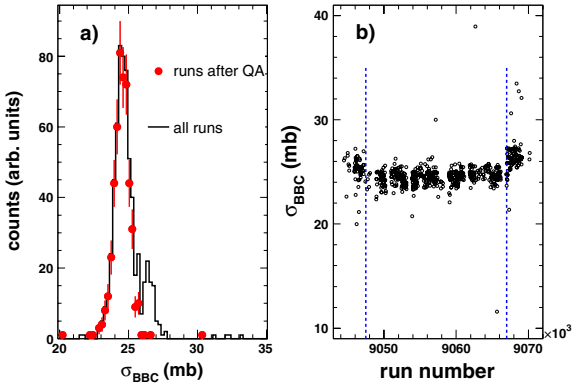

FIG. 13 (color online). (a) Distribution of the calculated σ_{BBC} before (solid lines) and after (closed circles) removing events at the beginning and the end of Run2008. (b) Variation of the calculated σ_{BBC} as a function of run number. The runs outside the region between the two dashed lines are rejected.

comparing the ratio of the isolated electron yield to the yield of electrons with partners in minimum-bias events to the same ratio in high-tower trigger events. We found that the difference is negligible at $p_T > 2.5$ GeV/c, while the trigger efficiency for photonic electron is 20%–30% higher than for nonphotonic electron in the lower p_T region.

F. Stability of the luminosity monitor

The BBC trigger was used to monitor the integrated luminosity for Run2005. During Run2008, because of the large beam background firing the BBC trigger, a high threshold high-tower trigger was used as the luminosity monitor. To quantify the stability of the monitor with respect to BBC, we calculate the BBC cross section as a function of run number using $\sigma_{\mathrm{BBC}} = N_{\mathrm{minbias}}/\mathcal{L}$, where $\mathcal{L} = N_{\mathrm{mon}}/\sigma_{\mathrm{mon}}$, σ_{mon} is the monitor cross section which is estimated to be 1.49μb using low luminosity runs, N_{minbias} and N_{mon} are, respectively, the number of events from the BBC trigger and the monitor after correcting for prescaling during data acquisition. Here a run refers to a block of short term ($\sim$ 30 minutes) data taking. Figure 13(a) shows the distribution of the calculated σ_{BBC}. There are two peaks in the figure. The dominant one centered around 25 mb contains most of the recorded luminosity in Run2008. The minor one centered at a higher value comes from events taken at the beginning and the end of Run2008 represented by the regions beyond the two dashed lines in Fig. 13(b) showing the calculated BBC cross section as a function of run number. After removing these runs taken at the beginning and the end of Run2008, the minor peak disappeared and the performance of the monitor appeared to be very stable.

In the data analysis, we also reject those with $\sigma_{\mathrm{BBC}} <$ 20 mb or $\sigma_{\mathrm{BBC}} > 30$ mb. We fit the σ_{BBC} distribution with a Gaussian function and assign the width of the function (2.3%) as the systematic uncertainty of the σ_{mon} with respect to BBC cross section.

The integrated luminosity sampled by the high-tower triggers are $\sim$2.6 and $\sim$2.8 pb^{-1} for Run2008 and Run2005, respectively.

G. Contribution from vector mesons

The main background sources of electrons that do not originate from photon conversion and Dalitz decay are electromagnetic decays of heavy (J/ψ, Υ) and light vector mesons (ρ, ω, and ϕ) as well as those from Drell-Yan process.

The electrons from J/ψ decay contribute noticeably to the observed nonphotonic electron signal as pointed out in Ref. [38]. In order to estimate the contribution from $\mathrm{J}/\psi \rightarrow \mathrm{e}^+\mathrm{e}^-$ to the nonphotonic electron yield, we combine the measured differential J/ψ cross sections from PHENIX [39] and STAR [40]. For each data point we add the statistical and systematic uncertainties, except the global uncertainties, in quadrature. Figure 14(a) shows the measured J/ψ differential cross section from the two experiments. While the PHENIX measurement dominates the low to medium-p_T region, the STAR measurement dominates the high-p_T region. The combined spectrum is fit using a power-law function of the form $Ed^3\sigma/d^3p|_{y=0} = A(\exp(ap_T - bp_T^2) + p_T/p_0)^{-n}$, where $A = 5.24 \pm 0.87$ mb $\cdot$ GeV$^{-2}c^3$, $a = 0.32 \pm 0.04$ GeV^{-1}c, $b = 0.06 \pm 0.03$ GeV$^{-2}c^2$, $p_0 = 2.59 \pm 0.21$ GeV/c, and $n = 8.44 \pm 0.61$ are fit parameters. The χ^2/NDF of the fit is 27.8/25. To obtain the uncertainty of the fit, the global uncertainties of the STAR and the PHENIX (10% [41]) measurements are assumed to be uncorrelated. We move the PHENIX data up by 10% and repeat the fit to obtain the band of 68% confidence intervals. The upper edge of the band is treated

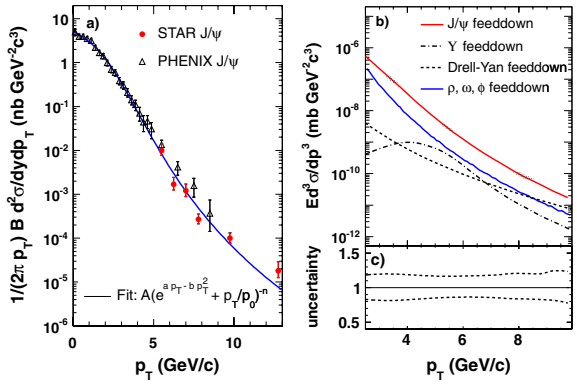

FIG. 14 (color online). (a) The J/ψ invariant cross-section measurement from STAR (closed circles) and PHENIX (open triangles), together with the fits using $A(\exp(ap_T - bp_T^2) + p_T/p_0)^{-n}$ (solid line). (b) Invariant cross section of the electron from decays of J/ψ (band), Υ (dot-dashed line), Drell-Yan (dotted line), and light vector mesons (solid line). The uncertainty of the J/ψ feed-down is represented by the band shown in (c) in linear scale.

as the upper bound of the fit. Following the same procedure except moving the PHENIX data down by 10%, we obtain the lower bound of the fit as the lower edge of the band. Furthermore, since we are considering a rather large p_T range ($p_T < 14.0$ GeV/c), we cannot assume that the p_T and rapidity distributions factorize. We use PYTHIA to generate $dN/dy(p_T)$ and implement a Monte Carlo program using the above functions as probability density functions to generate J/ψ and decay them into e^+e^- assuming the J/ψ to be unpolarized. The decay electrons are filtered through the same detector acceptance as used for the nonphotonic electrons. The band in Fig. 14(b) shows the invariant cross section of J/ψ decay electrons as a function of the electron p_T. The uncertainty of the derived yield comes from the uncertainty of the fit to the J/ψ spectra and is represented by the band which is also shown in Fig. 14(c) in linear scale.

The invariant cross section of electrons from Υ decays ($\Upsilon \to e^+e^-$), represented by the dot-dashed line in Fig. 14(b), is calculated in a similar fashion as that for the J/ψ except that the input Υ spectrum is from a next-to-leading-order perturbative quantum chromodynamics (pQCD) calculation in the color evaporation model (CEM) [42]. We have to rely on model calculations since so far no invariant p_T spectrum in our energy range has been measured. However, in a recent measurement STAR reported the overall production cross section for the sum of all three $\Upsilon(1S + 2S + 3S)$ states in $p + p$ collisions at $\sqrt{s} = 200$ GeV to be $B \times d\sigma/dy = 114 \pm 38^{+23}_{-24}$ pb, which is consistent with the CEM prediction [43]. Adding the statistical and systematic uncertainty in quadrature, the total relative uncertainty of this measurement is ~39%, which is the value we assigned as the total uncertainty of the Υ feed-down contribution to the nonphotonic electrons at all p_T.

The contribution to the nonphotonic electron yield from the light vector mesons is estimated using PYTHIA, assuming the meson spectra follow m_T scaling. We generate a sample of decay electrons using light vector mesons with flat spectra in p_T as input. To derive the differential cross section of the electrons, we keep only those electrons within the same detector acceptance as that for the nonphotonic electrons and weight them with the spectra of ρ, ω, and ϕ. The meson spectra are obtained by replacing the p_T with $\sqrt{p_T^2 + m_h^2 - m_{\pi^0}^2}$ in the same fit function as for the π^0 measurement (see Fig. 7). Here m_h is the mass of the vector meson. The relative yields of the mesons to π [17] are also taken into account during this process. We include the decay channels $\phi \to e^+e^-$, $\phi \to \eta e^+e^-$, $\omega \to e^+e^-$, $\omega \to \pi^0 e^+e^-$, and $\rho \to e^+e^-$ in the calculation. The derived electron differential cross section is represented by the solid line in Fig. 14(b). We assign a 50% systematic uncertainty to cover the uncertainty of the π^0 measurement and the meson to pion ratios.

The contribution to the nonphotonic electron yield from the Drell-Yan processes is represented by the dotted line in Fig. 14(b) and is estimated from a leading-order pQCD calculation using the CTEQ6M parton distribution function with a K-factor of 1.5 applied and without a cut on the electron pair mass [44]. No uncertainty is assigned to this estimate.

IV. RESULTS

A. Nonphotonic electron invariant cross section

The invariant cross section for nonphotonic electron production is calculated according to

$$E\frac{d^3\sigma}{dp^3} = \frac{1}{\mathcal{L}}\frac{1}{2\pi p_T \Delta p_T \Delta y}\frac{N_{\rm npe}}{\epsilon_{\rm rec}\epsilon_{\rm trig}\epsilon_{\rm eid}\epsilon_{\rm BBC}},$$

where $N_{\rm npe}$ is the nonphotonic electron raw yield with the V_z cuts, $\epsilon_{\rm rec}$ is the product of the single electron reconstruction efficiency and the correction factor for momentum resolution and finite spectrum bin width, $\epsilon_{\rm trig}$ is the high-tower trigger efficiency, $\epsilon_{\rm eid}$ is the electron identification efficiency, $\mathcal{L}$ is the integrated luminosity with the V_z cuts, and $\epsilon_{\rm BBC} = 0.866 \pm 0.08$ is the BBC trigger efficiency. The systematic uncertainties of all these quantities are listed in Table II. The relative uncertainty of $\mathcal{L} \cdot \epsilon_{\rm BBC}$ in maximum range is 14% including uncertainties in tracking efficiency [24]. Assuming a flat distribution within the range, we estimate the $\mathcal{L} \cdot \epsilon_{\rm BBC}$ uncertainty to be 8.1% in 1 standard deviation. The uncertainty of $N_{\rm npe}$ is the quadratic sum of the uncertainties from the estimation of $\epsilon_{\rm pho}$, purity and the light vector meson contribution. The uncertainty of $\epsilon_{\rm rec}$ is the quadratic sum of the uncertainties from

Article reprint

TABLE II. Sources of systematic uncertainty for the nonphotonic electron invariant yield in $p+p$ collisions. Type A are point to point uncertainties. Type B are scaling uncertainties which move data points in the same direction. Type C are the scaling uncertainties that are common to both Run2008 and Run2005. The range in each individual source covers the variation of the systematic uncertainty as a function of p_T.

source	Run2008	Run2005
$N_{\rm npe}$	5.0–48.1% (A)	8.5–38.0% (A)
$\epsilon_{\rm eid}$	6.5–25.2% (A)	0.7–2.0% (A)
$\epsilon_{\rm trg}$	1.8–10.0% (A)	0.3–16% (A)
	5.4% (B)	
$\epsilon_{\rm rec}$	2.3–33.3% (A)	1.0–3.5% (A)
	15.7% (B)	11.0% (B)
$\mathcal{L}\cdot\epsilon_{\rm BBC}$	2.3% (B)	
	8.1% (C)	8.1% (C)

correcting the track momentum resolution, the finite spectrum bin width as well as the estimation of single electron reconstruction efficiency. The range of the uncertainty for each individual quantity covers the variation of the uncertainty as a function of p_T. In order to compare with the result in Refs. [16,17], we do not subtract the J/ψ, Υ and Drell-Yan contribution from the nonphotonic electron invariant cross section shown in Figs. 15 and 16.

Figure 15(a) shows the ratio of nonphotonic to photonic electron yield as a function of p_T in $p+p$ collisions in Run2008 (closed circles) and Run2005 (open triangles). The ratio for Run2008 is much larger because there was much less material in front of the TPC for Run2008. Figure 15(b) shows the nonphotonic electron invariant cross section ($\frac{e^+ + e^-}{2}$) as a function of p_T in $p+p$ collisions from the Run2008 analysis (closed circles) and the Run2005 analysis (open triangles). Despite the large difference in photonic background, the two measurements are in good agreement.

Figure 16(a) shows the nonphotonic electron ($\frac{e^+ + e^-}{2}$) invariant cross section obtained by combining the Run2008 and the Run2005 results using the "best linear unbiased estimate" [45]. The corrected result of our early published measurement using year 2003 data [16] is shown in the plot as well. The published result exceeded pQCD predictions from FONLL calculations by about a factor of 4. We, however, uncovered a mistake in the corresponding analysis in calculating $\epsilon_{\rm pho}$. The details are described in the erratum [16]. To see more clearly the comparison, Fig. 16(b) shows the ratio of each individual measurement, including PHENIX results, to the FONLL calculation. One can see that all measurements at RHIC on nonphotonic

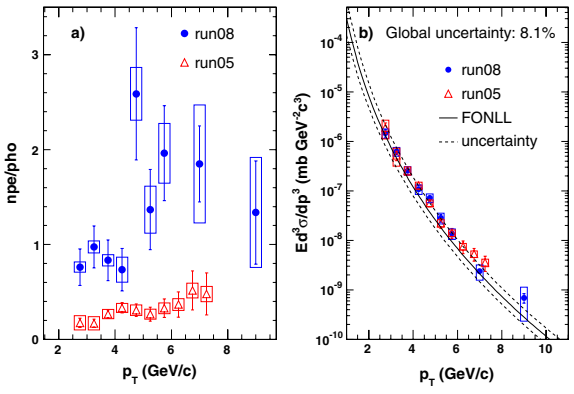

FIG. 15 (color online). (a) Ratio of nonphotonic to photonic electron yield from the Run2008 (closed circles) and the Run2005 (open triangles) analyses. (b) Invariant cross section for nonphotonic electron production ($\frac{e^+ + e^-}{2}$) in $p+p$ collisions from the Run2008 (closed circles) and the Run2005 (open triangles) analyses. The error bars and the boxes represent statistical and systematic uncertainty, respectively. The solid line is FONLL calculation and the dashed lines are the FONLL uncertainties [2].

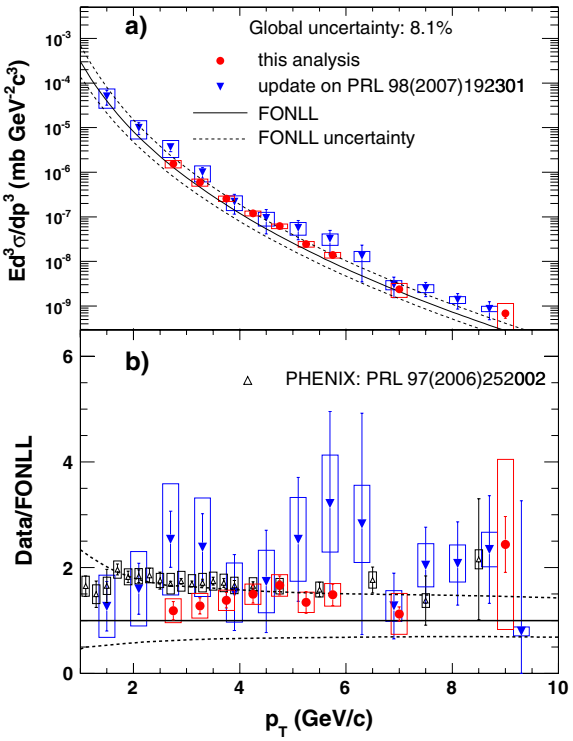

FIG. 16 (color online). (a) Invariant cross section of nonphotonic electron production ($\frac{e^+ + e^-}{2}$) in $p+p$ collisions from this analysis (closed circles) after combining results from Run2005 and Run2008. The published STAR result [16] (closed triangles) is also shown. (b) Ratio of data over FONLL [2] from all measurements at RHIC including PHENIX results [17] (open triangles).

Article reprint

electron production in $p + p$ collisions are now consistent with each other. The corrected run 2003 data points have large uncertainties because of the small integrated luminosity (~ 100 nb^{-1}) in that run. FONLL is able to describe the RHIC measurements within its theoretical uncertainties.

B. Invariant cross section of electrons from bottom and charm meson decays

Electrons from bottom and charm meson decays are the two dominant components of the nonphotonic electrons. Mostly due to the decay kinematics, the azimuthal correlations between the daughter electron and daughter hadron are different for bottom meson decays and charm meson decays. A study of these azimuthal correlations has been carried out on STAR data and is compared with a PYTHIA simulation to obtain the ratio of the bottom electron yield to the heavy-flavor decay electron yield ($e_B/(e_B + e_D)$) [19], where PYTHIA was tuned to reproduce STAR measurements of D mesons p_T spectra [46]. Using the measured $e_B/(e_B + e_D)$, together with the measured nonphotonic electron cross section with the electrons from J/ψ, Υ decay and Drell-Yan processes subtracted, we are able to disentangle these two components.

The bottom electron cross section is calculated as $e_B/(e_B + e_D)$ times the nonphotonic electron cross section with the contribution from J/ψ, Υ decay and Drell-Yan processes subtracted. The same procedure applies to the charm electrons except that $(1 - e_B/(e_B + e_D))$ is used instead. The specific location of p_T, where the $e_B/(e_B + e_D)$ is measured, is different from that of the nonphotonic electrons. To accommodate the difference, we calculate $e_B/(e_B + e_D)$ in any given p_T in nonphotonic electron measurements through a linear interpolation of the actual $e_B/(e_B + e_D)$ measurements. As an estimation of the systematic uncertainty of the interpolated value, we also repeat the same procedure using the curve predicted by FONLL. Figure 17 shows the invariant cross section of electrons ($\frac{e^+ + e^-}{2}$) from bottom (upper left) and charm (upper right) mesons as a function of p_T and the corresponding FONLL predictions, along with the ratio of each measurement to the FONLL calculations (lower panels). The statistical uncertainty of each data point is obtained by adding the relative statistical uncertainties of the corresponding data points in the nonphotonic electron and the $e_B/(e_B + e_D)$ measurement in quadrature. The systematic uncertainties are treated similarly, except that the uncertainties from the interpolation process are also included. The measured bottom electrons are consistent with the central value of FONLL calculation and the charm electrons are in between the central value and upper limit of the FONLL calculation, the uncertainties of which are from the variation of heavy quark masses and scales. From the measured spectrum, we determine the integrated cross section of electrons ($\frac{e^+ + e^-}{2}$) at

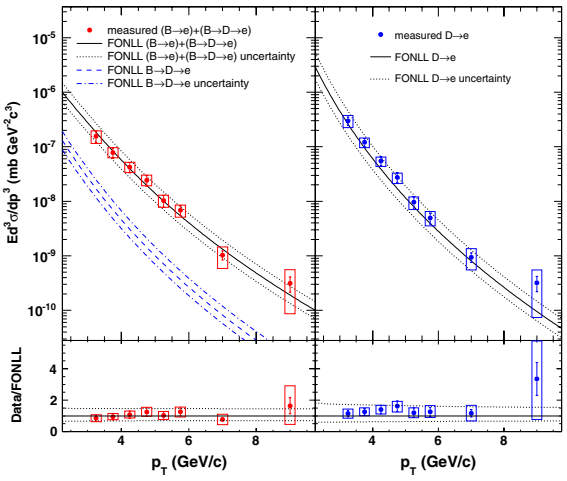

FIG. 17 (color online). Invariant cross section of electrons ($\frac{e^+ + e^-}{2}$) from bottom (upper left) and charm meson (upper right) decay, together with the ratio of the corresponding measurements to the FONLL predictions for bottom (lower left) and charm electrons (lower right). The solid circles are experimental measurements. The error bars and the boxes are, respectively, the statistical and systematic uncertainties. The solid and dotted curves are the FONLL predictions and their uncertainties. The dashed and dot-dashed curves are the FONLL prediction for B → D → e, i.e. electrons from the decays of D mesons which in turn come from B meson decays.

3 GeV/c < p_T < 10 GeV/c from bottom and charm meson decays to be, respectively,

$$\left.\frac{d\sigma_{(B\to e)+(B\to D\to e)}}{dy_e}\right|_{y_e=0} = 4.0 \pm 0.5(\text{stat}) \pm 1.1(\text{syst})\ \text{nb}\left.\frac{d\sigma_{D\to e}}{dy_e}\right|_{y_e=0} = 6.2 \pm 0.7(\text{stat}) \pm 1.5(\text{syst})\ \text{nb},$$

where y_e is the electron rapidity. The 8.1% global scale uncertainty from the BBC cross section is included in the total systematic uncertainty.

Relying on theoretical model predictions to extrapolate the measured results to the phase space beyond the reach of the experiment, one can estimate the total cross section for charm or bottom quark production. We perform a PYTHIA calculation with the same parameters as in Ref. [15]. After normalizing the p_T spectrum to our high-p_T measurements and extrapolating the results to the full kinematic phase space, we obtain a total bottom production cross section of 1.34μb. However, with the PYTHIA calculation using the same parameters except MSEL = 5, i.e. bottom production processes instead of minimum-bias processes as in the former calculation, we obtain a value of 1.83μb. The PYTHIA authors recommend the minimum-bias processes [31]. This large variation between the extracted total

Article reprint

bottom production cross sections comes mostly from the large difference in the shape of the bottom electron spectrum in the two PYTHIA calculations with MSEL = 1 and with MSEL = 5. Since both calculations are normalized to the measured data, the difference in the shape shows up at $p_T < 3$ GeV/c. The fact that the PYTHIA calculation with MSEL = 5 only includes leading-order diagrams of bottom production causes the difference between the PYTHIA calculations. Measurements in the low p_T region are therefore important for the understanding of bottom quark production at RHIC. Both values are consistent with the FONLL [2] prediction, $1.87^{+0.99}_{-0.67}$ μb, within its uncertainty.

V. CONCLUSIONS

STAR measurements of high p_T nonphotonic electron production in $p + p$ collisions at $\sqrt{s} = 200$ GeV using data from Run2005 and Run2008 agree with each other despite the large difference in background. This measurement and PHENIX measurement are consistent with each other within the quoted uncertainties. After correcting a mistake in the photonic electron reconstruction efficiency, the published STAR result using year 2003 data is consistent with our present measurements. We are able to disentangle the electrons from bottom and charm meson decays in the nonphotonic electron spectrum using the measured ratio of $e_B/(e_B + e_D)$ and the measured nonphotonic cross section. The integrated bottom and charm electron cross sections ($\frac{e^+ + e^-}{2}$) at 3 GeV/c < p_T < 10 GeV/c are determined separately as

$$\left.\frac{d\sigma_{(B\to e)+(B\to D\to e)}}{dy_e}\right|_{y_e=0} = 4.0 \pm 0.5(\text{stat}) \pm 1.1(\text{syst})\ \text{nb}\left.\frac{d\sigma_{D\to e}}{dy_e}\right|_{y_e=0} = 6.2 \pm 0.7(\text{stat}) \pm 1.5(\text{syst})\ \text{nb}.$$

FONLL can describe these measurements within its theoretical uncertainties. Future measurements on low-p_T electrons from bottom meson decay are important to overcome the large uncertainties of the derived total bottom quark production cross section that originate mostly from the large variations of theoretical model prediction in the low-p_T region.

ACKNOWLEDGMENTS

We thank the RHIC Operations Group and RCF at BNL, the NERSC Center at LBNL, and the Open Science Grid consortium for providing resources and support. This work was supported in part by the Offices of NP and HEP within the U.S. DOE Office of Science, the U.S. NSF, the Sloan Foundation, the DFG cluster of excellence "Origin and Structure of the Universe"of Germany, CNRS/IN2P3, FAPESP CNPq of Brazil, Ministry of Education and Science of the Russian Federation, NNSFC, CAS, MoST, and MoE of China, GA and MSMT of the Czech Republic, FOM and NWO of the Netherlands, DAE, DST, and CSIR of India, Polish Ministry of Science and Higher Education, Korea Research Foundation, Ministry of Science, Education and Sports of the Republic Of Croatia, and RosAtom of Russia.

[1] M. Cacciari, Nucl. Phys. **A783**, 189 (2007).
[2] M. Cacciari, P. Nason, and R. Vogt, Phys. Rev. Lett. **95**, 122001 (2005); R. Vogt (private communication).
[3] S. Frixione, Eur. Phys. J. C **43**, 103 (2005).
[4] A. D. Frawley, T. Ullrich, and R. Vogt, Phys. Rep. **462**, 125 (2008).
[5] M. G. Mustafa, D. Pal, D. K. Srivastava, and M. Thoma, Phys. Lett. B **428**, 234 (1998).
[6] M. Djordjevic, M. Gyulassy, R. Vogt, and S. Wicks, Phys. Lett. B **632**, 81 (2006).
[7] S. Wicks, W. Horowitz, M. Djordjevic, and M. Gyulassy, Nucl. Phys. **A784**, 426 (2007).
[8] M. Djordjevic and U. W. Heinz, Phys. Rev. Lett. **101**, 022302 (2008).
[9] R. Sharma, I. Vitev, and B. W. Zhang, Phys. Rev. C **80**, 054902 (2009).
[10] G. D. Moore and D. Teaney, Phys. Rev. C **71**, 064904 (2005).
[11] H. van Hees, V. Greco, and R. Rapp, Phys. Rev. C **73**, 034913 (2006).
[12] L. Grandchamp and R. Rapp, Nucl. Phys. **A715**, 545 (2003).
[13] B. I. Abelev *et al.* (STAR Collaboration), Phys. Rev. D **79**, 112006 (2009).
[14] S. Baumgart, Eur. Phys. J. C **62**, 3 (2009).
[15] J. Adams *et al.* (STAR Collaboration), Phys. Rev. Lett. **94**, 062301 (2005).
[16] B. I. Abelev *et al.* (STAR Collaboration), Phys. Rev. Lett. **98**, 192301 (2007); B. I. Abelev *et al.* (STAR Collaboration), arXiv:nucl-ex/0607012v3.
[17] A. Adare *et al.* (PHENIX Collaboration), Phys. Rev. Lett. **97**, 252002 (2006).
[18] S. S. Adler *et al.* (PHENIX Collaboration), Phys. Rev. Lett. **96**, 032301 (2006).
[19] M. M. Aggarwal *et al.* (STAR Collaboration), Phys. Rev. Lett. **105**, 202301 (2010).
[20] K. H. Ackermann *et al.*, Nucl. Instrum. Methods Phys. Res., Sect. A **499**, 624 (2003).
[21] M. Anderson *et al.*, Nucl. Instrum. Methods Phys. Res., Sect. A **499**, 659 (2003); M. Andersen *et al.*,

Article reprint

Nucl. Instrum. Methods Phys. Res., Sect. A **499**, 679 (2003).
[22] M. Beddo *et al.*, Nucl. Instrum. Methods Phys. Res., Sect. A **499**, 725 (2003).
[23] J. Kiryluk (STAR Collaboration), in Proceedings of the 16th International Spin Physics Symposium (World Scientific, Singapore, 2005), p. 718.
[24] J. Adams *et al.* (STAR Collaboration), Phys. Rev. Lett. **91**, 172302 (2003).
[25] W. J. Llope *et al.*, Nucl. Instrum. Methods Phys. Res., Sect. A **522**, 252 (2004).
[26] F. Jin (STAR Collaboration), J. Phys. G **36**, 064051 (2009).
[27] B. I. Abelev *et al.* (STAR Collaboration), Phys. Rev. C **81**, 064904 (2010).
[28] Y. Xu and Olga Barannikova *et al.*, arXiv:0807.4303v2.
[29] H. Bichsel, Nucl. Instrum. Methods Phys. Res., Sect. A **562**, 154 (2006).
[30] W. Dong, Ph.D. thesis, University of California Los Angeles, 2006, http://drupal.star.bnl.gov/STAR/files/startheses/2006/dong_eijiang.pdf.
[31] T. Sjostrand *et al.*, J. High Energy Phys. 05 (2006) 026.
[32] A. Adare *et al.* (PHENIX Collaboration), Phys. Rev. C **81**, 034911 (2010); Y. Akiba (private communication).
[33] S. S. Adler *et al.* (PHENIX Collaboration), Phys. Rev. Lett. **94**, 232301 (2005).
[34] GEANT 3.21, http://wwwasdoc.web.cern.ch/wwwasdoc/geant html3/geantall.html.
[35] N. M. Kroll and W. Wada, Phys. Rev. **98**, 1355 (1955).
[36] C. Amsler *et al.* (Particle Data Group), Phys. Lett. B **667**, 1 (2008).
[37] R. Arnaldi *et al.* (NA60 Collaboration), Phys. Lett. B **677**, 260 (2009).
[38] A. Adare *et al.* (PHENIX Collaboration), arXiv:1005.1627.
[39] A. Adare *et al.* (PHENIX Collaboration), Phys. Rev. D **82**, 012001 (2010).
[40] B. I. Abelev *et al.* (STAR Collaboration), Phys. Rev. C **80**, 041902 (2009).
[41] C. L. D. Silva (private communication).
[42] R. Vogt (private communication).
[43] B. I. Abelev *et al.* (STAR Collaboration), Phys. Rev. D **82**, 012004 (2010).
[44] W. Vogelsang (private communication).
[45] A. Valassi, Nucl. Instrum. Methods Phys. Res., Sect. A **500**, 391 (2003).
[46] X. Lin, arXiv:hep-ph/0602067.

Article reprint

PHYSICAL REVIEW D **86,** 072013 (2012)

Measurements of D^0 and D^* production in $p + p$ collisions at $\sqrt{s} = 200$ GeV

L. Adamczyk,[1] G. Agakishiev,[19] M. M. Aggarwal,[30] Z. Ahammed,[49] A. V. Alakhverdyants,[19] I. Alekseev,[17] J. Alford,[20] B. D. Anderson,[20] C. D. Anson,[28] D. Arkhipkin,[3] E. Aschenauer,[3] G. S. Averichev,[19] J. Balewski,[24] A. Banerjee,[49] Z. Barnovska,[12] D. R. Beavis,[3] R. Bellwied,[45] M. J. Betancourt,[24] R. R. Betts,[9] A. Bhasin,[18] A. K. Bhati,[30] H. Bichsel,[51] J. Bielcik,[11] J. Bielcikova,[12] L. C. Bland,[3] I. G. Bordyuzhin,[17] W. Borowski,[42] J. Bouchet,[20] A. V. Brandin,[27] S. G. Brovko,[5] E. Bruna,[53] S. Bueltmann,[29] I. Bunzarov,[19] T. P. Burton,[3] J. Butterworth,[37] X. Z. Cai,[41] H. Caines,[53] M. Calderón de la Barca Sánchez,[5] D. Cebra,[5] R. Cendejas,[6] M. C. Cervantes,[43] P. Chaloupka,[12] S. Chattopadhyay,[49] H. F. Chen,[39] J. H. Chen,[41] J. Y. Chen,[8] L. Chen,[8] J. Cheng,[46] M. Cherney,[10] A. Chikanian,[53] W. Christie,[3] P. Chung,[12] J. Chwastowski,[43] M. J. M. Codrington,[43] R. Corliss,[24] J. G. Cramer,[51] H. J. Crawford,[4] X. Cui,[39] A. Davila Leyva,[44] L. C. De Silva,[45] R. R. Debbe,[3] T. G. Dedovich,[19] J. Deng,[40] R. Derradi de Souza,[7] S. Dhamija,[16] L. Didenko,[3] F. Ding,[5] A. Dion,[3] P. Djawotho,[43] X. Dong,[23] J. L. Drachenberg,[43] J. E. Draper,[5] C. M. Du,[22] L. E. Dunkelberger,[6] J. C. Dunlop,[3] L. G. Efimov,[19] M. Elnimr,[52] J. Engelage,[4] G. Eppley,[37] L. Eun,[23] O. Evdokimov,[9] R. Fatemi,[21] S. Fazio,[3] J. Fedorisin,[19] R. G. Fersch,[21] P. Filip,[19] E. Finch,[53] Y. Fisyak,[3] C. A. Gagliardi,[43] D. R. Gangadharan,[28] F. Geurts,[37] S. Gliske,[2] Y. N. Gorbunov,[10] O. G. Grebenyuk,[23] D. Grosnick,[48] S. Gupta,[18] W. Guryn,[3] B. Haag,[5] O. Hajkova,[11] A. Hamed,[43] L-X. Han,[41] J. W. Harris,[53] J. P. Hays-Wehle,[24] S. Heppelmann,[32] A. Hirsch,[34] G. W. Hoffmann,[44] D. J. Hofman,[9] S. Horvat,[53] B. Huang,[3] H. Z. Huang,[6] P. Huck,[8] T. J. Humanic,[28] L. Huo,[43] G. Igo,[6] W. W. Jacobs,[16] C. Jena,[14] J. Joseph,[20] E. G. Judd,[4] S. Kabana,[42] K. Kang,[46] J. Kapitan,[12] K. Kauder,[9] H. W. Ke,[8] D. Keane,[20] A. Kechechyan,[19] A. Kesich,[5] D. Kettler,[51] D. P. Kikola,[34] J. Kiryluk,[23] A. Kisiel,[50] V. Kizka,[19] S. R. Klein,[23] D. D. Koetke,[48] T. Kollegger,[13] J. Konzer,[34] I. Koralt,[29] L. Koroleva,[17] W. Korsch,[21] L. Kotchenda,[27] P. Kravtsov,[27] K. Krueger,[2] L. Kumar,[20] M. A. C. Lamont,[3] J. M. Landgraf,[3] S. LaPointe,[52] J. Lauret,[3] A. Lebedev,[3] R. Lednicky,[19] J. H. Lee,[3] W. Leight,[24] M. J. LeVine,[3] C. Li,[39] L. Li,[44] W. Li,[41] X. Li,[34] X. Li,[40] Y. Li,[46] Z. M. Li,[8] L. M. Lima,[38] M. A. Lisa,[28] F. Liu,[8] T. Ljubicic,[3] W. J. Llope,[37] R. S. Longacre,[3] Y. Lu,[39] X. Luo,[8] A. Luszczak,[41] G. L. Ma,[41] Y. G. Ma,[41] D. M. M. D. Madagodagettige Don,[10] D. P. Mahapatra,[14] R. Majka,[53] O. I. Mall,[5] S. Margetis,[20] C. Markert,[44] H. Masui,[23] H. S. Matis,[23] D. McDonald,[37] T. S. McShane,[10] S. Mioduszewski,[43] M. K. Mitrovski,[3] Y. Mohammed,[43] B. Mohanty,[49] B. Morozov,[17] M. G. Munhoz,[38] M. K. Mustafa,[34] M. Naglis,[23] B. K. Nandi,[15] Md. Nasim,[49] T. K. Nayak,[49] L. V. Nogach,[33] J. Novak,[26] G. Odyniec,[23] A. Ogawa,[3] K. Oh,[35] A. Ohlson,[53] V. Okorokov,[27] E. W. Oldag,[44] R. A. N. Oliveira,[38] D. Olson,[23] P. Ostrowski,[50] M. Pachr,[11] B. S. Page,[16] S. K. Pal,[49] Y. X. Pan,[6] Y. Pandit,[20] Y. Panebratsev,[19] T. Pawlak,[50] B. Pawlik,[31] H. Pei,[9] C. Perkins,[4] W. Peryt,[50] P. Pile,[3] M. Planinic,[54] J. Pluta,[50] D. Plyku,[29] N. Poljak,[54] J. Porter,[23] A. M. Poskanzer,[23] C. B. Powell,[23] D. Prindle,[51] C. Pruneau,[52] N. K. Pruthi,[30] M. Przybycien,[1] P. R. Pujahari,[15] J. Putschke,[52] H. Qiu,[23] R. Raniwala,[36] S. Raniwala,[36] R. L. Ray,[44] R. Redwine,[24] R. Reed,[5] C. K. Riley,[53] H. G. Ritter,[23] J. B. Roberts,[37] O. V. Rogachevskiy,[19] J. L. Romero,[5] J. F. Ross,[10] L. Ruan,[3] J. Rusnak,[12] N. R. Sahoo,[49] I. Sakrejda,[23] S. Salur,[23] A. Sandacz,[50] J. Sandweiss,[53] E. Sangaline,[5] A. Sarkar,[15] J. Schambach,[44] R. P. Scharenberg,[34] A. M. Schmah,[23] B. Schmidke,[3] N. Schmitz,[25] T. R. Schuster,[13] J. Seele,[24] J. Seger,[10] P. Seyboth,[25] N. Shah,[6] E. Shahaliev,[19] M. Shao,[39] B. Sharma,[30] M. Sharma,[52] S. S. Shi,[8] Q. Y. Shou,[41] E. P. Sichtermann,[23] R. N. Singaraju,[49] M. J. Skoby,[34] D. Smirnov,[3] N. Smirnov,[53] D. Solanki,[36] P. Sorensen,[3] U. G. deSouza,[38] H. M. Spinka,[2] B. Srivastava,[34] T. D. S. Stanislaus,[48] S. G. Steadman,[24] J. R. Stevens,[16] R. Stock,[13] M. Strikhanov,[27] B. Stringfellow,[34] A. A. P. Suaide,[38] M. C. Suarez,[9] M. Sumbera,[12] X. M. Sun,[23] Y. Sun,[39] Z. Sun,[22] B. Surrow,[24] D. N. Svirida,[17] T. J. M. Symons,[23] A. Szanto de Toledo,[38] J. Takahashi,[7] A. H. Tang,[3] Z. Tang,[39] L. H. Tarini,[52] T. Tarnowsky,[26] D. Thein,[44] J. H. Thomas,[23] J. Tian,[41] A. R. Timmins,[45] D. Tlusty,[12] M. Tokarev,[19] T. A. Trainor,[51] S. Trentalange,[6] R. E. Tribble,[43] P. Tribedy,[49] B. A. Trzeciak,[50] O. D. Tsai,[6] J. Turnau,[31] T. Ullrich,[3] D. G. Underwood,[2] G. Van Buren,[3] G. van Nieuwenhuizen,[24] J. A. Vanfossen, Jr.,[20] R. Varma,[15] G. M. S. Vasconcelos,[7] F. Videbæk,[3] Y. P. Viyogi,[49] S. Vokal,[19] S. A. Voloshin,[52] A. Vossen,[16] M. Wada,[44] F. Wang,[34] G. Wang,[6] H. Wang,[26] J. S. Wang,[22] Q. Wang,[34] X. L. Wang,[39] Y. Wang,[46] G. Webb,[21] J. C. Webb,[3] G. D. Westfall,[26] C. Whitten, Jr.,[6,*] H. Wieman,[23] S. W. Wissink,[16] R. Witt,[47] W. Witzke,[21] Y. F. Wu,[8] Z. Xiao,[46] W. Xie,[34] K. Xin,[37] H. Xu,[22] N. Xu,[23] Q. H. Xu,[40] W. Xu,[6] Y. Xu,[39] Z. Xu,[3] L. Xue,[41] Y. Yang,[22] Y. Yang,[8] P. Yepes,[37] Y. Yi,[34] K. Yip,[3] I-K. Yoo,[35] M. Zawisza,[50] H. Zbroszczyk,[50] J. B. Zhang,[8] S. Zhang,[41] W. M. Zhang,[20] X. P. Zhang,[46] Y. Zhang,[39] Z. P. Zhang,[39] F. Zhao,[6] J. Zhao,[41] C. Zhong,[41] X. Zhu,[46] Y. H. Zhu,[41] and Y. Zoulkarneeva[19]

(STAR Collaboration)

[1]*AGH University of Science and Technology, Cracow, Poland*
[2]*Argonne National Laboratory, Argonne, Illinois 60439, USA*

Article reprint

[3]*Brookhaven National Laboratory, Upton, New York 11973, USA*
[4]*University of California, Berkeley, California 94720, USA*
[5]*University of California, Davis, California 95616, USA*
[6]*University of California, Los Angeles, California 90095, USA*
[7]*Universidade Estadual de Campinas, Sao Paulo, Brazil*
[8]*Central China Normal University (HZNU), Wuhan 430079, China*
[9]*University of Illinois at Chicago, Chicago, Illinois 60607, USA*
[10]*Creighton University, Omaha, Nebraska 68178, USA*
[11]*Czech Technical University in Prague, FNSPE, Prague, 115 19, Czech Republic*
[12]*Nuclear Physics Institute AS CR, 250 68 Řež/Prague, Czech Republic*
[13]*University of Frankfurt, Frankfurt, Germany*
[14]*Institute of Physics, Bhubaneswar 751005, India*
[15]*Indian Institute of Technology, Mumbai, India*
[16]*Indiana University, Bloomington, Indiana 47408, USA*
[17]*Alikhanov Institute for Theoretical and Experimental Physics, Moscow, Russia*
[18]*University of Jammu, Jammu 180001, India*
[19]*Joint Institute for Nuclear Research, Dubna, 141 980, Russia*
[20]*Kent State University, Kent, Ohio 44242, USA*
[21]*University of Kentucky, Lexington, Kentucky, 40506-0055, USA*
[22]*Institute of Modern Physics, Lanzhou, China*
[23]*Lawrence Berkeley National Laboratory, Berkeley, California 94720, USA*
[24]*Massachusetts Institute of Technology, Cambridge, Massachusetts 02139-4307, USA*
[25]*Max-Planck-Institut für Physik, Munich, Germany*
[26]*Michigan State University, East Lansing, Michigan 48824, USA*
[27]*Moscow Engineering Physics Institute, Moscow, Russia*
[28]*Ohio State University, Columbus, Ohio 43210, USA*
[29]*Old Dominion University, Norfolk, Virginia, 23529, USA*
[30]*Panjab University, Chandigarh 160014, India*
[31]*Institute of Nuclear Physics PAS, Cracow, Poland*
[32]*Pennsylvania State University, University Park, Pennsylvania 16802, USA*
[33]*Institute of High Energy Physics, Protvino, Russia*
[34]*Purdue University, West Lafayette, Indiana 47907, USA*
[35]*Pusan National University, Pusan, Republic of Korea*
[36]*University of Rajasthan, Jaipur 302004, India*
[37]*Rice University, Houston, Texas 77251, USA*
[38]*Universidade de Sao Paulo, Sao Paulo, Brazil*
[39]*University of Science and Technology of China, Hefei 230026, China*
[40]*Shandong University, Jinan, Shandong 250100, China*
[41]*Shanghai Institute of Applied Physics, Shanghai 201800, China*
[42]*SUBATECH, Nantes, France*
[43]*Texas A&M University, College Station, Texas 77843, USA*
[44]*University of Texas, Austin, Texas 78712, USA*
[45]*University of Houston, Houston, Texas, 77204, USA*
[46]*Tsinghua University, Beijing 100084, China*
[47]*United States Naval Academy, Annapolis, Maryland 21402, USA*
[48]*Valparaiso University, Valparaiso, Indiana 46383, USA*
[49]*Variable Energy Cyclotron Centre, Kolkata 700064, India*
[50]*Warsaw University of Technology, Warsaw, Poland*
[51]*University of Washington, Seattle, Washington 98195, USA*
[52]*Wayne State University, Detroit, Michigan 48201, USA*
[53]*Yale University, New Haven, Connecticut 06520, USA*
[54]*University of Zagreb, Zagreb, HR-10002, Croatia*

(Received 19 April 2012; revised manuscript received 15 October 2012; published 31 October 2012)

We report measurements of charmed-hadron (D^0, D^*) production cross sections at midrapidity in $p + p$ collisions at a center-of-mass energy of 200 GeV by the STAR experiment. Charmed hadrons were reconstructed via the hadronic decays $D^0 \to K^-\pi^+$, $D^{*+} \to D^0\pi^+ \to K^-\pi^+\pi^+$ and their charge conjugates, covering the p_T range of 0.6–2.0 and 2.0–6.0 GeV/c for D^0 and D^{*+}, respectively. From this analysis,

[*]Deceased.

Article reprint

the charm-pair production cross section at midrapidity is $d\sigma/dy|_{y=0}^{c\bar{c}} = 170 \pm 45(\text{stat})^{+38}_{-59}(\text{sys})\ \mu\text{b}$. The extracted charm-pair cross section is compared to perturbative QCD calculations. The transverse momentum differential cross section is found to be consistent with the upper bound of a fixed-order next-to-leading logarithm calculation.

DOI: 10.1103/PhysRevD.86.072013 PACS numbers: 25.75.−q, 25.75.Cj

I. INTRODUCTION

The primary goal of ultrarelativistic heavy-ion experiments at the Relativistic Heavy Ion Collider (RHIC) is to search for and characterize the new state of matter with partonic degrees of freedom, namely, the quark-gluon plasma, predicted by quantum chromodynamics (QCD) [1]. In high-energy collisions at RHIC, heavy quarks (c, b) are expected to be created from initial hard scatterings [2] and the relative changes in their masses are small by the strong interactions with the QCD medium [3]. Thus they carry clean information from the system at the early stage. The interaction between heavy quarks and the medium is sensitive to the medium dynamics; therefore, heavy quarks are suggested as an ''ideal'' probe to quantify the properties of the strongly interacting QCD matter [4–6]. Consequently, measurements of heavy-quark production over a wide transverse momentum (p_T) region in proton-proton ($p + p$) collisions are critical to provide a baseline for understanding the results from heavy-ion collisions. In particular, precise knowledge of the total charm production cross sections from $p + p$ to central heavy-ion collisions is critical to understand both open charm and charmonium production mechanisms in the quark-gluon plasma medium formed in central heavy-ion collisions at RHIC [7,8].

In elementary particle collisions, processes involving heavy quarks with masses much larger than the QCD scale (Λ_{QCD}) are, in principle, amenable to perturbative QCD (pQCD) calculations. For heavy-quark production cross sections at large momentum transfer Q^2, fixed-order next-to-leading logarithm (FONLL) pQCD calculations, where $p_T \gg m_c$, are expected to work reasonably well [9]. However, calculations of the charm cross section at low p_T become complicated because charm quarks cannot be treated as a massless flavor. Furthermore, in the low momentum transfer region there is a large uncertainty in the gluon density function, and the strong coupling constant increases dramatically. Thus, perturbative QCD calculations have little predictive power for the total charm cross section in high-energy hadron-hadron collisions [10]. In view of these theoretical issues, experimental measurements become necessary and in turn provide constraints that improve theoretical calculations.

Measurements of inclusive charm production have been carried out through two main approaches: (i) single leptons from heavy-flavor semileptonic decays and (ii) charmed hadrons from hadronic decays. The advantages of the first method include an experimentally triggerable observable and relatively large decay branching ratios, thus resulting in relatively large statistics. However, interpretations of the experimental results contain ambiguities because (a) leptons are produced by various charmed and bottomed hadron decays, and (b) heavy-flavor hadrons contributing to leptons at a certain p_T can come from a wide kinematic region due to the decay smearing. The second method suffers from a large combinatorial background when all particles from the collision vertex are included, without any reconstruction of the secondary weak-decay vertices. This background is particularly large (S/B is on the order of $1{:}10^3$) in heavy-ion collisions.

There are many measurements of the charm production cross section in low energy $p + p$ or $p + \text{A}$ collisions via both semileptonic and hadronic decays at CERN and Fermilab [11,12]. Results for the total charm cross sections (from measurements with reasonable extrapolations) are consistent with next-to-leading-order pQCD calculations. At high energies, the Collider Detector at Fermilab (CDF) Collaboration at the Tevatron measured the charmed-hadron cross sections at $p_T > 5$ GeV/c in $p + \bar{p}$ collisions at $\sqrt{s} = 1.96$ TeV, and results for D^0, D^+ and D^{*+} mesons are consistent with the upper bounds of FONLL pQCD calculations [13]. At RHIC energies, charm production has been studied mainly via semileptonic decay electrons from $p + p$ to Au + Au collisions [14–18]. The result from $p + p$ collisions is also consistent with the upper bound of FONLL pQCD calculations at $p_T(e) > 2$ GeV/c. Measurements of the D^0 cross section by the reconstruction of hadronic decays were carried out in $d + \text{Au}$ collisions [14], but no measurement of the charmed-hadron production cross section in $p + p$ collisions has been made at RHIC until now.

In this paper, we report measurements from the STAR experiment of the charmed-hadron (D^0, D^*) production cross section at midrapidity in $p + p$ collisions at $\sqrt{s} =$ 200 GeV. Charmed hadrons, D^0 and D^*, were reconstructed via hadronic decays in the transverse momentum ranges of 0.6–2.0 and 2–6 GeV/c, respectively. The p_T differential production cross sections are compared to pQCD theoretical calculations, and a total charm cross section is extracted.

The paper is organized as follows: Section II describes the experimental setup, the data set, and the particle-identification method used in this analysis. Section III explains the hadronic reconstruction for D^0 and D^* mesons in detail. Section IV discusses the reconstruction efficiency, acceptance, and trigger and vertex corrections.

Details of the systematic uncertainties are discussed in Sec. V. The transverse momentum differential production cross section is presented in Sec. VI and it is compared with pQCD FONLL and PYTHIA [19] calculations. The results are summarized in Sec. VII.

II. EXPERIMENTAL SETUP

A. Detector apparatus

The data used in this analysis were recorded by the Solenoidal Tracker at RHIC (STAR) detector [20]. The STAR detector is a multipurpose spectrometer with large rapidity coverage. The major subsystems at midrapidity sit inside a solenoidal magnet which provides a uniform magnetic field of 0.5 T along the beam axis. Subsystems used in this analysis are the time projection chamber (TPC) [21], the time-of-flight (TOF) detector [22], the barrel and end cap electromagnetic calorimeters [23,24], and two trigger detector subsystems: the vertex position detector (VPD) [25] and the beam beam counters (BBCs) [26].

The TPC is the main tracking detector, covering the full azimuthal angle at pseudorapidity $|\eta| < 1$ for tracks crossing all 45 padrows [21]. It measures the charged-particle momenta and provides particle-identification (PID) capability via the ionization energy loss (dE/dx) in the TPC gas, allowing a clean separation between charged kaons and pions up to momentum $p \sim 0.6$ GeV/c. The barrel TOF detector is a newly installed subsystem, utilizing the multigap resistive plate chamber technology [22]. The full system consists of 120 trays covering the full azimuth at $|\eta| < 0.9$ surrounding the TPC cylinder. In the year 2009 run, 84 trays out of 120 for the full barrel were installed and used for this analysis. The TOF detector uses the timing recorded in the forward VPD as the start time to calculate the particle time of flight, which is combined with the momentum from the TPC to identify particles. The timing resolution of the TOF system, including the start timing resolution in $\sqrt{s} = 200$ GeV $p + p$ collisions, is about 110 ps, allowing separation of K and π up to $p \sim 1.5$ GeV/c. The barrel and end cap electromagnetic calorimeters are designed to identify electrons and photons, covering the full azimuthal angle at $|\eta| < 1$ and $1 < \eta < 2$, respectively [23,24]. They are fast-response detectors (< 100 ns) and were used to suppress the TPC pileup-track contribution in the event-vertex finder by matching with charged tracks from the TPC.

In addition to providing the start time for the barrel TOF detector, the VPD is also one of the trigger detectors in STAR. It has two parts surrounding the beam pipe, located on the east and west sides, 5.7 m away from the center of the STAR detector and covering $4.24 < |\eta| < 5.1$ [25]. The minimum-bias trigger was defined as a coincidence signal in the east and west VPDs and a selection was made on the vertex position along the beam axis (V_z) to be within 40 cm of the center of the STAR detector. The BBC [26] consists of two identical counters located on each side of the TPC covering full azimuth and $2.1 < |\eta| < 5.0$ in pseudorapidity. Each part consists of a set of hexagonal scintillator tiles grouped into a ring and mounted around the beam pipe at a distance of 3.7 m from the center of STAR. The BBC detector had been used to define the main minimum-bias trigger in $p + p$ collisions before the minimum-bias trigger was used in 2009. A small sample of BBC minimum-bias-triggered events were collected in 2009 to check for a trigger bias. Details of the minimum-bias trigger bias and correction will be discussed in Sec. IV.

B. Data sets and event selection

The data sample used in this analysis consisted of minimum-bias-triggered $p + p$ collisions at $\sqrt{s} =$ 200 GeV, recorded in 2009 by the STAR experiment at RHIC.

The intrinsic drift time for electrons from the center to one end of the TPC is on the order of 40 μs. Thus, in high-luminosity $p + p$ collisions, one TPC event usually contains tracks from collisions originating from nontriggered bunch crossings. These "pileup events" will lead to additional tracks recorded in the TPC, in addition to those from the triggered event. This effect was not significant in previous RHIC runs, but the increase in the collision rate during 2009 to several hundred kilohertz made this a significant effect. The V_z position from offline VPD data has a resolution of 2.5 cm for minimum-bias events, which can provide a useful constraint to select the real event that fired the trigger. Figure 1, upper panel, shows the correlation between the V_z positions from the TPC and the VPD. Events with TPC vertices along the diagonal correlated band are real ones that fired the VPD minimum-bias trigger. In Fig. 1, bottom panel, the solid black histogram shows the 1D V_z difference between the first TPC-determined vertex position and VPD-determined vertex position. By applying a V_z difference cut $|\Delta Vz| < 6$ cm, most of the TPC pileup events can be removed. There still remain random associated correlations that enter into this cut window ($\sim 7\%$ level, calculated using a two-Gaussian fit). To further suppress this contamination, we required the TPC event vertices to have at least two tracks that match with hits in the barrel and end cap electromagnetic calorimeters (this vertex is treated as a "good" vertex). The red dashed histogram in Fig. 1, bottom panel, shows the ΔVz distribution after this selection. The random associated pileup events in the V_z difference cut window are now suppressed to $\sim 2\%$ of the total, while the corresponding loss of real events is $\sim 15\%$. In total, 105×10^6 minimum-bias events were used in the charmed-hadron analysis.

C. Track reconstruction and particle identification

Charged-particle tracks are required to point within $|\eta| < 1$ in order minimize TPC acceptance effects during reconstruction. Tracks must have 15 out of a maximum of 45 points used in track fitting (nFitPts) and at least 52% of

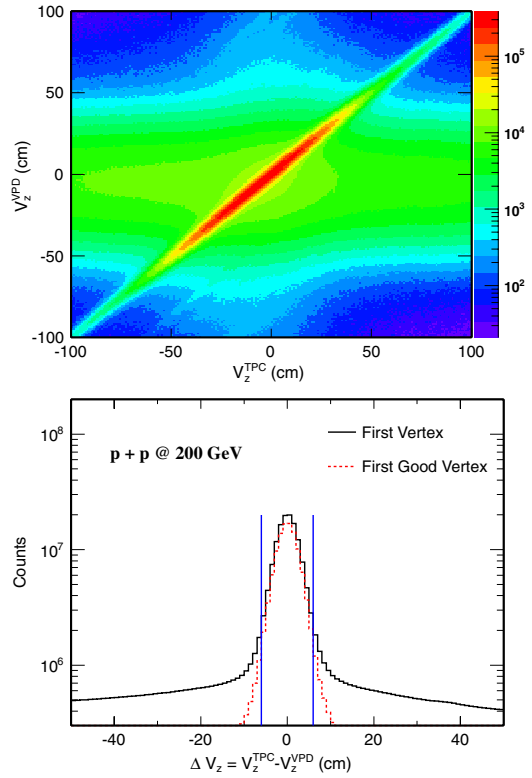

FIG. 1 (color online). Upper panel: Correlation of V_z^{TPC} versus V_z^{VPD}. Bottom panel: ΔV_z distributions. A good vertex requirement rejects most of the pileup events. Blue vertical lines indicate the cuts for the V_z selection.

the total possible fit points in order to avoid double-counting split tracks. Tracks are required to have a distance-of-closest-approach (DCA) to the collision vertex of less than 2 cm to suppress background tracks produced by secondary scattering in the detector and also long-lived particle decays. The STAR track pointing resolution with the TPC alone does not have the precision to separate charm secondary decay vertices from the collision vertices.

Particle identification for final-state charged hadrons was carried out with a combination of dE/dx in the TPC and the particle velocity (β) measurement from the barrel TOF detector. Thus the normalized $dE/dx(n\sigma_X^{dE/dx})$ and $1/\beta(n\sigma_X^{\mathrm{TOF}})$ distributions were used to select daughter particle candidates. They are defined as follows:

$$n\sigma_X^{dE/dx} = \frac{\ln \frac{\langle dE/dx \rangle^{\mathrm{mea}}}{dE/dx_X^{\mathrm{th}}}}{R_{dE/dx}}, \quad (1)$$

$$n\sigma_X^{\mathrm{TOF}} = \frac{\frac{1}{\beta^{\mathrm{mea}}} - \frac{1}{\beta_X^{\mathrm{th}}}}{R_{1/\beta}}, \quad (2)$$

where the superscripts "mea" and "th" are measured and theoretical values, respectively. The X denotes expected values which are calculated with respect to one kind of particle species (π or K). $R_{dE/dx}$ and $R_{1/\beta}$ are the experimental dE/dx and $1/\beta$ resolutions, respectively. With the above definitions, the two resulting distributions can be approximated by Gaussian distributions with mean ~ 0 and $\sigma \sim 1$). Figure 2 shows the $n\sigma_K^{dE/dx}$, $n\sigma_\pi^{dE/dx}$, and $n\sigma_K^{\mathrm{TOF}}$ distributions versus particle momentum.

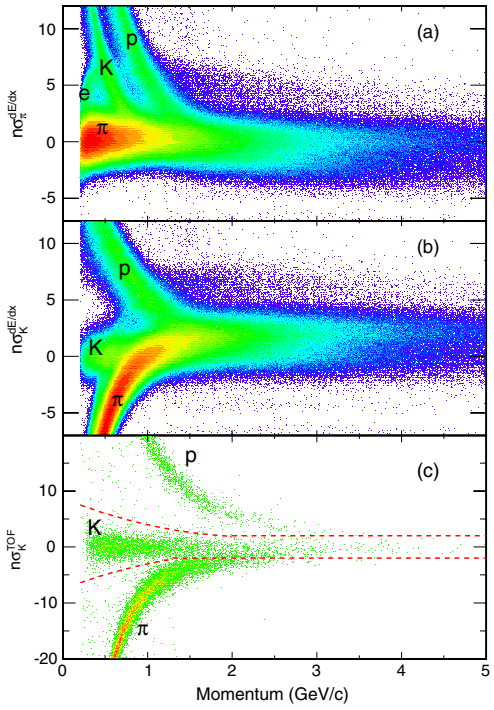

FIG. 2 (color online). Distributions of $n\sigma_\pi^{dE/dx}$, $n\sigma_K^{dE/dx}$, and $n\sigma_K^{\mathrm{TOF}}$ versus momentum are shown in panels (a), (b), and (c), respectively. The latter is shown after dE/dx cuts were applied.

Daughter kaon (pion) candidates are selected by requiring $|n\sigma_K^{dE/dx}| < 2$ ($|n\sigma_\pi^{dE/dx}| < 2$). In addition, to improve the significance of the reconstructed D^0 signal, the kaon daughter tracks were required to have a valid hit in the TOF detector and then selected with a TOF PID cut, which is denoted as the red dashed lines in Fig. 2(c). In order to have good efficiency and considering pion identification is good enough with dE/dx only, we did not require pion to match with TOF.

III. CHARMED-HADRON RECONSTRUCTION AND RAW YIELD EXTRACTION

A. D^0 Reconstruction

D^0 and $\bar{D}^0$ mesons were reconstructed via the hadronic decay $D^0(\bar{D}^0) \to K^{\mp}\pi^{\pm}$ with a branching ratio of 3.89%. The analysis technique is the same as that used for a D^0 analysis in d + Au collisions [14]. In $p + p$ collisions, the

Article reprint

mixed-events technique is not suitable for describing the background due to the large contribution of correlated jets. Therefore, two different techniques were used to reproduce the background: the like-sign and track-rotation methods. Since the π^- and π^+ production is symmetric in the STAR uniform acceptance and their yield ratio is measured to be 0.988 ± 0.043 [27], the like-sign (LS) method is used and a pair combination with the same charged sign is expected to reproduce the background without the signal correlation. The opposite-sign backgrounds, which go into the residual background, are only several percent of the total background and will be discussed later. The track-rotation (Rot) technique has been used in many measurements [28]. This method is based on the assumption that by rotating the daughter kaon track by 180° in azimuth, the decay kinematics are destroyed. Thus the invariant mass distribution after rotation is able to reproduce the random combinatorial background. Figure 3 shows the invariant mass distributions of $K\pi$ candidates. Figure 3(a) shows the invariant mass distributions for $K\pi$ pairs [$0.6 < p_T(K\pi) < 2.0$ GeV/c] with unlike sign (US) before background subtraction, with like sign, and with rotated kaon momentum. The distributions from the like-sign and track-rotation techniques describe the background well. Figure 3(b) is the unlike-sign $K\pi$ invariant mass distribution after combinatorial background subtraction. A significant $K^*(892)$ peak is observed. The secondary small peak at about 1.4 GeV/c^2 is the $K_2^*(1430)$. A direct zoom-in view of the vicinity around the D^0 mass region is shown in Fig. 4 [panel (a) for subtraction of like-sign background, and panel (b) for the rotational case]. Solid symbols depict the same distributions as shown in Figs. 3 and 5 in two different D^0 p_T bins. One can see there is still some "residual" background after like-sign or rotational background subtraction. The possible sources to the residual background have been investigated using PYTHIA simulations. We performed the same reconstruction as we did on the data, for the foreground and background distributions.

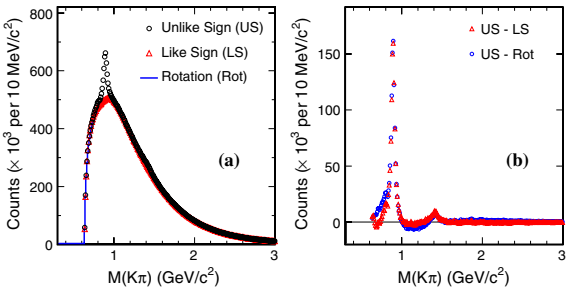

FIG. 3 (color online). (a) Invariant mass distributions of raw $K\pi$ combinations for unlike-sign pairs (circles), like-sign pairs (triangles), and kaon momentum rotated pairs (line). (b) Residual distributions after subtracting the like-sign distribution (triangles) and rotation pair distribution (dots) from the unlike-sign distribution.

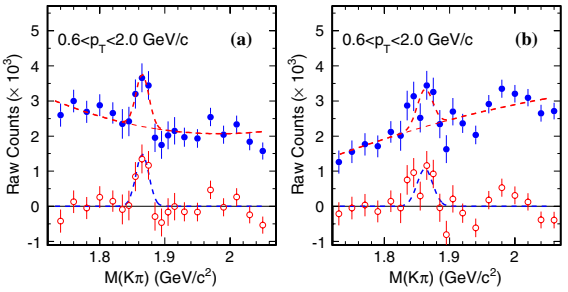

FIG. 4 (color online). Invariant $K\pi$ mass distributions in the D^0 mass region after like-sign (a) and track-rotation (b) background subtraction. Solid circles show the signal and a residual background. A Gaussian function and a second-order polynomial function were used to describe the signal and residual background, respectively. Open circles show the signal after residual background subtraction.

From these simulations, we have learned that the possible sources that can contribute to this residual correlated background include: correlated hadron pairs from decays (mostly resonances) where the real daughters were misidentified as $K\pi$ pairs; $K\pi$ pair from other decay channels of D^0 (e.g. $K^-\pi^+\pi^0$) where the other daughters are missed in the reconstruction; same-charge $K^-\pi^-$ pairs from multibody decays of $D^0 \to K^-\pi^+\pi^+\pi^-$; $K\pi$ pairs from jet fragmentations; etc. The different shape of the residual background from LS and Rot background subtraction in the data can be qualitatively reproduced by PYTHIA simulation. The magnitude of the residual background depends

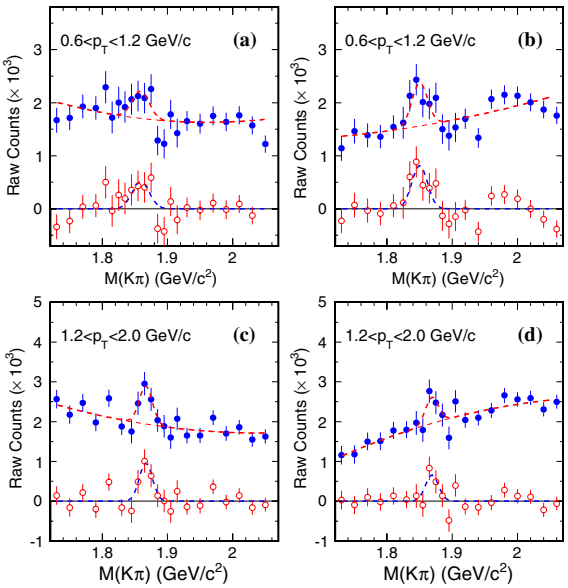

FIG. 5 (color online). Raw D^0 signals in different p_T bins after like-sign (a),(c) and track-rotation (b),(d) subtraction.

TABLE I. D^0 raw yields.

p_T range (GeV/c)	0.6–1.2	1.2–2
p_T (GeV/c)	0.908	1.57
Raw yields $\times 10^3$ (Rot)	2.45 ± 0.66	1.65 ± 0.63
Raw yields $\times 10^3$ (LS)	1.67 ± 0.74	2.40 ± 0.64

on how to choose the normalization for the like-sign or rotational background, as qualitatively understood from the PYTHIA simulations. However, the change of the residual background magnitude due to different normalizations has a very small impact on the final extracted signal counts, and it has been included in the systematic uncertainties. We used an empirical polynomial function to describe it and the choice of this empirical function was also included as one of the systematic source to the raw yields. A Gaussian function is used to fit the signal. The raw yield of the D^0 is obtained by fitting the data (blue solid circles) with a fit function representing the sum of signal and background (red dashed curve) in the mass region of $1.72 < M_{K\pi} < 2.05$ GeV/c^2. The signal after the residual background subtraction is shown as the red open circles. The Gaussian function used to describe the signal is shown as the blue dashed curve. The total D^0 signal consists of 4085 ± 938 counts.

The signals after background subtraction for two p_T bins are shown in Fig. 5. Panels (a), (c) and (b), (d) show the signals from LS and Rot background subtraction, respectively. The D^0 raw yields and statistical errors extracted from the two background methods are listed in Table I. The average values of the D^0 counts from the LS and Rot background methods are used to calculate the final D^0 raw yield in each p_T bin. The mean and width from the Gaussian fits are compared with Monte Carlo (MC) simulation in Fig. 6 (left panels). The single D^0 and D^* are embedded into the real data and simulated in the full STAR GEANT reconstruction chain, taking into account detector response and material effect. The D^0 signal mean value from an open-parameter fit shifts to lower mass due to kaon energy loss at low p_T, which is not fully accounted in the simulation due to possibly missing material budget. The systematic uncertainty in determining the D^0 raw yields as well as the potential double-counting issue due to particle misidentification will be discussed in Sec. VA.

B. D^* Reconstruction

$D^{*\pm}$ mesons were reconstructed via the decay sequence $D^{*+} \to D^0\pi^+(\mathrm{BR} = 67.7\%)$, $D^0 \to K^-\pi^+$ and its charge conjugate. We followed the same analysis technique as described in Ref. [29]. The daughter particles were still identified by dE/dx in the TPC because (a) most of the D^* decay daughter particles that fall inside the STAR acceptance with higher momenta are located in the region where the TOF PID improvement is very limited and (b) the

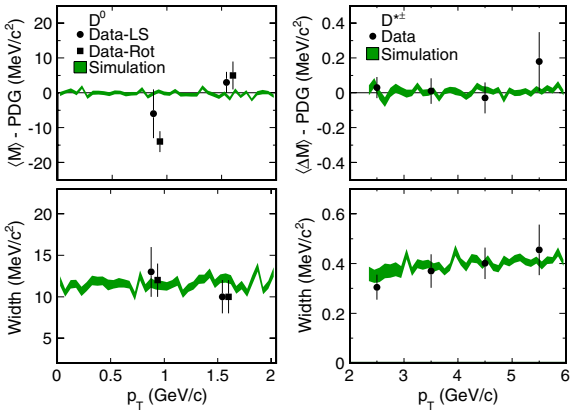

FIG. 6 (color online). The mean and width from Gaussian fit to data (symbols) compared with MC simulations (bands) for D^0 and D^* are shown in left and right panels, respectively.

signal suffers significant losses due to incomplete TOF acceptance in 2009. Compared to the cuts used in Ref. [29], the p_T threshold cut for the π^+ (from D^* decays), denoted as π_s^+, was lowered to 0.15 GeV/c. The ratio r of transverse momenta from the D^0 and π_s^+ was required to be $7 < r < 20$. These two changes were implemented to improve the statistics near the lower bound in p_T. The remainder of the analysis cuts were the same as those used in Ref. [29].

The invariant mass difference $\Delta M = M(K\pi\pi) - M(K\pi)$ was calculated in reconstructing the D^* signal to take advantage of the partial cancellation in the detector resolution in measured mass distributions. The ΔM distributions are shown in the upper panel of Fig. 7. The "right-sign" combinations $K^\mp\pi^\pm\pi_s^\pm$ were used to select the $D^{*\pm}$ candidates. Two independent methods—"wrong-sign" combinations $K^\pm\pi^\mp\pi_s^\pm$ and D^0 "sideband" combinations—were used for combinatorial background reconstruction. The plot illustrates that both methods reproduce the combinatorial background very well. The events displayed in this figure are all minimum-bias events without event-vertex selections, which demonstrates the significance of D^* signal. The lower panel in Fig. 7 shows the $K\pi$ invariant mass distribution after requiring the D^* candidate cut $(0.144 < \Delta M < 0.147$ GeV/$c^2)$. The cross-hatched area indicates D^0 candidate mass selection in the $K\pi\pi$ right-sign and wrong-sign combination reconstruction. The line-hatched area indicates the D^0 sideband region $[1.72 < M(K\pi)/(\mathrm{GeV}/c^2) < 1.80$ or $1.92 < M(K\pi)/(\mathrm{GeV}/c^2) < 2.00]$ used in sideband combinatorial background reconstruction for D^*. The sideband combinatorial background was used to obtain the raw D^* yields for better statistics and also because sideband distributions do not suffer from the double-counting issue due to particle misidentification. The difference between the yields obtained from the sideband method and the

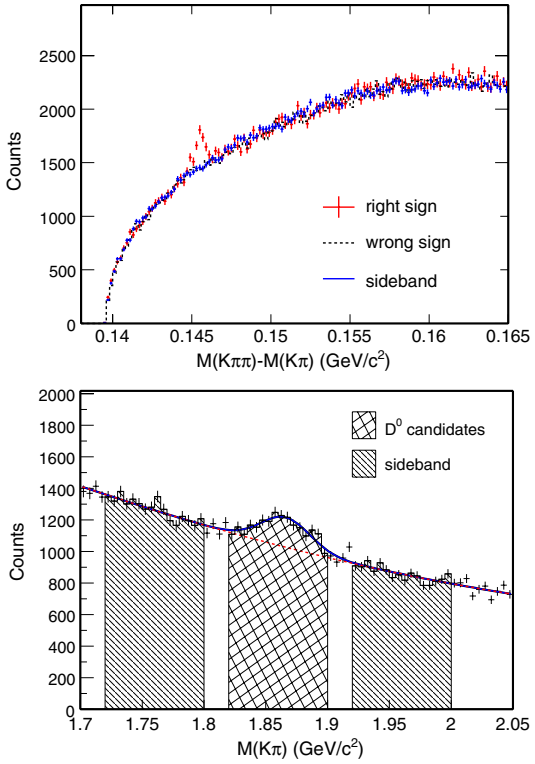

FIG. 7 (color online). Upper: Raw D^* candidate signal from the right-sign combinations in all $p+p$ minimum-bias events. Histograms are combinatorial background distributions from wrong-sign and sideband methods. Lower: Raw D^0 candidates after requiring the D^* candidate cut ($0.144 < \Delta M < 0.147$ GeV/c^2).

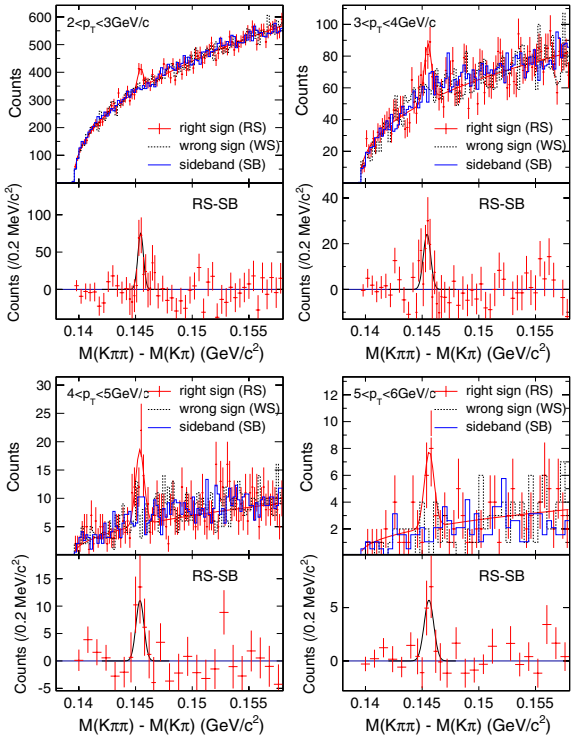

FIG. 8 (color online). Raw D^* signals in different p_T bins. In each plot, the bottom panel distribution is generated by subtracting the sideband background from the right-sign distribution. Variable binning is used in the bottom panel for better illustration.

wrong-sign method was included in the systematic uncertainties. Details in determining the uncertainties on the raw D^* yields including the double-counting effect will be discussed in Sec. VA. The D^* raw yields are summarized in Table II.

To obtain the cross section, the event-selection criteria described in the previous section were applied. The raw distributions were further divided into p_T slices to obtain the raw D^* yields in each p_T bin. Figure 8 shows the D^* candidates and background distributions in different p_T bins. The bottom panel on each plot was generated by subtracting the sideband background from the right-sign candidates. The mean and width from Gaussian fits are compared with MC simulation in the right panel of Fig. 6,

TABLE II. D^* raw yields.

p_T range (GeV/c)	2–3	3–4	4–5	5–6
p_T (GeV/c)	2.45	3.44	4.45	5.45
Raw yields	209 ± 58	98 ± 35	27 ± 11	12.3 ± 4.1

and it shows the obtained D^* peak positions and widths agree with the MC simulation well. From this analysis, the total signal consisted of 364 ± 68 counts, and the raw yield ratio of D^{*-}/D^{*+} is 0.93 ± 0.37.

IV. EFFICIENCY AND TRIGGER OR VERTEX BIAS CORRECTION

The final charmed-hadron cross section in $p+p$ collisions is calculated as follows:

$$E\frac{d^3\sigma}{dp^3} = \frac{1}{2\pi}\cdot\frac{1}{\epsilon_{\rm rec}}\cdot\frac{1}{\rm BR}\cdot\frac{\Delta N_D}{p_T\Delta p_T\Delta y}\cdot\frac{\sigma_{\rm NSD}}{N_{\rm MB}}\cdot f_{\rm trg,vtx}, \quad (3)$$

where $\sigma_{\rm NSD}$ is the total nonsingly diffractive (NSD) cross section, which is measured at STAR to be 30.0 ± 2.4 mb [30]. $N_{\rm MB}$ is the total number of minimum-bias events used for the analysis. ΔN_D is the raw charmed-hadron signal in each p_T bin within a rapidity window Δy. BR is the hadronic decay branching ratio for the channel of interest. There are two correction factors: $\epsilon_{\rm rec}$, which is the reconstruction efficiency including geometric acceptance, track selection efficiency, PID efficiency, and analysis cut efficiency; and $f_{\rm trg,vtx}(p_T)$, which is the correction factor to

account for the bias between the minimum-bias sample used in this analysis and the total NSD sample. This bias is mainly caused by the VPD trigger and event-vertex reconstruction, and it may have a dependence on the charmed-hadron p_T. In the following sections of the paper, the condition that requires the event to fire the VPD trigger and to have a good vertex will be referred to as the "analysis condition."

A. Reconstruction efficiency

The reconstruction efficiency for charmed hadrons was obtained by embedding MC simulated charmed-hadron tracks into the real minimum-bias events. The MC charmed-hadron tracks were processed through a full GEANT detector simulation [31] with a representation of the 2009 STAR geometry. The raw detector-response signals were mixed together with those from the real data and processed through the full STAR offline reconstruction chain to obtain the detector-response efficiency in a realistic environment. The input MC track multiplicity was constrained to have negligible effect on the final tracking efficiency due to increased occupancy in the TPC.

Figures 9 and 10 show the D^0 and D^* reconstruction efficiency versus p_T within $|y| < 1$. In Fig. 9, the solid squares denote the reconstruction efficiency for both daughters selected and identified by the TPC, while the solid circles denote the reconstruction efficiency with additional PID selection from the TOF detector for the kaon daughter. The combined TOF efficiency, including the acceptance, matching between TPC tracks and TOF hits, and PID selection efficiency, is around 45% studied from the data in 2009.

B. Trigger and vertex bias corrections

The trigger and vertex bias corrections were studied by simulating PYTHIA events [19] processed through the full GEANT detector-response and offline reconstruction. The PYTHIA generator versions 6.205 and 6.416 were both used

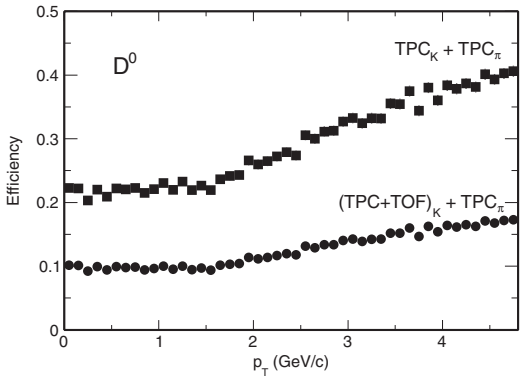

FIG. 9. Total D^0 reconstruction efficiency versus $D^0 p_T$.

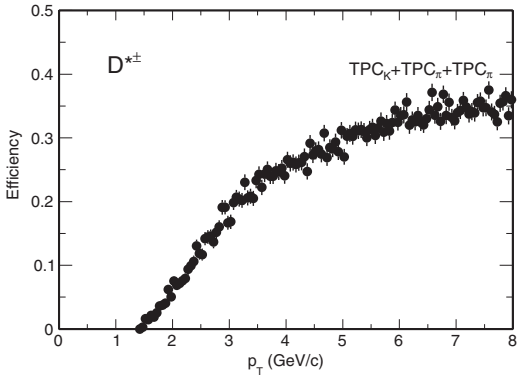

FIG. 10. Total D^* reconstruction efficiency versus $D^* p_T$.

in this study. We chose the PYTHIA version 6.205 with minimum-bias processes selected and with the CDF TUNEA settings [32] to give the centroid value of the correction factor because it gives better description for the particle production in the forward rapidities than the 6.416 version [33]. The differences between the two versions as well as different parameter settings have been included to estimate the systematic uncertainty of the trigger and vertex bias correction factor.

To validate the PYTHIA generator in simulating particle production in the forward region for the VPD trigger study, we first compared the VPD trigger efficiencies (from the BBC triggered minimum-bias sample) from MC simulation and real data. The BBC trigger has been well studied and was used to calculate the $p + p$ NSD cross section [16]. Figure 11 shows the comparison of the VPD trigger efficiency, with the requirement that there is a BBC trigger and a good vertex. The efficiency is studied as a function of the charged hadron p_T. The real data used are BBC triggered minimum-bias events taken in 2009 during a very low luminosity run, which minimizes TPC pileup tracks.

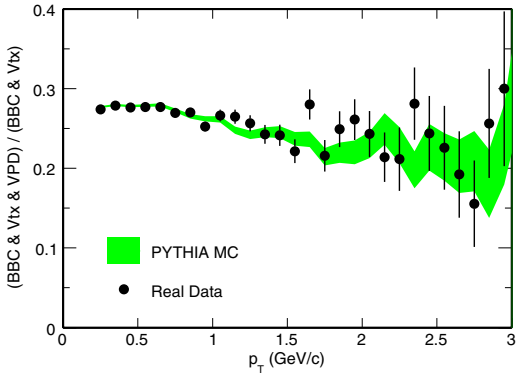

FIG. 11 (color online). VPD trigger efficiency comparison between data and Monte Carlo versus charged-particle p_T in BBC minimum-bias conditions.

Article reprint

Figure 11 shows that the efficiency goes down with increasing p_T of midrapidity particles indicating an anticorrelation between midrapidity particle production and forward VPD triggering. Most importantly, within the momentum range under study, the PYTHIA MC simulation agrees well with the data. This agreement provides confidence in using PYTHIA simulations to evaluate this correction.

The correction factor $f_{\mathrm{trg,vtx}}$ can be related to the ratio (N_D/N_{mb}) for the pure minimum-bias condition and the analysis condition, i.e.

$$f_{\mathrm{trg,vtx}}(p_T) \equiv \frac{N_D(p_T)/N_{\mathrm{mb}}}{N_D^{\mathrm{trg,vtx}}(p_T)/N_{\mathrm{mb}}^{\mathrm{trg,vtx}}}. \quad (4)$$

Two simulation samples were generated to obtain the correction factor. One sample consisted of PYTHIA-simulated $p + p$ events and was used to obtain the fraction of minimum-bias events that satisfy the analysis condition $N_{\mathrm{mb}}^{\mathrm{trg,vtx}}/N_{\mathrm{mb}}$. This fraction was found to be 12.7% from this PYTHIA simulation. The other simulation sample was generated using the same PYTHIA settings, but only events with at least one charmed hadron were saved to enhance the statistics. This sample was used to obtain the fraction of charmed-hadron signals that satisfy the analysis condition $N_D^{\mathrm{trg,vtx}}/N_D$. We also studied this fraction as a function of charmed-hadron p_T. Figure 12 shows the calculated efficiencies for D^* from different event-selection criteria. The BBC coincidence study provides a baseline for this simulation, which demonstrates consistency with previous STAR results [30]. As expected, the vertex finding efficiency increases with increasing p_T. The VPD trigger efficiency shows an anticorrelation with increasing $D^* p_T$, similar to that observed with increasing charged-hadron p_T. The final efficiency (with requirements for both vertexing and VPD triggering) is almost flat versus p_T, leveling off at ~19%. The simulation for D^0 hadrons shows very

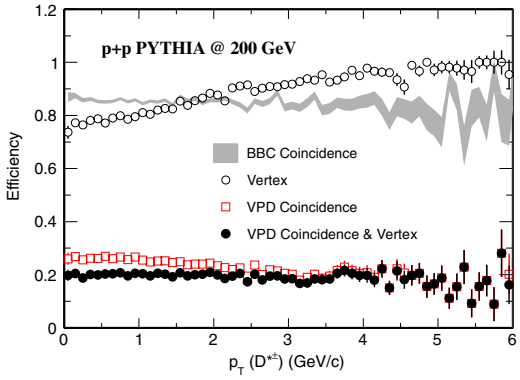

FIG. 12 (color online). D^* efficiency versus D^* p_T with different event-selection criteria.

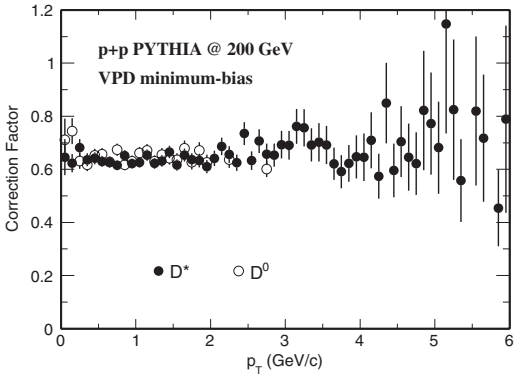

FIG. 13. The correction factor $f_{\mathrm{trg,vtx}}$ versus charmed-hadron p_T for cross section calculations for D^0 and D^*.

similar results. Figure 13 shows the correction factor $f_{\mathrm{trg,vtx}}$ for cross section calculations for D^0 and D^*.

V. SYSTEMATIC UNCERTAINTIES

Sources that contribute to the systematic uncertainties in the final D-meson cross sections include: (a) uncertainty in determining the raw D-meson yields; (b) uncertainty in determining the reconstruction efficiency; (c) uncertainty of the total NSD cross section; and (d) uncertainty in determining the trigger or vertex correction factor. Uncertainties due to particle identifications will enter in both (a) and (b) which will be discussed in the following subsections. We consider (a) as point-by-point uncorrelated systematic uncertainties. Although (b) is correlated in p_T, it is not simply a normalization uncertainty, and the exact correlation in p_T is not known. Therefore we include (b) in the point-by-point uncorrelated systematic uncertainties. Finally, (c) and (d) are overall normalization uncertainties.

A. Uncertainty in raw yields

Different choices on background reconstruction methods, function fits and mass binning were used to evaluate the systematic uncertainty in the raw D-meson yields. In the D^0 analysis, the difference between the yields extracted from Rot and LS methods is 15.6%–18.9%. Fitting the D^0 peak with fixed parameters from simulation estimates lower yields of 28.2% and 6.1% for the two D^0 p_T bins. The systematic uncertainties from different mass binning and different fit regions are estimated to be ~5%–7%. The systematic uncertainties in determining the raw D^* yields include contributions from the difference obtained between the sideband and the wrong-sign methods, and the difference between bin counting and Gaussian fitting methods, varying ~6%–11% in the p_T range 2–6 GeV/c. The choice of mass binning and fitting range had a negligible effect on the extracted yields.

Article reprint

In D^0 meson reconstruction, if the kaon (pion) daughter is misidentified as a pion (kaon), then two daughters from a real D^0 decay will show up as additional $\bar{D}^0$ combinations with a wider mass distribution due to wrong mass assignments. Thus one D^0 signal will be counted twice, once as a D^0 and again as a $\bar{D}^0$. A Monte Carlo simulation was used to evaluate the fraction of such double-counting occurrences in the D^0 reconstruction. Based on realistic dE/dx and TOF PID resolutions extracted from real data, the probability that kaons (pions) can be misidentified as pions (kaons) at a given p_T, using these PID selections, was obtained. Assuming a D^0 candidate, this procedure provides an estimate of the probability that both daughters are misidentified and then reconstructed as a $\bar{D}^0$. In Fig. 14, the open and closed circles show the double-counting fraction, relative to the total real signal, for two different PID selections: (a) both daughters are identified by TPC dE/dx; (b) the kaon daughters are identified by the TOF, while pions are identified by the TPC. The sharp increase at very low p_T (identifying both daughters using dE/dx) is due to the case where a D^0 decays almost at rest ($p_T \sim 0$), and the two daughters are produced in the momentum region where the kaon and pion dE/dx bands cross, therefore maximizing the misidentification probability. The plot shows that when the kaon daughter is identified by the TOF, the double-counting fraction is negligible in our D^0 p_T coverage region (0.6–2.0 GeV/c).

Double counting the D^0 may also impact reconstruction of D^*. However, the impact is different because of a charge sign requirement on the soft pions. If both daughters from a D^0 are misidentified (D^0 is reconstructed as $\bar{D}^0$), then the combination from the same signal will become $K^+\pi^-\pi^+$. It will not contribute to the right-sign distributions but, instead, will enter into the wrong-sign (background) distributions if the mass also falls into the D^0 ($\bar{D}^0$) mass selection window. Thus the double counting in wrong-sign background will contribute to an undercounting in the total signal if the wrong-sign background is subtracted from the right-sign distribution. Since the right-sign combination was also required, the misidentification does not affect the sideband background distributions. In the real analysis, the sideband background subtraction was used to extract the raw signal, but also the difference between sideband and wrong-sign methods was used for systematic uncertainty estimation. Since the wrong-sign distribution can be overestimated due to particle misidentification, the systematic error from the difference between the two methods would be overestimated. This was avoided with better understanding of the wrong-sign overcounting. The red triangles in Fig. 14 denote the overcounting fraction in the D^* wrong-sign background to real signals. It is very close to the D^0 double-counting fraction, since they are from the same source. The slight difference comes from the additional D^0 candidate selection cuts used in the D^* reconstruction. This fraction was used to compensate for the difference between the two background methods and as a way to improve the assessment of the systematic uncertainties in the extraction of the raw D^* yields.

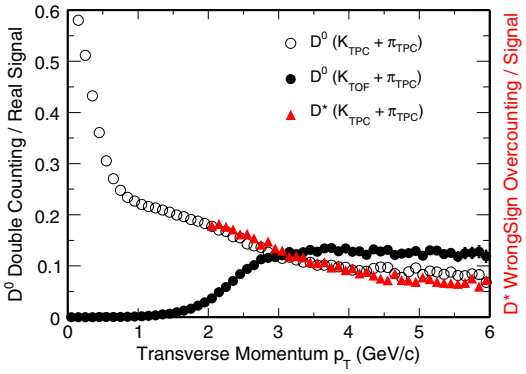

FIG. 14 (color online). D^0 double-counting fraction due to particle misidentification in two PID selections and D^* wrong-sign over counting fraction versus D-meson p_T.

B. Uncertainty in reconstruction efficiency

The systematic uncertainties of the reconstruction efficiencies were obtained following similar methods used in other particle cross section measurements by changing the daughter track selection criteria and comparing the difference between the data and the MC. In this analysis, it was studied by changing the minimum number of fit points (nFitPts) in the TPC from 15 to 25 and the DCA to the collision vertex from 2 to 1 cm. The uncertainty was then quantified by the difference in the remaining fractions after cut changes between the data and the MC. For each cut change, the uncertainties were calculated for each decay daughter and added together linearly to obtain the total for D^0 and D^*. The systematic uncertainties on the PID cut efficiencies (from both dE/dx and TOF) were estimated to be $<1\%$ and neglected in the total uncertainty. Then the uncertainties from the cut changes on nFitPts and DCA were added in quadrature to obtain the total systematic uncertainty on the reconstruction efficiency.

The point-by-point systematic errors including uncertainties in raw yields and reconstruction efficiency for the D^0 and D^* cross sections in each p_T bin are summarized in Table III.

TABLE III. D^0 (0.6–2 GeV/c) and D^* (2–6 GeV/c) point-by-point systematic errors (%).

p_T (GeV/c)	0.6–1.2	1.2–2	2–3	3–4	4–5	5–6
Raw yields	$^{+18.9}_{-33.9}$	$^{+15.6}_{-16.8}$	9.4	6.5	11.0	6.6
nFitPts 15 → 25	3.8	3.2	7.2	4.7	5.9	4.7
DCA 2 → 1 (cm)	6.6	7.1	13.6	12.7	11.6	10.7
Quadratic sum	$^{+20.8}_{-34.8}$	$^{+17.8}_{-18.5}$	18.1	15.1	17.1	13.5

Article reprint

C. Overall normalization uncertainty

The overall normalization uncertainty for the total NSD cross section has been studied before and reported in a previous STAR publication [30]. It was estimated to be 8.1%, including the uncertainty from measuring the absolute BBC cross section and that of BBC triggering efficiency. The uncertainty from the trigger or vertex bias correction factor amounts to 5.2% by varying different PYTHIA versions (6.205 vs 6.416) and different parameter settings in the simulation. We also considered the impact from pileup TPC tracks as an additional systematic source on the correction factor, and the uncertainty was estimated to be 4.0% by comparing the result with a conservative luminosity level for this data set to that from pure PYTHIA simulation without pileup.

These uncertainties were added in quadrature, which gives 10.4% overall normalization uncertainty for the D-meson cross sections.

VI. RESULT AND DISCUSSION

After the reconstruction efficiency and trigger or vertex bias correction factor were applied, the differential production cross sections for D^0 and D^* in $p + p$ collisions at $\sqrt{s} = 200$ GeV were extracted, as shown in Fig. 15. The vertical bars on the data points indicate the statistical uncertainties, while the brackets indicate the bin-to-bin systematic uncertainties described in the previous section. The D^0 and D^* cross sections were divided by the charm quark fragmentation ratios 0.565 ± 0.032 ($c \to D^0$) and 0.224 ± 0.028 ($c \to D^{*+}$), respectively, to convert to the $c\bar{c}$ production cross section. The charm quark fragmentation ratios are measured from CLEO and BELLE experiments near the Υ resonance [34]. The uncertainties of the fragmentation ratios are taken into account as systematic errors in calculating the $c\bar{c}$ production cross section. A power-law fit to the data points was performed with the following function [14]:

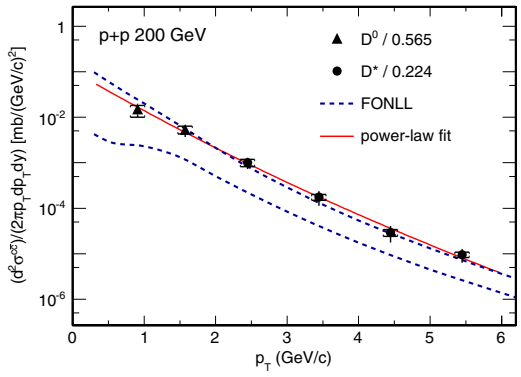

FIG. 15 (color online). $c\bar{c}$ production cross section as inferred from D^0 and D^* production in $p + p$ collisions at $\sqrt{s} = 200$ GeV compared with FONLL calculations. The D^0 and D^* data points were divided by the charm quark fragmentation ratios 0.565 ($c \to D^0$) and 0.224 ($c \to D^{*+}$) [34], respectively, to convert to the $c\bar{c}$ production cross section.

$$E\frac{d^3\sigma}{dp^3} = \frac{d\sigma}{dy}\frac{2(n-1)(n-2)}{\pi(n-3)^2\langle p_T\rangle^2}\left(1 + \frac{p_T}{\langle p_T\rangle(n-3)/2}\right)^{-n} \tag{5}$$

and shown as the solid red line in the figure. The fit quality with the power-law function, measured as χ^2/ndf, is $0.9/3$ with statistical errors and $3.7/3$ with point-by-point systematic errors, respectively. The latter was used to extract the systematic uncertainty on the p_T integrated cross section from point-by-point systematic sources. The obtained $c\bar{c}$ production cross section at midrapidity is

$$\left.\frac{d\sigma}{dy}\right|_{y=0}^{c\bar{c}} = 170 \pm 45(\mathrm{stat})^{+38}_{-59}(\mathrm{sys})\ \mu\mathrm{b}. \tag{6}$$

The term with sys includes the uncertainty arising from the bin-to-bin systematic uncertainties and from the extrapolation to the low-p_T region, which is not measured. The FONLL upper limit and PYTHIA + tune fits are used for the low-p_T extrapolation, which gives +6.2% and −16.4% uncertainties, respectively. At midrapidity, about 67% of the D meson yield falls in the measured p_T region. The mean transverse momentum of charmed mesons is found to be $1.06 \pm 0.14(\mathrm{stat}) \pm 0.09(\mathrm{sys})$ GeV/c. The charm-pair cross section at midrapidity from this measurement is consistent with STAR's previous measurement in d + Au collisions [14] at 1.7σ (σ is the averaged total uncertainty between two results), providing negligible nuclear effects in d + Au collisions.

Also shown in Fig. 15 are the upper and lower edges (blue dashed lines) of a FONLL pQCD calculation taken from Ref. [9]. Our results are consistent with the upper limit of the FONLL pQCD calculation in a wide p_T region. It is observed that the charmed-hadron cross sections measured by CDF [13] and ALICE [35] at energies up to 7 TeV are also close to the upper limits of FONLL pQCD calculations. This may help set constraints on the parameters used in the FONLL calculations, e.g. on the choice of renormalization or factorization scales, which are the main parameters varied to obtain the upper and lower limits on these calculations. However one should note the valid p_T region of FONLL calculations when applying such an analysis since FONLL calculations are supposed to work when $p_T \gg m_c$.

The charm cross section at midrapidity was extrapolated to full phase space using the same extrapolation factor, 4.7 ± 0.7, as in a previous publication [14], and the extracted charm total cross section at $\sqrt{s} = 200$ GeV is

$$\sigma_{c\bar{c}} = 797 \pm 210(\mathrm{stat})^{+208}_{-295}(\mathrm{sys})\ \mu\mathrm{b}. \tag{7}$$

Shown in Fig. 16, the data were also compared with PYTHIA calculations. PYTHIA version 6.416 was used as it has been tuned to describe the midrapidity Tevatron data.

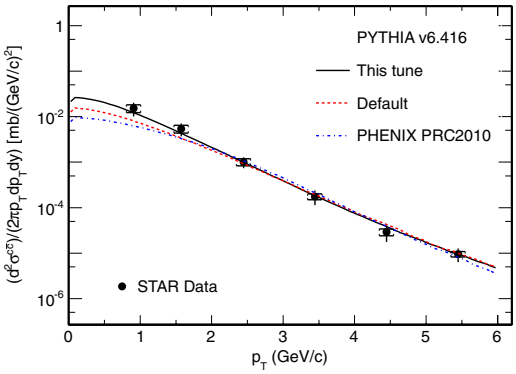

FIG. 16 (color online). $c\bar{c}$ production cross section as inferred from D^0 and D^* production in $p+p$ collisions at $\sqrt{s} =$ 200 GeV compared with PYTHIA calculations. Data are fitted with PYTHIA spectra with an overall scale parameter for the purpose of shape comparison only.

We tried PYTHIA calculations with the following sets of parameters to compare with our measurements:

(a) Default MSEL = 1.

(b) PHENIX tune: MSEL = 0 with MSUB(11, 12, 13, 28, 53, 68) on, PARP(91) $(\langle k_\perp \rangle) =$ 1.5 GeV/c, MSTP(32) (Q^2 scale) = 4, CKIN(3) (min. parton $\hat{p}_\perp$) = 2 GeV.

(c) This tune: MSEL = 1, PARP(91) $(\langle k_\perp \rangle) =$ 1.0 GeV/c, PARP(67) (parton shower level) = 1.0.

The choice of modifying the primordial $\langle k_\perp \rangle$ (the Gaussian width of primordial k_T in hadrons) and the parton shower level parameters from default values (2 GeV/c and 4, respectively) in this tune was suggested by the matching of scales in heavy-flavor production at lower energies [36], which has been noted in PYTHIA [19]. The CDF TUNEA parameters [32], which were tuned to reproduce midrapidity jet and "underlying event" results at Tevatron energies, are included as defaults in PYTHIA v6.416. "PHENIX tune" parameters are those used in the PHENIX charm continuum contribution estimation from dielectron measurements [37]. The default parton distribution function (CTEQ5L) was used in all three cases.

All ground-state charmed hadrons (D^0, D^+, D_s^+, and Λ_c^+) were added together in the rapidity window $|y| < 1$ to obtain charm cross sections. The data were then fitted with the PYTHIA calculations with an overall scale factor as the unique free parameter. The charm production p_T spectrum with this tune gives best χ^2: 1.41 (this tune), 4.97 (default), 5.96 (PHENIX tune). This is the first direct D-meson measurement that goes down to such a low p_T, which constrains the model parameters better.

VII. SUMMARY

In summary, measurement on the charmed meson (D^0 and D^*) production cross sections via their hadronic decays in $p+p$ collisions at $\sqrt{s} = 200$ GeV has been reported. The charm-pair production cross section at midrapidity extracted from this analysis is $d\sigma/dy|_{y=0}^{c\bar{c}} = 170 \pm 45(\text{stat})^{+38}_{-59}(\text{sys})$ μb. The charm total cross section at $\sqrt{s} =$ 200 GeV is estimated as $797 \pm 210(\text{stat})^{+208}_{-295}(\text{sys})$ μb. The reconstructed charmed mesons cover the p_T range 0.6–6 GeV/c. The charm-pair transverse momentum differential cross sections from this analysis are consistent with the upper bound of a fixed-order next-to-leading logarithm perturbative QCD calculation. When comparing to PYTHIA model calculations, we found that a calculation with smaller primordial $\langle k_\perp \rangle$ and parton shower level compared to CDF TUNEA settings describes the shape of the p_T distribution of data.

ACKNOWLEDGMENTS

We thank the RHIC Operations Group and RCF at BNL, the NERSC Center at LBNL and the Open Science Grid consortium for providing resources and support. This work was supported in part by the Offices of NP and HEP within the U.S. DOE Office of Science, the U.S. NSF, the Sloan Foundation, the DFG cluster of excellence "Origin and Structure of the Universe" of Germany, CNRS/IN2P3, FAPESP CNPq of Brazil, Ministry of Education and Science of the Russian Federation, NNSFC, CAS, MoST, and MoE of China, GA and MSMT of the Czech Republic, FOM and NWO of the Netherlands, DAE, DST, and CSIR of India, Polish Ministry of Science and Higher Education, Korea Research Foundation, Ministry of Science, Education and Sports of the Republic of Croatia, and RosAtom of Russia.

[1] J. Adams *et al.* (STAR Collaboration), Nucl. Phys. **A757**, 102 (2005).
[2] Z. Lin and M. Gyulassy, Phys. Rev. C **51**, 2177 (1995); **52**, 440(E) (1995).
[3] B. Mueller, Nucl. Phys. **A750**, 84 (2005).
[4] G. D. Moore and D. Teaney, Phys. Rev. C **71**, 064904 (2005).
[5] H. van Hees and R. Rapp, Phys. Rev. C **71**, 034907 (2005); R. Rapp and H. van Hees, arXiv:0803.0901.
[6] J. Uphoff, O. Fochler, Z. Xu, and C. Greiner, Phys. Rev. C **82**, 044906 (2010).
[7] R. L. Thews, M. Schroedter, and J. Rafelski, Phys. Rev. C **63**, 054905 (2001).

Article reprint

[8] A. Andronic, P. Braun-Munzinger, K. Redlich, and J. Stachel, Phys. Lett. B **571**, 36 (2003).
[9] M. Cacciari, P. Nason, and R. Vogt, Phys. Rev. Lett. **95**, 122001 (2005).
[10] R. Vogt, Eur. Phys. J. Special Topics **155**, 213 (2008).
[11] S. P. K. Tavernier, Rep. Prog. Phys. **50**, 1439 (1987).
[12] X. Dong, Ph.D. thesis, University of Science and Technology of China, 2005, arXiv:nucl-ex/0509011, Appendix C and references therein.
[13] D. Acosta *et al.* (CDF Collaboration), Phys. Rev. Lett. **91**, 241804 (2003).
[14] J. Adams *et al.* (STAR Collaboration), Phys. Rev. Lett. **94**, 062301 (2005).
[15] B. I. Abelev *et al.* (STAR Collaboration), Phys. Rev. Lett. **106**, 159902(E) (2011).
[16] H. Agakishiev *et al.* (STAR Collaboration), Phys. Rev. D **83**, 052006 (2011).
[17] A. Adare *et al.* (PHENIX Collaboration), Phys. Rev. Lett. **97**, 252002 (2006).
[18] S. S. Adler *et al.* (PHENIX Collaboration), Phys. Rev. Lett. **96**, 032301 (2006); A. Adare *et al.* (PHENIX Collaboration), Phys. Rev. Lett. **98**, 172301 (2007).
[19] T. Sjöstrand, S. Mrenna, and P. Skands, J. High Energy Phys. 05 (2006) 026.
[20] Special Issue on RHIC and Its Detectors, edited by M. Harrison, T. Ludlam, and S. Ozaki [Nucl. Instrum. Methods Phys. Res., Sect. A **499**, No. 2–3 (2003)].
[21] M. Anderson *et al.*, Nucl. Instrum. Methods Phys. Res., Sect. A **499**, 659 (2003).
[22] STAR TOF proposal, http://drupal.star.bnl.gov/STAR/files/future/proposals/tof-5-24-2004.pdf.
[23] M. Beddo *et al.*, Nucl. Instrum. Methods Phys. Res., Sect. A **499**, 725 (2003).
[24] C. E. Allgower *et al.*, Nucl. Instrum. Methods Phys. Res., Sect. A **499**, 740 (2003).
[25] W. J. Llope, in *Proceedings of 24th Winter Workshop on Nuclear Dynamics, 2008* (unpublished).
[26] J. Kiryluk, AIP Conf. Proc. **675**, 424 (2003).
[27] B. I. Abelev *et al.* (STAR Collaboration), Phys. Rev. C **79**, 034909 (2009).
[28] C. Adler *et al.* (STAR Collaboration), Phys. Rev. Lett. **89**, 132301 (2002); J. Adams *et al.* (STAR Collaboration), Phys. Rev. Lett. **95**, 122301 (2005); Phys. Rev. C **70**, 44902 (2004); B. I. Abelev *et al.* (STAR Collaboration), Science **328**, 58 (2010); K. Aamodt *et al.* (ALICE Collaboration), Phys. Lett. B **704**, 442 (2011).
[29] B. I. Abelev *et al.* (STAR Collaboration), Phys. Rev. D **79**, 112006 (2009).
[30] J. Adams *et al.* (STAR Collaboration), Phys. Rev. Lett. **91**, 172302 (2003).
[31] GEANT 3.21, CERN program library. http://wwwasdoc.web.cern.ch/wwwasdoc/22geanthtml3/geantall.html.
[32] R. D. Field *et al.*, arXiv:hep-ph/0510198.
[33] N. Poljak (for the STAR Collaboration), Nuovo Cimento Soc. Ital. Fis. C **035N2**, 193 (2012).
[34] C. Amsler *et al.*, Phys. Lett. B **667**, 1 (2008).
[35] A. Dainese *et al.* (ALICE Collaboration), J. Phys. G **38**, 124032 (2011).
[36] E. Norrbin and T. Sjöstrand, Phys. Lett. B **442**, 407 (1998); Eur. Phys. J. C **17**, 137 (2000).
[37] A. Adare *et al.* (PHENIX Collaboration), Phys. Rev. C **81**, 034911 (2010), footnote in reference [51].

Kapitola 3

Produkcia kvarkov ťažkých vôní v jadro-jadrových zrážkach

Zhášanie výtryskov častíc v centrálnych jadro-jadrových zrážkach je dôsledkom straty energie gluónov a ľahkých kvarkov, vzniknutých v tvrdých procesoch, pri prelete cez kvarkovo-gluónovú plazmu. Pôvodné teoretické výpočty odhadovali, že radiačné straty energie ťažkých kvarkov prechádzajúcich horúcou a hustou jadrovou hmotou by mali byť menšie ako u ľahkých partónov [R26]. Toto by malo byť spôsobené potlačením vyžarovania gluónov pod malými uhlami vzhľadom k letu kvarku (efekt mŕtveho kužeľu) a tento jav je silnejší u kvarkov s vyššou hmotnosťou [R27]. Z tohto dôvodu sa očakávala hierarchia v potlačení produkcie D a B mezónov alebo elektrónov pochádzajúcich z ich semileptónových rozpadov pri $p_T \approx 5$ - 10 GeV/c. B mezóny by mali byť potlačené menej ako D mezóny a tie menej ako π a podobne i elektróny pochádzajúce z ich rozpadov [R28]. Straty energie závisia tiež od vlastností jadrovej hmoty a preto sa meraním jadrového modifikačného faktora tieto vlastnosti dajú študovať a konfrontovať predpovede modelových výpočtov. Cieľom je komplexne popísať produkciu ľahkých aj ťažkých kvarkov zároveň pri rovnakých parametroch charakterizujúcich jadrovú hmotu. Doposiaľ sa nepodarilo zároveň popísať R_{AA} a eliptický tok mezónov z ľahkých a ťažkých kvarkov pri RHIC a LHC energiách [R29]. Fundamentálnym parametrom, ktorý samostatne charakterizuje QCD hmotu je difúzny parameter ťažkých kvarkov D_s. Systematickým štúdiom dát z LHC a modelov sa ukázalo, že hodnota tohto parametru v podmienkach LHC je menšia ako $D_s(2\pi T) = 6$ [R30]. Upresnenie tohto parametru pre hmotu tvorenú na RHIC vyžaduje presné experimentálne merania.

Ako už bolo zmienené v predošlej kapitole, najpresnejšiu informáciu o pôvabných a krásnych kvarkoch by sme získali pomocou merania mezónov D a B. V jadro-jadrových zrážkach na RHIC sa podarilo publikovať výsledky z priamej rekonštrukcie pôvabných mezónov v zrážkach d+Au v roku 2005 [R21], avšak prvé poznatky o energetických stratách ťažkých kvarkov na experimentoch na RHIC zo zrážok Au+Au pochádzajú z meraní nefotonických elektrónov, ktoré som prezentoval na konferencii Quark Matter 2005. Predbežné výsledky boli následne publikované v príslušnom recenzovanom článku

do zborníku konferencie [24]. Finálne výsledky boli publikované v článku B. I. Abelev *et al.*, *Transverse momentum and centrality dependence of high-p_T non-photonic electron suppression in Au+Au collisions at 200 GeV*, Phys. Rev. Lett. **98**, 192301 (2007). Podobné merania potlačenia ťažkých kvarkov zo zrážok Au+Au pri energii $\sqrt{s_{NN}} = 200$ GeV boli tiež publikované experimentom PHENIX [R31–R33].

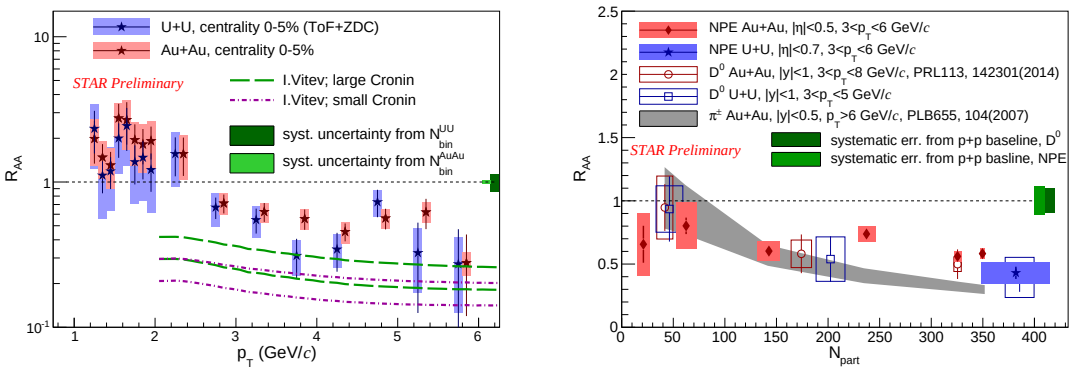

Obr. 3.1: Vľavo: Predbežné meranie závislosti jadrového modifikačného faktora na priečnej hybnosti získaného z meraní nefotónových elektrónov v 0-5% centrálnych zrážkach Au+Au pri energii $\sqrt{s_{NN}} = 200$ GeV a U+U pri energii $\sqrt{s_{NN}} = 193$ GeV. Experimentálne dáta sú porovnané s modelom z Ref. [R35, R36]. Vpravo: Jadrový modifikačný faktor v závislosti na priemernom počte účastníkov v zrážke z meraní nefotónových elektrónov, D^0 a $\pi^{\pm}$ mezónov zrážkach Au+Au pri energii $\sqrt{s_{NN}} = 200$ GeV a U+U pri energii $\sqrt{s_{NN}} = 193$ GeV.

Merania experimentu STAR majú výhodu, že sa nám podarilo jednak využiť veľké azimutálne geometrické pokrytie fázového priestoru vyletujúcich nefotonických elektrónov a jednak sa nám podarilo využiť detektor EMC v spúšťači a merať prednostne zrážky, ktoré obsahujú elektrón s vysokou hybnosťou dávajúce v EMC dostatočný signál. Tým sa nám podarilo zmerať spektrum nefotónových elektrónov až do $p_T \approx 8$ GeV/c. Pri identifikácii elektrónov sme použili kombináciu informácie z TPC (špecifické straty energie častíc dE/dx) a EMC (pomer hybnosti častice k zmeranej energie E/p). Pri analýze nefotónových elektrónov je dôležité stanoviť výťažok fotónových elektrónov v inkluzívnom spektre. Pre výťažok fotónových elektrónov je dôležité rozloženie detekčných systémov a radiačná dĺžka materiálu od bodu zrážky až po TPC, kde je možné dráhy častíc zmerať. V zrážke jadier vzniká veľké množstvo π^0 a tie následne môžu konvertovať na $e^+ - e^-$ páry. V prípade, že obe dráhy v páre sa podarí rekonštruovať je možné tieto elektróny identifikovať a odčítať. Avšak to sa podarí len u približne polovice prípadov. Keďže pomer všetkých elektrónov k fotónovým je približne 1,1 až 1,3 (viz. FIG. 1c), je veľmi dôležité určiť presne účinnosť rekonštrukcie fotónového pozadia. Zámena korekčných parametrov v tomto kroku bola dôvodom nutnosti opraviť pôvodnú publikáciu týchto dát. Po vydelení stanovených celkových výťažkov v zrážkach Au+Au

referenčnými p+p meraniami, násobenými priemerným počtom binárnych zrážok pre rôzne centrality, sme určili jadrový modifikačný faktor R_{AA}. Pozorovali sme, že na rozdiel od produkcie nefotónových elektrónov v zrážkach d+Au, kde je R_{AA} v rámci nepresností merania blízky 1, je produkcia v centrálnych Au+Au zrážkach potlačená a hodnota R_{AA} je $\approx$ 0,2 - 0,3 pre $p_T >$ 0,3 GeV/c (viz. FIG. 4). Toto potlačenie je podobné ako pozorujeme u hadrónov vzniknutých z ľahkých kvarkov a partónov, čo je neočakávané. Potlačenie je dôsledkom energetických strát ťažkých kvarkov, avšak nie je možné odlíšiť od seba elektróny pochádzajúce z rozpadov pôvabných kvarkov a krásnych kvarkov. V článku sme meranie porovnali s niekoľkými modelmi energetických strát a v rámci nepresností meraní sa javí, že len zahrnutím oboch zložiek energetických strát: radiačných a zrážkových je možné dáta lepšie popísať. So študentkou Katarínou Gajdošovou sme previedli štúdium produkcie nefotónových elektrónov v zrážkach U+U pri energii $\sqrt{s_{NN}}$ = 193 GeV [D6, R34]. V centrálnych zrážkach U+U je možné dosiahnúť o 10 - 20% vyššiu jadrovú hustotu ako v zrážkach Au+Au. Na Obr. 3.1 (vľavo) je predbežné meranie závislosť jadrového modifikačného faktora na priečnej hybnosti získaného z meraní nefotónových elektrónov v 0-5% centrálnych zrážkach Au+Au pri energii $\sqrt{s_{NN}}$ = 200 GeV a U+U pri energii $\sqrt{s_{NN}}$ = 193 GeV. Zistili sme, že pozorujeme podobné potlačenie nefotónových elektrónov. Dáta sú porovnané s modelovým výpočtom [R35,R36], ktorý obsahuje efekty QGP, effekty studenej jadrovej hmoty (Croninov jav) a disociáciu D a B mezónov zrážkami v jadrovej hmote. Model popisuje dáta kvalitatívne dobre, avšak predpovedá väčšie potlačenie. Na Obr. 3.1 (vpravo) je pre oba zrážkové systémy vykreslený jadrový modifikačný faktor v závislosti na priemernom počte účastníkov v zrážke (počas zrážky interagujúce nukléony) z meraní nefotónových elektrónov, D^0 a $\pi^{\pm}$ mezónov pre $p_T >$ 3 GeV/c ($p_T >$ 6 GeV/c u piónov). Vidíme, že pre všetky častice polačenie produkcie rastie so zväčšujúcim sa počtom účastníkov, t.j. zväčšujúcou sa centralitou zrážky. Potlačenie piónov sa javí pri najcentrálnejších zrážkach trochu väčšie ako pre ostatné častice. Avšak nepresnosti meraní znemožnujú jednoznačný záver.

Experimentu STAR sa podarilo v roku 2014 publikovať prvé meranie produkcie D^0 mezónov v Au+Au pri energii 200 GeV na RHIC [235], ktoré potvrdilo, že produkcia pôvabných mezónov je potlačená v centrálnych zrážkach. V rokoch 2014 a 2016 experiment STAR meral s novým detektorom HFT. Podarilo sa nám pomocou využitia informácie z HFT o dráhe častíc blízko hlavného vrcholu zrážky, lepšie potlačiť pozadie náhodných kombinácií dcérskych častíc D mezónov a previesť presnejšie meranie D^0 a tiež $D^{\pm}$ v trojčasticovom rozpadovom kanáli. Analýzu $D^{\pm}$ sme previedli s Jakubom Kvapilom [D9] a hlavný výsledok je na Obr. 3.2. Vidíme, že i tu pozorujeme, že produkcia pôvabných mezónov je potlačená pri vysokej hodnote p_T .

Na lepšie pochopenie toho, ktorý fenomenologický model lepšie popisuje mechanizmy energetických strát, je dôležité tiež súčasné porovnanie meraní a výpočtov eliptického toku. Experiment STAR v roku 2017 publikoval tieto merania nielen pre ne-

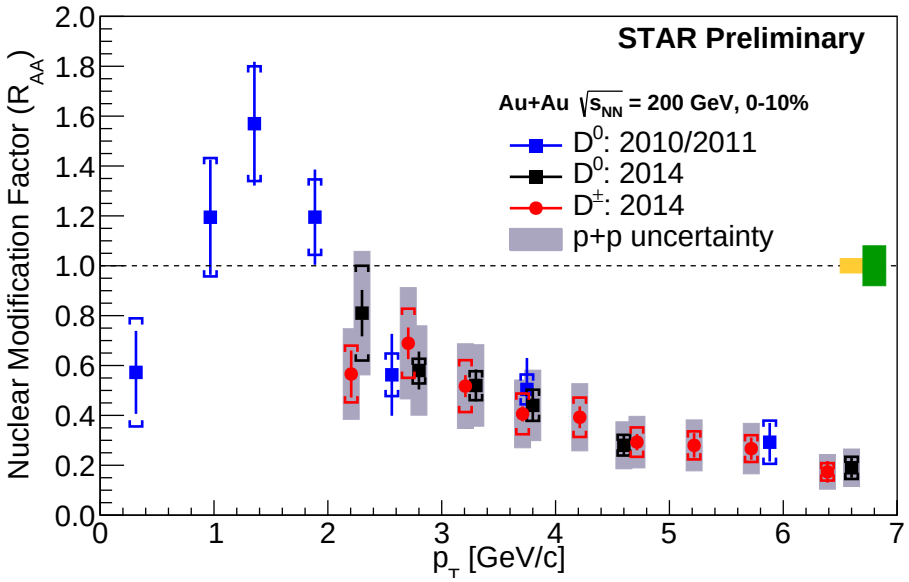

Obr. 3.2: Závislosť jadrového modifikačného faktora na priečnej hybnosti získaného z meraní $D^{\pm}$ a D^0 v 0-10% centrálnych zrážkach Au+Au pri energii $\sqrt{s_{NN}} = 200$ GeV. Meranie z roku 2010/2011 je z Ref. [235], ostatné sú predbežné merania.

fotónové elektróny [249], ale aj pre D^0 [360]. U D^0 sa jednalo o prvé publikované meranie využívajúce topologickú rekonštrukciu pomocou detektoru HFT. Avšak až finálne spracovanie dát z rokov 2014 a 2016 umožní dosiahnuť potrebnú presnosť na diskrimináciu fenomenologických modelov a upresnenie odhadu difúzneho parametra ťažkých kvarkov D_s. Na základe súčasných poznatkov z experimentu STAR je jeho najpravdepodobnejšia hodnota v intervale $D_s(2\pi T) = 2$ - 12 [360].

Z dôvodu malého účinného prierezu produkcie kvarku b je meranie signálov spojených s energetickými stratami b kvarkov v jadrovej hmote náročné. Doposiaľ len experiment CMS na LHC meral priamo produkciu B mezónu v hadrónovom rozpade $B^{\pm} \rightarrow J/\psi + K^{\pm}$ v p + p a Pb+Pb zrážkach pri energii $\sqrt{s_{NN}} = 5{,}02$ TeV [R37]. V zrážkach s najmenším zaujatím sú namerané hodnoty R_{AA} od 0,3 do 0,6 v intervale priečnych hybností p_T od 7 do 50 GeV/c . V porovnaní s D mezónmi je potlačenie menšie [R38], avšak dáta nie sú dostatočne presné, aby bolo možné jednoznačne potvrdiť hierarchiu v potlačení produkcie ťažkých kvarkov. Alternatívne je možné skúmať produkciu B mezónov pomocou merania J/ψ vychádzajúceho mimo hlavný vrchol zrážky a taktiež pomocou nefotónových elektrónov s odlíšením príspevku c a b rozpadov. V experimentoch ALICE a STAR sa aktuálne sústredíme na tieto dva kanály.

Article reprint

PRL **98,** 192301 (2007) PHYSICAL REVIEW LETTERS week ending 11 MAY 2007

Transverse Momentum and Centrality Dependence of High-p_T Nonphotonic Electron Suppression in Au + Au Collisions at $\sqrt{s_{\mathrm{NN}}} = 200$ GeV

B. I. Abelev,[9] M. M. Aggarwal,[30] Z. Ahammed,[45] B. D. Anderson,[20] D. Arkhipkin,[13] G. S. Averichev,[12] Y. Bai,[28] J. Balewski,[17] O. Barannikova,[9] L. S. Barnby,[2] J. Baudot,[18] S. Baumgart,[50] V. V. Belaga,[12] A. Bellingeri-Laurikainen,[40] R. Bellwied,[48] F. Benedosso,[28] R. R. Betts,[9] S. Bhardwaj,[35] A. Bhasin,[19] A. K. Bhati,[30] H. Bichsel,[47] J. Bielcik,[50] J. Bielcikova,[50] L. C. Bland,[3] S-L. Blyth,[22] M. Bombara,[2] B. E. Bonner,[36] M. Botje,[28] J. Bouchet,[40] A. V. Brandin,[26] A. Bravar,[3] T. P. Burton,[2] M. Bystersky,[11] R. V. Cadman,[1] X. Z. Cai,[39] H. Caines,[50] M. Calderón de la Barca Sánchez,[6] J. Callner,[9] O. Catu,[50] D. Cebra,[6] Z. Chajecki,[29] P. Chaloupka,[11] S. Chattopadhyay,[45] H. F. Chen,[38] J. H. Chen,[39] J. Y. Chen,[49] J. Cheng,[43] M. Cherney,[10] A. Chikanian,[50] W. Christie,[3] S. U. Chung,[3] J. P. Coffin,[18] T. M. Cormier,[48] M. R. Cosentino,[37] J. G. Cramer,[47] H. J. Crawford,[5] D. Das,[45] S. Dash,[15] M. Daugherity,[42] M. M. de Moura,[37] T. G. Dedovich,[12] M. DePhillips,[3] A. A. Derevschikov,[32] L. Didenko,[3] T. Dietel,[14] P. Djawotho,[17] S. M. Dogra,[19] X. Dong,[22] J. L. Drachenberg,[41] J. E. Draper,[6] F. Du,[50] V. B. Dunin,[12] J. C. Dunlop,[3] M. R. Dutta Mazumdar,[45] V. Eckardt,[24] W. R. Edwards,[22] L. G. Efimov,[12] V. Emelianov,[26] J. Engelage,[5] G. Eppley,[36] B. Erazmus,[40] M. Estienne,[18] P. Fachini,[3] R. Fatemi,[23] J. Fedorisin,[12] A. Feng,[49] P. Filip,[13] E. Finch,[50] V. Fine,[3] Y. Fisyak,[3] J. Fu,[49] C. A. Gagliardi,[41] L. Gaillard,[2] M. S. Ganti,[45] E. Garcia-Solis,[9] V. Ghazikhanian,[7] P. Ghosh,[45] Y. G. Gorbunov,[10] H. Gos,[46] O. Grebenyuk,[28] D. Grosnick,[44] S. M. Guertin,[7] K. S. F. F. Guimaraes,[37] N. Gupta,[19] B. Haag,[6] T. J. Hallman,[3] A. Hamed,[41] J. W. Harris,[50] W. He,[17] M. Heinz,[50] T. W. Henry,[41] S. Heppelmann,[31] B. Hippolyte,[18] A. Hirsch,[33] E. Hjort,[22] A. M. Hoffman,[23] G. W. Hoffmann,[42] D. Hofman,[9] R. Hollis,[9] M. J. Horner,[22] H. Z. Huang,[7] E. W. Hughes,[4] T. J. Humanic,[29] G. Igo,[7] A. Iordanova,[9] P. Jacobs,[22] W. W. Jacobs,[17] P. Jakl,[11] F. Jia,[21] P. G. Jones,[2] E. G. Judd,[5] S. Kabana,[40] K. Kang,[43] J. Kapitan,[11] M. Kaplan,[8] D. Keane,[20] A. Kechechyan,[12] D. Kettler,[47] V. Yu. Khodyrev,[32] B. C. Kim,[34] J. Kiryluk,[22] A. Kisiel,[46] E. M. Kislov,[12] S. R. Klein,[22] A. G. Knospe,[50] A. Kocoloski,[23] D. D. Koetke,[44] T. Kollegger,[14] M. Kopytine,[20] L. Kotchenda,[26] V. Kouchpil,[11] K. L. Kowalik,[22] P. Kravtsov,[26] V. I. Kravtsov,[32] K. Krueger,[1] C. Kuhn,[18] A. I. Kulikov,[12] A. Kumar,[30] P. Kurnadi,[7] A. A. Kuznetsov,[12] M. A. C. Lamont,[50] J. M. Landgraf,[3] S. Lange,[14] S. LaPointe,[48] F. Laue,[3] J. Lauret,[3] A. Lebedev,[3] R. Lednicky,[13] C.-H. Lee,[34] S. Lehocka,[12] M. J. LeVine,[3] C. Li,[38] Q. Li,[48] Y. Li,[43] G. Lin,[50] X. Lin,[49] S. J. Lindenbaum,[27] M. A. Lisa,[29] F. Liu,[49] H. Liu,[38] J. Liu,[36] L. Liu,[49] T. Ljubicic,[3] W. J. Llope,[36] R. S. Longacre,[3] W. A. Love,[3] Y. Lu,[49] T. Ludlam,[3] D. Lynn,[3] G. L. Ma,[39] J. G. Ma,[7] Y. G. Ma,[39] D. Magestro,[29] D. P. Mahapatra,[15] R. Majka,[50] L. K. Mangotra,[19] R. Manweiler,[44] S. Margetis,[20] C. Markert,[42] L. Martin,[40] H. S. Matis,[22] Yu. A. Matulenko,[32] C. J. McClain,[1] T. S. McShane,[10] Yu. Melnick,[32] A. Meschanin,[32] J. Millane,[23] M. L. Miller,[23] N. G. Minaev,[32] S. Mioduszewski,[41] C. Mironov,[20] A. Mischke,[28] J. Mitchell,[36] B. Mohanty,[22] D. A. Morozov,[32] M. G. Munhoz,[37] B. K. Nandi,[16] C. Nattrass,[50] T. K. Nayak,[45] J. M. Nelson,[2] N. S. Nepali,[20] P. K. Netrakanti,[33] L. V. Nogach,[32] S. B. Nurushev,[32] G. Odyniec,[22] A. Ogawa,[3] V. Okorokov,[26] M. Oldenburg,[22] D. Olson,[22] M. Pachr,[11] S. K. Pal,[45] Y. Panebratsev,[12] A. I. Pavlinov,[48] T. Pawlak,[46] T. Peitzmann,[28] V. Perevoztchikov,[3] C. Perkins,[5] W. Peryt,[46] S. C. Phatak,[15] M. Planinic,[51] J. Pluta,[46] N. Poljak,[51] N. Porile,[33] A. M. Poskanzer,[22] M. Potekhin,[3] E. Potrebenikova,[12] B. V. K. S. Potukuchi,[19] D. Prindle,[47] C. Pruneau,[48] J. Putschke,[22] I. A. Qattan,[17] R. Raniwala,[35] S. Raniwala,[35] R. L. Ray,[42] D. Relyea,[4] A. Ridiger,[26] H. G. Ritter,[22] J. B. Roberts,[36] O. V. Rogachevskiy,[12] J. L. Romero,[6] A. Rose,[22] C. Roy,[40] L. Ruan,[22] M. J. Russcher,[28] R. Sahoo,[15] I. Sakrejda,[22] T. Sakuma,[23] S. Salur,[50] J. Sandweiss,[50] M. Sarsour,[41] P. S. Sazhin,[12] J. Schambach,[42] R. P. Scharenberg,[33] N. Schmitz,[24] J. Seger,[10] I. Selyuzhenkov,[48] P. Seyboth,[24] A. Shabetai,[18] E. Shahaliev,[12] M. Shao,[38] M. Sharma,[30] W. Q. Shen,[39] S. S. Shimanskiy,[12] E. P. Sichtermann,[22] F. Simon,[23] R. N. Singaraju,[45] N. Smirnov,[50] R. Snellings,[28] P. Sorensen,[3] J. Sowinski,[17] J. Speltz,[18] H. M. Spinka,[1] B. Srivastava,[33] A. Stadnik,[12] T. D. S. Stanislaus,[44] D. Staszak,[7] R. Stock,[14] M. Strikhanov,[26] B. Stringfellow,[33] A. A. P. Suaide,[37] M. C. Suarez,[9] N. L. Subba,[20] M. Sumbera,[11] X. M. Sun,[22] Z. Sun,[21] B. Surrow,[23] T. J. M. Symons,[22] A. Szanto de Toledo,[37] J. Takahashi,[37] A. H. Tang,[3] T. Tarnowsky,[33] J. H. Thomas,[22] A. R. Timmins,[2] S. Timoshenko,[26] M. Tokarev,[12] T. A. Trainor,[47] S. Trentalange,[7] R. E. Tribble,[41] O. D. Tsai,[7] J. Ulery,[33] T. Ullrich,[3] D. G. Underwood,[1] G. Van Buren,[3] N. van der Kolk,[28] M. van Leeuwen,[22] A. M. Vander Molen,[25] R. Varma,[16] I. M. Vasilevski,[13] A. N. Vasiliev,[32] R. Vernet,[18] S. E. Vigdor,[17] Y. P. Viyogi,[15] S. Vokal,[12] S. A. Voloshin,[48] W. T. Waggoner,[10] F. Wang,[33] G. Wang,[7] J. S. Wang,[21] X. L. Wang,[38] Y. Wang,[43] J. W. Watson,[20] J. C. Webb,[44] G. D. Westfall,[25] A. Wetzler,[22] C. Whitten, Jr.,[7] H. Wieman,[22] S. W. Wissink,[17] R. Witt,[50] J. Wu,[38] Y. Wu,[49] N. Xu,[22] Q. H. Xu,[22] Z. Xu,[3] P. Yepes,[36] I-K. Yoo,[34] Q. Yue,[43] V. I. Yurevich,[12] W. Zhan,[21] H. Zhang,[3] W. M. Zhang,[20] Y. Zhang,[38] Z. P. Zhang,[38] Y. Zhao,[38] C. Zhong,[39] J. Zhou,[36] R. Zoulkarneev,[13] Y. Zoulkarneeva,[13] A. N. Zubarev,[12] and J. X. Zuo[39]

Article reprint

PRL **98,** 192301 (2007) PHYSICAL REVIEW LETTERS week ending 11 MAY 2007

(STAR Collaboration)

[1]*Argonne National Laboratory, Argonne, Illinois 60439, USA*
[2]*University of Birmingham, Birmingham, United Kingdom*
[3]*Brookhaven National Laboratory, Upton, New York 11973, USA*
[4]*California Institute of Technology, Pasadena, California 91125, USA*
[5]*University of California, Berkeley, California 94720, USA*
[6]*University of California, Davis, California 95616, USA*
[7]*University of California, Los Angeles, California 90095, USA*
[8]*Carnegie Mellon University, Pittsburgh, Pennsylvania 15213, USA*
[9]*University of Illinois, Chicago, Illinois 61801, USA*
[10]*Creighton University, Omaha, Nebraska 68178, USA*
[11]*Nuclear Physics Institute AS CR, 250 68 Řež/Prague, Czech Republic*
[12]*Laboratory for High Energy (JINR), Dubna, Russia*
[13]*Particle Physics Laboratory (JINR), Dubna, Russia*
[14]*University of Frankfurt, Frankfurt, Germany*
[15]*Institute of Physics, Bhubaneswar 751005, India*
[16]*Indian Institute of Technology, Mumbai, India*
[17]*Indiana University, Bloomington, Indiana 47408, USA*
[18]*Institut de Recherches Subatomiques, Strasbourg, France*
[19]*University of Jammu, Jammu 180001, India*
[20]*Kent State University, Kent, Ohio 44242, USA*
[21]*Institute of Modern Physics, Lanzhou, China*
[22]*Lawrence Berkeley National Laboratory, Berkeley, California 94720, USA*
[23]*Massachusetts Institute of Technology, Cambridge, Massachusetts 02139-4307, USA*
[24]*Max-Planck-Institut für Physik, Munich, Germany*
[25]*Michigan State University, East Lansing, Michigan 48824, USA*
[26]*Moscow Engineering Physics Institute, Moscow Russia*
[27]*City College of New York, New York City, New York 10031, USA*
[28]*NIKHEF and Utrecht University, Amsterdam, The Netherlands*
[29]*Ohio State University, Columbus, Ohio 43210, USA*
[30]*Panjab University, Chandigarh 160014, India*
[31]*Pennsylvania State University, University Park, Pennsylvania 16802, USA*
[32]*Institute of High Energy Physics, Protvino, Russia*
[33]*Purdue University, West Lafayette, Indiana 47907, USA*
[34]*Pusan National University, Pusan, Republic of Korea*
[35]*University of Rajasthan, Jaipur 302004, India*
[36]*Rice University, Houston, Texas 77251, USA*
[37]*Universidade de Sao Paulo, Sao Paulo, Brazil*
[38]*University of Science & Technology of China, Hefei 230026, China*
[39]*Shanghai Institute of Applied Physics, Shanghai 201800, China*
[40]*SUBATECH, Nantes, France*
[41]*Texas A&M University, College Station, Texas 77843, USA*
[42]*University of Texas, Austin, Texas 78712, USA*
[43]*Tsinghua University, Beijing 100084, China*
[44]*Valparaiso University, Valparaiso, Indiana 46383, USA*
[45]*Variable Energy Cyclotron Centre, Kolkata 700064, India*
[46]*Warsaw University of Technology, Warsaw, Poland*
[47]*University of Washington, Seattle, Washington 98195, USA*
[48]*Wayne State University, Detroit, Michigan 48201, USA*
[49]*Institute of Particle Physics, CCNU (HZNU), Wuhan 430079, China*
[50]*Yale University, New Haven, Connecticut 06520, USA*
[51]*University of Zagreb, Zagreb, HR-10002, Croatia*

(Received 11 July 2006; revised manuscript received 15 January 2007; published 10 May 2007)

The STAR collaboration at the BNL Relativistic Heavy-Ion Collider (RHIC) reports measurements of the inclusive yield of nonphotonic electrons, which arise dominantly from semileptonic decays of heavy flavor mesons, over a broad range of transverse momenta ($1.2 < p_T < 10$ GeV/c) in $p + p$, $d +$ Au, and Au + Au collisions at $\sqrt{s_{\mathrm{NN}}} = 200$ GeV. The nonphotonic electron yield exhibits an unexpectedly large suppression in central Au + Au collisions at high p_T, suggesting substantial heavy-quark energy loss at

Article reprint
PRL 98, 192301 (2007) PHYSICAL REVIEW LETTERS week ending 11 MAY 2007

RHIC. The centrality and p_T dependences of the suppression provide constraints on theoretical models of suppression.

DOI: 10.1103/PhysRevLett.98.192301 PACS numbers: 25.75.Dw, 13.20.Fc, 13.20.He, 13.85.Qk

High p_T hadron production measurements at the Relativistic Heavy-Ion Collider (RHIC) show a strong suppression of the single-particle inclusive yields in nuclear collisions [1–3]. The suppression is commonly thought to arise from partonic energy loss in dense matter due to induced gluon radiation [4], with its magnitude depending strongly on the color charge density of the medium. This makes it a sensitive probe of the matter created in heavy-ion collisions, where a quark-gluon plasma may form if sufficient energy density is achieved.

Charm and bottom quarks are produced dominantly through high-Q^2 partonic interactions. Heavy flavor cross sections and p_T spectra have been calculated at next-to-leading-order (NLO) for both $p + p$ and $A + A$ collisions [5–7], including nuclear matter effects [7]. Although pQCD calculations agree well with heavy-quark production in collider experiments at higher $\sqrt{s}$ [8], they disagree with recent RHIC measurements [9,10]. Nevertheless, measurements of heavy-quark production potentially provide new constraints on partonic energy loss mechanisms [11–17]. Gluon radiation in a forward cone is suppressed for heavy quarks at moderate energy (dead cone effect) [11,12], with corresponding reduction in medium induced energy loss and less suppression of heavy-quark mesons than light quark mesons.

Direct reconstruction of heavy flavor mesons via hadronic decay channels [9] is difficult in the complex environment of high energy nuclear collisions. Heavy-quark production can also be studied through measurements of electrons (positrons) from semileptonic D and B decays. This Letter reports STAR Collaboration measurements of the nonphotonic electron yield, $(e^+ + e^-)/2$, in $p + p$, d + Au, and Au + Au collisions at nucleon-nucleon center of mass energy $\sqrt{s_{\rm NN}} = 200$ GeV. The data extend significantly the p_T range of previous electron suppression studies [18], to a region of phase space where bottom decays are expected to be dominant. Large differences in energy loss are expected between c and b quarks in this region [14], and these measurements provide important new constraints on partonic energy loss mechanisms.

STAR is a large acceptance apparatus comprising several detector subsystems within a 0.5 T solenoidal magnet field [19]. The main detectors for this analysis are the Time Projection Chamber (TPC) [20] and the barrel Electromagnetic Calorimeter (EMC) [21]. The EMC has a gas-filled Shower Maximum Detector (SMD) at a depth of $\sim 5X_0$ to measure shower shape and position. A fast trigger based on single EMC tower energy enriches the electron sample at high p_T. Electrons at moderate p_T were reconstructed from minimum bias and centrality triggered Au + Au event samples, while EMC triggered events were used for $p_T > 3 - 4\text{GeV}/c$. Au + Au data were divided into 3 centrality classes based on the track multiplicity measured at midrapidity. The integrated luminosity sampled by the EMC trigger is 100 nb^{-1} for $p + p$, 370 μb^{-1} for d + Au and 26 μb^{-1} for the most central Au + Au events. The charged particle acceptance is $0 < \eta < 0.7$ and $0 < \phi < 2\pi$, selected to minimize the radiation length of detector material interior to the EMC within the available EMC acceptance.

The analysis has three main steps: selection of electrons, subtraction of background from decays and interactions in material, and residual corrections to the signal yield. Table I shows the major correction factors and uncertainties, which we now discuss in detail.

Electron PID.—Electron identification utilizes ionization energy loss (dE/dx) and track momentum from the TPC, together with energy and shower shapes from the EMC. Tracks with momentum $p > 1.5\text{GeV}/c$ are accepted if they originate from the primary vertex (distance of closest approach less than 1.5 cm) and project to an active EMC tower, with acceptance $\alpha_{\rm EMC} \sim 75\%$–$85\%$ of the EMC instrumented coverage. This reduced acceptance is due to dead or noisy electronics channels. Initial electron identification is based on $p/E < 2$, where p is the TPC track momentum and E is the energy of the EMC tower. Simulations show that this cut excludes $\sim 7\%$ of real electrons due to sharing of shower energy between towers. Additional hadron rejection is based on the shower shape measured by the SMD. Figure 1(a) shows the dE/dx distribution for tracks passing the p/E and shower shape cuts. The curves show Gaussian functions fit to the distribution, representing the yields of $p + K$, pions and electrons [22]. The parameters in the fit are the yields, widths, and overall dE/dx scale, with widths and the distances between centroids being quasifree parameters, constrained by a model of energy deposition in the TPC gas [23].

Electrons are selected by cutting on TPC energy loss $dE/dx_{\rm min} < dE/dx < 5.1$ keV/cm. $dE/dx_{\rm min}$ is around 3.5 keV/cm, with the specific value having weak dependence on the event multiplicity and increasing slowly with track momentum, to optimize electron efficiency and hadron rejection while preserving more than 50% of the electrons in the dE/dx distribution. The residual hadron background satisfying the dE/dx cut is estimated based on Gaussian fits similar to those in Fig. 1.

Table I shows the combined electron tracking and identification efficiency (''PID efficiency''), determined by embedding simulated electrons into real events. It is significantly below unity due to tracking efficiency ($\sim 70\%$),

PRL 98, 192301 (2007) PHYSICAL REVIEW LETTERS week ending 11 MAY 2007

TABLE I. Corrections and systematic uncertainties for the nonphotonic electron yield at $p_T = 2$ and 8 GeV/c.

Correction	$p + p$		Central Au + Au	
	2 GeV/c	8 GeV/c	2 GeV/c	8 GeV/c
Acceptance	0.84 ± 0.05		0.75 ± 0.15	
PID efficiency	0.25 ± 0.03	0.50 ± 0.03	0.13 ± 0.03	0.45 ± 0.03
Hadron contamination	<0.01	0.20 ± 0.04	0.03 ± 0.03	0.22 ± 0.05
Background reconstruction efficiency (ε_B)	0.65 ± 0.06	0.55 ± 0.06	0.56 ± 0.06	0.50 ± 0.06
Bremsstrahlung & $\delta p/p$	0.86 ± 0.14	1.05 ± 0.05	0.9 ± 0.1	1.1 ± 0.1
EMC $\varepsilon_{\text{trigger}}$	-	1.00 ± 0.08	-	1.00 ± 0.05
Cross section	± 0.14		-	

exclusion of electrons due to the energy leakage to neighboring towers, and SMD response. Its increase from $p_T =$ 2 to 8 GeV/c is due to increasing SMD efficiency.

Electron background.—Background from photonic sources is due largely to photon conversions (~85%) in the detector material between the interaction point and the TPC ($X/X_0 \sim 4.5\%$) and π^0 and η Dalitz decays [24] (~15%). The photonic electron yield is measured using the invariant mass distribution of track pairs detected in the TPC. One track of the pair is required to fall in the EMC acceptance, satisfying $p > 1.5$ GeV/c and electron PID cuts, with the other track having $p_T > 0.15$ GeV/c within the TPC acceptance and a loose cut around the electron dE/dx band. Figure 1(b) shows the invariant mass distribution of pairs with the same or opposite charge sign. The same-sign distribution is due to random (combinatorial) pairs. An alternative combinatorial distribution formed by embedding single simulated electrons into real events agrees with the same-sign distribution within statistical uncertainties.

The shaded region in Fig. 1(b) is the difference between the opposite and same-sign distributions and represents the photonic yield. It exhibits a peak at zero invariant mass due to conversions, and a tail at nonzero mass due to Dalitz decays [24]. Selecting $m < 150$ MeV/c^2 accepts ~98% of all π^0 and η Dalitz pairs in this distribution. The efficiency $\varepsilon_B(p_T)$ to identify a photonic electron in the EMC by this procedure was estimated by embedding [25] the main background sources (π^0 and γ) with a realistic momentum distribution derived from recent RHIC data [26] into real events.

The photonic electron yield N_{ph} is calculated in each p_T bin via $N_{\text{ph}} = (N_{\text{unlike}} - N_{\text{like}})/\varepsilon_B$. Additional background, mainly from ω, ϕ, and ρ decays, was estimated using PYTHIA [27] and HIJING [28] simulations to be ~2%–4% of N_{ph} [9] and is included in the systematic uncertainty of N_{ph}. Figure 1(c) depicts the ratio of the inclusive to the photonic electron spectra for $p + p$ and Au + Au collisions. The figure shows a clear electron excess. Within uncertainties, the nonphotonic excess is independent of centrality at high p_T.

Nonphotonic electron yield.—The trigger efficiency was determined by comparing the electron candidate spectrum in the minimum bias and triggered data sets. At high-p_T the ratio of the spectra is compatible with the online scale-down factor applied to minimum bias events. The nonphotonic spectrum is the difference of the inclusive and photonic spectra. Additional corrections are applied for momentum resolution and bremsstrahlung, determined from simulations.

Systematic uncertainties.—Systematic uncertainties were determined by varying cut parameters within reasonable limits. The uncorrelated systematic uncertainty of the electron yield is dominated by the electron identification efficiency and photonic background reconstruction at low p_T and the correction for residual hadron background at high p_T.

Figure 2 shows the fully corrected nonphotonic electron spectra for 200 GeV $p + p$, $d +$ Au, and Au + Au collisions. The curves correspond to fixed order next-to-leading log (FONLL) predictions [7] for semileptonic D and B

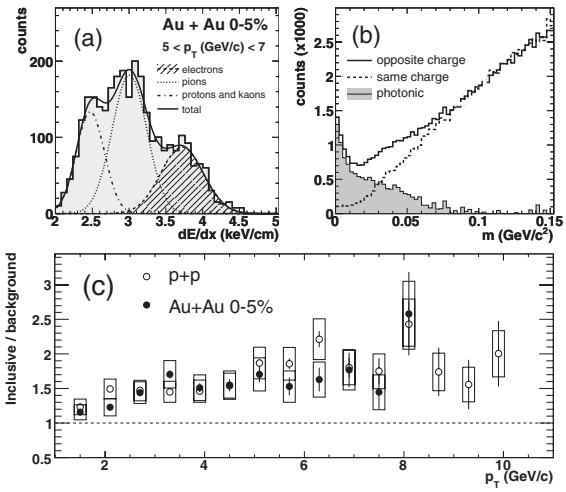

FIG. 1. (a) dE/dx projections for $5 < p_T(\text{GeV}/c) < 7$ in central Au + Au events after EMC and SMD cuts. The lines are Gaussian fits for $p + K$, π, and electron yields. (b) Invariant e^+e^- mass spectrum. (c) Ratio of inclusive and background electron yield vs p_T for $p + p$ and Au + Au collisions. Vertical bars are statistical errors, boxes are systematic uncertainties.

PRL 98, 192301 (2007) PHYSICAL REVIEW LETTERS week ending 11 MAY 2007

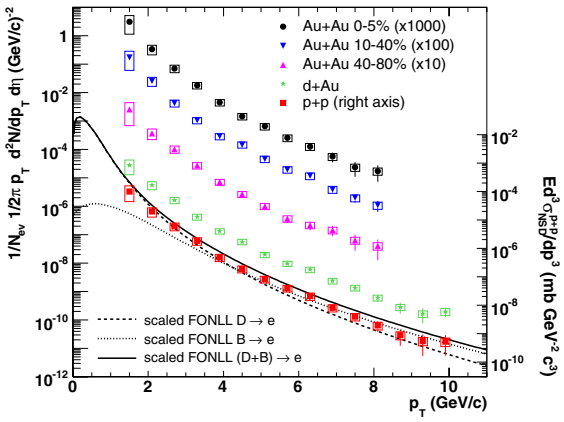

FIG. 2 (color online). Nonphotonic electron spectra. Vertical bars are statistical errors, boxes are systematic uncertainties. The curves are scaled pQCD predictions for $p + p$ [7]. Cross section on right axis applies to $p + p$ spectrum only.

meson decays. The calculated spectrum is scaled by 5.5 (see below).

Figure 3, upper part (points), shows the ratio of measured to unscaled FONLL-calculated nonphotonic electron yield for $p + p$ collisions. The calculation describes the *shape* of the measured spectra relatively well, though with a large difference in their overall scale. Better agreement is found at larger $\sqrt{s}$ [8]. The same ratio is shown for published STAR [9] and PHENIX [10] measurements. The horizontal dashed line is at $5.5 \pm 0.8(\text{stat}) \pm 1.7(\text{syst})$, corresponding to the ratio between the total charm cross section measured by STAR [9] to the central value predicted by FONLL [7,8]. The shaded band around that line shows the experimental uncertainty in this ratio. PHENIX data [10] exhibit a lower ratio and appear not to be consistent with the data reported here. The lower part (curves) shows the relative contribution to the FONLL calculation of charm and bottom decays, with the variation due to NLO uncertainties [7,29]. The B-decay contribution is expected to be significant in the upper p_T range of this measurement.

Modification of the inclusive particle production is measured by the nuclear modification factor [1] [$R_{AA}(p_T)$]. R_{AA} is unity for hard processes without nuclear effects. Figure 4 shows $R_{AA}(p_T)$ for nonphotonic electrons in d + Au and central Au + Au collisions. Error bars show the statistical uncertainties, boxes show uncorrelated systematic uncertainties, and the filled band at unity is the overall normalization uncertainty. R_{AA} for d + Au is consistent with a moderate Cronin enhancement. $R_{AA} \sim 0.2$ for central Au + Au collisions at $p_T > 3$ GeV/c, consistent with a previous measurement at lower p_T [18]. The suppression is similar to that for light hadrons at $p_T > 6$ GeV/c [2].

Figure 4 shows predictions for electron R_{AA} from semileptonic D- and B-meson decay in central Au + Au collisions using calculations of heavy-quark energy loss. Curve I uses DGLV radiative energy loss via few hard scatterings [14] with initial gluon density $dN_g/dy = 1000$, consistent with light quark suppression. Curve II uses BDMPS radiative energy loss via multiple soft collisions [15], with transport coefficient $\hat{q}$. $\hat{q}$ is set to 14 GeV^2/fm, though light quark hadron suppression provides only a loose constraint $4 < \hat{q} < 14$ GeV^2/fm [15]. Both calculations predict much less suppression than observed.

This discrepancy may indicate significant collisional (elastic) energy loss for heavy quarks [13,30]. Curve III is a DGLV-based calculation including both radiative *and* collisional energy loss, together with path length fluctua-

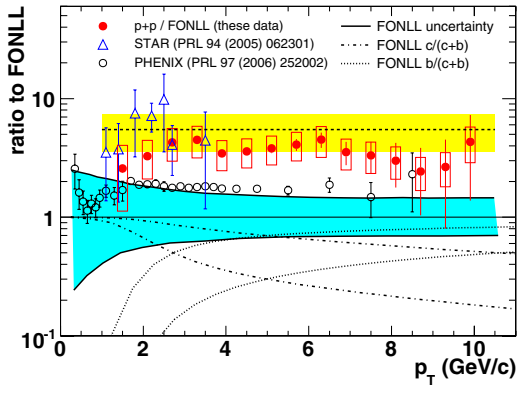

FIG. 3 (color online). Upper: ratio between measured nonphotonic electron yield and FONLL pQCD calculations [7] for $p + p$ collisions. Lower: relative contributions to FONLL distribution of c and b decays.

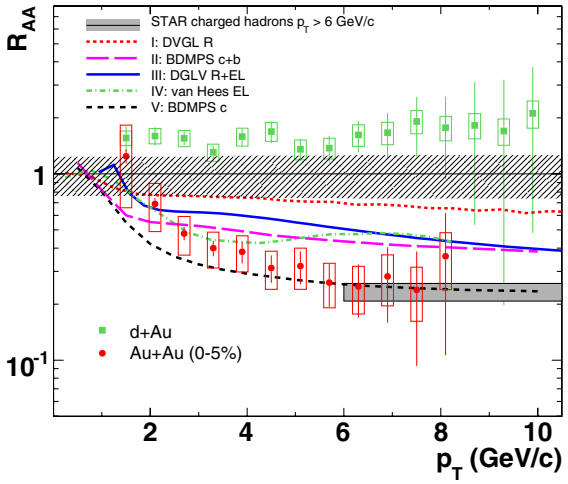

FIG. 4 (color online). The nuclear modification factor, R_{AA}, for d + Au and Au + Au collisions at $\sqrt{s_{\text{NN}}} = 200$ GeV. Error bars and uncertainties are described in text.

Article reprint
PRL 98, 192301 (2007) PHYSICAL REVIEW LETTERS week ending 11 MAY 2007

tions [16]. The calculated suppression is also markedly less than that observed. For curve IV, the heavy-quark energy loss is due to elastic scattering mediated by resonance excitations (D and B) and LO t-channel gluon exchange [17]. This calculation also predicts significantly less suppression than observed.

Dead cone reduction of energy loss is expected to be more significant for bottom than charm quarks in the reported p_T range. Curve V, which is the same calculation as curve II but for D-meson decays only, agrees better with the data. Since there is better agreement of data and theory for bottom than charm production at the Tevatron [8], the scale factor 5.5 between calculated and measured $p + p$ electron yields may overestimate the B decay contribution at RHIC; i.e., D decays may in fact dominate the electron yields in the reported p_T range, favoring calculation V. A direct measurement of D mesons at high-p_T is required to understand energy loss of heavy quarks in detail. Finally, multibody mechanisms may also contribute to heavy-quark energy loss [31].

We have reported the measurement of high-p_T nonphotonic electrons in $p + p$, $d + \mathrm{Au}$, and $\mathrm{Au} + \mathrm{Au}$ collisions at $\sqrt{s_{\mathrm{NN}}} = 200$ GeV. A pQCD calculation for heavy-quark production in $p + p$ collisions underpredicts the data, although it describes the overall shape of the p_T distribution relatively well. Large yield suppression is observed in central $\mathrm{Au} + \mathrm{Au}$ collisions, consistent with substantial energy loss of heavy quarks in dense matter. The suppression is larger than that expected from radiative energy loss calculations, suggesting that other processes contribute significantly to heavy-quark energy loss. This unique sensitivity to the energy loss mechanisms makes the measurement of heavy-quark suppression an essential component of the study of dense matter. Full description of the interaction between partons and the medium will require further detailed measurements of charm and bottom separately.

We thank the RHIC Operations Group and RCF at BNL, and the NERSC Center at LBNL for their support. This work was supported in part by the HENP Divisions of the Office of Science of the U. S. DOE; the U. S. NSF; the BMBF of Germany; IN2P3, RA, RPL, and EMN of France; EPSRC of the United Kingdom; FAPESP of Brazil; the Russian Ministry of Science and Technology; the Ministry of Education and the NNSFC of China; IRP and GA of the Czech Republic, FOM of the Netherlands, DAE, DST, and CSIR of the Government of India; Swiss NSF; the Polish State Committee for Scientific Research; STAA of Slovakia, and the Korea Sci. & Eng. Foundation.

[1] C. Adler *et al.*, Phys. Rev. Lett. **89**, 202301 (2002).
[2] J. Adams *et al.*, Phys. Rev. Lett. **91**, 172302 (2003).
[3] J. Adams *et al.*, Phys. Rev. Lett. **91**, 072304 (2003).
[4] R. Baier *et al.*, Annu. Rev. Nucl. Part. Sci. **50**, 37 (2000); M. Gyulassy *et al.*, arXiv:nucl-th/0302077.
[5] S. Frixione *et al.*, Adv. Ser. Dir. High Energy Phys. **15**, 609 (1998).
[6] R. Vogt, Heavy Ion Physics **18**, 11 (2003).
[7] M. Cacciari *et al.*, Phys. Rev. Lett. **95**, 122001 (2005); FONLL calculations with CTEQ6M, $m_c = 1.5\ \mathrm{GeV}/c^2$, $m_b = 5\ \mathrm{GeV}/c^2$, and $\mu_{R,F} = m_T$.
[8] S. Frixione, Eur. Phys. J. C **43**, 103 (2005).
[9] J. Adams *et al.*, Phys. Rev. Lett. **94**, 062301 (2005).
[10] A. Adare *et al.*, Phys. Rev. Lett. **97**, 252002 (2006).
[11] Yu. L. Dokshitzer and D. E. Kharzeev, Phys. Lett. B **519**, 199 (2001).
[12] B. W. Zhang *et al.*, Phys. Rev. Lett. **93**, 072301 (2004).
[13] M. G. Mustafa, Phys. Rev. C **72**, 014905 (2005).
[14] M. Djordjevic *et al.*, Phys. Lett. B **632**, 81 (2006).
[15] N. Armesto *et al.*, Phys. Lett. B **637**, 362 (2006).
[16] S. Wicks *et al.*, Nucl. Phys. **A784**, 426 (2007).
[17] H. van Hees, V. Greco, and R. Rapp, Phys. Rev. C **73**, 034913 (2006); (private comunication).
[18] S. S. Adler *et al.*, Phys. Rev. Lett. **96**, 032301 (2006).
[19] K. H. Ackermann *et al.*, Nucl. Instrum. Methods Phys. Res., Sect. A **499**, 624 (2003).
[20] M. Anderson *et al.*, Nucl. Instrum. Methods Phys. Res., Sect. A **499**, 659 (2003).
[21] M. Beddo *et al.*, Nucl. Instrum. Methods Phys. Res., Sect. A **499**, 725 (2003).
[22] M. Shao *et al.*, Nucl. Instrum. Methods Phys. Res., Sect. A **558**, 419 (2006).
[23] H. Bichsel, Nucl. Instrum. Methods Phys. Res., Sect. B **562**, 154 (2006).
[24] S. Eidelman *et al.*, Phys. Lett. B **592**, 1 (2004).
[25] J. Adams *et al.*, arXiv:nucl-ex/0311017.
[26] S. S. Adler *et al.*, Phys. Rev. Lett. **98**, 172302 (2007).
[27] T. Sjostrand *et al.*, arXiv:hep-ph/0308153.
[28] M. Gyulassy and X. N. Wang, Comput. Phys. Commun. **83**, 307 (1994).
[29] R. Vogt (private communication).
[30] M. Djordjevic, Phys. Rev. C **74**, 064907 (2006).
[31] W. Liu and C. M. Ko, arXiv:nucl-th/0603004.

Article reprint

PRL **106,** 159902 (2011) PHYSICAL REVIEW LETTERS week ending 15 APRIL 2011

Erratum: Transverse Momentum and Centrality Dependence of High-p_T Nonphotonic Electron Suppression in Au + Au Collisions at $\sqrt{s_{NN}} = 200$ GeV [Phys. Rev. Lett. 98, 192301 (2007)]

B. I. Abelev, M. M. Aggarwal, Z. Ahammed, B. D. Anderson, D. Arkhipkin, G. S. Averichev, Y. Bai, J. Balewski, O. Barannikova, L. S. Barnby, J. Baudot, S. Baumgart, V. V. Belaga, A. Bellingeri-Laurikainen, R. Bellwied, F. Benedosso, R. R. Betts, S. Bhardwaj, A. Bhasin, A. K. Bhati, H. Bichsel, J. Bielcik, J. Bielcikova, L. C. Bland, S-L. Blyth, M. Bombara, B. E. Bonner, M. Botje, J. Bouchet, A. V. Brandin, A. Bravar, T. P. Burton, M. Bystersky, R. V. Cadman, X. Z. Cai, H. Caines, M. Calderón de la Barca Sánchez, J. Callner, O. Catu, D. Cebra, Z. Chajecki, P. Chaloupka, S. Chattopadhyay, H. F. Chen, J. H. Chen, J. Y. Chen, J. Cheng, M. Cherney, A. Chikanian, W. Christie, S. U. Chung, J. P. Coffin, T. M. Cormier, M. R. Cosentino, J. G. Cramer, H. J. Crawford, D. Das, S. Dash, M. Daugherity, M. M. de Moura, T. G. Dedovich, M. DePhillips, A. A. Derevschikov, L. Didenko, T. Dietel, P. Djawotho, S. M. Dogra, X. Dong, J. L. Drachenberg, J. E. Draper, F. Du, V. B. Dunin, J. C. Dunlop, M. R. Dutta Mazumdar, V. Eckardt, W. R. Edwards, L. G. Efimov, V. Emelianov, J. Engelage, G. Eppley, B. Erazmus, M. Estienne, P. Fachini, R. Fatemi, J. Fedorisin, A. Feng, P. Filip, E. Finch, V. Fine, Y. Fisyak, J. Fu, C. A. Gagliardi, L. Gaillard, M. S. Ganti, E. Garcia-Solis, V. Ghazikhanian, P. Ghosh, Y. G. Gorbunov, H. Gos, O. Grebenyuk, D. Grosnick, S. M. Guertin, K. S. F. F. Guimaraes, N. Gupta, B. Haag, T. J. Hallman, A. Hamed, J. W. Harris, W. He, M. Heinz, T. W. Henry, S. Heppelmann, B. Hippolyte, A. Hirsch, E. Hjort, A. M. Hoffman, G. W. Hoffmann, D. Hofman, R. Hollis, M. J. Horner, H. Z. Huang, E. W. Hughes, T. J. Humanic, G. Igo, A. Iordanova, P. Jacobs, W. W. Jacobs, P. Jakl, F. Jia, P. G. Jones, E. G. Judd, S. Kabana, K. Kang, J. Kapitan, M. Kaplan, D. Keane, A. Kechechyan, D. Kettler, V. Yu. Khodyrev, B. C. Kim, J. Kiryluk, A. Kisiel, E. M. Kislov, S. R. Klein, A. G. Knospe, A. Kocoloski, D. D. Koetke, T. Kollegger, M. Kopytine, L. Kotchenda, V. Kouchpil, K. L. Kowalik, P. Kravtsov, V. I. Kravtsov, K. Krueger, C. Kuhn, A. I. Kulikov, A. Kumar, P. Kurnadi, A. A. Kuznetsov, M. A. C. Lamont, J. M. Landgraf, S. Lange, S. LaPointe, F. Laue, J. Lauret, A. Lebedev, R. Lednicky, C -H. Lee, S. Lehocka, M. J. LeVine, C. Li, Q. Li, Y. Li, G. Lin, X. Lin, S. J. Lindenbaum, M. A. Lisa, F. Liu, H. Liu, J. Liu, L. Liu, T. Ljubicic, W. J. Llope, R. S. Longacre, W. A. Love, Y. Lu, T. Ludlam, D. Lynn, G. L. Ma, J. G. Ma, Y. G. Ma, D. Magestro, D. P. Mahapatra, R. Majka, L. K. Mangotra, R. Manweiler, S. Margetis, C. Markert, L. Martin, H. S. Matis, Yu. A. Matulenko, C. J. McClain, T. S. McShane, Yu. Melnick, A. Meschanin, J. Millane, M. L. Miller, N. G. Minaev, S. Mioduszewski, C. Mironov, A. Mischke, J. Mitchell, B. Mohanty, D. A. Morozov, M. G. Munhoz, B. K. Nandi, C. Nattrass, T. K. Nayak, J. M. Nelson, N. S. Nepali, P. K. Netrakanti, L. V. Nogach, S. B. Nurushev, G. Odyniec, A. Ogawa, V. Okorokov, M. Oldenburg, D. Olson, M. Pachr, S. K. Pal, Y. Panebratsev, A. I. Pavlinov, T. Pawlak, T. Peitzmann, V. Perevoztchikov, C. Perkins, W. Peryt, S. C. Phatak, M. Planinic, J. Pluta, N. Poljak, N. Porile, A. M. Poskanzer, M. Potekhin, E. Potrebenikova, B. V. K. S. Potukuchi, D. Prindle, C. Pruneau, J. Putschke, I. A. Qattan, R. Raniwala, S. Raniwala, R. L. Ray, D. Relyea, A. Ridiger, H. G. Ritter, J. B. Roberts, O. V. Rogachevskiy, J. L. Romero, A. Rose, C. Roy, L. Ruan, M. J. Russcher, R. Sahoo, I. Sakrejda, T. Sakuma, S. Salur, J. Sandweiss, M. Sarsour, P. S. Sazhin, J. Schambach, R. P. Scharenberg, N. Schmitz, J. Seger, I. Selyuzhenkov, P. Seyboth, A. Shabetai, E. Shahaliev, M. Shao, M. Sharma, W. Q. Shen, S. S. Shimanskiy, E. P. Sichtermann, F. Simon, R. N. Singaraju, N. Smirnov, R. Snellings, P. Sorensen, J. Sowinski, J. Speltz, H. M. Spinka, B. Srivastava, A. Stadnik, T. D. S. Stanislaus, D. Staszak, R. Stock, M. Strikhanov, B. Stringfellow, A. A. P. Suaide, M. C. Suarez, N. L. Subba, M. Sumbera, X. M. Sun, Z. Sun, B. Surrow, T. J. M. Symons, A. Szanto de Toledo, J. Takahashi, A. H. Tang, T. Tarnowsky, J. H. Thomas, A. R. Timmins, S. Timoshenko, M. Tokarev, T. A. Trainor, S. Trentalange, R. E. Tribble, O. D. Tsai, J. Ulery, T. Ullrich, D. G. Underwood, G. Van Buren, N. van der Kolk, M. van Leeuwen, A. M. Vander Molen, R. Varma, I. M. Vasilevski, A. N. Vasiliev, R. Vernet, S. E. Vigdor, Y. P. Viyogi, S. Vokal, S. A. Voloshin, W. T. Waggoner, F. Wang, G. Wang, J. S. Wang, X. L. Wang, Y. Wang, J. W. Watson, J. C. Webb, G. D. Westfall, A. Wetzler, C. Whitten, Jr., H. Wieman, S. W. Wissink, R. Witt, J. Wu, Y. Wu, N. Xu, Q. H. Xu, Z. Xu, P. Yepes, I. -K. Yoo, Q. Yue, V. I. Yurevich, W. Zhan, H. Zhang, W. M. Zhang, Y. Zhang, Z. P. Zhang, Y. Zhao, C. Zhong, J. Zhou, R. Zoulkarneev, Y. Zoulkarneeva, A. N. Zubarev, and J. X. Zuo

(STAR Collaboration)

(Received 4 February 2011; published 13 April 2011)

DOI: 10.1103/PhysRevLett.106.159902 PACS numbers: 25.75.Dw, 13.20.Fc, 13.20.He, 13.85.Qk, 99.10.Cd

Article reprint

PRL **106,** 159902 (2011) PHYSICAL REVIEW LETTERS week ending 15 APRIL 2011

In the original Letter [1] we reported on measurements of the transverse momentum spectra of nonphotonic electrons in $p + p$, $d +$ Au, and Au + Au collisions at $\sqrt{s_{\mathrm{NN}}} = 200$ GeV.

We have uncovered a mistake in the application of the background finding efficiency in the subtraction of the background from Dalitz decays and photon conversion. While the effective background reconstruction efficiency quoted in the original Letter is correct, the ones actually applied were 10%–15% higher. Because of this the background levels reported were underestimated and consequently the yields of nonphotonic electrons published were higher than their actual values. This mistake affected results from all three collision systems used in [1].

Figure 1 shows the revised ratio of inclusive over background electron yield as a function of p_T for $p + p$ and Au + Au collisions. Because of the increase in background the ratio decreased systematically over the full p_T range.

Figure 2 shows the corrected nonphotonic electron spectra for 200 GeV $p + p$, $d +$ Au, and Au + Au collisions. The curves correspond to FONLL (Fixed Order Next-to-Leading Log) predictions [2] for semileptonic D and B meson decays.

Recent studies reported that feed-down from J/ψ decays contributes noticeably to the observed nonphotonic electron signal [3]. This correction is not applied to the spectra shown in Fig. 2 but will be included and discussed in detail in a recent analysis of high statistics data [4].

Comparisons of the corrected $p + p$ spectrum with a pQCD FONLL calculation and the result from the PHENIX collaboration [5] are shown in Fig. 3. Within statistical errors our measurement agrees well with the pQCD calculation and the STAR and PHENIX results are consistent with each other. The results at low p_T that were derived from a separate analysis using STAR's time of flight detector [6] were also investigated and found to be correct.

Since the mistake made in the background finding efficiency affects the $p + p$, $d +$ Au, and Au + Au data in a similar fashion, the nuclear modification factor, R_{AA}, for $d +$ Au and Au + Au collisions shown in Fig. 4 shifts only slightly in

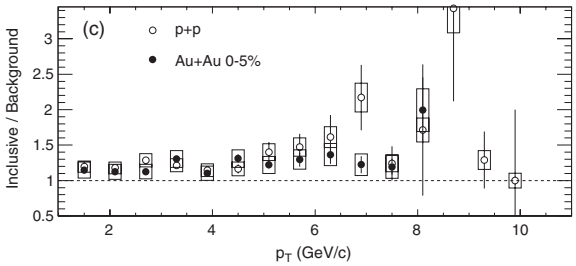

FIG. 1. (c) Ratio of inclusive and background electron yield vs p_T for $p + p$ and Au + Au collisions. Vertical bars are statistical errors, boxes are systematic uncertainties.

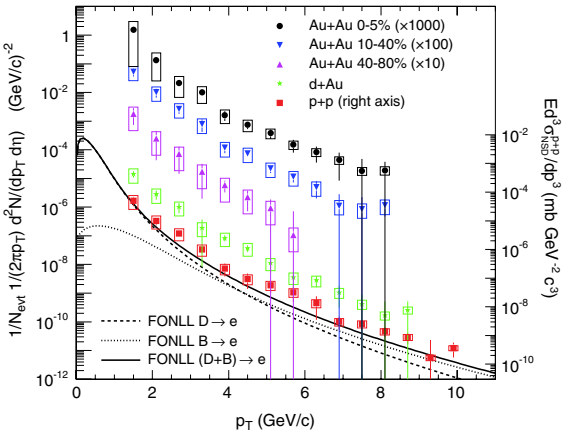

FIG. 2 (color online). Nonphotonic electron spectra. Vertical bars are statistical errors, boxes are systematic uncertainties. The curves are pQCD predictions for $p + p$ [2] (not scaled). Cross section on right axis applies to $p + p$ spectrum only.

Article reprint
PRL 106, 159902 (2011) PHYSICAL REVIEW LETTERS week ending 15 APRIL 2011

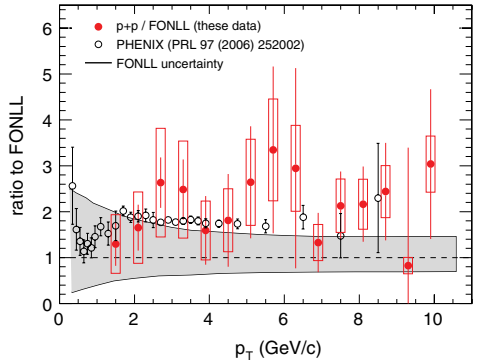

FIG. 3 (color online). Ratio between measured nonphotonic electron spectra and FONLL pQCD calculations [2]. The shaded band around that line reflects the experimental uncertainty in this ratio.

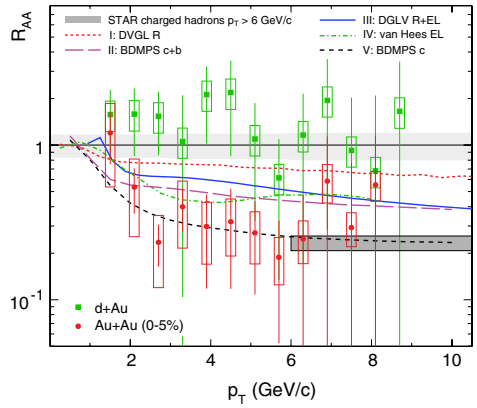

FIG. 4 (color online). The nuclear modification factor, R_{AA}, for d + Au and Au + Au collisions at $\sqrt{s_{\mathrm{NN}}} = 200$ GeV.

central value, but the statistical errors are larger than those in [1]. The main conclusion of the original Letter remains valid: a large suppression of nonphotonic electron yield in central Au + Au collisions is observed, consistent with substantial energy loss of heavy quarks in dense matter created at RHIC.

The authors wish to thank Wei Xie and Xin Li from Purdue University for their contributions in identifying the mistake and reanalyzing the data.

[1] B. I. Abelev *et al.* (STAR Collaboration), Phys. Rev. Lett. **98**, 192301 (2007).
[2] M. Cacciari, P. Nason, and R. Vogt, Phys. Rev. Lett. **95**, 122001 (2005) [arXiv:hep-ph/0502203]; FONLL calculations with CTEQ6M, $m_c = 1.5$ GeV/c^2, $m_b = 5$ GeV/c^2, and $\mu_{R,F} = m_T$.
[3] A. Adare *et al.* (PHENIX Collaboration), arXiv:1005.1627.
[4] H. Agakishiev *et al.* (STAR Collaboration), Phys. Rev. D **83**, 052006 (2011).
[5] A. Adare *et al.* (PHENIX Collaboration), Phys. Rev. Lett. **97**, 252002 (2006).
[6] J. Adams *et al.* (STAR Collaboration), Phys. Rev. Lett. **94**, 062301 (2005).

Kapitola 4

Produkcia kvarkónií v protón-protónových zrážkach

Pôvabné kvarkónia majú v problematike kvarkovo-gluónovej plazmy špeciálne miesto. Je to z dôvodu, že boli považované za významný prejav jej existencie, ako sme uviedli v úvodnej kapitole. Experimenty na RHIC previedli ich podrobné merania v rôznych zrážkových systémoch a energiách. Jadro-jadrovým zrážkam sa budeme podrobne venovať v budúcej kapitole. Teraz sa zameráme na merania v protón-protónových zrážkach. Je pozoruhodné, že i po viac než štyroch dekádach od objavenia J/ψ nie je dostatočne presne teoreticky popísaná produkcia pôvabných kvarkónií ani v elementárnych zrážkach. Základné modely produkcie, ktoré sa pri výpočtoch používajú sú color-singlet model (CSM) a nerelativistický QCD model (NRQCD), zahrňujúci produkciu i cez color-octet mechanizmus. Prehľadný popis modelov je možné nájsť v Ref. [R39]. Samotné spektrá priečných hybností sú, v rámci ich aplikovateľnosti, modelmi s dobrou presnosťou popísané, viz Obr. 4.1. Na tomto obrázku je predbežné meranie závislosti inkluzívneho účinného prierezu mezónu J/ψ na priečnej hybosti z dielektrónového a dimuónového kanálu meraného experimentom STAR v p + p zrážkach pri energii 200 GeV [R40]. Experimentálne dáta pokrývajú rozsah p_T v intervale 0 až 14 GeV/c a sú porovnané s výpočtami z teoretických modelov CGC+NRQCD [R41], NLO+NRQCD [R42] a ICEM [R43]. Kým ostatný model popisuje dobre spektrá do $p_T \approx 3$ GeV/c, prvé dva modely popisujú dobre spektrá nad 1 GeV/c . NRQCD model je úspešný aj v popise spektier na LHC a Tevatrone [R41].

Veličina, ktorá je ďalším výborným testom teoretických výpočtov, je polarizácia, t.j. zarovnanie vektora spinu častice vzhľadom k vektoru hybnosti častice. Parameter polarizácie sa stanovuje obvykle v konkrétnej vzťažnej sústave. My sme v článku priloženom v tejto kapitole použili tzv. helicitnú sústavu. Z dôvodu nedostatočnej veľkosti súboru dát pre presnejšie merania, sme študovali len polárny polarizačný parameter λ_θ a cez azimutálnu závislosť sme preintegrovali. Hodnotu polarizácie je možné v tomto prípade získať z uhlového rozdelenia elektrónov z rozpadu J/ψ, kde nás zajíma polárny uhol θ medzi vektorom hybnosti pozitrónu v kľudovej sústave J/ψ a hybnosťou J/ψ v labo-

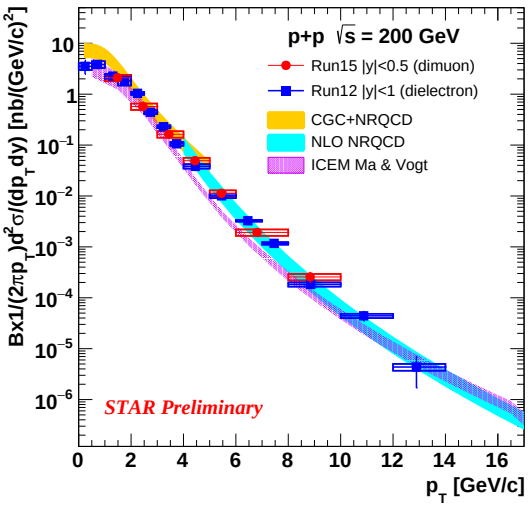

Obr. 4.1: Predbežný inkluzívny účinný prierez mezónu J/ψ z dielektrónového a dimuónového kanálu meraný experimentom STAR v p + p zrážkach pri energii $\sqrt{s}$ = 200 GeV. Experimentálne dáta sú porovnané s výpočtami z teoretických modelov CGC+NRQCD [R41], NLO+NRQCD [R42] a ICEM [R43]. Prevzaté z Ref. [R40].

ratórnej sústave.

$$\frac{dN}{d(\cos\theta)} \propto 1 + \lambda_\theta \cos^2\theta\,, \tag{4.1}$$

Pri takejto voľbe sústavy a parametru λ_θ je parameter zložený z príspevku z oboch typov polarizácie: pozdĺžnej i priečnej. Avšak pri hraničných hodnotách platí, že $\lambda_\theta = 1$ znamená plnú priečnu polarizáciu a λ_θ = -1 znamená plnú pozdĺžnu polarizáciu.

Výpočty polarizácie pomocou NRQCD nesúhlasia s experimentálnymi meraniami z experimentu CDF (p_T od 5 GeV/c do 30 GeV/c) [R44] pri energii 1.96 TeV. Výpočty predpovedajú priečnu polarizáciu, avšak merania odpovedajú miernej pozdĺžnej polarizácii. Podobne je to u meraní na LHC z experimentu CMS (p_T od 14 GeV/c do 70 GeV/c) pri energii 7 TeV [R45]. Kým merania ukazujú na hodnotu λ_θ blízku nule a teda na žiadnu polarizáciu, výpočty predpovedajú priečnu polarizáciu. Merania polarizácie pri zhodnej energii, ale doprednej rapidite z experimentu ALICE (p_T od 2 GeV/c do 8 GeV/c) [140] a z experimentu LHCb (p_T od 2 GeV/c do 15 GeV/c) [R46] ukazujú na žiadnu, prípadne malú, pozdĺžnu polarizáciu a sú bližšie výpočtom NRQCD ako CSM modelu, ktorý predpovedá silnú pozdĺžnu polarizáciu.

V článku priloženom v tejto kapitole L. Adamczyk *et al.*, *J/ψ polarization in p+p collisions at $\sqrt{s}$=200 GeV*, Phys. Lett. B **739**, 180 (2014), sme previedli prvú analýzu polarizácie J/ψ na experimente STAR. Zamerali sme sa na experimentálne dáta, ktoré boli merané pomocou nastavenia HT spúšťača (viz. predošlá kapitola). Cieľom bolo rekonštruovať J/ψ v e^+e^- rozpadovom kanáli s čo najvyššou priečnou hybnosťou, kde

sa predpovede modelov líšia. Dáta z meraní v roku 2009 umožnili zmerať parameter λ_θ v helicitnej sústave pre J/ψ s priečnymi hybnosťami od 2 GeV/c do 6 GeV/c . V našej analýze sme nedokázali rozlíšiť od seba rôzne zdroje produkcie J/ψ a meranie je preto inkluzívne, zahrňujúce J/ψ z priamej produkcie, z rozpadov vyšších $c\bar{c}$ stavov a tiež z rozpadov B mezónu. V kombinácii s meraniami polarizácie inkluzívnych J/ψ experimentom PHENIX z našich výsledkov vyplýva (Fig. 4 v priloženom článku), že pri energiách na urýchľovači RHIC je so zvyšujúcou sa priečnou hybnosťou polarizácia inkluzívnych J/ψ pozdĺžna. Oproti tomu porovnateľné merania pri vyšších energiach na experimentoch CDF, CMS či ALICE ukazujú na nulovú, alebo malú pozdĺžnu polarizáciu. Predpovede polarizácie z teoretických modelov sú relatívne nepresné: model LO COM (model farebného oktetu v prvom ráde poruchoveho priblíženia) [R47] predpovedá s rastúcou priečnou hybnosťou priečnu polarizáciu pre priame J/ψ, model NLO+ CSM (model farebného singletu v druhom ráde poruchového priblíženia) [R48] predpovedá hodnoty parametru λ_θ v širokom rozsahu -0,4 až 0, pre priame J/ψ, s tým, že hodnota sa s priečnou hybnosťou nemení. Naše meranie je v rámci nepresností zhodné s výpočtami NLO+ CSM.

Toto prvé meranie polarizácie na experimente STAR prinieslo významné informácie pre porovnanie s modelmi produkcie J/ψ. V rámci kolaborácie STAR pracujeme na analýze väčších súborov dát, ktore umožnia merať i parameter λ_ϕ a taktiež merania polarizačných parametrov budú mať menšie štatistické chyby a budú môcť modely produkcie lepšie rozlíšiť.

Article reprint

Physics Letters B 739 (2014) 180–188

Contents lists available at ScienceDirect

Physics Letters B

www.elsevier.com/locate/physletb

J/ψ polarization in $p+p$ collisions at $\sqrt{s}=200$ GeV in STAR

STAR Collaboration

L. Adamczyk [a], J.K. Adkins [w], G. Agakishiev [u], M.M. Aggarwal [ai], Z. Ahammed [bb], I. Alekseev [s], J. Alford [v], C.D. Anson [af], A. Aparin [u], D. Arkhipkin [d], E.C. Aschenauer [d], G.S. Averichev [u], J. Balewski [aa], A. Banerjee [bb], Z. Barnovska [n], D.R. Beavis [d], R. Bellwied [ax], A. Bhasin [t], A.K. Bhati [ai], P. Bhattarai [aw], H. Bichsel [bd], J. Bielcik [m], J. Bielcikova [n], L.C. Bland [d], I.G. Bordyuzhin [s], W. Borowski [at], J. Bouchet [v], A.V. Brandin [ad], S.G. Brovko [f], S. Bültmann [ag], I. Bunzarov [u], T.P. Burton [d], J. Butterworth [ao], H. Caines [be], M. Calderón de la Barca Sánchez [f], D. Cebra [f], R. Cendejas [aj], M.C. Cervantes [av], P. Chaloupka [m], Z. Chang [av], S. Chattopadhyay [bb], H.F. Chen [aq], J.H. Chen [as], L. Chen [i], J. Cheng [ay], M. Cherney [l], A. Chikanian [be], W. Christie [d], J. Chwastowski [k], M.J.M. Codrington [aw], R. Corliss [aa], J.G. Cramer [bd], H.J. Crawford [e], X. Cui [aq], S. Das [p], A. Davila Leyva [aw], L.C. De Silva [ax], R.R. Debbe [d], T.G. Dedovich [u], J. Deng [ar], A.A. Derevschikov [ak], R. Derradi de Souza [h], S. Dhamija [r], B. di Ruzza [d], L. Didenko [d], C. Dilks [aj], F. Ding [f], P. Djawotho [av], X. Dong [z], J.L. Drachenberg [ba], J.E. Draper [f], C.M. Du [y], L.E. Dunkelberger [g], J.C. Dunlop [d], L.G. Efimov [u], J. Engelage [e], K.S. Engle [az], G. Eppley [ao], L. Eun [z], O. Evdokimov [j], R. Fatemi [w], S. Fazio [d], J. Fedorisin [u], P. Filip [u], E. Finch [be], Y. Fisyak [d], C.E. Flores [f], C.A. Gagliardi [av], D.R. Gangadharan [af], D. Garand [al], F. Geurts [ao], A. Gibson [ba], M. Girard [bc], S. Gliske [b], D. Grosnick [ba], Y. Guo [aq], A. Gupta [t], S. Gupta [t], W. Guryn [d], B. Haag [f], O. Hajkova [m], A. Hamed [av], L.-X. Han [as], R. Haque [ae], J.W. Harris [be], J.P. Hays-Wehle [aa], S. Heppelmann [aj], A. Hirsch [al], G.W. Hoffmann [aw], D.J. Hofman [j], S. Horvat [be], B. Huang [d], H.Z. Huang [g], X. Huang [ay], P. Huck [i], T.J. Humanic [af], G. Igo [g], W.W. Jacobs [r], H. Jang [x], E.G. Judd [e], S. Kabana [at], D. Kalinkin [s], K. Kang [ay], K. Kauder [j], H.W. Ke [d], D. Keane [v], A. Kechechyan [u], A. Kesich [f], Z.H. Khan [j], D.P. Kikola [bc], I. Kisel [o], A. Kisiel [bc], D.D. Koetke [ba], T. Kollegger [o], J. Konzer [al], I. Koralt [ag], W. Korsch [w], L. Kotchenda [ad], P. Kravtsov [ad], K. Krueger [b], I. Kulakov [o], L. Kumar [ae], R.A. Kycia [k], M.A.C. Lamont [d], J.M. Landgraf [d], K.D. Landry [g], J. Lauret [d], A. Lebedev [d], R. Lednicky [u], J.H. Lee [d], W. Leight [aa], M.J. LeVine [d], C. Li [aq], W. Li [as], X. Li [al], X. Li [au], Y. Li [ay], Z.M. Li [i], L.M. Lima [ap], M.A. Lisa [af], F. Liu [i], T. Ljubicic [d], W.J. Llope [ao], R.S. Longacre [d], X. Luo [i], G.L. Ma [as], Y.G. Ma [as], D.M.M.D. Madagodagettige Don [l], D.P. Mahapatra [p], R. Majka [be], S. Margetis [v], C. Markert [aw], H. Masui [z], H.S. Matis [z], D. McDonald [ao], T.S. McShane [l], N.G. Minaev [ak], S. Mioduszewski [av], B. Mohanty [ae], M.M. Mondal [av], D.A. Morozov [ak], M.G. Munhoz [ap], M.K. Mustafa [z], B.K. Nandi [q], Md. Nasim [ae], T.K. Nayak [bb], J.M. Nelson [c], L.V. Nogach [ak], S.Y. Noh [x], J. Novak [ac], S.B. Nurushev [ak], G. Odyniec [z], A. Ogawa [d], K. Oh [am], A. Ohlson [be], V. Okorokov [ad], E.W. Oldag [aw], R.A.N. Oliveira [ap], M. Pachr [m], B.S. Page [r], S.K. Pal [bb], Y.X. Pan [g], Y. Pandit [j], Y. Panebratsev [u], T. Pawlak [bc], B. Pawlik [ah], H. Pei [i], C. Perkins [e], W. Peryt [bc], P. Pile [d], M. Planinic [bf], J. Pluta [bc], D. Plyku [ag], N. Poljak [bf], J. Porter [z], A.M. Poskanzer [z], N.K. Pruthi [ai], M. Przybycien [a], P.R. Pujahari [q], H. Qiu [z], A. Quintero [v], S. Ramachandran [w], R. Raniwala [an], S. Raniwala [an], R.L. Ray [aw], C.K. Riley [be],

http://dx.doi.org/10.1016/j.physletb.2014.10.049

Article reprint

STAR Collaboration / Physics Letters B 739 (2014) 180–188 181

H.G. Ritter [z], J.B. Roberts [ao], O.V. Rogachevskiy [u], J.L. Romero [f], J.F. Ross [l], A. Roy [bb], L. Ruan [d], J. Rusnak [n], N.R. Sahoo [bb], P.K. Sahu [p], I. Sakrejda [z], S. Salur [z], A. Sandacz [bc], J. Sandweiss [be], E. Sangaline [f], A. Sarkar [q], J. Schambach [aw], R.P. Scharenberg [al], A.M. Schmah [z], W.B. Schmidke [d], N. Schmitz [ab], J. Seger [l], P. Seyboth [ab], N. Shah [g], E. Shahaliev [u], P.V. Shanmuganathan [v], M. Shao [aq], B. Sharma [ai], W.Q. Shen [as], S.S. Shi [z], Q.Y. Shou [as], E.P. Sichtermann [z], R.N. Singaraju [bb], M.J. Skoby [r], D. Smirnov [d], N. Smirnov [be], D. Solanki [an], P. Sorensen [d], U.G. deSouza [ap], H.M. Spinka [b], B. Srivastava [al], T.D.S. Stanislaus [ba], J.R. Stevens [aa], R. Stock [o], M. Strikhanov [ad], B. Stringfellow [al], A.A.P. Suaide [ap], M. Sumbera [n], X. Sun [z], X.M. Sun [z], Y. Sun [aq], Z. Sun [y], B. Surrow [au], D.N. Svirida [s], T.J.M. Symons [z], A. Szanto de Toledo [ap], J. Takahashi [h], A.H. Tang [d], Z. Tang [aq], T. Tarnowsky [ac], J.H. Thomas [z], A.R. Timmins [ax], D. Tlusty [n], M. Tokarev [u], S. Trentalange [g], R.E. Tribble [av], P. Tribedy [bb], B.A. Trzeciak [bc,*], O.D. Tsai [g], J. Turnau [ah], T. Ullrich [d], D.G. Underwood [b], G. Van Buren [d], G. van Nieuwenhuizen [aa], J.A. Vanfossen Jr. [v], R. Varma [q], G.M.S. Vasconcelos [h], A.N. Vasiliev [ak], R. Vertesi [n], F. Videbæk [d], Y.P. Viyogi [bb], S. Vokal [u], A. Vossen [r], M. Wada [aw], M. Walker [aa], F. Wang [al], G. Wang [g], H. Wang [d], J.S. Wang [y], X.L. Wang [aq], Y. Wang [ay], Y. Wang [j], G. Webb [w], J.C. Webb [d], G.D. Westfall [ac], H. Wieman [z], S.W. Wissink [r], R. Witt [az], Y.F. Wu [i], Z. Xiao [ay], W. Xie [al], K. Xin [ao], H. Xu [y], N. Xu [z], Q.H. Xu [ar], Y. Xu [aq], Z. Xu [d], W. Yan [ay], C. Yang [aq], Y. Yang [y], Y. Yang [i], Z. Ye [j], P. Yepes [ao], L. Yi [al], K. Yip [d], I.-K. Yoo [am], Y. Zawisza [aq], H. Zbroszczyk [bc], W. Zha [aq], J.B. Zhang [i], J.L. Zhang [ar], S. Zhang [as], X.P. Zhang [ay], Y. Zhang [aq], Z.P. Zhang [aq], F. Zhao [g], J. Zhao [i], C. Zhong [as], X. Zhu [ay], Y.H. Zhu [as], Y. Zoulkarneeva [u], M. Zyzak [o]

[a] *AGH University of Science and Technology, Cracow, Poland*
[b] *Argonne National Laboratory, Argonne, IL 60439, USA*
[c] *University of Birmingham, Birmingham, United Kingdom*
[d] *Brookhaven National Laboratory, Upton, NY 11973, USA*
[e] *University of California, Berkeley, CA 94720, USA*
[f] *University of California, Davis, CA 95616, USA*
[g] *University of California, Los Angeles, CA 90095, USA*
[h] *Universidade Estadual de Campinas, Sao Paulo, Brazil*
[i] *Central China Normal University (HZNU), Wuhan 430079, China*
[j] *University of Illinois at Chicago, Chicago, IL 60607, USA*
[k] *Cracow University of Technology, Cracow, Poland*
[l] *Creighton University, Omaha, NE 68178, USA*
[m] *Czech Technical University in Prague, FNSPE, Prague, 115 19, Czech Republic*
[n] *Nuclear Physics Institute AS CR, 250 68 Řež/Prague, Czech Republic*
[o] *Frankfurt Institute for Advanced Studies FIAS, Germany*
[p] *Institute of Physics, Bhubaneswar 751005, India*
[q] *Indian Institute of Technology, Mumbai, India*
[r] *Indiana University, Bloomington, IN 47408, USA*
[s] *Alikhanov Institute for Theoretical and Experimental Physics, Moscow, Russia*
[t] *University of Jammu, Jammu 180001, India*
[u] *Joint Institute for Nuclear Research, Dubna, 141 980, Russia*
[v] *Kent State University, Kent, OH 44242, USA*
[w] *University of Kentucky, Lexington, KY 40506-0055, USA*
[x] *Korea Institute of Science and Technology Information, Daejeon, Republic of Korea*
[y] *Institute of Modern Physics, Lanzhou, China*
[z] *Lawrence Berkeley National Laboratory, Berkeley, CA 94720, USA*
[aa] *Massachusetts Institute of Technology, Cambridge, MA 02139-4307, USA*
[ab] *Max-Planck-Institut für Physik, Munich, Germany*
[ac] *Michigan State University, East Lansing, MI 48824, USA*
[ad] *Moscow Engineering Physics Institute, Moscow, Russia*
[ae] *National Institute of Science Education and Research, Bhubaneswar 751005, India*
[af] *Ohio State University, Columbus, OH 43210, USA*
[ag] *Old Dominion University, Norfolk, VA 23529, USA*
[ah] *Institute of Nuclear Physics PAN, Cracow, Poland*
[ai] *Panjab University, Chandigarh 160014, India*
[aj] *Pennsylvania State University, University Park, PA 16802, USA*
[ak] *Institute of High Energy Physics, Protvino, Russia*
[al] *Purdue University, West Lafayette, IN 47907, USA*
[am] *Pusan National University, Pusan, Republic of Korea*
[an] *University of Rajasthan, Jaipur 302004, India*
[ao] *Rice University, Houston, TX 77251, USA*
[ap] *Universidade de Sao Paulo, Sao Paulo, Brazil*
[aq] *University of Science & Technology of China, Hefei 230026, China*
[ar] *Shandong University, Jinan, Shandong 250100, China*
[as] *Shanghai Institute of Applied Physics, Shanghai 201800, China*
[at] *SUBATECH, Nantes, France*

Article reprint

[au] Temple University, Philadelphia, PA 19122, USA
[av] Texas A&M University, College Station, TX 77843, USA
[aw] University of Texas, Austin, TX 78712, USA
[ax] University of Houston, Houston, TX 77204, USA
[ay] Tsinghua University, Beijing 100084, China
[az] United States Naval Academy, Annapolis, MD 21402, USA
[ba] Valparaiso University, Valparaiso, IN 46383, USA
[bb] Variable Energy Cyclotron Centre, Kolkata 700064, India
[bc] Warsaw University of Technology, Warsaw, Poland
[bd] University of Washington, Seattle, WA 98195, USA
[be] Yale University, New Haven, CT 06520, USA
[bf] University of Zagreb, Zagreb, HR-10002, Croatia

ARTICLE INFO

Article history:
Received 8 November 2013
Received in revised form 7 October 2014
Accepted 22 October 2014
Available online 30 October 2014
Editor: M. Doser

Keywords:
Charmonia
Polarization
Spin alignment
STAR
RHIC

ABSTRACT

We report on a polarization measurement of inclusive J/ψ mesons in the di-electron decay channel at mid-rapidity at $2 < p_T < 6$ GeV/c in $p+p$ collisions at $\sqrt{s} = 200$ GeV. Data were taken with the STAR detector at RHIC. The J/ψ polarization measurement should help to distinguish between different models of the J/ψ production mechanism since they predict different p_T dependences of the J/ψ polarization. In this analysis, J/ψ polarization is studied in the helicity frame. The polarization parameter λ_θ measured at RHIC becomes smaller towards high p_T, indicating more longitudinal J/ψ polarization as p_T increases. The result is compared with predictions of presently available models.

1. Introduction

The J/ψ is a bound state of charm (c) and anti-charm ($\bar{c}$) quarks. Charmonia physical states have to be colorless, however they can be formed via a color-singlet or a color-octet intermediate $c\bar{c}$ state. The first model of charmonia production, the Color Singlet Model (CSM) [1–8], assumed that $c\bar{c}$ pairs are created in the color-singlet state only. This early prediction failed to describe the measured charmonia cross-section which has led to the development of new models. For example, Non-Relativistic QCD (NRQCD) [9] calculations were proposed in which a $c\bar{c}$ color-octet intermediate state, in addition to a color-singlet state, can bind to form a charmonium.

Different models of J/ψ production are able to describe the measured J/ψ production cross section reasonably well [10–17] and therefore other observables are needed to discriminate between different J/ψ production mechanisms. J/ψ spin alignment, commonly known as polarization, can be used for this purpose, since various models predict different transverse momentum (p_T) dependence for the polarization. The predictions of different models deviate the most at high p_T. Therefore a high-p_T J/ψ polarization measurement is of particular interest since it can help to discriminate between the models.

NRQCD calculations with color-octet contributions [18] are in good agreement with observed J/ψ p_T spectra in different experiments at different energies, at the Relativistic Heavy Ion Collider (RHIC) [11,12], the Tevatron [13,14] and the Large Hadron Collider (LHC) [16,17,19]. But the calculations fail to describe the J/ψ polarization at high p_T ($p_T > 5$ GeV/c) measured by the CDF experiment at FermiLab at $\sqrt{s} = 1.96$ TeV [20]. NRQCD calculations predict transverse polarization for $p_T > 5$ GeV/c and the growth of the polarization parameter λ_θ with increasing p_T [21]. However, the CDF polarization measurement becomes slightly longitudinal with increasing p_T, for $5 < p_T < 30$ GeV/c [20]. Also, the CMS J/ψ polarization measurement in $p+p$ collisions at $\sqrt{s} = 7$ TeV for high transverse momenta [22] is in disagreement with existing next-to-leading-order (NLO) NRQCD calculations [21,23]. In addition, the J/ψ polarization measurements at the same energy and for lower p_T were performed by ALICE (inclusive J/ψ production) [24] and LHCb (prompt J/ψ production) [25] experiments at forward rapidity. The ALICE experiment observed zero polarization while LHCb λ_θ results indicate small longitudinal polarization (with other coefficients consistent with zero). Data from both experiments favor NLO NRQCD over NLO CSM [21,25]. At RHIC energies, at intermediate p_T ($1.5 < p_T \lesssim 5$ GeV/c) and for mid-rapidity, the tuned leading-order (LO) NRQCD model [26] predicts slightly longitudinal J/ψ polarization and describes the PHENIX result [27] well.

In the case of the Color Singlet Model, the Next-to-Leading Order calculations (NLO$^+$ CSM) [28] for the p_T spectrum are in near agreement with the RHIC data at low and mid p_T and these CSM calculations predict longitudinal J/ψ polarization at intermediate p_T ($1.5 < p_T < 6$ GeV/c) at mid-rapidity which is in agreement with the PHENIX result [28]. At the Tevatron and LHC energies, the upper bound of NNLO* prediction [29] is very close to the experimental cross section data, similar to RHIC [28]. Also, the upper edge of this prediction for the polarization is in good agreement with the CDF data [29]. However, NLO CSM calculations [21,25] do not describe J/ψ polarization results from ALICE and LHCb well.

For the lower p_T range at RHIC energies, the LO NRQCD calculations [26] and NLO$^+$ CSM [28] have similar predictions regarding the J/ψ polarization, which is longitudinal, and describe the experimental results [27] well. However, these models predict different p_T dependence: in the case of the NRQCD prediction, the trend is towards the transverse polarization with increasing p_T, while the NLO$^+$ CSM shows almost no p_T dependence. Thus, it is especially important to measure a p_T dependence of the J/ψ polarization and go to high p_T.

In this paper, we report a J/ψ polarization measurement in $p+p$ collisions at $\sqrt{s} = 200$ GeV at rapidity (y) $|y| < 1$, in the p_T range $2 < p_T < 6$ GeV/c from the STAR experiment at RHIC. The

* Corresponding author.
E-mail address: barbara.trzeciak@gmail.com (B.A. Trzeciak).

Article reprint

STAR Collaboration / Physics Letters B 739 (2014) 180–188

analysis is done using data with a high-p_T electron (so-called High Tower) trigger. The J/ψ is reconstructed via its di-electron decay channel. The angular distribution parameter (polarization parameter) λ_θ for electron decay of the J/ψ is extracted in the helicity frame [30] as a function of J/ψ p_T, in three p_T bins. The obtained result is compared with predictions of NLO$^+$ CSM [28] and LO NRQCD calculations (COM) [26].

1.1. Angular distribution of decay products

J/ψ polarization is analyzed via the angular distribution of the decay electrons in the helicity frame [30]. In this analysis, we are interested in the polar angle θ. It is the angle between the positron momentum vector in the J/ψ rest frame and the J/ψ momentum vector in the laboratory frame. The full angular distribution, which is derived from the density matrix elements of the production amplitude using parity conservation rules, is described by:

$$\frac{d^2N}{d(\cos\theta)d\phi} \propto 1 + \lambda_\theta \cos^2\theta + \lambda_\phi \sin^2\theta \cos 2\phi + \lambda_{\theta\phi} \sin 2\theta \cos\phi, \quad (1)$$

where θ and ϕ are polar and azimuthal angles, respectively; λ_θ and λ_ϕ are the angular decay coefficients. The angular distribution integrated over the azimuthal angle is parametrized as

$$\frac{dN}{d(\cos\theta)} \propto 1 + \lambda_\theta \cos^2\theta, \quad (2)$$

where λ_θ is called the polarization parameter. This parameter contains both the longitudinal and transverse components of the J/ψ cross section; $\lambda_\theta = 1$ indicates full transverse polarization, and $\lambda_\theta = -1$ corresponds to full longitudinal polarization.

The measurement presented in this Letter is limited to the θ angle analysis due to statistical limitations. Extraction of the λ_θ parameter in the helicity frame allows one to compare the result with the available model predictions and draw model dependent conclusions. A measurement of the θ angle with a better precision, as well as the ϕ angle, will be possible with a newer STAR data at $\sqrt{s} = 500$ GeV. Then, the frame invariant parameter, also in different reference frames, can be calculated providing model independent information about the J/ψ polarization [31].

2. Data analysis

2.1. Data set and electron identification

The $p+p$ 200 GeV data used in this analysis were recorded by the STAR experiment in the year 2009. The STAR detector [32] is a multi-purpose detector. It consists of many subsystems and has cylindrical geometry and a large acceptance with a full azimuthal coverage. The most important subsystems for this analysis are briefly described below. The Time Projection Chamber (TPC) [33] is the main tracking detector for charged particles. It is also used to identify particles using the ionization energy loss (dE/dx). Outside the TPC is the Time Of Flight (TOF) detector [34] which extends STAR particle identification capabilities to momentum ranges where TPC dE/dx alone is inadequate. Between the TOF and the STAR magnet there is the STAR Barrel Electromagnetic Calorimeter (BEMC) [35]. The BEMC is constructed so that an electron should deposit all its energy in the BEMC towers while hadrons usually deposit only a fraction of their energy. The energy deposited by a particle in the BEMC can thus be used to discriminate between electrons and hadrons, by looking at the E/p ratio. The BEMC is also used to trigger on high-p_T electrons. Together with the TOF, the BEMC is utilized to discriminate against pile-up tracks in the TPC, since both detectors are fast. Most of the STAR detector subsystems are enclosed in a room temperature solenoid magnet with a uniform magnetic field of maximum value of 0.5 T [36].

The analyzed data were collected with the High Tower (HT) trigger, which requires transverse energy deposited in at least one single tower of the BEMC to be within $2.6 < E_T \leq 4.3$ GeV. The HT trigger also requires a coincidence signal from two Vertex Position Detectors [37]. We have analyzed ∼33 M events with the HT trigger and with a primary vertex z position $|V_z| < 65$ cm. This corresponds to an integrated luminosity of ∼1.6 pb^{-1}. The J/ψ is reconstructed via its di-electron decay channel, $J/\psi \to e^+e^-$, with the branching ratio $5.94\% \pm 0.06\%$ [38].

Charged tracks are reconstructed using the STAR TPC which has 2π azimuthal coverage and a pseudorapidity (η) coverage of $|\eta| < 1$. Tracks that originate from the primary vertex and have a distance of closest approach (DCA) to the primary vertex of less than 2 cm are used. In 2009 STAR did not have a vertex detector that would help to distinguish between prompt and non-prompt J/ψ, and TPC resolution alone is not enough to select non-prompt J/ψ from B meson decays. In order to ensure a good track quality, tracks are required to have at least 15 points used in the track reconstruction in the TPC, and to have at least 52% of the maximum number of possible track reconstruction points. Cuts of $|\eta| < 1$ and $p_T > 0.4$ GeV/c are also applied. The transverse momentum cut is chosen to optimize the acceptance in $\cos\theta$ and the significance of the J/ψ signal. Applying higher p_T cut causes a loss of statistics at $|\cos\theta| \sim 1$ while a lower p_T cut reduces the J/ψ signal significance. Efficient identification of electrons with low p_T was possible using available information from the TOF detector. During the analyzed run in 2009, 72% of the full TOF detector was installed. The TOF pseudorapidity coverage is $|\eta| < 0.9$.

In order to identify electrons and reject hadrons, information from the TPC, TOF and BEMC detectors is used. The TPC provides information about dE/dx of a particle in the detector. Electron candidates are required to have $n\sigma_{\text{electron}}$ within $-1 < n\sigma_{\text{electron}} < 2$, where $n\sigma_{\text{electron}} = \log[(dE/dx)/(dE/dx|_{\text{Bichsel}})]/\sigma_{dE/dx}$, dE/dx is the measured energy loss in the TPC, $dE/dx\,|_{\text{Bichsel}}$ is the expected value of dE/dx from the Bichsel function prediction [39] and $\sigma_{dE/dx}$ is the dE/dx resolution. The Bichsel function is used to calculate the energy dependence of the most probable energy loss of the ionization spectrum from a detector. In a thin material such as the TPC gas, it has been shown that the Bichsel function is a very good approximation for the dE/dx curves [40]. At lower momenta ($p \lesssim 1.5$ GeV/c), where electron and hadron dE/dx bands overlap, the TOF detector is used to reject slow hadrons. For $p < 1.4$ GeV/c, a cut on the speed of a particle, β, of $|1/\beta - 1| < 0.03$ is applied. At higher momenta, the BEMC rejects hadrons efficiently. For momenta above 1.4 GeV/c, a cut on $E/p > 0.5c$ is used for electron identification, where E is the energy deposited in a single BEMC tower ($\Delta\eta \times \Delta\phi = 0.05 \times 0.05$). For electrons, the ratio of total energy deposited in the BEMC to the particle's momentum is expected to be ≈ 1. In the analysis we use energy deposited in a single BEMC tower but an electron can deposit its energy in more towers, therefore the value of the E/p cut is $0.5c$.

It is also required that at least one of the electrons from the J/ψ decay satisfies the HT trigger conditions. In order to ensure that a selected electron indeed fired the trigger, an additional cut of $p_T > 2.5$ GeV/c is applied for that electron. The HT trigger requirements reduce significantly the combinatorial background under the J/ψ signal and lead to a clear J/ψ signal at $2 < p_T < 6$ GeV/c.

Article reprint

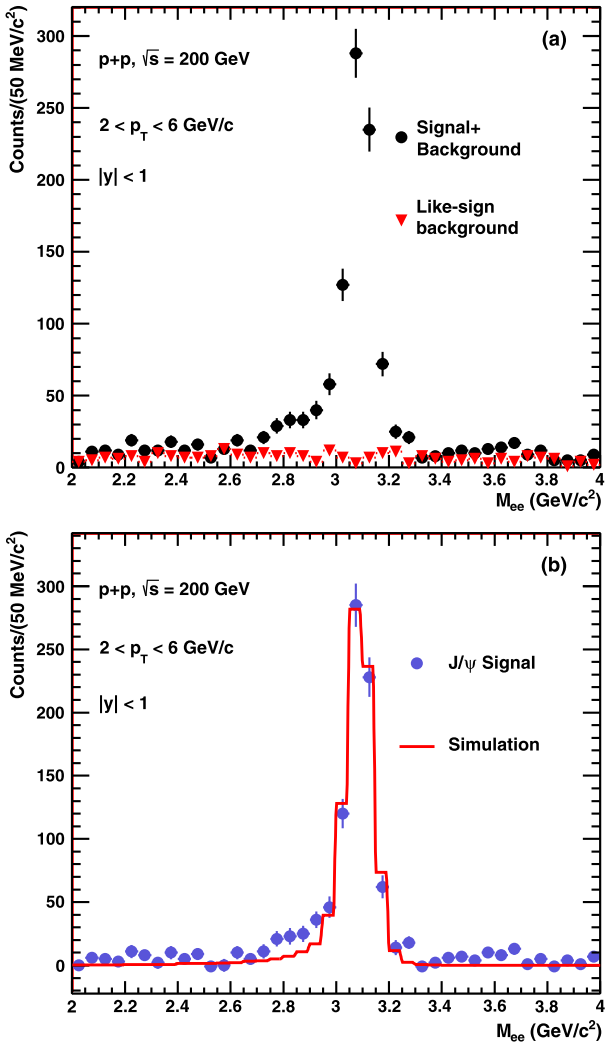

Fig. 1. (Color online.) (a) Invariant mass distributions of unlike-sign (black circles) and like-sign (red triangles) electron/positron pairs, for $2 < p_T < 6$ GeV/c and $|y| < 1$. (b) J/ψ signal after the combinatorial background subtraction (closed blue circles) and MC simulation (histogram).

2.2. J/ψ signal and $\cos\theta$ distributions

Electrons and positrons that pass track quality and electron identification (eID) cuts are paired in each event. Fig. 1(a) shows the invariant mass distribution for di-electron pairs with $|y| < 1$ and p_T of 2–6 GeV/c. The unlike-sign pairs are represented by circles. The combinatorial background is estimated using the like-sign technique, and is defined as a sum of all e^+e^+ and e^-e^- pairs in an event, represented by triangles. The J/ψ signal is obtained by subtracting the combinatorial background from the unlike-sign pair distribution. Fig. 1(b) shows the invariant mass distribution for J/ψ as circles, and the histogram is the J/ψ signal obtained from a Monte Carlo (MC) simulation (see Section 2.3). Momentum resolution of electrons and positrons from the MC simulation is additionally smeared in order that the simulated J/ψ signal width matches the width of the J/ψ signal obtained from the data. The simulation does not include the J/ψ radiative decay channel, $J/\psi \to e^+e^-\gamma$ [11,38], leading to the discrepancy between data and simulation for invariant mass ~2.7–2.9 GeV/c^2. The tail in the data at low invariant mass is due to electron bremsstrahlung and missing photons in the case of the J/ψ radiative decay reconstruction. We select J/ψ candidates in the invariant mass range 2.9–3.3 GeV/c^2 and so the discrepancy between the data and the simulation for the lower mass range does not influence our result.

In the analyzed ranges of rapidity, p_T, and invariant mass, the signal to background ratio is 15. A strong J/ψ signal is seen with a significance of 26σ. The number of J/ψ, obtained by counting data entries in the J/ψ mass window, is 791 ± 30. For the polarization analysis, we split the entire J/ψ sample into 3 p_T bins with a comparable number of J/ψ in each bin: 2–3 GeV/c, 3–4 GeV/c and 4–6 GeV/c.

Raw $\cos\theta$ distributions for J/ψ (after the combinatorial background subtraction) are obtained by bin counting, using distributions from the data. Figs. 2(a)–(c) show uncorrected $\cos\theta$ distributions (full squares).

2.3. Corrections

In order to obtain the $\cos\theta$ corrections, unpolarized Monte Carlo J/ψ particles with uniform p_T and rapidity distributions are embedded into real events, and the STAR detector response is simulated. Since the input p_T and rapidity shapes influence efficiencies, J/ψ distributions are then weighted according to the J/ψ p_T and rapidity shapes observed in the STAR [11] and PHENIX [41] experiments. Corrected $\cos\theta$ distributions are obtained by dividing raw $\cos\theta$ distributions by the corrections calculated as a function of $\cos\theta$, in each analyzed p_T bin.

Efficiencies as a function of $\cos\theta$ are calculated by applying the same cuts used in the data analysis to the embedding (simulation) sample. Most corrections related to the TPC response, such as the acceptance (with the p_T and η cuts) and tracking efficiency, and all BEMC efficiencies, are obtained from the simulation. The $n\sigma_{\text{electron}}$ and the TOF response are not simulated accurately in embedding. Therefore the $n\sigma_{\text{electron}}$ cut and TOF cut efficiencies are calculated using the data.

For the calculation of the $n\sigma_{\text{electron}}$ cut efficiency, the $n\sigma_{\text{electron}}$ distribution from the data is approximated with a sum of Gaussian functions (one Gaussian function for electrons and two Gaussian functions for hadrons), in narrow momentum bins. In order to improve the fitting, the TOF and BEMC eID cuts are applied and the position of the Gaussian fit for electrons is constrained using a high-purity (almost 100%) electron sample obtained by selecting photonic electrons and subtracting a background from like-sign electron pairs. Photonic electrons are produced from photon conversion in the detector material and Dalitz decay of π^0 and η mesons. These electrons are isolated using a cut on the invariant mass of a pair of tracks of $m_{e^-e^+} < 100$ MeV/c^2 and additional electron identification cuts: $|1/\beta - 1| < 0.03$ for $p < 1.5$ GeV/c and $E/p > 0.5c$ for momenta above 1.5 GeV/c.

TOF matching efficiency is calculated using a low luminosity data sample (with almost no pile-up). Since the TOF detector did not have full coverage in 2009, the TOF matching efficiency is applied in the total efficiency calculation as a function of η. The efficiency of the $1/\beta$ cut is calculated by using a pure electron sample obtained by selecting photonic electrons with $-0.2 < n\sigma_e < 2$ and with the invariant mass of a pair of tracks less than 15 MeV/c^2. The $1/\beta$ cut efficiency is calculated in narrow momentum bins and then a constant function is fitted to obtain the final $1/\beta$ cut efficiency.

The total J/ψ efficiency calculations include contributions from the acceptance, the tracking efficiency, the electron identification efficiency, and the HT trigger efficiency, and are shown as a function of $\cos\theta$ in Fig. 2(d)–(f) (blue triangles). The systematic

Article reprint

STAR Collaboration / Physics Letters B 739 (2014) 180–188 185

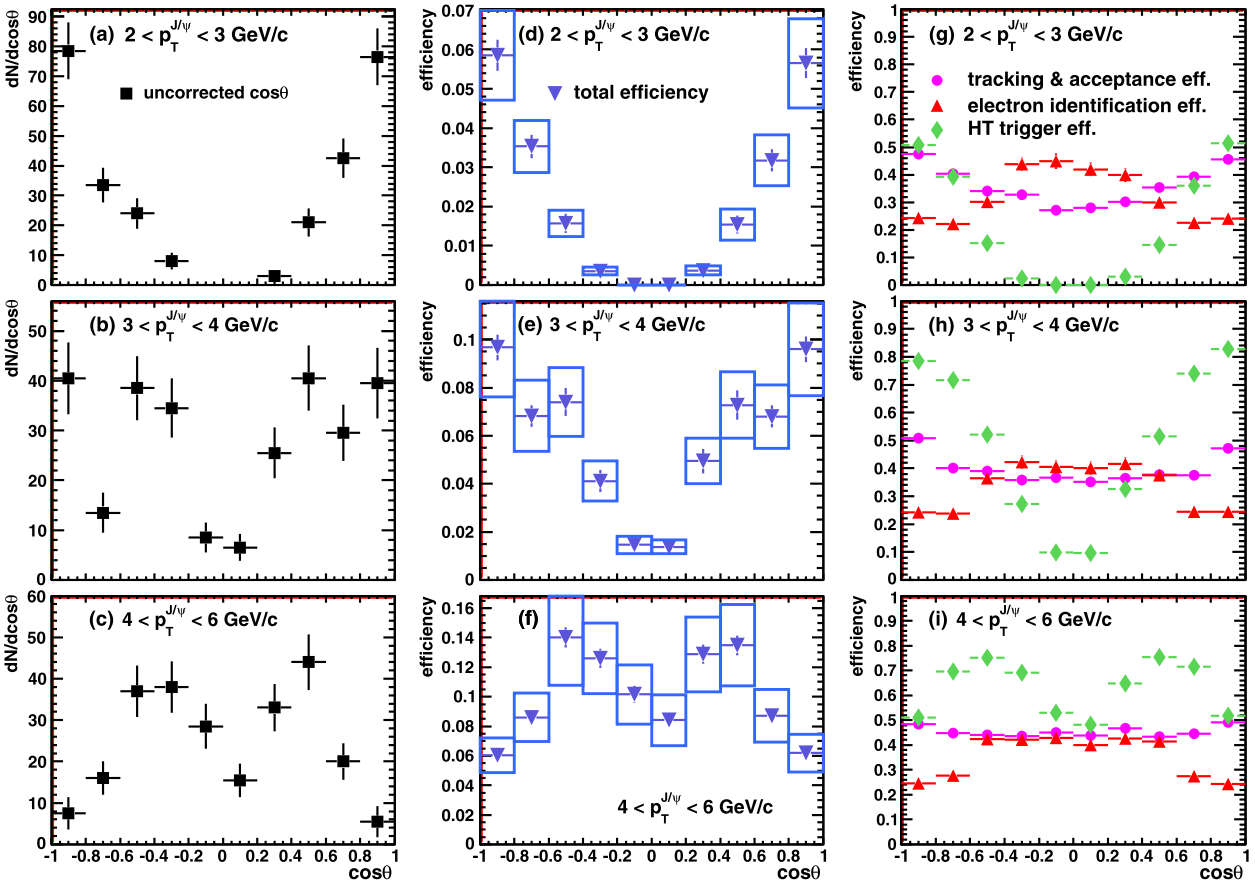

Fig. 2. (Color online.) Panels (a)–(c) show uncorrected $\cos\theta$ distributions after the combinatorial background subtraction, for each analyzed p_T bin. Panels (d)–(f) show total efficiencies as a function of $\cos\theta$. Systematic errors are shown as boxes. Panels (g)–(i) show different efficiencies that contribute to the total efficiency.

uncertainties (discussed in Subsection 3.2) on the total efficiency are also shown in the figure. The right-hand panels, Fig. 2(g)–(i), show separately the efficiencies that contribute to the total efficiency.

The most important factor influencing the shape of the total efficiency is the HT trigger efficiency, which is shown as green diamonds in Fig. 2(g)–(i). At least one of the electrons from the J/ψ decay is required to satisfy the trigger conditions and must have p_T above 2.5 GeV/c. Due to the decay kinematics this cut causes significant loss in the number of observed J/ψ at lower J/ψ p_T, and the efficiency decreases with decreasing $|\cos\theta|$. This pattern is clearly visible in the HT trigger efficiency plot for $2 < p_T < 3$ GeV/c in Fig. 2(g), where all entries at $\cos\theta \sim 0$ are zero. With increasing J/ψ p_T, the trigger efficiency increases. Since the trigger has also an upper threshold ($E_T \leq 4.3$ GeV), a decrease of the efficiency at $|\cos\theta| \sim 1$ at higher p_T is seen, as evident in Fig. 2(i).

3. Results and discussion

3.1. Corrected $\cos\theta$ distributions

The corrected $\cos\theta$ distributions are fitted with

$$f(\cos\theta) = C\left(1 + \lambda_\theta \cos^2\theta\right) \quad (3)$$

where C is a normalization factor and λ_θ is the polarization parameter. The fitting procedure is carried out with no constraints applied to the fit parameters. The corrected $\cos\theta$ distributions with the fits are shown in Fig. 3. The errors shown are statistical only. The solid line represents the most likely fit. The band around the line is a 1σ uncertainty contour on the fit, which takes into account uncertainties on both fit parameters and correlations between them. The measured values of the polarization parameter, in each analyzed p_T bin, are listed in Table 1 together with a mean p_T ($\langle p_T \rangle$) in each bin and statistical and systematic uncertainties.

3.2. Systematic uncertainties

The systematic uncertainties on the polarization parameter λ_θ are summarized in Table 2. All sources, except the last two, contribute to the error on the total efficiency and are included in the systematic uncertainties shown in Fig. 2(d)–(f). Each contribution is described below. Each systematic uncertainty is the maximum deviation from the central value of λ_θ. The systematic uncertainties are combined assuming that they are uncorrelated, and are added in quadrature.

3.2.1. Tracking efficiency

The systematic uncertainty on the tracking efficiency arises from small differences between the simulation of the TPC response in the embedding calculation and the data. Track properties, DCA and the number of points used in the track reconstruction in the TPC (fitPts), are compared between simulation and data. The systematic uncertainty is due to a shift of the fitPts distribution (by

Article reprint

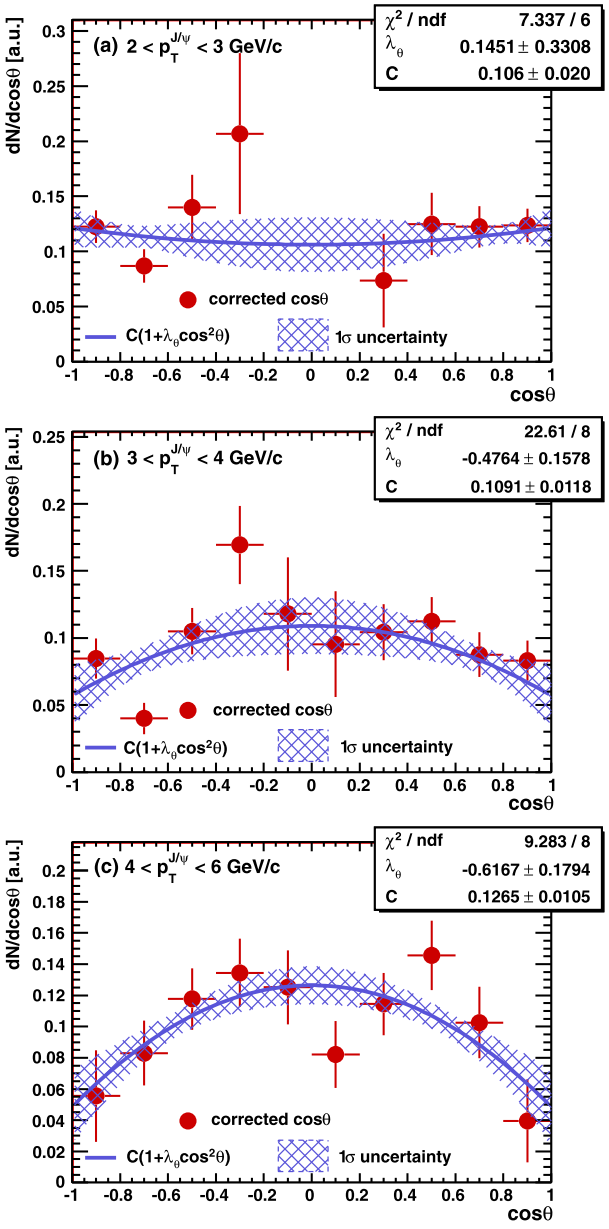

Fig. 3. (Color online.) Corrected $\cos\theta$ distributions fitted with the function in Eq. (3). The plotted errors are statistical. The solid blue lines represent the most likely fits, and the hatched blue bands represent the 1σ uncertainty on the fits.

2 points) in the simulation. The uncertainty is considered symmetric.

3.2.2. TPC eID efficiency

The systematic uncertainty from TPC electron identification is estimated by changing constraints on the mean and width of the Gaussian fit for electrons and recalculating the total efficiency. The constraints put on the mean and width are allowed to vary by 3σ.

3.2.3. TOF efficiency

Since the TOF detector did not have full coverage in 2009, the TOF matching efficiency is applied in the total efficiency calculation as a function of η. The systematic uncertainty is estimated with the TOF matching efficiency also being a function of azimuthal angle ϕ. The $1/\beta$ cut efficiency estimated from the data in small p_T bins may be sensitive to fluctuations. The $1/\beta$ distribution obtained from the data is well described by the Gaussian function. So the systematic uncertainty on the $1/\beta$ cut efficiency is estimated by applying the efficiency calculated for the whole momentum range of $0.4 < p < 1.4$ GeV/c from a Gaussian fit to the $1/\beta$ distribution.

Table 1
The polarization parameter λ_θ.

p_T (GeV/c)	$\langle p_T \rangle$ (GeV/c)	λ_θ
$2 < p_T < 3$	2.48	0.15 ± 0.33 (stat.) ± 0.30 (sys.)
$3 < p_T < 4$	3.52	-0.48 ± 0.16 (stat.) ± 0.16 (sys.)
$4 < p_T < 6$	4.74	-0.62 ± 0.18 (stat.) ± 0.26 (sys.)

Table 2
Systematic uncertainties.

Source	Systematic uncertainty on λ_θ, in p_T (GeV/c) bins		
	2–3	3–4	4–6
Tracking efficiency	0.024	0.009	0.008
TPC eID efficiency	0.009	0.006	0.012
TOF efficiency	0.057	0.018	0.014
BEMC efficiency	0.035	0.024	0.068
HT trigger efficiency	0.049	0.006	0.003
Input J/ψ distributions in the simulation	0.190	0.019	0.027
Errors from the simulation	0.077	0.028	0.004
Polarization of the continuum background	0.025	0.034	0.034
J/ψ signal extraction	0.195	0.149	0.246
Total	±0.297	±0.160	±0.260

3.2.4. BEMC efficiency

Differences between the simulated BEMC response and the BEMC response in the real data may affect the matching of a TPC track to the BEMC detector and the efficiency of the E/p cut. The matching efficiency of a TPC track to the BEMC and the E/p distribution are compared between data and simulation. A pure electron sample from the data is obtained by selecting photonic electrons with $-0.2 < n\sigma_e < 2$ and with the invariant mass of a pair of tracks less than 15 MeV/c^2. The systematic uncertainty of the BEMC efficiency is estimated by applying BEMC matching and E/p cut efficiencies obtained from the data instead of using simulated BEMC response, in the total efficiency calculation.

3.2.5. HT trigger efficiency

HT trigger response in the simulation, energy in a BEMC tower, is compared with the BEMC response in the data. The systematic uncertainty on the HT trigger efficiency is estimated by varying the trigger turn-on conditions in the simulation by the difference seen between data and simulation, which is 3%.

3.2.6. Input J/ψ distribution in the simulation

Since the input J/ψ transverse momentum and rapidity distributions in the simulation are flat, they need to be weighted with realistic p_T and rapidity spectra. In order to estimate a systematic uncertainty, the p_T and rapidity weights are changed. The p_T weight is varied by changing the ranges in which the Kaplan [42] function is fitted to the p_T spectrum. The weight used for rapidity is obtained by fitting a Gaussian function to the rapidity spectrum, and the systematic uncertainty is estimated by assuming that the rapidity shape is flat at mid-rapidity.

Also, the J/ψ particles in the simulation are unpolarized (the input $\cos\theta$ distribution is flat). The acceptance of electron and

Article reprint

STAR Collaboration / Physics Letters B 739 (2014) 180–188 187

positron from the J/ψ decay in the detector depends on the J/ψ polarization. In order to estimate the effect of the unknown J/ψ polarization on the acceptance calculation, fully transverse ($\lambda_\theta = 1$) and fully longitudinal ($\lambda_\theta = -1$) J/ψ polarization is assumed in the embedding analysis. A systematic uncertainty is estimated as a difference between the result obtained with no input J/ψ polarization and the result when J/ψ in the simulation is polarized. An average uncertainty from the two input J/ψ polarizations, longitudinal and transverse, is taken as a systematic uncertainty in this study.

3.2.7. Errors from the simulation

Statistical errors on the total efficiencies, determined using the MC simulation, are included in the systematic uncertainties.

3.2.8. Polarization of the continuum background

In Fig. 1(b), it is seen that there is still some residual continuum background after the combinatorial background subtraction. This background consists of correlated $c\bar{c} \to e^+e^-$ and $b\bar{b} \to e^+e^-$. The continuum background is about 5% of the measured J/ψ in the analyzed invariant mass range. Due to the small statistics of the continuum background, we are not able to estimate a polarization of the correlated background using our data. Instead, we use the value obtained by the PHENIX experiment [27]. They found that the continuum polarization is between -0.3 and 0.3. We estimate a systematic uncertainty by simulating $\cos\theta$ distributions for the residual background taking two extreme values of λ_θ: -0.3 and 0.3. Then those $\cos\theta$ distributions are subtracted from the corrected $\cos\theta$ distributions from the data, assuming that the residual background is 5% of the J/ψ yield, in order to estimate the influence of the continuum background polarization on the measured λ_θ.

3.2.9. J/ψ signal extraction

The systematic uncertainty associated with the J/ψ signal extraction is estimated by counting the number of J/ψ particles using the simulated J/ψ signal shape. The J/ψ signal from the simulation is extracted in each p_T and $\cos\theta$ bin and fitted to the data.

3.3. Polarization parameter λ_θ

Fig. 4 shows the polarization parameter λ_θ as a function of J/ψ p_T for inclusive J/ψ production. The result includes direct J/ψ production, as well as J/ψ from feed-down from heavier charmonium states, ψ' and χ_C (about 40% of the prompt J/ψ yield [43]), as well as from B meson decays (non-prompt J/ψ) [11]. The non-direct J/ψ production may influence the observed polarization. The STAR result (red stars) is compared with the PHENIX mid-rapidity ($|y| < 0.35$) J/ψ polarization result for inclusive J/ψ [27] (black solid circles). The blue line is a linear fit, which takes into account both statistical and systematic uncertainties, to all RHIC points. The fit gives a negative slope parameter -0.16 ± 0.07 with $\chi^2/\text{ndf} = 1.5/4$. A trend towards longitudinal J/ψ polarization is seen in the RHIC data.

STAR observes longitudinal J/ψ polarization in the helicity frame at $p_T > 3$ GeV/c. The STAR and PHENIX measurements are consistent with each other in the overlapping p_T region. Our result can be compared to the polarization measurements from CDF [20] and CMS [22] at mid-rapidity for prompt J/ψ. At $p_T \sim 5$ GeV/c, CDF observes almost no polarization, $\lambda_\theta \sim 0$ (the polarization becomes slightly longitudinal as p_T increases) while STAR observes a strong longitudinal polarization in that p_T region. At LHC $\sqrt{s} = 7$ TeV, CMS reports zero polarization at mid-rapidity up to $p_T \sim 70$ GeV/c [22]. In addition, the ALICE experiment also reports

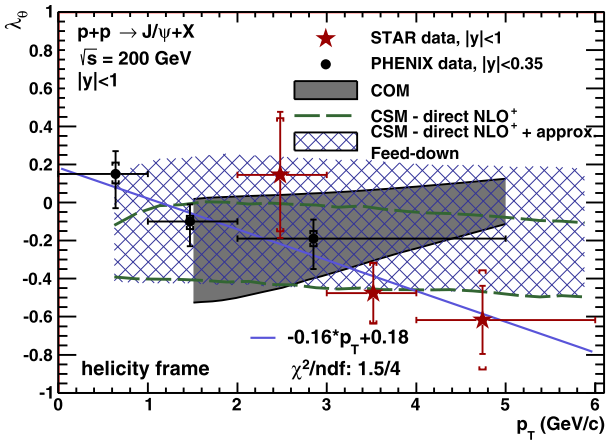

Fig. 4. (Color online.) Polarization parameter λ_θ as a function of J/ψ p_T (red stars) for $|y| < 1$. The data is compared with the PHENIX result (black solid circles) [27] and two model predictions: NLO$^+$ Color Singlet Model (CSM) (green dashed lines represent a range of λ_θ for the direct J/ψ, and the hatched blue band is an extrapolation of λ_θ for the prompt J/ψ) [28] and LO NRQCD calculations with color-octet contributions (COM) [26] (gray shaded area). The p_T coverages of the CSM and COM models are ~0.6–6.0 GeV/c and ~1.5–5.0 GeV/c, respectively. The horizontal error bars represent widths of p_T bins. The blue line is a linear fit ($Ax + B$) to RHIC points.

very small polarization within $2 < p_T < 8$ GeV/c at forward rapidity [24]. However, if the J/ψ production is x_T dependent [10], the RHIC result at $p_T \sim 2$ GeV/c is comparable with the CDF result at $p_T \sim 20$ GeV/c and with the CMS result at $p_T \sim 70$ GeV/c ($x_T \sim 0.02$, $x_T = 2p_T/\sqrt{s}$).

The data are compared with two model predictions for λ_θ at mid-rapidity: NLO$^+$ CSM [28] and LO COM [26]. The prediction of the COM [26] for direct J/ψ production, the gray shaded area, moves towards the transverse J/ψ polarization as p_T increases [20]. The trend seen in the STAR and PHENIX results is towards longitudinal J/ψ polarization with increasing p_T, and a linear fit to the RHIC data has a negative slope parameter. The difference between the central value of the COM model calculations and the STAR data in terms of χ^2/ndf (P value) is 6.7/3 (8.2×10^{-2}). The COM failed to describe the polarization measurements by the CDF and CMS experiments at higher energies.

Green dashed lines represent a range of λ_θ for the direct J/ψ production from the NLO$^+$ CSM prediction and an extrapolation of λ_θ for the prompt J/ψ production is shown as the hatched blue band [28]. It predicts a weak p_T dependence of λ_θ, and within the experimental and theoretical uncertainties, the RHIC result is consistent with the NLO$^+$ CSM model prediction. Comparison between the central value of the NLO$^+$ CSM prediction and the STAR data gives χ^2/ndf (P value) of 3.0/3 (3.9×10^{-1}) and 5.1/3 (1.6×10^{-1}) for the direct and prompt J/ψ production, respectively.

4. Summary and outlook

This paper reports the first STAR measurement of J/ψ polarization and contributes to the evolving understanding of the J/ψ production mechanisms. J/ψ polarization is measured in $p + p$ collisions at $\sqrt{s} = 200$ GeV in the helicity frame at $|y| < 1$ and $2 < p_T < 6$ GeV/c. RHIC data indicates a trend towards longitudinal J/ψ polarization as p_T increases. The result is consistent, within experimental and theoretical uncertainties, with the NLO$^+$ CSM model.

Newer data at $\sqrt{s} = 500$ GeV, taken in 2011 with much higher luminosity, may help to further distinguish between J/ψ

Article reprint

production models, and may permit analysis of the full angular distribution. Furthermore, uncertainties in the models need to be reduced in order to draw more precise conclusions from experimental measurements.

Acknowledgements

We thank the RHIC Operations Group and RCF at BNL, the NERSC Center at LBNL, the KISTI Center in Korea and the Open Science Grid consortium for providing resources and support. This work was supported in part by the Offices of NP and HEP within the U.S. DOE Office of Science, the U.S. NSF, CNRS/IN2P3, FAPESP CNPq of Brazil, Ministry of Ed. and Sci. of the Russian Federation, NNSFC, CAS, MoST and MoE of China, the Korean Research Foundation, GA and MSMT of the Czech Republic, FIAS of Germany, DAE, DST, and CSIR of India, National Science Centre of Poland, National Research Foundation (NRF-2012004024), Ministry of Sci., Ed. and Sports of the Rep. of Croatia, and RosAtom of Russia.

References

[1] M. Einhorn, S. Ellis, Phys. Rev. D 12 (1975) 2007.
[2] S. Ellis, M.B. Einhorn, C. Quigg, Phys. Rev. Lett. 36 (1976) 1263.
[3] C. Carlson, R. Suaya, Phys. Rev. D 14 (1976) 3115.
[4] C. Chang, Nucl. Phys. B 172 (1980) 425–434.
[5] E.L. Berger, D.L. Jones, Phys. Rev. D 23 (1981) 1521–1530.
[6] R. Baier, R. Ruckl, Phys. Lett. B 102 (1981) 364.
[7] R. Baier, R. Ruckl, Nucl. Phys. B 201 (1982) 1.
[8] R. Baier, R. Ruckl, Z. Phys. C 19 (1983) 251.
[9] E. Braaten, S. Fleming, T.C. Yuan, Annu. Rev. Nucl. Part. Sci. 46 (1996) 197–235.
[10] B. Abelev, et al., STAR Collaboration, Phys. Rev. C 80 (2009) 041902.
[11] L. Adamczyk, et al., STAR Collaboration, Phys. Lett. B 722 (2013) 55–62.
[12] A. Adare, et al., PHENIX Collaboration, Phys. Rev. D 85 (2012) 092004.
[13] F. Abe, et al., CDF Collaboration, Phys. Rev. Lett. 79 (1997) 572–577.
[14] D. Acosta, et al., CDF Collaboration, Phys. Rev. D 71 (2005) 032001.
[15] G. Aad, et al., ATLAS Collaboration, Nucl. Phys. B 850 (2011) 387–444.
[16] V. Khachatryan, et al., CMS Collaboration, Eur. Phys. J. C 71 (2011) 1575.
[17] R. Aaij, et al., LHCb Collaboration, Eur. Phys. J. C 71 (2011) 1645.
[18] E. Braaten, B.A. Kniehl, J. Lee, Phys. Rev. D 62 (2000) 094005.
[19] M. Butenschoen, B.A. Kniehl, Nucl. Phys. Proc. Suppl. 222–224 (2012) 151–161.
[20] A. Abulencia, et al., CDF Collaboration, Phys. Rev. Lett. 99 (2007) 132001.
[21] M. Butenschoen, B.A. Kniehl, Phys. Rev. Lett. 108 (2012) 172002.
[22] S. Chatrchyan, et al., CMS Collaboration, arXiv:1307.6070, 2013.
[23] B. Gong, L.-P. Wan, J.-X. Wang, H.-F. Zhang, Phys. Rev. Lett. 110 (2013) 042002.
[24] B. Abelev, et al., ALICE Collaboration, Phys. Rev. Lett. 108 (2012) 082001.
[25] R. Aaij, et al., LHCb Collaboration, Eur. Phys. J. C 73 (2013) 2631.
[26] H.S. Chung, C. Yu, S. Kim, J. Lee, Phys. Rev. D 81 (2010) 014020.
[27] A. Adare, et al., PHENIX Collaboration, Phys. Rev. D 82 (2010) 012001.
[28] J. Lansberg, Phys. Lett. B 695 (2011) 149–156, and private communication (2013).
[29] J. Lansberg, J. Phys. G 38 (2011) 124110.
[30] C.S. Lam, W.-K. Tung, Phys. Rev. D 18 (1978) 2447–2461.
[31] P. Faccioli, C. Lourenco, J. Seixas, H.K. Wohri, Eur. Phys. J. C 69 (2010) 657–673.
[32] K. Ackermann, et al., STAR Collaboration, Nucl. Instrum. Methods A 499 (2003) 624–632.
[33] M. Anderson, et al., Nucl. Instrum. Methods A 499 (2003) 659–678.
[34] W.J. Llope, et al., Nucl. Instrum. Methods A 661 (2012) 110–113.
[35] M. Beddo, et al., STAR Collaboration, Nucl. Instrum. Methods A 499 (2003) 725–739.
[36] F. Bergsma, et al., Nucl. Instrum. Methods A 499 (2003) 633–639.
[37] W.J. Llope, et al., Nucl. Instrum. Methods A 522 (2004) 252–273.
[38] J. Beringer, et al., Particle Data Group, The branching ratio for $J/\psi \to e^+e^-$ is (5.94 ± 0.06)%, including (0.88 ± 0.14)% for $J/\psi \to e^+e^-\gamma$, Phys. Rev. D 86 (2012) 010001.
[39] H. Bichsel, 2001, STAR Note SN0439.
[40] H. Bichsel, Nucl. Instrum. Methods A 562 (2006) 154–197.
[41] A. Adare, et al., PHENIX Collaboration, Phys. Rev. Lett. 98 (2007) 232002.
[42] D. Kaplan, et al., Phys. Rev. Lett. 40 (1978) 435–438.
[43] S.J. Brodsky, J.-P. Lansberg, Phys. Rev. D 81 (2010) 051502.

Kapitola 5

Produkcia kvarkónií v jadro-jadrových zrážkach

Pred viac než tridsiatimi rokmi T. Matsui a H. Satz [R49] predpovedali, že produkcia pôvabných kvarkónií bude v prítomnosti horúcej a hustej jadrovej hmoty potlačená. Toto potlačenie je z dôvodu farebného tienenia dikvarkového potenciálu z okolitých kvarkov a gluónov. Očakávalo sa, že prípadné experimentálne potvrdenie tejto predpovede by mohlo slúžiť ako dôkaz existencie kvarkovo-gluónovej plazmy. Následné prvé merania z experimentov na urýchľovači SPS (Super Proton Synchrotron) v CERN prevedené kolaboráciou NA38 preukázali, že v dvojmiónovom rozpadovom kanáli je produkcia J/ψ potlačená faktorom 0,64 $\pm$ 0,06 v centrálnych zrážkach O+U pri energii 200 GeV na nukleón vzhľadom k periferálnym zrážkam [R50]. Na produkciu J/ψ majú v jadro-jadrových zrážkach vplyv aj ďalšie fyzikálne procesy. Sú to effekty tzv. studenej jadrovej hmoty, ako napríklad jadrové tienenie partónovej distribučnej funkcie, partónová saturácia pri malých Feymanových x, viacnásobný rozptyl partónov pred a po tvrdom rozptyle (Croninov jav) a jadrová absorpcia $c\bar{c}$ párov v jadrovej hmote dôsledkom nepružných zrážok. Taktiež je možné, že v prípade väčšieho množstva $c\bar{c}$ párov vytvorených v jednej zrážke, po rozpade J/ψ na pôvabné kvarky opäť náhodne rekombinujú naspäť na J/ψ mezón. Príspevky sa môžu navzájom čiastočne kompenzovať. Pre správnu interpretáciu meraní v jadro-jadrových zrážkach je nutné stanoviť jednotlivé možné príspevky z ďalších meraní.

V prvom článku priloženom v tejto kapitole, L. Adamczyk *et al.*, *Energy dependence of J/ψ production in Au +Au collisions at $\sqrt{s}$= 39, 62.4 and 200 GeV*, Phys. Lett. B **771**, 13 (2017), sme previedli meranie produkcie J/ψ v jadro-jadrových zrážkach pri troch energiách. Využili sme k tomu dáta z prvej fázy programu energetickej prehliadky BES (Beam Energy Scan), ktorého účelom je pri meraniach jadro-jadrových zrážok s postupne menšími energiami hľadať hraničné prejavy kvarkovo-gluónovej plazmy. Aj pri tomto meraní sme použili na identifikáciu J/ψ rozpadový kanál e^+e^- a keďže sme pri meraní nemohli rozlíšiť rôzne zdroje J/ψ produkcie, jednalo sa o meranie inkluzívnych J/ψ mezónov. Všeobecne sme čakali, že potlačenie produkcie J/ψ mezónov, vyjadrené

jadrovým modifikačným faktorom R_{AA}, bude pri zrážkach s menšou energiou menšie, z dôvodu prípadnej absencie QGP alebo menšej hustoty či teploty. Podarilo sa nám rekonštruovať J/ψ v rozmezí priečnych hybností 0 až 3 GeV/c pre energie 39 a 62,4 GeV a 0 až 5 GeV/c pre energiu 200 GeV, pre štyri rôzne centrality zrážky: 0-20%, 20-40%, 40-60% a 0-60%. Experimentálne údaje sme namerali v rokoch 2010 a 2011. V tejto analýze sme na identifikáciu elektrónov použili kombináciu informácie z detektorov TPC, TOF a EMC. V neskorších meraniach po roku 2012 sa na rekonštrukciu J/ψ začal používať tiež dvojmiónový rozpadový kanál, keďže sa postupne nainštaloval Muónový Teleskopický Detektor. Zásadným problémom, s ktorým sme sa museli potýkať pri stanovení jadrového modifikačného faktora, bola absencia referenčného p+p merania pri energiách 39 GeV a 62,4 GeV. Použili sme parameterizáciu, ktorá bola vytvorená empirickou extrapoláciou z existujúcich meraní pri iných energiách v Ref. [R51]. Určili sme závislosť R_{AA} na priemernom počte účastníkov zrážky $\langle N_{part} \rangle$ a na priečnej hybnosti J/ψ (Fig. 4). Naše merania sme porovnali s meraniami pri nižšej energii na SPS $\sqrt{s} = 17$ GeV a meraniami na LHC pri energii $\sqrt{s} = 2{,}76$ TeV. V rámci chýb meraní je R_{AA} závislosť na $\langle N_{part} \rangle$ zhodná pre všetky energie do 200 GeV, vrátane. Pri periferálnych zrážkach (malé hodnoty $\langle N_{part} \rangle$) je R_{AA} blízke 1, avšak so zväčšujúcou sa hodnotou $\langle N_{part} \rangle$ a teda aj centralitou R_{AA} klesá až k $R_{AA} \approx 0.3$. Avšak R_{AA} pri energii na LHC je iné, jednak je jeho hodnota väčšia ($R_{AA} \approx 0.8$) a jednak viac-menej nezávisí na centralite zrážky. Podobne je to aj pri závislosti R_{AA} na p_T, opäť je závislosť iná pre energiu na LHC a ostatné nižšie energie majú rovnaký trend, keď pri malých p_T je potlačenie výrazné a potom sa potlačenie so zväčšujúcou priečnou hybnosťou zmenšuje. Na obrázku Fig. 6 sme z dôvodu lepšej interpretácie meraní porovnali závislosť R_{AA} na $\langle N_{part} \rangle$ s výpočtami z teoretického modelu z Ref. [R52], kde sme vykreslili jednotlivo príspevok z potlačenia zapríčineného farebným tienením a tiež príspevok z regenerácie J/ψ, z dôvodu rekombinácie $c\bar{c}$ párov. Model popisuje naše merania kvalitatívne celkom dobre. Pri nižších energiách je príspevok rekombinácie malý až zanedbateľný, avšak pri energii 200 GeV je tento príspevok pri najcentrálnejších zrážkach približne rovnakej veľkosti ako ten z farebného tienenia. Príspevok rekombinácie rastie so zväčšujúcou sa energiou, čo vysvetluje meranie R_{AA} s vyššou energiou na LHC. Vyplýva to tiež zo závislosti jadrového modifikačného faktora na energii zrážky pre centralitu 0-20% (Fig. 7). Pri energiách na LHC príspevok z rekombinácie takmer kompenzuje potlačenie z farebného tienenia a toto objasnuje celkovo malé potlačenie produkcie J/ψ na LHC v porovnaní s energiami na RHIC.

V druhom článku, ktorý je zaradený do tejto kapitoly, L. Adamczyk *et al. Measurement of J/ψ Azimuthal Anisotropy in Au+Au Collisions at $\sqrt{s}$= 200 GeV*, Phys. Rev. Lett. **111**, no. 5, 052301 (2013), sme sa zaoberali meraním azimutálnej anizotropie J/ψ v zrážkach Au+Au pri energii 200 GeV meraných roku 2010. Hlavnou motiváciou bolo tiež skúmať vplyv rekombinácie $c\bar{c}$ na produkciu J/ψ v týchto zrážkach. Konkrétne sme sa zamerali na určenie eliptického toku - v_2, druhého člena vo Furierovom rozvoji

azimutálnej uhlovej závislosti produkcie J/ψ vzhľadom k rovine zrážky. J/ψ mezóny, ktoré vznikajú priamo v tvrdých procesoch na začiatku zrážky, by nemali mať žiadnu azimutálnu závislosť produkcie. V necentrálnych zrážkach je priečny tvar objemu prekryvu jadier pri zrážke mandľovitý, tj. v rovine zrážky je užší ako v na ňu kolmom smere. Vzhľadom k tomu, že pravdepodobnosť rozbitia J/ψ z dôvodu farebného tienenia väzbového potenciálu je úmerná dráhe, ktorú častica v jadrovej hmote uletí, môže tento proces viesť k asymetrii vzhľadom na rovinu zrážky. Na druhej strane v prípade, že sa pôvabné kvarky v jadrovej hmote tiež termalizujú a získajú podobné kolektívne chovanie ako ľahké kvarky a tým pádom tiež budú mať eliptický tok, po ich náhodnej rekombinácii výsledné J/ψ bude mať tiež úmerne tomu nenulový eliptický tok v_2. Keďže doba termalizácie častice s veľkou hmotnosťou ako pôvabný kvark je dlhá, znamenalo by to, že ľahké kvarky by sa museli termalizovať rýchlo po zrážke. I v tejto analýze sme na identifikáciu elektrónov použili kombinovanú informáciu z detektorov TPC, TOF a EMC. Podarilo sa nám určiť parameter v_2, jednak pre zrážky s centralitou 0-60%, a jednak pre centralitné intervaly 0-10%, 10-40% a 40-80% pre J/ψ s priečnymi hybnosťami od 0 do 10 GeV/c . Ako sme diskutovali v článku priloženom v prvej kapitole, na meranie kolektívneho toku môžu mať vplyv rozpady rezonancií a výtrysky častíc. Vplyv týchto dvoj a viačasticových korelácií iných častíc s J/ψ efektívne mení rovinu zrážky a tým pádom zvyšuje hodnotu nameraného parametru v_2. Tento vplyv sme odhadli pomocou veľkosti hadrón-J/ψ korelácií z p + p zrážok pri rovnakej energii. Zistili sme prekvapivú skutočnosť, že J/ψ nemá podobné kolektívne chovanie ako všetky iné doposiaľ skúmané hadróny, ale pre priečne hybnosti väčšie ako 2 GeV/c má hodnotu eliptického toku zhodnú s nulou, v rámci chýb merania (Fig. 3 z priloženého druhého článku). Z porovnania s rôznymi modelmi produkcie J/ψ vyplýva, že model založený hlavne na produkcii J/ψ rekombináciou termalizovaných $c\bar{c}$ kvarkov je s nameraným v_2 najviac v rozpore. Fyzikálny záver z oboch článkov v tejto kapitole je teda veľmi podobný. V experimente ALICE na LHC sme tiež merali parameter eliptického toku v_2 pre inkluzívne J/ψ v zrážkach Pb-Pb pri energii $\sqrt{s_{NN}} = 5.02$ TeV v strednej a doprednej rapidite [386]. Pri tejto energii sme namerali nenulovú hodnotu v_2, čo je v súlade s dôležitosťou príspevku z rekombinovaných termalizovaných $c\bar{c}$ párov na LHC.

Article reprint

Physics Letters B 771 (2017) 13–20

Contents lists available at ScienceDirect

Physics Letters B

www.elsevier.com/locate/physletb

Energy dependence of J/ψ production in Au + Au collisions at $\sqrt{s_{NN}} = 39, 62.4$ and 200 GeV

STAR Collaboration

L. Adamczyk [a], J.K. Adkins [s], G. Agakishiev [q], M.M. Aggarwal [ae], Z. Ahammed [ax], N.N. Ajitanand [an], I. Alekseev [o,z], D.M. Anderson [ap], R. Aoyama [at], A. Aparin [q], D. Arkhipkin [c], E.C. Aschenauer [c], M.U. Ashraf [as], A. Attri [ae], G.S. Averichev [q], X. Bai [g], V. Bairathi [aa], A. Behera [an], R. Bellwied [ar], A. Bhasin [p], A.K. Bhati [ae], P. Bhattarai [aq], J. Bielcik [j], J. Bielcikova [k], L.C. Bland [c], I.G. Bordyuzhin [o], J. Bouchet [r], J.D. Brandenburg [aj], A.V. Brandin [z], D. Brown [w], I. Bunzarov [q], J. Butterworth [aj], H. Caines [bb], M. Calderón de la Barca Sánchez [e], J.M. Campbell [ac], D. Cebra [e], I. Chakaberia [c], P. Chaloupka [j], Z. Chang [ap], N. Chankova-Bunzarova [q], A. Chatterjee [ax], S. Chattopadhyay [ax], X. Chen [ak], J.H. Chen [am], X. Chen [u], J. Cheng [as], M. Cherney [i], W. Christie [c], G. Contin [v], H.J. Crawford [d], S. Das [g], L.C. De Silva [i], R.R. Debbe [c], T.G. Dedovich [q], J. Deng [al], A.A. Derevschikov [ag], L. Didenko [c], C. Dilks [af], X. Dong [v], J.L. Drachenberg [t], J.E. Draper [e], L.E. Dunkelberger [f], J.C. Dunlop [c], L.G. Efimov [q], N. Elsey [az], J. Engelage [d], G. Eppley [aj], R. Esha [f], S. Esumi [at], O. Evdokimov [h], J. Ewigleben [w], O. Eyser [c], R. Fatemi [s], S. Fazio [c], P. Federic [k], P. Federicova [j], J. Fedorisin [q], Z. Feng [g], P. Filip [q], E. Finch [au], Y. Fisyak [c], C.E. Flores [e], J. Fujita [i], L. Fulek [a], C.A. Gagliardi [ap], D. Garand [ah], F. Geurts [aj], A. Gibson [aw], M. Girard [ay], D. Grosnick [aw], D.S. Gunarathne [ao], Y. Guo [r], A. Gupta [p], S. Gupta [p], W. Guryn [c], A.I. Hamad [r], A. Hamed [ap], A. Harlenderova [j], J.W. Harris [bb], L. He [ah], S. Heppelmann [af], S. Heppelmann [e], A. Hirsch [ah], G.W. Hoffmann [aq], S. Horvat [bb], B. Huang [h], H.Z. Huang [f], T. Huang [ab], X. Huang [as], T.J. Humanic [ac], P. Huo [an], G. Igo [f], W.W. Jacobs [n], A. Jentsch [aq], J. Jia [c,an], K. Jiang [ak], S. Jowzaee [az], E.G. Judd [d], S. Kabana [r], D. Kalinkin [n], K. Kang [as], K. Kauder [az], H.W. Ke [c], D. Keane [r], A. Kechechyan [q], Z. Khan [h], D.P. Kikoła [ay], I. Kisel [l], A. Kisiel [ay], L. Kochenda [z], M. Kocmanek [k], T. Kollegger [l], L.K. Kosarzewski [ay], A.F. Kraishan [ao], P. Kravtsov [z], K. Krueger [b], N. Kulathunga [ar], L. Kumar [ae], J. Kvapil [j], J.H. Kwasizur [n], R. Lacey [an], J.M. Landgraf [c], K.D. Landry [f], J. Lauret [c], A. Lebedev [c], R. Lednicky [q], J.H. Lee [c], Y. Li [as], X. Li [ak], W. Li [am], C. Li [ak], J. Lidrych [j], T. Lin [n], M.A. Lisa [ac], Y. Liu [ap], H. Liu [n], F. Liu [g], P. Liu [an], T. Ljubicic [c], W.J. Llope [az], M. Lomnitz [v], R.S. Longacre [c], S. Luo [h], X. Luo [g], G.L. Ma [am], L. Ma [am], Y.G. Ma [am], R. Ma [c], N. Magdy [an], R. Majka [bb], D. Mallick [aa], S. Margetis [r], C. Markert [aq], H.S. Matis [v], K. Meehan [e], J.C. Mei [al], Z.W. Miller [h], N.G. Minaev [ag], S. Mioduszewski [ap], D. Mishra [aa], S. Mizuno [v], B. Mohanty [aa], M.M. Mondal [m], D.A. Morozov [ag], M.K. Mustafa [v], Md. Nasim [f], T.K. Nayak [ax], J.M. Nelson [d], M. Nie [am], G. Nigmatkulov [z], T. Niida [az], L.V. Nogach [ag], T. Nonaka [at], S.B. Nurushev [ag], G. Odyniec [v], A. Ogawa [c], K. Oh [ai], V.A. Okorokov [z], D. Olvitt Jr. [ao], B.S. Page [c], R. Pak [c], Y. Pandit [h], Y. Panebratsev [q], B. Pawlik [ad], H. Pei [g], C. Perkins [d], P. Pile [c], J. Pluta [ay], K. Poniatowska [ay], J. Porter [v], M. Posik [ao], N.K. Pruthi [ae], M. Przybycien [a], J. Putschke [az], H. Qiu [ah], A. Quintero [ao], S. Ramachandran [s], R.L. Ray [aq], R. Reed [w], M.J. Rehbein [i], H.G. Ritter [v], J.B. Roberts [aj], O.V. Rogachevskiy [q], J.L. Romero [e], J.D. Roth [i], L. Ruan [c],

http://dx.doi.org/10.1016/j.physletb.2017.04.078

Article reprint

J. Rusnak [k], O. Rusnakova [j], N.R. Sahoo [ap], P.K. Sahu [m], S. Salur [v], J. Sandweiss [bb], M. Saur [k], J. Schambach [aq], A.M. Schmah [v], W.B. Schmidke [c], N. Schmitz [x], B.R. Schweid [an], J. Seger [i], M. Sergeeva [f], P. Seyboth [x], N. Shah [am], E. Shahaliev [q], P.V. Shanmuganathan [w], M. Shao [ak], A. Sharma [p], M.K. Sharma [p], W.Q. Shen [am], S.S. Shi [g], Z. Shi [v], Q.Y. Shou [am], E.P. Sichtermann [v], R. Sikora [a], M. Simko [k], S. Singha [r], M.J. Skoby [n], N. Smirnov [bb], D. Smirnov [c], W. Solyst [n], L. Song [ar], P. Sorensen [c], H.M. Spinka [b], B. Srivastava [ah], T.D.S. Stanislaus [aw], M. Strikhanov [z], B. Stringfellow [ah], T. Sugiura [at], M. Sumbera [k], B. Summa [af], X. Sun [g], Y. Sun [ak], X.M. Sun [g], B. Surrow [ao], D.N. Svirida [o], A.H. Tang [c], Z. Tang [ak], A. Taranenko [z], T. Tarnowsky [y], A. Tawfik [ba], J. Thäder [v], J.H. Thomas [v], A.R. Timmins [ar], D. Tlusty [aj], T. Todoroki [c], M. Tokarev [q], S. Trentalange [f], R.E. Tribble [ap], P. Tribedy [c], S.K. Tripathy [m], B.A. Trzeciak [j], O.D. Tsai [f], T. Ullrich [c], D.G. Underwood [b], I. Upsal [ac], G. Van Buren [c], G. van Nieuwenhuizen [c], A.N. Vasiliev [ag], F. Videbæk [c], S. Vokal [q], S.A. Voloshin [az], A. Vossen [n], G. Wang [f], Y. Wang [g], F. Wang [ah], Y. Wang [as], J.C. Webb [c], G. Webb [c], L. Wen [f], G.D. Westfall [y], H. Wieman [v], S.W. Wissink [n], R. Witt [av], Y. Wu [r], Z.G. Xiao [as], W. Xie [ah], G. Xie [ak], J. Xu [g], N. Xu [v], Q.H. Xu [al], Y.F. Xu [am], Z. Xu [c], Y. Yang [ab], Q. Yang [ak], C. Yang [al], S. Yang [c], Z. Ye [h], Z. Ye [h], L. Yi [bb], K. Yip [c], I.-K. Yoo [ai], N. Yu [g], H. Zbroszczyk [ay], W. Zha [ak,*], Z. Zhang [am], X.P. Zhang [as], J.B. Zhang [g], S. Zhang [ak], J. Zhang [u], Y. Zhang [ak], J. Zhang [v], S. Zhang [am], J. Zhao [ah], C. Zhong [am], L. Zhou [ak], C. Zhou [am], X. Zhu [as], Z. Zhu [al], M. Zyzak [l]

[a] *AGH University of Science and Technology, FPACS, Cracow 30-059, Poland*
[b] *Argonne National Laboratory, Argonne, Illinois 60439*
[c] *Brookhaven National Laboratory, Upton, New York 11973*
[d] *University of California, Berkeley, California 94720*
[e] *University of California, Davis, California 95616*
[f] *University of California, Los Angeles, California 90095*
[g] *Central China Normal University, Wuhan, Hubei 430079*
[h] *University of Illinois at Chicago, Chicago, Illinois 60607*
[i] *Creighton University, Omaha, Nebraska 68178*
[j] *Czech Technical University in Prague, FNSPE, Prague, 115 19, Czech Republic*
[k] *Nuclear Physics Institute AS CR, 250 68 Prague, Czech Republic*
[l] *Frankfurt Institute for Advanced Studies FIAS, Frankfurt 60438, Germany*
[m] *Institute of Physics, Bhubaneswar 751005, India*
[n] *Indiana University, Bloomington, Indiana 47408*
[o] *Alikhanov Institute for Theoretical and Experimental Physics, Moscow 117218, Russia*
[p] *University of Jammu, Jammu 180001, India*
[q] *Joint Institute for Nuclear Research, Dubna, 141 980, Russia*
[r] *Kent State University, Kent, Ohio 44242*
[s] *University of Kentucky, Lexington, Kentucky, 40506-0055*
[t] *Lamar University, Physics Department, Beaumont, Texas 77710*
[u] *Institute of Modern Physics, Chinese Academy of Sciences, Lanzhou, Gansu 730000*
[v] *Lawrence Berkeley National Laboratory, Berkeley, California 94720*
[w] *Lehigh University, Bethlehem, Pennsylvania 18015*
[x] *Max-Planck-Institut fur Physik, Munich 80805, Germany*
[y] *Michigan State University, East Lansing, Michiagan 48824*
[z] *National Research Nuclear University MEPhI, Moscow 115409, Russia*
[aa] *National Institute of Science Education and Research, Bhubaneswar 751005, India*
[ab] *National Cheng Kung University, Tainan 70101*
[ac] *Ohio State University, Columbus, Ohio 43210*
[ad] *Institute of Nuclear Physics PAN, Cracow 31-342, Poland*
[ae] *Panjab University, Chandigarh 160014, India*
[af] *Pennsylvania State University, University Park, Pennsylyania 16802*
[ag] *Institute of High Energy Physics, Protvino 142281, Russia*
[ah] *Purdue University, West Lafayette, Indiana 47907*
[ai] *Pusan National University, Pusan 46241, Republic of Korea*
[aj] *Rice University, Houston, Texas 77251*
[ak] *University of Science and Technology of China, Hefei, Anhui 230026*
[al] *Shandong University, Jinan, Shandong 250100*
[am] *Shanghai Institute of Applied Physics, Chinese Academy of Sciences, Shanghai 201800*
[an] *State University Of New York, Stony Brook, New York 11794*
[ao] *Temple University, Philadelphia, Pennsylvania 19122*
[ap] *Texas A&M University, College Station, Texas 77843*
[aq] *University of Texas, Austin, Texas 78712*
[ar] *University of Houston, Houston, Texas 77204*
[as] *Tsinghua University, Beijing 100084*
[at] *University of Tsukuba, Tsukuba, Ibaraki, Japan*
[au] *Southern Connecticut State University, New Haven, Connecticut 06515*
[av] *United States Naval Academy, Annapolis, Maryland 21402*
[aw] *Valparaiso University, Valparaiso, Indiana 46383*

Article reprint

[ax] *Variable Energy Cyclotron Centre, Kolkata 700064, India*
[ay] *Warsaw University of Technology, Warsaw 00-661, Poland*
[az] *Wayne State University, Detroit, Michigan 48201*
[ba] *World Laboratory for Cosmology and Particle Physics (WLCAPP), Cairo 11571, Egypt*
[bb] *Yale University, New Haven, Connecticut 06520*

ARTICLE INFO

Article history:
Received 26 July 2016
Received in revised form 11 April 2017
Accepted 20 April 2017
Available online 10 May 2017
Editor: M. Doser

ABSTRACT

The inclusive J/ψ transverse momentum spectra and nuclear modification factors are reported at mid-rapidity ($|y| < 1.0$) in Au + Au collisions at $\sqrt{s_{NN}} = 39$, 62.4 and 200 GeV taken by the STAR experiment. A suppression of J/ψ production, with respect to the production in $p + p$ scaled by the number of binary nucleon–nucleon collisions, is observed in central Au + Au collisions at these three energies. No significant energy dependence of nuclear modification factors is found within uncertainties. The measured nuclear modification factors can be described by model calculations that take into account both suppression of direct J/ψ production due to the color screening effect and J/ψ regeneration from recombination of uncorrelated charm–anticharm quark pairs.

1. Introduction

The Relativistic Heavy Ion Collider (RHIC) was built to investigate strongly interacting matter at high temperature and energy density in the laboratory through high-energy heavy-ion collisions. At extremely high temperatures and baryon densities, a transition from the hadronic phase of matter to a new deconfined partonic phase, the Quark–Gluon Plasma (QGP), is predicted by Quantum Chromodynamics (QCD) [1–8]. It has been proposed that the color potential in quarkonia could be screened by quarks and gluons in the QGP [9]. Quarkonia are bound states of charm–anticharm ($c\bar{c}$) or bottom–antibottom ($b\bar{b}$) quark pairs. As a consequence, quarkonium production cross sections in heavy-ion collisions divided by the corresponding number of binary nucleon–nucleon collisions, N_{coll}, are expected to be suppressed compared to those in $p + p$ collisions if QGP is formed in heavy-ion collisions.

The J/ψ is the most abundantly produced quarkonium state accessible to experiments. Over the past twenty years, J/ψ suppression in hot and dense media has been a topic of growing interest. Various measurements of J/ψ production in heavy ion collisions have been performed in different collision systems and at different energies, and indeed a suppression of J/ψ production has been observed [10–13]. A similar centrality dependent suppression was found at SPS (S + U $\sqrt{s_{NN}} = 19.4$ GeV [14], Pb + Pb $\sqrt{s_{NN}} = 17.2$ GeV [15] and In + In $\sqrt{s_{NN}} = 17.2$ GeV [12]) and at RHIC (Au + Au $\sqrt{s_{NN}} = 200$ GeV [16,17]) for mid-rapidity, even though the temperature and energy density reached in these studies are significantly different [18]. Furthermore, a stronger suppression at forward rapidity ($1.2 < |y| < 2.2$) compared to mid-rapidity ($|y| < 0.35$) was observed at RHIC [16]. These observations indicate that effects other than color screening are important for J/ψ production. Among these effects, J/ψ production from the recombination of $c\bar{c}$ [19,20], together with color screening effect, play important roles in explaining the similar suppressions at SPS and RHIC [21]. With the higher temperature and density at RHIC, the increased contribution due to regeneration from the larger charm quark density could compensate for the enhanced suppression. This could also explain a stronger suppression at forward rapidity at RHIC where the charm quark density is lower compared to mid-rapidity [20–23]. In addition to the color screening and regeneration effects, there are also modifications from cold nuclear matter (CNM) effects, such as nuclear parton distribution function modification [24], energy loss by the colliding nuclei [25], Cronin effect [26], and other final state effects, such as nuclear absorption [27] and dissociation by co-movers [28]. The suppression due to these effects has been systematically studied experimentally via $p + A$ collisions [29–39]. However, the extrapolation from $p + A$ to $A + A$ is still model dependent.

The nuclear modification factor of J/ψ production in Pb + Pb collisions at $\sqrt{s_{NN}} = 2.76$ TeV has been measured at the LHC [40–42]. In comparison with results from RHIC in Au + Au collisions at $\sqrt{s_{NN}} = 200$ GeV, the J/ψ production is significantly less suppressed, which suggests significantly more recombination contribution at LHC energies. The measurement of J/ψ production at forward rapidity ($1.2 < |y| < 2.2$) in Au + Au collisions by the PHENIX experiment at $\sqrt{s_{NN}} = 39$ and 62.4 GeV indicates a similar suppression level as that at $\sqrt{s_{NN}} = 200$ GeV [43]. Measurements of J/ψ invariant yields at different collision energies at RHIC in different centralities at mid-rapidity can shed new light on the interplay of the mechanisms for J/ψ production and medium properties.

In this letter, we further study the collision energy dependence of J/ψ production and test the hypothesis of the two competing mechanisms of color screening and regeneration. We present measurements of the J/ψ production at mid-rapidity ($|y| < 1$) with the STAR experiment in Au + Au collisions at $\sqrt{s_{NN}} = 39$, 62.4 using data collected in year 2010 and at $\sqrt{s_{NN}} = 200$ GeV using the combined data in year 2010 [17] and 2011 and study the nuclear modification factors at these energies.

2. Experiment and analysis

The STAR experiment is a large-acceptance multi-purpose detector which covers full azimuth in the pseudorapidity interval $|\eta| < 1$ [44]. The Vertex Position Detector (VPD) was used to select Au + Au collisions that were within ±15 cm of the center of the STAR detector [45]. The minimum-bias trigger utilized in this analysis required a coincidence between the East and West VPD. In order to avoid the VPD inefficiency in peripheral Au + Au collisions, only data in 0–60% central collisions are accepted. The total numbers of 0–60% central events that are used in this analysis are 182 million, 94 million, and 360 million for 39, 62.4 and 200 GeV, respectively. The J/ψ is reconstructed through its decay into electron–positron pairs, $J/\psi \to e^+e^-$ (branching ratio $\mathrm{Br}(J/\psi \to e^+e^-) = 5.97 \pm 0.03\%$ [46]). The primary detectors used in this analysis are the Time Projection Chamber (TPC)

* Corresponding author.
E-mail address: wangmei@rcf.rhic.bnl.gov (W. Zha).

Article reprint

Table I
Summary of centrality bins, average number of participants $\langle N_{part}\rangle$, number of binary collisions $\langle N_{coll}\rangle$, and nuclear overlap function $\langle T_{AA}\rangle$ from MC Glauber simulation of Au + Au at $\sqrt{s_{NN}} = 39$, 62 and 200 GeV. The errors indicate uncertainties from the MC Glauber calculations.

$\sqrt{s_{NN}}$ (GeV)	Centrality (%)	$\langle N_{part}\rangle$	$\langle N_{coll}\rangle$	$\langle T_{AA}\rangle$ (fm^{-2})
39	0–20	273 ± 6	629 ± 26	187 ± 5
	20–40	137 ± 11	245 ± 26	71 ± 7
	40–60	59 ± 10	79 ± 17	23 ±5
	0–60	156 ± 8	316 ± 22	93 ± 6
62	0–20	276 ± 5	664 ± 25	187 ± 5
	20–40	139 ± 10	258 ± 27	71 ± 7
	40–60	60 ± 10	82 ± 18	23 ± 5
	0–60	157 ± 9	332 ± 23	93 ± 6
200	0–20	280 ± 6	785 ± 29	187 ± 5
	20–40	142 ± 11	300 ± 31	71 ± 7
	40–60	62 ± 10	95 ± 21	23 ± 5
	0–60	161 ± 9	393 ± 27	93 ± 6

[47], the Time-of-Flight (TOF) detector [48], and the Barrel Electromagnetic Calorimeter (BEMC) [49]. The TPC provides tracking and particle identification via the ionization energy loss ($\langle dE/dx\rangle$) of charge particles. The TOF [48] measures the velocity of particles, which greatly improved electron identification at low momentum. This detector, combined with the TPC [47], clearly identifies electrons by rejecting hadrons in the low and intermediate momentum range ($p < 1.5$ GeV/c). The BEMC [49], a lead-scintillator calorimeter, is used to improve the electron identification at high momentum ($p > 1.5$ GeV/c). The electron identification method is similar to Refs. [17,50].

Collision centrality was determined from the uncorrected charged particle multiplicity $dN/d\eta$ within $|\eta| < 0.5$ using a Monte Carlo (MC) Glauber model [51]. The dependence of $dN/d\eta$ on the collision vertex position V_z and the beam luminosity has been included to take acceptance and efficiency changes on the measured $dN/d\eta$ into account. For each collision centrality, an average nuclear overlap function, $\langle T_{AA}\rangle$, average number of participants, $\langle N_{part}\rangle$, and average number of binary collisions, $\langle N_{coll}\rangle$, were related to an observed multiplicity range. Centrality definitions in Au + Au collisions for $\sqrt{s_{NN}} = 39$, 62.4 and 200 GeV are summarized in Table I.

The daughter tracks of the J/ψ candidates are required to have at least 25 out of the 45 possible TPC hits, and a distance of closest approach (DCA) from the primary vertex of less than 3 cm. Low momentum ($p < 1.5$ GeV/c) electron and positron candidates are separated from hadrons by selecting on the inverse velocity, $|1/\beta - 1| < 0.03$, where β is the velocity measured in the TOF normalized by the speed of light. The cut value is determined using a three standard deviation window. At high momentum ($p >$ 1.5 GeV/c), a cut on the ratio of momentum to energy deposited in towers from BEMC ($0.3 < pc/E < 1.5$) is used to suppress hadrons. The electron and positron candidates are then identified by their specific energy loss ($\langle dE/dx\rangle$) in the TPC. More than 15 TPC hits are required to calculate $\langle dE/dx\rangle$. The normalized $\langle dE/dx\rangle$ is defined as follows:

$$n\sigma_e = \frac{ln(\langle dE/dx\rangle^m / \langle dE/dx\rangle_e^{th})}{R_{dE/dx}} \quad (1)$$

where $\langle dE/dx\rangle^m$ and $\langle dE/dx\rangle^{th}$ represent measured and theoretical values, respectively, and $R_{dE/dx}$ is the experimental $ln(dE/dx)$ resolution. The $n\sigma_e$ cut for electron identification is $-1.5 < n\sigma_e < 2$. The combination of these cuts enables the identification of electrons and positrons over a wide momentum range [17]. The electron sample purity integrated over the measured momentum region is over 90%. Our measurement of J/ψ covers the rapidity range $|y| < 1$ due to the STAR acceptance and decay kinematics.

The J/ψ signal is extracted by subtracting combinatorial background reconstructed from the unlike-sign mixed-events spectrum. The like-sign distributions can be used as normalization references for the mixed-events method. The like-sign and mixed-events distributions are obtained as follows:

1) Like-sign: Electrons (or positrons) of the same charge sign are paired within the same event.
2) Mixed-events: Events are categorized according to the position along the beam line of the primary vertex and centrality of the event. Electrons from one event are paired with positrons from other random events from an event pool with similar global features such as collision centrality and vertex position. The vertex position is divided into 20 bins and the event centrality into 10 bins to ensure that the mixing is done using tracks from similar conditions.

The invariant mass distribution of e^+e^- pairs before and after the combinatorial background subtraction in 0–60% central Au + Au collisions are shown in Fig. 1 for $\sqrt{s_{NN}} = 39$, 62.4, and 200 GeV. The mixed-event background is normalized to the like-sign distribution in a mass range of 2.0–4.0 GeV/c^2 and the normalized shapes show close agreement. The normalization technique is described in Ref. [52]. The mass distribution of e^+e^- is fitted by the J/ψ signal shape obtained from MC simulation, which includes the resolution of the TPC, bremsstrahlung of the daughter electrons in the detector and internal radiation of J/ψ, combined with a straight line for residual background. The residual background mainly comes from the correlated open charm decays and Drell–Yan processes. The raw J/ψ signal is obtained from bin counting in the mass range 2.7–3.2 GeV/c^2 after combinatorial and residual background subtraction. The fraction of J/ψ counts outside of the mass window was determined from the J/ψ MC simulated signal shape and was found to be ∼9%. This was used to correct the number of J/ψ counts. Signal-to-background ratios for these three energies are observed to be 0.62, 0.39, and 0.04, respectively for the transverse momentum (p_T) interval 0–3 GeV/c (39 and 62 GeV) and 0–5 GeV/c (200 GeV). The J/ψ invariant yield is defined as

$$\mathrm{Br}_{J/\psi\to e^+e^-}\frac{d^2N}{2\pi\, p_T dp_T dy} = \frac{1}{2\pi\, p_T \Delta p_T \Delta y}\frac{N_{J/\psi\to e^+e^-}}{A\epsilon N_{EVT}} \quad (2)$$

where $N_{J/\psi\to e^+e^-}$ is the uncorrected number of reconstructed J/ψ, N_{EVT} is the number of events in the relevant Au + Au centrality selection, $A\epsilon$ is the detector's geometric acceptance times its efficiency (about 0.05 ∼ 0.12 depending on p_T, centrality and collision energy), and Δp_T and Δy are the bin width in p_T and y, respectively. Acceptance and efficiency corrections (TPC and BEMC related) are estimated by MC simulations with GEANT3 package [53]. Some of the efficiency corrections such as those corresponding to the TOF and dE/dx related cuts are extracted directly from data [52]. The acceptance and efficiency correction procedure is similar to Refs. [17,50].

The systematic uncertainties in this analysis include uncertainties from the particle identification efficiency using the TPC, TOF, and BEMC, the tracking efficiency from TPC, and the yield extraction methods. The systematic uncertainty on the efficiency correction and particle identification is estimated by comparing the difference for the related cut distributions between simulation and data. In order to account for the contributions from radiation losses and correlated background in the yield extraction procedure, the mass window and methods for signal counting have also been varied to evaluate the uncertainties. Table II contains a summary of

Article reprint

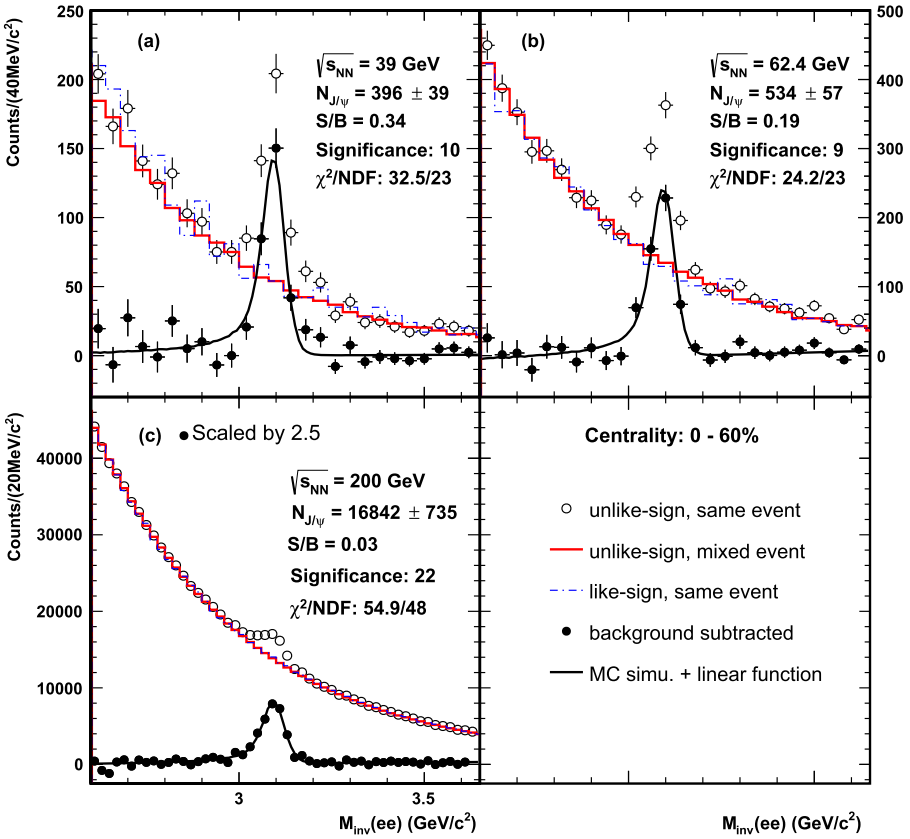

Fig. 1. The e^+e^- invariant mass distribution of J/ψ candidates (black open circles), like-sign combinatorial background (blue dashed line), mixed event combinatorial background (red solid line), and J/ψ candidates with mixed event background subtracted (black solid circles) in Au + Au collisions at $\sqrt{s_{NN}}$ = 39 (a), 62.4 (b), and 200 GeV (c) for centrality 0–60%. The J/ψ signal shape from a MC simulation is combined with a linear residual background and is fitted to the combinatorial background subtracted data (black solid line). (For interpretation of the references to color in this figure legend, the reader is referred to the web version of this article.)

the contributions from the different sources. The ranges in the table are corresponding to the p_T, centrality and collision energy dependence of uncertainties. The uncertainties are partially correlated among the p_T and centrality intervals. The total systematic uncertainties in the integrated p_T range are 20%, 11%, and 10% at $\sqrt{s_{NN}}$ = 39, 62.4, and 200 GeV, respectively. At $\sqrt{s_{NN}}$ = 39 GeV, the large systematic uncertainty on the particle identification BEMC related cuts is due to the large uncertainties associated to the cuts themselves. The normalization uncertainty on the nuclear modification factor includes the uncertainty from $\langle T_{AA}\rangle$ and the statistical and systematic uncertainty of the J/ψ cross section in $p+p$. The centrality and transverse momentum dependence of the total systematic uncertainties are reflected in the results shown in Section 3.

3. Results

The J/ψ invariant yields as a function of p_T in Au + Au collisions at $\sqrt{s_{NN}}$ = 39, 62.4, and 200 GeV for different centrality bins are shown in Fig. 2. As expected, the J/ψ invariant yields are larger in Au + Au collisions at larger center-of-mass energies. Results from the current measurements (year 2011) are compared with the published results from data taken in 2010, they show close agreement with each other. These two measurements are combined together to cumulate more statistics for the nuclear modification factors in this paper.

Table II
The contributions of systematic uncertainty sources for $\sqrt{s_{NN}}$ = 39, 62.4 and 200 GeV. The uncertainties are partially correlated among the p_T and centrality intervals.

Systematic uncertainty source	39 GeV	62.4 GeV	200 GeV
TPC tracking cuts (%)	8	7	6
BEMC related cuts (%)	17–25	3–5	1–2
TOF related cuts (%)	2	2	2
Yield extraction (%)	6–12	2–7	5–11
Total (%)	19–29	10–12	8–12
$\langle N_{coll}\rangle$ (%)	4–22	4–22	4–22
$\langle T_{AA}\rangle$ (%)	3–22	3–22	3–22
$\sigma^{pp}_{J/\psi}$ (%)	12	7	14

Nuclear modification factors (R_{CP}, R_{AA}) are used to quantify the suppression of J/ψ production. R_{CP} is a ratio of the J/ψ yield in central collisions to peripheral collisions (centrality: 40–60%) and defined as follows:

$$R_{CP} = \frac{\frac{dN/dy}{\langle N_{coll}\rangle}(central)}{\frac{dN/dy}{\langle N_{coll}\rangle}(peripheral)} \quad (3)$$

where $\langle N_{coll}\rangle$ and dN/dy are the average number of nucleon–nucleon collisions and J/ψ yield in a given centrality, respectively. dN/dy is obtained from the integration of the J/ψ p_T spectrum. The extrapolation of the p_T spectrum to the full coverage ($p_T > 0$ GeV/c) is based on the two following functions:

Article reprint

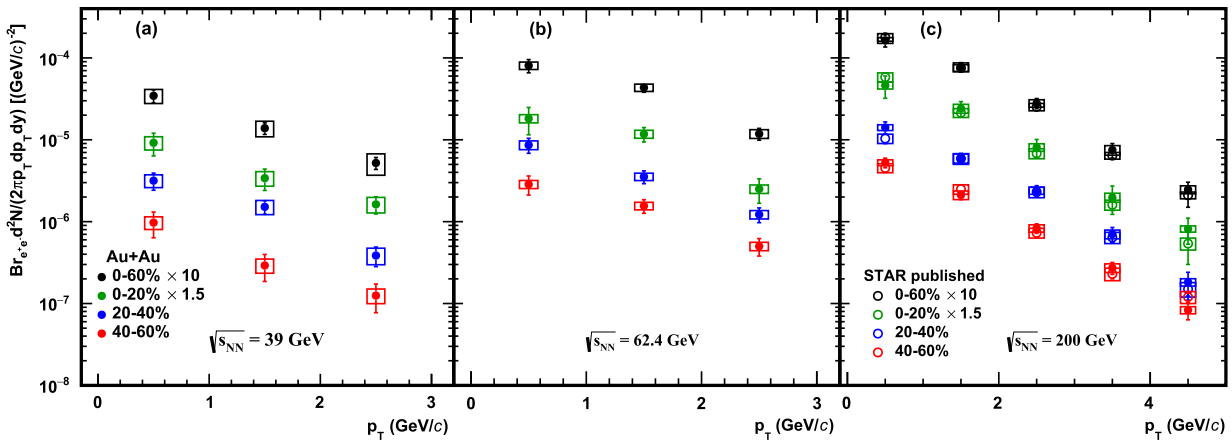

Fig. 2. J/ψ invariant yields in Au + Au collisions at $\sqrt{s_{NN}}$ = 39, 62.4 and 200 GeV as a function of p_T for different centralities. The error bars represent the statistical uncertainties. The boxes represent the systematic uncertainties. The STAR published results are from Refs. [50] and [17].

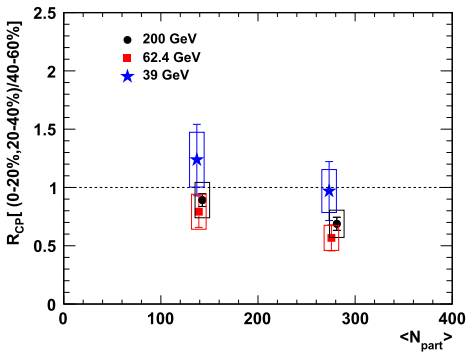

Fig. 3. J/ψ R_{CP} results (with respect to 40–60% peripheral collisions) for Au + Au as a function of $\langle N_{part}\rangle$. The error bars represent the statistical uncertainties. The boxes represent the systematic uncertainties combined with uncertainties from $\langle N_{coll}\rangle$ in different centrality bins.

$$\frac{dN}{dp_T} = a \times \frac{p_T}{(1 + b^2 p_T^2)^n} \tag{4}$$

$$\frac{dN}{dp_T} = l \times p_T \times \exp^{-\frac{m_T}{h}}, \qquad m_T = \sqrt{p_T^2 + m_{J/\psi}^2} \tag{5}$$

where a, b, n, h and l are free parameters. The fit results from Eq. (4) have been assigned as central value, and the differences (< 2%) between these two functional fits have been taken as a source of systematic uncertainty. Note that R_{CP} reflects only relative suppression – if the modification of J/ψ yield in central and peripheral bins is the same, R_{CP} is equal to 1. The R_{CP}, as a function of the average number of participant nucleons ($\langle N_{part}\rangle$), for Au + Au collisions at $\sqrt{s_{NN}}$ = 39, 62.4 and 200 GeV, are shown in Fig. 3. Note that the peripheral bin selection is 40–60% central Au + Au collisions for these three energies. The systematic uncertainties for R_{CP} are mainly from $\langle N_{coll}\rangle$ and yield extraction. Systematic uncertainties originating from TPC, BEMC and TOF related cuts, are negligible or mostly cancel. A suppression is observed in central Au + Au collisions at $\sqrt{s_{NN}}$ = 62.4 GeV, which is similar to that at $\sqrt{s_{NN}}$ = 200 GeV.

R_{AA} is obtained from comparing J/ψ production in A + A collisions to $p + p$ collisions, defined as follows:

$$R_{AA} = \frac{1}{\langle T_{AA}\rangle} \frac{d^2N_{AA}/dp_T dy}{d^2\sigma_{pp}/dp_T dy} \tag{6}$$

where $d^2N_{AA}/dp_T dy$ is the J/ψ yield in A + A collisions and $d^2\sigma_{pp}/dp_T dy$ is the J/ψ cross section in $p + p$ collisions. The nuclear overlap function with impact parameter **b** is defined as $T_{AA}(\mathbf{b}) = \int T_A(\mathbf{s}) T_A(\mathbf{s} - \mathbf{b}) d^2s$, where $T_A(\mathbf{s})$ is the probability per unit transverse area of a nucleon being located in the target flux tube. The uncertainties from T_{AA} are estimated by varying the radius and skin depth of the nuclei in the Glauber calculations. If there are no hot or cold nuclear matter effects, the value of R_{AA} should be unity.

To obtain R_{AA} at $\sqrt{s_{NN}}$ = 39 and 62.4 GeV, we have to derive the J/ψ cross section in $p + p$ collisions because there are no measurements available for the $p + p$ references at STAR for these two energies. There are several $p + p$ measurements from fixed target $p + A$ experiments [54–56] and from Intersecting Storage Ring (ISR) collider experiments [57,58] near these two energies. However, the p_T shapes from Ref. [57] and Ref. [58] at $\sqrt{s}$ = 63 GeV are inconsistent with each other and the cross section measurements at $\sqrt{s}$ = 39 GeV are comparable to (or even larger than) that at $\sqrt{s}$ = 63 GeV. Therefore, we use the cross section derived in Ref. [59] as our $p + p$ reference baselines for $\sqrt{s_{NN}}$ = 39 and 62.4 GeV. In Ref. [59], the world-wide experimental data on J/ψ cross sections and kinematic distributions in $p + p$ and $p + A$ collisions at $\sqrt{s}$ = 6.8–7000 GeV are examined in a systematic way. The authors explore the $\sqrt{s}$ dependence of the inclusive cross section, rapidity and transverse momentum distributions phenomenologically and develop a strategy for the interpolation of the J/ψ cross section and kinematics at RHIC energies. This approach is found to describe the world-wide J/ψ data reasonably well. With this strategy, the predicted J/ψ cross section times branching ratio at $\sqrt{s}$ = 39 and 62.4 GeV in mid-rapidity are $\mathrm{Br}(J/\psi \to e^+e^-) d\sigma/dy|_{|y|<1.0} = 9.0 \pm 0.6$ and 17.6 ± 2.1 nb, respectively.

With the derived $p + p$ references for $\sqrt{s}$ = 39 and 62.4 GeV, and the measured $p + p$ baseline at $\sqrt{s}$ = 200 GeV [50,60], we obtain the R_{AA} of J/ψ for $p_T > 0$ as a function of $\langle N_{part}\rangle$ in Au + Au collisions at $\sqrt{s_{NN}}$ = 39, 62.4, and 200 GeV, as shown in Fig. 4 (a). The p_T-differential J/ψ R_{AA} is shown in Fig. 4 (b). The bars and boxes on the data points represent the statistical and systematic uncertainties, respectively. The shaded and hatched bands indicate the uncertainties on the baseline J/ψ cross section in $p + p$ collisions [50,59,60] and $\langle T_{AA}\rangle$, respectively. The bands on the vertical axes indicate global uncertainties, while those on the data points represent bin to bin uncertainties. The measurements from SPS [12,14,15] and LHC [61] and the expected R_{AA} with complete

Article reprint

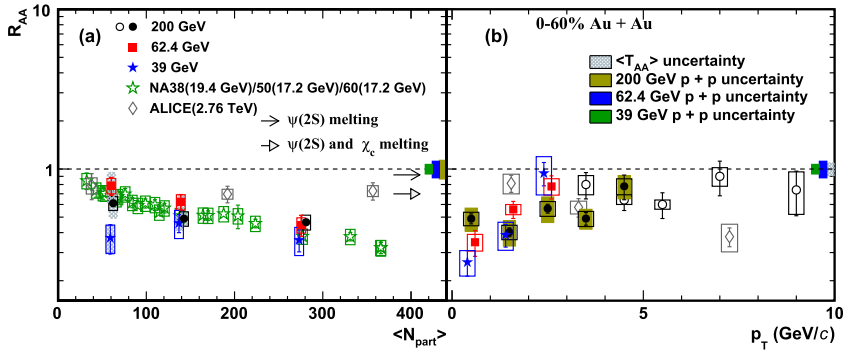

Fig. 4. The results of J/ψ R_{AA} as a function of $\langle N_{part}\rangle$ (a) and p_T (b) in Au + Au collisions at $\sqrt{s_{NN}}$ = 39, 62.4 and 200 GeV. The error bars represent the statistical uncertainties. The boxes represent the systematic uncertainties. The shaded and hatched bands indicate the uncertainties on the baseline J/ψ cross section in $p + p$ collisions [50,59,60] and $\langle T_{AA}\rangle$, respectively. The ALICE points are from [61]. The ratio of feed-down J/ψ from higher chamonium states to inclusive J/ψ is from [63]. The STAR high-p_T ($3 < p_T < 10$ GeV/c) results, represented as open circles, are from [50].

$\psi(2S)$ and χ_c melting and no modification of the J/ψ yield [63] are also included for comparison. Suppression of J/ψ production is observed in Au + Au collisions from $\sqrt{s_{NN}}$ = 39 to 200 GeV with respect to the production in $p + p$ scaled by $\langle T_{AA}\rangle$. For R_{AA} as a function of $\langle N_{part}\rangle$, no significant energy dependence is observed within uncertainties from $\sqrt{s_{NN}}$ = 17.2 to 200 GeV. For the J/ψ R_{AA} as a function of p_T, significant suppression is observed at low p_T ($p_T < 2$ GeV/c) from $\sqrt{s_{NN}}$ = 39 to 200 GeV. The modification of J/ψ production is consistent within the systematic uncertainties for these collision energies. The ALICE [61] points are also shown for comparison. As shown in the figure, the ALICE R_{AA} results are higher than the measurements at RHIC and SPS and show a different trend as a function of p_T. Fig. 5 shows the comparison of R_{AA} between mid-rapidity from STAR and forward rapidity from PHENIX from $\sqrt{s_{NN}}$ = 39 to 200 GeV. The suppression of J/ψ shows no significant rapidity dependence at $\sqrt{s_{NN}}$ = 39 nor 62.4 GeV within uncertainties.

As shown in Fig. 6, theoretical calculations [21] with initial suppression and J/ψ regeneration describe the data within 1.6 standard deviation for these three collision energies. The R_{AA} results as a function of collision energy for 0–20% centrality are also shown in Fig. 7. Theoretical calculations are also included for comparison. The calculations include two components: direct suppression and regeneration. The direct suppression represent the "anomalous" suppression of primordial J/ψs due to CNM and color screening effects. According to the model calculations [21], the R_{AA} is about

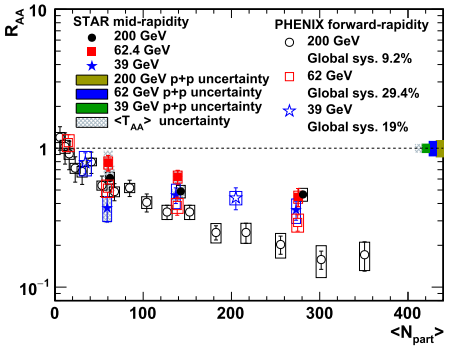

Fig. 5. J/ψ R_{AA} results as a function of $\langle N_{part}\rangle$ in Au + Au collisions at $\sqrt{s_{NN}}$ = 39, 62.4 and 200 GeV. The error bars represent the statistical uncertainties. The boxes represent the systematic uncertainties. The shaded and hatched bands indicate the uncertainties on the baseline J/ψ cross section in $p + p$ collisions [50,59,60] and $\langle T_{AA}\rangle$, respectively. The PHENIX results are from [43,62].

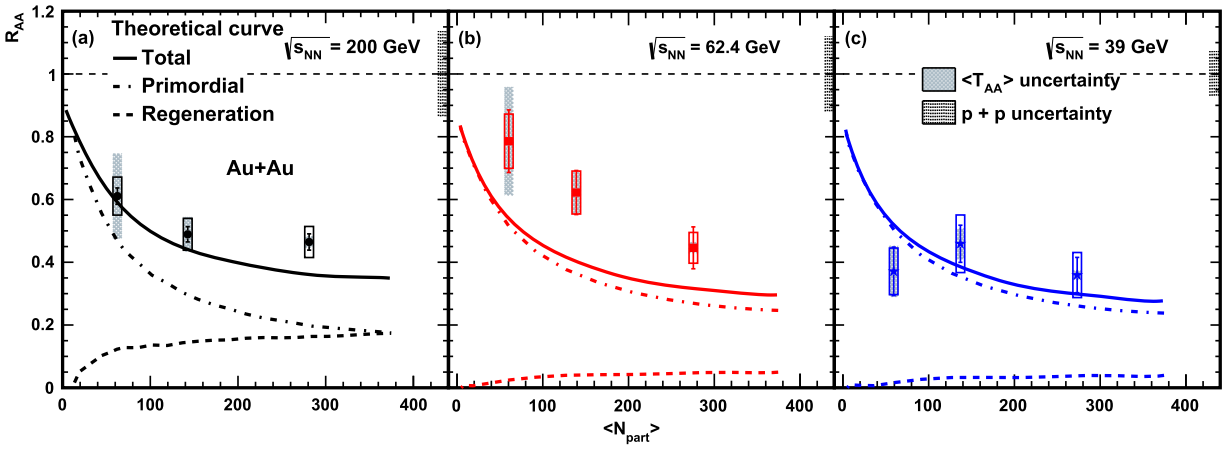

Fig. 6. The results of J/ψ R_{AA} as a function of $\langle N_{part}\rangle$, in comparison with model calculations [21], for Au + Au collisions at $\sqrt{s_{NN}}$ = 200 (a), 62.4 (b) and 39 GeV (c), respectively. The error bars represent the statistical uncertainties. The boxes represent the systematic uncertainties. The dotted and hatched bands indicate the uncertainties on the baseline J/ψ cross section in $p + p$ collisions [50,59,60] and $\langle T_{AA}\rangle$, respectively. Solid lines are J/ψ modification factors from model [21]; dash-dotted line are suppressed primordial production; dashed lines are regeneration component.

Article reprint

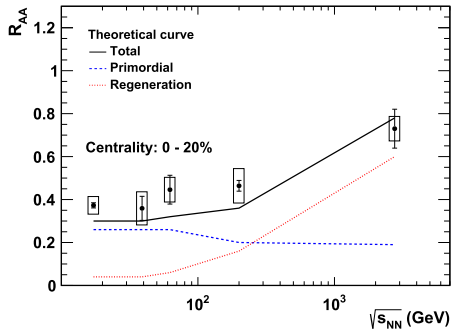

Fig. 7. The results of J/ψ R_{AA} as a function of collision energy for centrality 0–20%, in comparison with model calculations [21]. The SPS result ($\sqrt{s_{NN}}$ = 17.2 GeV) is from [10,15]; the ALICE point ($\sqrt{s_{NN}}$ = 2.76 TeV) is from [61]. The error bars represent the statistical uncertainties and the boxes represent the systematic uncertainties. The boxes include the systematic uncertainties, the uncertainties on the baseline J/ψ cross section in $p+p$ collisions [50,59,60] and the uncertainties from $\langle T_{AA}\rangle$. Solid line is the total J/ψ modification factors from model; dash-dotted line is the suppressed primordial production; dashed line is the regeneration component. The theory calculations are only done for the five specific energy points, and connected by straight lines. Note: since ALICE data show no significant centrality dependence, it is appropriate to use the available 0–10% data at 2.76 TeV in this figure.

0.6 for central Au + Au collisions at $\sqrt{s_{NN}}$ = 200 GeV with only CNM effects. The regeneration component is responsible for the contribution from the recombination of correlated or uncorrelated $c\bar{c}$ pairs. The feed-down to J/ψ from χ_c and ψ' has been taken into account in the calculations. No significant energy dependence of R_{AA} for 0–20% centrality is observed at $\sqrt{s_{NN}}$ < 200 GeV. As the collision energy increases the QGP temperature increases, thus the J/ψ color screening becomes more significant. However, in the theoretical calculation [21], the regeneration contribution increases with collision energy due to the increase in the charm pair production, and compensates the enhanced suppression arising from the higher temperature. The higher R_{AA} at ALICE may indicate that the surviving J/ψs are mainly coming from the recombination contribution. The model calculation describes the energy dependence of J/ψ production from SPS to LHC.

4. Summary

In summary, we report on recent STAR measurements of J/ψ production at mid-rapidity in Au + Au collisions at $\sqrt{s_{NN}}$ = 39, 62.4 and 200 GeV. Suppression of J/ψ production, with respect to the production in $p+p$ scaled by the number of binary nucleon–nucleon collisions, is observed at these three energies. No significant energy dependence of the nuclear modification factor (either R_{AA} or R_{CP}) is found within uncertainties. Model calculations, which include direct suppression and regeneration, reasonably describe the centrality and energy dependence of J/ψ production in high-energy heavy ion collisions.

Acknowledgements

We thank the RHIC Operations Group and RCF at BNL, the NERSC Center at LBNL, the KISTI Center in Korea, and the Open Science Grid consortium for providing resources and support. This work was supported in part by the Office of Nuclear Physics within the U.S. DOE Office of Science, the U.S. NSF, the Ministry of Education and Science of the Russian Federation, NSFC, CAS, MoST and MoE of China, the National Research Foundation of Korea, NCKU (Taiwan), GA and MSMT of the Czech Republic, FIAS of Germany, DAE, DST, and UGC of India, the National Science Centre of Poland, National Research Foundation, the Ministry of Science, Education and Sports of the Republic of Croatia, and RosAtom of Russia.

References

[1] E.V. Shuryak, Phys. Rep. 61 (1980) 71.
[2] S. Digal, P. Petreczky, H. Satz, Phys. Rev. D 64 (2001) 094015.
[3] F. Karsch, D. Kharzeev, H. Satz, Phys. Lett. B 637 (2006) 75.
[4] P. Braun-Munzinger, J. Stachel, Nature 448 (2007) 302.
[5] J. Adams, et al., STAR Collaboration, Nucl. Phys. A 757 (2005) 102.
[6] K. Adcox, et al., PHENIX Collaboration, Nucl. Phys. A 757 (2005) 184.
[7] B.B. Back, et al., PHOBOS Collaboration, Nucl. Phys. A 757 (2005) 28.
[8] I. Arsene, et al., BRAHMS Collaboration, Nucl. Phys. A 757 (2005) 1.
[9] T. Matsui, H. Satz, Phys. Lett. B 178 (1986) 416.
[10] L. Kluberg, Eur. Phys. J. C 43 (2005) 145.
[11] M.C. Abreu, et al., Phys. Lett. B 449 (1999) 128.
[12] R. Arnaldi, et al., Phys. Rev. Lett. 99 (2007) 132302.
[13] E.T. Atomssa, Eur. Phys. J. C 61 (2009) 683.
[14] M.C. Abreu, et al., Phys. Lett. B 466 (1999) 408.
[15] M.C. Abreu, et al., Phys. Lett. B 477 (2000) 28.
[16] A. Adare, et al., Phys. Rev. Lett. 98 (2007) 232301.
[17] L. Adamczyk, et al., Phys. Rev. C 90 (2014) 024906.
[18] K.J. Eskola, et al., Nucl. Phys. B 570 (2000) 379.
[19] P. Braun-Munzinger, J. Stachel, Phys. Lett. B 490 (2000) 196.
[20] L. Grandchamp, R. Rapp, G.E. Brown, Phys. Rev. Lett. 92 (2004) 212301.
[21] X. Zhao, R. Rapp, Phys. Rev. C 82 (2010) 064905 (private communication).
[22] R. Rapp, et al., Prog. Part. Nucl. Phys. 65 (2010) 209.
[23] Y. Liu, et al., Int. J. Mod. Phys. E 24 (2015) 1530015.
[24] J.L. Nagle, et al., Phys. Rev. C 84 (2011) 044911.
[25] J.L. Nagle, M.J. Bennett, Phys. Lett. B 465 (1999) 21.
[26] J.W. Cronin, et al., Phys. Rev. D 11 (1975) 3105.
[27] R. Vogt, Nucl. Phys. A 700 (2002) 539.
[28] E.G. Ferreiro, Phys. Lett. B 749 (2015) 98.
[29] D. Alde, et al., Phys. Rev. Lett. 66 (1991) 133.
[30] M. Leitch, et al., Nucl. Phys. A 544 (1992) 197c.
[31] M. Leitch, et al., Phys. Rev. Lett. 84 (2000) 3256.
[32] B. Alessandro, et al., Eur. Phys. J. C 33 (2004) 31.
[33] B. Alessandro, et al., Eur. Phys. J. C 39 (2005) 335.
[34] R. Arnaldi, et al., Phys. Lett. B 706 (2012) 263.
[35] A. Adare, et al., Phys. Rev. C 87 (2013) 034904.
[36] A. Adare, et al., Phys. Rev. Lett. 107 (2011) 142301.
[37] A. Adare, et al., Phys. Rev. Lett. 111 (2013) 202301.
[38] B. Abelev, et al., J. High Energy Phys. 02 (2014) 073.
[39] W.K. Brooks (for ATLAS Collaboration), Nucl. Part. Phys. Proc. 276–278 (2016) 149.
[40] B. Abelev, et al., Phys. Rev. Lett. 109 (2012) 072301.
[41] G. Aad, et al., Phys. Lett. B 697 (2011) 294.
[42] S. Chatrchyan, et al., J. High Energy Phys. 05 (2012) 063.
[43] A. Adare, et al., Phys. Rev. C 86 (2012) 064901.
[44] K.H. Ackermannn, et al., Nucl. Instrum. Methods A 499 (2003) 624.
[45] W.J. Llope, et al., Nucl. Instrum. Methods 759 (2014) 23.
[46] K.A. Olive, et al., Chin. Phys. C 38 (2014) 090001.
[47] M. Anderson, et al., Nucl. Instrum. Methods 499 (2003) 659.
[48] W.J. Llope, Nucl. Instrum. Methods 661 (2012) S110.
[49] M. Beddo, et al., Nucl. Instrum. Methods 499 (2003) 725.
[50] L. Adamczyk, et al., Phys. Lett. B 722 (2013) 55.
[51] M.L. Miller, et al., Annu. Rev. Nucl. Part. Sci. 57 (2007) 205.
[52] L. Adamczyk, et al., Phys. Rev. C 92 (2015) 024912.
[53] B.I. Abelev, et al., Phys. Rev. C 79 (2009) 034909.
[54] T. Alexopoulos, et al., Phys. Rev. D 55 (1997) 3927.
[55] M.H. Schub, et al., Phys. Rev. D 52 (1995) 1307.
[56] A. Gribushin, et al., Phys. Rev. D 62 (2000) 012001.
[57] A.G. Clark, et al., Nucl. Phys. B 142 (1978) 29.
[58] C. Kourkoumelis, et al., Phys. Lett. B 91 (1980) 481.
[59] W. Zha, et al., Phys. Rev. C 93 (2016) 024919.
[60] A. Adare, et al., Phys. Rev. D 82 (2010) 012001.
[61] B. Abelev, et al., Phys. Lett. B 734 (2014) 314.
[62] A. Adare, et al., Phys. Rev. C 84 (2011) 054912.
[63] P. Faccioli, et al., J. High Energy Phys. 10 (2008) 004.

Article reprint

PRL **111,** 052301 (2013) PHYSICAL REVIEW LETTERS week ending 2 AUGUST 2013

Measurement of J/ψ Azimuthal Anisotropy in Au + Au Collisions at $\sqrt{s_{NN}} = 200$ GeV

L. Adamczyk,[1] J. K. Adkins,[23] G. Agakishiev,[21] M. M. Aggarwal,[34] Z. Ahammed,[53] I. Alekseev,[19] J. Alford,[22] C. D. Anson,[31] A. Aparin,[21] D. Arkhipkin,[4] E. Aschenauer,[4] G. S. Averichev,[21] J. Balewski,[26] A. Banerjee,[53] Z. Barnovska,[14] D. R. Beavis,[4] R. Bellwied,[49] M. J. Betancourt,[26] R. R. Betts,[10] A. Bhasin,[20] A. K. Bhati,[34] P. Bhattarai,[48] H. Bichsel,[55] J. Bielcik,[13] J. Bielcikova,[14] L. C. Bland,[4] I. G. Bordyuzhin,[19] W. Borowski,[45] J. Bouchet,[22] A. V. Brandin,[29] S. G. Brovko,[6] E. Bruna,[57] S. Bültmann,[32] I. Bunzarov,[21] T. P. Burton,[4] J. Butterworth,[40] X. Z. Cai,[44] H. Caines,[57] M. Calderón de la Barca Sánchez,[6] D. Cebra,[6] R. Cendejas,[35] M. C. Cervantes,[47] P. Chaloupka,[13] Z. Chang,[47] S. Chattopadhyay,[53] H. F. Chen,[42] J. H. Chen,[44] J. Y. Chen,[9] L. Chen,[9] J. Cheng,[50] M. Cherney,[12] A. Chikanian,[57] W. Christie,[4] P. Chung,[14] J. Chwastowski,[11] M. J. M. Codrington,[48] R. Corliss,[26] J. G. Cramer,[55] H. J. Crawford,[5] X. Cui,[42] S. Das,[16] A. Davila Leyva,[48] L. C. De Silva,[49] R. R. Debbe,[4] T. G. Dedovich,[21] J. Deng,[43] R. Derradi de Souza,[8] S. Dhamija,[18] B. di Ruzza,[4] L. Didenko,[4] F. Ding,[6] A. Dion,[4] P. Djawotho,[47] X. Dong,[25] J. L. Drachenberg,[52] J. E. Draper,[6] C. M. Du,[24] L. E. Dunkelberger,[7] J. C. Dunlop,[4] L. G. Efimov,[21] M. Elnimr,[56] J. Engelage,[5] G. Eppley,[40] L. Eun,[25] O. Evdokimov,[10] R. Fatemi,[23] S. Fazio,[4] J. Fedorisin,[21] R. G. Fersch,[23] P. Filip,[21] E. Finch,[57] Y. Fisyak,[4] E. Flores,[6] C. A. Gagliardi,[47] D. R. Gangadharan,[31] D. Garand,[37] F. Geurts,[40] A. Gibson,[52] S. Gliske,[2] O. G. Grebenyuk,[25] D. Grosnick,[52] A. Gupta,[20] S. Gupta,[20] W. Guryn,[4] B. Haag,[6] O. Hajkova,[13] A. Hamed,[47] L-X. Han,[44] J. W. Harris,[57] J. P. Hays-Wehle,[26] S. Heppelmann,[35] A. Hirsch,[37] G. W. Hoffmann,[48] D. J. Hofman,[10] S. Horvat,[57] B. Huang,[4] H. Z. Huang,[7] P. Huck,[9] T. J. Humanic,[31] G. Igo,[7] W. W. Jacobs,[18] C. Jena,[30] E. G. Judd,[5] S. Kabana,[45] K. Kang,[50] J. Kapitan,[14] K. Kauder,[10] H. W. Ke,[9] D. Keane,[22] A. Kechechyan,[21] A. Kesich,[6] D. P. Kikola,[37] J. Kiryluk,[25] I. Kisel,[25] A. Kisiel,[54] S. R. Klein,[25] D. D. Koetke,[52] T. Kollegger,[15] J. Konzer,[37] I. Koralt,[32] W. Korsch,[23] L. Kotchenda,[29] P. Kravtsov,[29] K. Krueger,[2] I. Kulakov,[25] L. Kumar,[22] M. A. C. Lamont,[4] J. M. Landgraf,[4] K. D. Landry,[7] S. LaPointe,[56] J. Lauret,[4] A. Lebedev,[4] R. Lednicky,[21] J. H. Lee,[4] W. Leight,[26] M. J. LeVine,[4] C. Li,[42] W. Li,[44] X. Li,[37] X. Li,[46] Y. Li,[50] Z. M. Li,[9] L. M. Lima,[41] M. A. Lisa,[31] F. Liu,[9] T. Ljubicic,[4] W. J. Llope,[40] R. S. Longacre,[4] Y. Lu,[42] X. Luo,[9] A. Luszczak,[11] G. L. Ma,[44] Y. G. Ma,[44] D. M. M. D. Madagodagettige Don,[12] D. P. Mahapatra,[16] R. Majka,[57] S. Margetis,[22] C. Markert,[48] H. Masui,[25] H. S. Matis,[25] D. McDonald,[40] T. S. McShane,[12] S. Mioduszewski,[47] M. K. Mitrovski,[4] Y. Mohammed,[47] B. Mohanty,[30] M. M. Mondal,[47] M. G. Munhoz,[41] M. K. Mustafa,[37] M. Naglis,[25] B. K. Nandi,[17] Md. Nasim,[53] T. K. Nayak,[53] J. M. Nelson,[3] L. V. Nogach,[36] J. Novak,[28] G. Odyniec,[25] A. Ogawa,[4] K. Oh,[38] A. Ohlson,[57] V. Okorokov,[29] E. W. Oldag,[48] R. A. N. Oliveira,[41] D. Olson,[25] M. Pachr,[13] B. S. Page,[18] S. K. Pal,[53] Y. X. Pan,[7] Y. Pandit,[10] Y. Panebratsev,[21] T. Pawlak,[54] B. Pawlik,[33] H. Pei,[10] C. Perkins,[5] W. Peryt,[54] P. Pile,[4] M. Planinic,[58] J. Pluta,[54] N. Poljak,[58] J. Porter,[25] A. M. Poskanzer,[25] C. B. Powell,[25] C. Pruneau,[56] N. K. Pruthi,[34] M. Przybycien,[1] P. R. Pujahari,[17] J. Putschke,[56] H. Qiu,[25] S. Ramachandran,[23] R. Raniwala,[39] S. Raniwala,[39] R. L. Ray,[48] C. K. Riley,[57] H. G. Ritter,[25] J. B. Roberts,[40] O. V. Rogachevskiy,[21] J. L. Romero,[6] J. F. Ross,[12] L. Ruan,[4] J. Rusnak,[14] N. R. Sahoo,[53] P. K. Sahu,[16] I. Sakrejda,[25] S. Salur,[25] A. Sandacz,[54] J. Sandweiss,[57] E. Sangaline,[6] A. Sarkar,[17] J. Schambach,[48] R. P. Scharenberg,[37] A. M. Schmah,[25] B. Schmidke,[4] N. Schmitz,[27] T. R. Schuster,[15] J. Seger,[12] P. Seyboth,[27] N. Shah,[7] E. Shahaliev,[21] M. Shao,[42] B. Sharma,[34] M. Sharma,[56] S. S. Shi,[9] Q. Y. Shou,[44] E. P. Sichtermann,[25] R. N. Singaraju,[53] M. J. Skoby,[18] D. Smirnov,[4] N. Smirnov,[57] D. Solanki,[39] P. Sorensen,[4] U. G. deSouza,[41] H. M. Spinka,[2] B. Srivastava,[37] T. D. S. Stanislaus,[52] J. R. Stevens,[26] R. Stock,[15] M. Strikhanov,[29] B. Stringfellow,[37] A. A. P. Suaide,[41] M. C. Suarez,[10] M. Sumbera,[14] X. M. Sun,[25] Y. Sun,[42] Z. Sun,[24] B. Surrow,[46] D. N. Svirida,[19] T. J. M. Symons,[25] A. Szanto de Toledo,[41] J. Takahashi,[8] A. H. Tang,[4] Z. Tang,[42] L. H. Tarini,[56] T. Tarnowsky,[28] J. H. Thomas,[25] J. Tian,[44] A. R. Timmins,[49] D. Tlusty,[14] M. Tokarev,[21] S. Trentalange,[7] R. E. Tribble,[47] P. Tribedy,[53] B. A. Trzeciak,[54] O. D. Tsai,[7] J. Turnau,[33] T. Ullrich,[4] D. G. Underwood,[2] G. Van Buren,[4] G. van Nieuwenhuizen,[26] J. A. Vanfossen, Jr.,[22] R. Varma,[17] G. M. S. Vasconcelos,[8] F. Videbæk,[4] Y. P. Viyogi,[53] S. Vokal,[21] S. A. Voloshin,[56] A. Vossen,[18] M. Wada,[48] F. Wang,[37] G. Wang,[7] H. Wang,[4] J. S. Wang,[24] Q. Wang,[37] X. L. Wang,[42] Y. Wang,[50] G. Webb,[23] J. C. Webb,[4] G. D. Westfall,[28] C. Whitten, Jr.,[7] H. Wieman,[25] S. W. Wissink,[18] R. Witt,[51] Y. F. Wu,[9] Z. Xiao,[50] W. Xie,[37] K. Xin,[40] H. Xu,[24] N. Xu,[25] Q. H. Xu,[43] W. Xu,[7] Y. Xu,[42] Z. Xu,[4] L. Xue,[44] Y. Yang,[24] Y. Yang,[9] P. Yepes,[40] L. Yi,[37] K. Yip,[4] I-K. Yoo,[38] M. Zawisza,[54] H. Zbroszczyk,[54] J. B. Zhang,[9] S. Zhang,[44] X. P. Zhang,[50] Y. Zhang,[42] Z. P. Zhang,[42] F. Zhao,[7] J. Zhao,[44] C. Zhong,[44] X. Zhu,[50] Y. H. Zhu,[44] Y. Zoulkarneeva,[21] and M. Zyzak[25]

Article reprint

PRL **111,** 052301 (2013) PHYSICAL REVIEW LETTERS week ending 2 AUGUST 2013

(STAR Collaboration)

[1]*AGH University of Science and Technology, Cracow, Poland*
[2]*Argonne National Laboratory, Argonne, Illinois 60439, USA*
[3]*University of Birmingham, Birmingham, United Kingdom*
[4]*Brookhaven National Laboratory, Upton, New York 11973, USA*
[5]*University of California, Berkeley, California 94720, USA*
[6]*University of California, Davis, California 95616, USA*
[7]*University of California, Los Angeles, California 90095, USA*
[8]*Universidade Estadual de Campinas, Sao Paulo, Brazil*
[9]*Central China Normal University (HZNU), Wuhan 430079, China*
[10]*University of Illinois at Chicago, Chicago, Illinois 60607, USA*
[11]*Cracow University of Technology, Cracow, Poland*
[12]*Creighton University, Omaha, Nebraska 68178, USA*
[13]*Czech Technical University in Prague, FNSPE, Prague 115 19, Czech Republic*
[14]*Nuclear Physics Institute AS CR, 250 68 Řež/Prague, Czech Republic*
[15]*University of Frankfurt, Frankfurt, Germany*
[16]*Institute of Physics, Bhubaneswar 751005, India*
[17]*Indian Institute of Technology, Mumbai, India*
[18]*Indiana University, Bloomington, Indiana 47408, USA*
[19]*Alikhanov Institute for Theoretical and Experimental Physics, Moscow, Russia*
[20]*University of Jammu, Jammu 180001, India*
[21]*Joint Institute for Nuclear Research, Dubna 141 980, Russia*
[22]*Kent State University, Kent, Ohio 44242, USA*
[23]*University of Kentucky, Lexington, Kentucky 40506-0055, USA*
[24]*Institute of Modern Physics, Lanzhou, China*
[25]*Lawrence Berkeley National Laboratory, Berkeley, California 94720, USA*
[26]*Massachusetts Institute of Technology, Cambridge, Massachusetts 02139-4307, USA*
[27]*Max-Planck-Institut für Physik, Munich, Germany*
[28]*Michigan State University, East Lansing, Michigan 48824, USA*
[29]*Moscow Engineering Physics Institute, Moscow, Russia*
[30]*National Institute of Science and Education and Research, Bhubaneswar 751005, India*
[31]*Ohio State University, Columbus, Ohio 43210, USA*
[32]*Old Dominion University, Norfolk, Virginia 23529, USA*
[33]*Institute of Nuclear Physics PAN, Cracow, Poland*
[34]*Panjab University, Chandigarh 160014, India*
[35]*Pennsylvania State University, University Park, Pennsylvania 16802, USA*
[36]*Institute of High Energy Physics, Protvino, Russia*
[37]*Purdue University, West Lafayette, Indiana 47907, USA*
[38]*Pusan National University, Pusan, Republic of Korea*
[39]*University of Rajasthan, Jaipur 302004, India*
[40]*Rice University, Houston, Texas 77251, USA*
[41]*Universidade de Sao Paulo, Sao Paulo, Brazil*
[42]*University of Science and Technology of China, Hefei 230026, China*
[43]*Shandong University, Jinan, Shandong 250100, China*
[44]*Shanghai Institute of Applied Physics, Shanghai 201800, China*
[45]*SUBATECH, Nantes, France*
[46]*Temple University, Philadelphia, Pennsylvania 19122, USA*
[47]*Texas A&M University, College Station, Texas 77843, USA*
[48]*University of Texas, Austin, Texas 78712, USA*
[49]*University of Houston, Houston, Texas 77204, USA*
[50]*Tsinghua University, Beijing 100084, China*
[51]*United States Naval Academy, Annapolis, Maryland 21402, USA*
[52]*Valparaiso University, Valparaiso, Indiana 46383, USA*
[53]*Variable Energy Cyclotron Centre, Kolkata 700064, India*
[54]*Warsaw University of Technology, Warsaw, Poland*
[55]*University of Washington, Seattle, Washington 98195, USA*
[56]*Wayne State University, Detroit, Michigan 48201, USA*
[57]*Yale University, New Haven, Connecticut 06520, USA*

Article reprint

PRL 111, 052301 (2013) PHYSICAL REVIEW LETTERS week ending 2 AUGUST 2013

[58]University of Zagreb, Zagreb, HR-10002, Croatia

(Received 13 December 2012; revised manuscript received 10 May 2013; published 2 August 2013)

The measurement of J/ψ azimuthal anisotropy is presented as a function of transverse momentum for different centralities in Au + Au collisions at $\sqrt{s_{NN}} = 200$ GeV. The measured J/ψ elliptic flow is consistent with zero within errors for transverse momentum between 2 and 10 GeV/c. Our measurement suggests that J/ψ particles with relatively large transverse momenta are not dominantly produced by coalescence from thermalized charm quarks, when comparing to model calculations.

DOI: 10.1103/PhysRevLett.111.052301 PACS numbers: 25.75.Cj, 12.38.Mh, 14.40.Pq

Quantum chromodynamics (QCD) predicts a quark-gluon plasma (QGP) phase at extremely high temperature and/or density, consisting of deconfined quarks and gluons. Over the past twenty years, heavy quarkonia production in hot and dense nuclear matter has been a topic attracting growing interest. In relativistic heavy-ion collisions the $c\bar{c}$ bound state is subject to dissociation due to the color screening effect in the deconfined medium. As a consequence, the production of the J/ψ is expected to be suppressed compared to proton + proton ($p + p$) collisions scaled by number of binary collisions, and such suppression has been proposed as a signature of QGP formation [1]. However, the J/ψ suppression observed in experiments [2–6] can also be affected by additional cold [7,8] and hot [9–14] nuclear effects. In particular, the recombination of the J/ψ from a thermalized charm quark and its antiquark [11–14] has not been unambiguously established experimentally at the top RHIC energy. By measuring J/ψ azimuthal anisotropy, especially its second Fourier coefficient v_2 (elliptic flow), one may infer the relative contribution of J/ψ particles from direct perturbative QCD (pQCD) processes and from recombination. J/ψ particles produced from direct pQCD processes, which do not have initial collective motion, should have little azimuthal preference. In noncentral collisions, the produced J/ψ particles will then gain limited azimuthal anisotropy from azimuthally different absorption due to the different path lengths in azimuth. On the other hand, J/ψ particles produced from recombination of thermalized charm quarks will inherit the flow of charm quarks, exhibiting considerable flow.

Many models that describe the experimental results of heavy-ion collisions depend on the assumption that light flavor quarks in the medium reach thermalization on a short time scale (~ 0.5 fm/c) [15,16]. However, this rapid full thermalization has not been directly certified. The flow pattern of heavy quarks provides a unique tool to test the thermalization. With much larger mass than that of light quarks, heavy quarks are more resistant to having their velocity changed, and are thus expected to thermalize much more slowly than light partons. If charm quarks are observed to have sizable collective motion, then light partons, which dominate the medium, should be fully thermalized. The charm quark flow can be measured through open [17] and closed charm particles. The J/ψ is the most prominent for experiment among the latter. However, because the J/ψ production mechanism is not well understood, there is significant uncertainty associated with this probe, since only J/ψ particles from recombination of charm quarks inherit their flow. A detailed comparison between experimental measurements and models on J/ψ v_2 vs transverse momentum (p_T) and centrality, in addition to nuclear modification factor, will shed light on the J/ψ production mechanism and charm quark flow.

This analysis benefits from a large amount of data taken during the RHIC [18] $\sqrt{s_{NN}} = 200$ GeV Au + Au run in the year 2010 by the new data acquisition system of STAR [19], capable of an event rate up to 1 kHz. In addition, the newly installed time of flight (TOF) detector [20] allows STAR to improve electron identification, and background electrons from photon conversion are reduced by one order of magnitude due to less material around the center of the detector setup. The data presented consist of 360 million minimum bias (MB) events triggered by the coincidence of two vertex position detectors [21], 270 million central events triggered by a large hit multiplicity in the TOF detector [20], and a set of high tower events triggered by signals in the towers of the barrel electromagnetic calorimeter (BEMC) [22] exceeding certain thresholds (2.6, 3.5, 4.2, and 5.9 GeV). The high tower sample is equivalent to approximately 7 billion MB events for J/ψ production in the high-p_T region. In addition, in order to cope with the large data volume coming from collisions at high luminosity, a high level trigger (HLT) was implemented to reconstruct charged tracks online, select events with J/ψ candidates and tag them for fast analysis. There are 16 million J/ψ enriched events selected by the HLT.

The J/ψ particles were reconstructed through the $J/\psi \to e^+e^-$ channel, which has a branching ratio of 5.9%. The daughter tracks of the J/ψ particles were required to have more than 20 hits in the time projection chamber (TPC) [23], and a distance of closest approach less than 1 cm from the primary vertex. Low-momentum electrons and positrons can be separated from hadrons by selecting on the inverse velocity ($0.97 < 1/\beta < 1.03$), which is calculated from the time of flight measured by the TOF detector [20] and the path length measured by the TPC. At large momentum ($p > 1.5$ GeV/c), with the energy measured by towers from the BEMC [22], a cut of the momentum to energy ratio ($0.3 < p/E < 1.5$) was applied to select electrons and positrons. The electrons and

Article reprint

PRL 111, 052301 (2013) PHYSICAL REVIEW LETTERS week ending 2 AUGUST 2013

TABLE I. Event plane resolution (R) for different centralities.

Centrality (%)	0–10	10–20	20–30	30–40	40–50	50–60	60–70	70–80
R	0.600	0.748	0.805	0.787	0.719	0.608	0.478	0.364

positrons were then identified by their specific energy loss ($\langle dE/dx\rangle$) inside the TPC. More than 15 TPC hits were required to calculate $\langle dE/dx\rangle$. The $\langle dE/dx\rangle$ cut is asymmetric around the expected value for electrons, because the lower side is where the hadron $\langle dE/dx\rangle$ lies. It also varies according to whether the candidate track passes the $1/\beta$ and/or p/E cut to optimize efficiency and purity. The combination of cuts on $1/\beta$, p/E, and $\langle dE/dx\rangle$ enables electron and positron identification in a wide momentum range. Our measured J/ψ particles cover the rapidity range $-1 < y < 1$, favoring J/ψ particles near $y = 0$ because of detection efficiency variation due to acceptance and decay kinematics. A total of just over 13 000 J/ψ particles were reconstructed in the entire p_T range of 0–10 GeV/c.

The following method has been used to calculate the v_2 of the J/ψ. First, measurements of ϕ-Ψ, ranging from 0 to π, were divided into 10 bins. Here ϕ is the azimuthal angle of the J/ψ candidate, and Ψ is the azimuthal angle of the event plane reconstructed from TPC tracks with the azimuthally nonuniform detector efficiency corrected for [24]. The event plane resolution [24] (R) is different for different centrality ranges, as listed in Table I. Then two bins at supplementary angles were combined into one. For example, the bin at 0–0.1π is combined with 0.9π–π, and the invariant mass distribution of electron and positron pairs in this combined ϕ-Ψ bin is shown in the top of Fig. 1. To avoid bias from different event plane resolution for different centrality, entries in the histogram were weighted by $1/R$ accordingly [25]. The weighted J/ψ yield within this combined ϕ-Ψ bin was obtained by fitting the e^+e^- invariant mass distribution with a Crystal Ball function [26] signal on top of a second order polynomial background, as shown in the plot. The Crystal Ball function connects a Gaussian core with a power-law tail at low mass to account for daughter energy loss fluctuations and J/ψ radiative decays. Then v_2 was obtained by fitting the weighted J/ψ yield vs ϕ-Ψ with a functional form of $A[1+2v_2\cos\{2(\phi\text{-}\Psi)\}]$, as shown in the bottom of Fig. 1. Finally, the observed v_2 was scaled by $\langle 1/R\rangle$ to obtain the true v_2 [25].

Three dominant sources of systematic error have been investigated for this measurement: assumptions in the v_2 calculation method, hadron contamination for the daughter e^+e^- pairs, and the nonflow effect. The first source can be estimated from the difference in v_2 calculated by methods with different assumptions. Two other methods are used here. One is similar to the original method, except that the J/ψ yield in each combined ϕ-Ψ bin was not obtained from fitting, but from subtracting the like-sign background from unlike-sign distribution within the

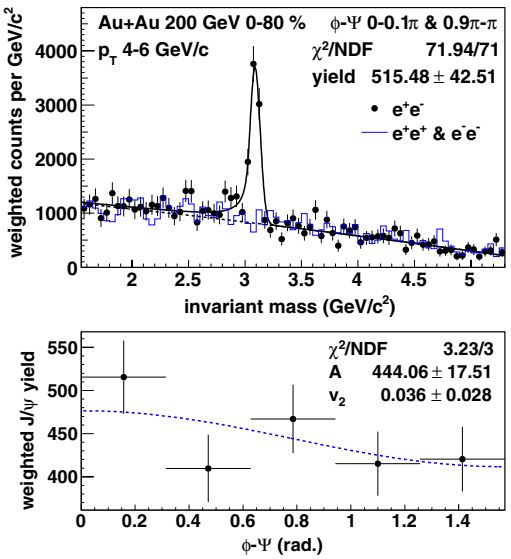

FIG. 1 (color online). Top: $1/R$ weighted invariant mass spectrum of electron and positron pairs for ϕ-Ψ in 0–0.1π and 0.9π–π, $4 < p_T < 6$ GeV/c, in 0%–80% central collisions. The points are unlike-sign pairs with the J/ψ signal, fitted by a Crystal Ball plus second order polynomial function. The polynomial background component of the fit is shown by the dashed line. The solid line histogram shows the like-sign background. Bottom: $1/R$ weighted J/ψ yield vs ϕ-Ψ with fitted v_2.

possible invariant mass range of the J/ψ (2.9–3.3 GeV/c^2). In the other method, the overall v_2 of both signal and background was measured first as a function of invariant mass, and then it was fitted with an average of J/ψ v_2 and background v_2 weighted by their respective yields vs invariant mass [27]. The systematic error from hadron contamination can be estimated from the difference in calculated v_2 with different electron (positron) identification cuts. While the original cuts aim for the best J/ψ significance, a purer electron (positron) sample can be obtained from a set of tighter cuts. The overall systematic uncertainty for the first two sources was estimated from the maximum difference between the calculated v_2 with the $3 \times 2 = 6$ combinations of v_2 methods and electron (positron) identification cut sets mentioned above. Besides elliptic flow, there are also some other two- and many-particle correlations due to, for example, resonance decay and jet production. When v_2 of a particle is measured, other particles having nonflow correlations with the measured particle are more likely to be azimuthally nearby, drawing the reconstructed event plane closer to the measured particle, and make the measured v_2 larger than its real value. To estimate this nonflow influence on the v_2 measurement, a method of scaling nonflow in $p + p$ collisions to that in Au + Au collisions [28] was employed. This method assumes that 1) J/ψ-hadron correlation in

Article reprint
PRL 111, 052301 (2013) PHYSICAL REVIEW LETTERS week ending 2 AUGUST 2013

$p + p$ collisions is entirely due to nonflow, and 2) the nonflow correlation to other particles per J/ψ in Au + Au collisions is similar to that in $p + p$ collisions. Under these assumptions, it can be deduced that the nonflow influence on measured J/ψ v_2 in Au + Au collisions is $\langle \sum_i \cos 2(\phi_{J/\psi} - \phi_i) \rangle / M \overline{v_2}$. Here, the sum is over all measured charged hadrons and the average is over J/ψ particles in $p + p$ collisions. M and $\overline{v_2}$ are the multiplicity and average elliptic flow of charged hadrons in Au + Au collisions, respectively. Since the away side correlation may be greatly modified by the medium in heavy-ion collisions, this procedure gives an upper limit of the nonflow effect. Detector acceptance and efficiency variation with p_T, centrality, and rapidity may lead to a biased J/ψ sample, which may induce some systematic effects when v_2 also changes with these parameters. But these effects are estimated to be negligible compared to statistical errors.

Figure 2 shows J/ψ v_2 as a function of transverse momentum for different centralities. Due to the nonflow effect, the real v_2 can be lower than the measured value shown in the plot. The boxes indicate the maximum magnitude of the nonflow influence. Data from the central trigger, minimum bias trigger and high tower triggers are used for the 0%–10% most central bin, while only minimum bias and high tower triggered events are used for other centrality bins. Considering errors and the magnitude of nonflow, J/ψ v_2 is consistent with 0 for $p_T > 2$ GeV/c for all measured centrality bins. Light particles usually have a larger v_2 in the intermediate centrality than in the most central and peripheral collisions. This can be explained by a larger initial spatial eccentricity in the intermediate centrality, which is transferred into final state momentum anisotropy due to different pressure gradients in different directions, when there are sufficient interactions in the medium. However, no strong centrality dependence for J/ψ v_2 has been observed with the statistical significance of the data.

The top panel of Fig. 3 shows J/ψ v_2 for 0%–80% central collisions as a function of transverse momentum. For reference, two other sets of v_2 measurements are also plotted, one is for charged hadrons (dominated by pions) [29] and the other is for the ϕ meson [30] which is heavier than the pion but not as heavy as the J/ψ. Unlike v_2 of hadrons consisting of light quarks, J/ψ v_2 at $p_T > 2$ GeV/c is found to be consistent with zero within statistical errors. However, the significant mass difference between the J/ψ and light particles makes the direct comparison of v_2 vs p_T less conclusive. For example, for the same velocity at $y = 0$, the p_T of J/ψ particles at 3.0 GeV/c corresponds to p_T of pions (ϕ) at 0.14 (1.0) GeV/c. Thus, comparisons between the experimental result and theoretical calculations are needed.

In the bottom panel of Fig. 3, a comparison is made between the measured J/ψ v_2 and various theoretical calculations, and a quantitative level of difference is shown in Table II by χ^2/NDF and the p value. v_2 of J/ψ particles produced by initial pQCD processes is predicted to stay

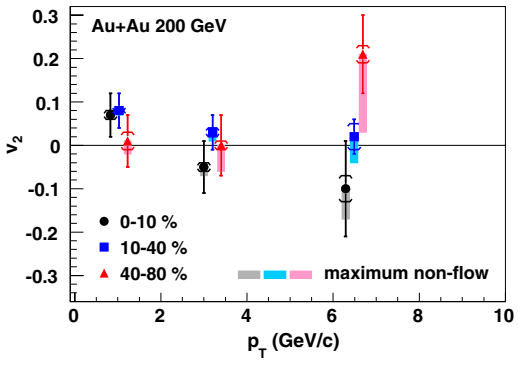

FIG. 2 (color online). v_2 vs p_T for J/ψ particles in different centrality bins. The brackets represent systematic errors estimated from differences between different methods and cuts. The boxes show the estimated maximum possible range of v_2 if the nonflow influence is corrected (see text). The p_T bins for J/ψ particles are 0–2, 2–5, and 5–10 GeV/c. The mean p_T in each bin for the J/ψ sample used for v_2 calculation is drawn, but is shifted a little for some centralities so that all points can be seen clearly.

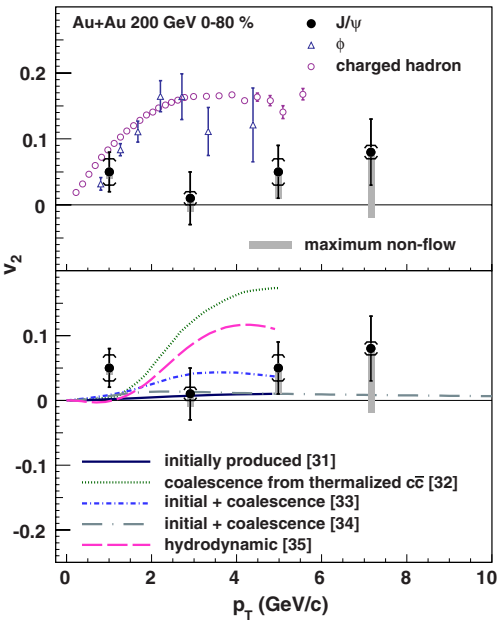

FIG. 3 (color online). v_2 vs p_T for J/ψ particles in 0%–80% central events comparing with charged hadrons [29] and the ϕ meson [30] (upper panel) and theoretical calculations [31–35] (lower panel). The brackets represent systematic errors estimated from differences between different methods and cuts. The boxes show the estimated maximum possible range of v_2 if the nonflow influence is corrected. The p_T bins for J/ψ particles are 0–2, 2–4, 4–6, and 6–10 GeV/c, and the mean p_T in each bin for the J/ψ sample used for v_2 calculation is drawn.

Article reprint

PRL 111, 052301 (2013) PHYSICAL REVIEW LETTERS week ending 2 AUGUST 2013

TABLE II. Difference between model calculations and data (where NDF stands for the number of degrees of freedom). The p value is the probability of observing a χ^2 that exceeds the current measured χ^2 by chance, even for a correct model. The estimated upper limit of nonflow effect is not included in this calculation.

Theoretical calculation	χ^2/NDF	p value
Initially produced [31]	2.6/3	4.6×10^{-1}
Coalescence from thermalized $c\bar{c}$ [32]	16.2/3	1.0×10^{-3}
Initial + coalescence [33]	2.0/3	5.8×10^{-1}
Initial + coalescence [34]	4.2/4	3.8×10^{-1}
Hydrodynamic [35]	7.0/3	7.2×10^{-2}

close to zero [31]. Although anomalous suppression in the hot medium due to color screening are considered in the model, the azimuthally different suppression along the different path lengths in azimuth leads to a limited v_2 beyond the sensitivity of the current measurement. On the contrary, if charm quarks get fully thermalized and J/ψ particles are produced by coalescence from the thermalized flowing charm quarks at the freeze-out, the v_2 of the J/ψ is predicted to reach almost the same maximum magnitude as v_2 of light flavor mesons, although at a larger p_T (around 4 GeV/c) due to the significantly larger mass of the J/ψ [32]. This is nearly 3σ above the measurement for $p_T >$ 2 GeV/c, leading to a large χ^2/NDF of 16.2/3 and a small p value of 1.0×10^{-3}, and is, thus, inconsistent with the data. Models that include J/ψ particles from both initial production and coalescence production in the transport model [31,36] predict a much smaller v_2 [33,34], and are consistent with our measurement. In these models, J/ψ particles are formed continuously through the system evolution rather than at the freeze-out, so many J/ψ particles could be formed from charm quarks whose v_2 has still not fully developed. Furthermore, the initial production of J/ψ particles with very limited v_2 dominates at high p_T, thus, the overall J/ψ v_2 does not rise rapidly as for light hadrons. This kind of model also describes the measured J/ψ nuclear modification factor over a wide range of p_T and centrality [5]. The hydrodynamic model, which assumes local thermal equilibrium, can be tuned to describe v_2 for light hadrons, but it predicts a J/ψ v_2 that rises strongly with p_T in the region $p_T < 4$ GeV/c, and thus, fails to describe the main feature of the data [35]. For heavy particles such as the J/ψ, hydrodynamic predictions suffer from large uncertainties related to viscous corrections (δf) at freeze-out and the assumed freeze-out time or temperature.

In summary, J/ψ elliptic flow is presented as a function of transverse momentum for different centralities in $\sqrt{s_{NN}} = 200$ GeV Au + Au collisions. Unlike light flavor hadrons, J/ψ v_2 at $p_T > 2$ GeV/c is consistent with zero within statistical errors. Comparing to model calculations, the measured J/ψ v_2 values disfavor the scenario that J/ψ particles with $p_T > 2$ GeV/c are produced dominantly by coalescence from (anti-)charm quarks which are thermalized and flow with the medium.

We thank the RHIC Operations Group and RCF at BNL, the NERSC Center at LBNL and the Open Science Grid consortium for providing resources and support. This work was supported in part by the Offices of NP and HEP within the U.S. DOE Office of Science, the U.S. NSF, the Sloan Foundation; CNRS/IN2P3, FAPESP CNPq of Brazil; Ministry of Education and Science of the Russian Federation; NNSFC, CAS, MoST, and MoE of China; GA and MSMT of the Czech Republic; FOM and NWO of the Netherlands; DAE, DST, and CSIR of India; Polish Ministry of Science and Higher Education; National Research Foundation (NRF-2012004024), Ministry of Science, Education, and Sports of the Republic of Croatia; and RosAtom of Russia.

[1] T. Matsui and H. Satz, Phys. Lett. B **178**, 416 (1986).
[2] M. C. Abreu *et al.*, Phys. Lett. B **499**, 85 (2001).
[3] A. Adare *et al.*, Phys. Rev. Lett. **98**, 232301 (2007).
[4] A. Adare *et al.*, Phys. Rev. C **77**, 024912 (2008).
[5] L. Adamczyk *et al.*, Phys. Lett. B **722**, 55 (2013).
[6] B. Abelev *et al.*, Phys. Rev. Lett. **109**, 072301 (2012).
[7] M. B. Johnson *et al.*, Phys. Rev. Lett. **86**, 4483 (2001).
[8] V. Guzey, M. Strikman, and W. Vogelsang, Phys. Lett. B **603**, 173 (2004).
[9] R. Baier, D. Schiff, and B. G. Zakharov, Annu. Rev. Nucl. Part. Sci. **50**, 37 (2000).
[10] S. Gavin and R. Vogt, Nucl. Phys. **A610**, 442 (1996).
[11] R. L. Thews, Eur. Phys. J. C **43**, 97 (2005).
[12] R. L. Thews and M. L. Mangano, Phys. Rev. C **73**, 014904 (2006).
[13] A. Andronic, P. Braun-Munzinger, K. Redlich, and J. Stachel, Nucl. Phys. **A789**, 334 (2007).
[14] A. Capella, L. Bravina, E. G. Ferreiro, A. B. Kaidalov, K. Tywoniuk, and E. Zabrodin, Eur. Phys. J. C **58**, 437 (2008).
[15] P. F. Kolb and U. W. Heinz, in *Quark Gluon Plasma*, edited by R. C. Hwa and X. N. Wang (World Scientific, Singapore, 2003), pp. 634–714.
[16] P. Huovinen and P. V. Ruuskanen, Annu. Rev. Nucl. Part. Sci. **56**, 163 (2006).
[17] S. S. Adler *et al.*, Phys. Rev. C **72**, 024901 (2005).
[18] H. Hahn *et al.*, Nucl. Instrum. Methods Phys. Res., Sect. A **499**, 245 (2003).
[19] K. H. Ackermann *et al.*, Nucl. Instrum. Methods Phys. Res., Sect. A **499**, 624 (2003).
[20] B. Bonner, H. Chen, G. Eppley, F. Geurts, J. Lamas-Valverde, Ch. Li, W. J. Llope, T. Nussbaum, E. Platner, and J. Roberts, Nucl. Instrum. Methods Phys. Res., Sect. A **508**, 181 (2003).
[21] W. J. Llope *et al.*, Nucl. Instrum. Methods Phys. Res., Sect. A **522**, 252 (2004).
[22] M. Beddo *et al.*, Nucl. Instrum. Methods Phys. Res., Sect. A **499**, 725 (2003).

Article reprint

PRL **111,** 052301 (2013) PHYSICAL REVIEW LETTERS week ending 2 AUGUST 2013

[23] M. Anderson *et al.*, Nucl. Instrum. Methods Phys. Res., Sect. A **499**, 659 (2003).
[24] A. M. Poskanzer and S. A. Voloshin, Phys. Rev. C **58**, 1671 (1998).
[25] H. Masui and A. Schmah, arXiv:1212.3650.
[26] J. Gaiser, Ph.D. thesis, Standford University, appendix F [Report No. SLAC-R-255, 1982 (unpublished)].
[27] N. Borghini and J. Y. Ollitrault, Phys. Rev. C **70**, 064905 (2004).
[28] J. Adams *et al.*, Phys. Rev. Lett. **93**, 252301 (2004).
[29] J. Adams *et al.*, Phys. Rev. Lett. **92**, 062301 (2004).
[30] B. I. Abelev *et al.*, Phys. Rev. Lett. **99**, 112301 (2007).
[31] L. Yan, P. Zhuang, and N. Xu, Phys. Rev. Lett. **97**, 232301 (2006).
[32] V. Greco, C. M. Ko, and R. Rapp, Phys. Lett. B **595**, 202 (2004).
[33] X. Zhao and R. Rapp, arXiv:0806.1239.
[34] Y. Liu, N. Xu, and P. Zhuang, Nucl. Phys. **A834**, 317c (2010).
[35] U. W. Heinz and C. Shen, (private communication).
[36] L. Ravagli and R. Rapp, Phys. Lett. B **655**, 126 (2007).

Kapitola 6

Diskusia a záver

Táto habilitačná práca zhrňuje výber fyzikálnej problematiky, ktorou sa autor profesne zaoberal v rámci svojej činnosti na experimente STAR v BNL v rokoch 2004 až 2017. Hlavnou motiváciou a hybnou silou tejto činnosti je experimentálne zmerať a interpretovať produkciu častíc obsahujúcich ťažké kvarky v studenej a horúcej jadrovej hmote. Podarilo sa preukázať pomocou meraní nefotónových elektrónov z D a B mezónov a priamym meraním pôvabných mezónov v p+p zrážkach, že produkciu ťažkých kvarkov je možné popísať pomocou výpočtov poruchovej kvantovej chromodynamiky. Ďalej sa podarilo ukázať, že produkcia pôvabných kvarkov v centrálnych jadro-jadrových zrážkach je potlačená podobne ako produkcia ľahkých kvarkov. Z dôvodu efektu mŕtveho kužela sa očakávalo, že oba ťažké kvarky budú potlačené menej ako ľahké, avšak v poslednej dobe fenomenologické modely ukazujú, že menšie potlačenie je len u krásnych (b) kvarkov. Podobná závislosť sa ukazuje aj z meraní na experimentoch ALICE a CMS na LHC. Na experimentoch na urýchľovači RHIC sme zatiaľ jednoznačne neukázali, aké je potlačenie u krásnych kvarkov. V súčasnosti sa venujeme hlavne analýze údajov zo zrážok p+Au a d+Au, aby sme pre pôvabné mezóny experimentálne stanovili efekty studenej jadrovej hmoty. Taktiež finalizujeme analýzu pôvabných mezónov z celkového súboru dát z rokov 2014 a 2016, aby sme previedli doposiaľ ich najpresnejšie meranie jadrového modifikačného faktora a eliptického toku za účelom stanoviť difúzny transportný koeficient pôvabného kvarku pre energie na RHIC. Potlačenie krásnych kvarkov študujeme pomocou elektrónov zo semileptónového rozpadu B. Získané výsledky umožnia v najbližších rokoch zavŕšiť tento fyzikálny program.

Pri meraní produkcie J/ψ v p+p sme významne rozšírili experimentálne údaje určením polarizačného parametru. Podstatne podrobnejšie meranie sme previedli aj v zrážkach pri enegii 500 GeV, predbežné výsledky sú zhodné s meraniami pri energii 200 GeV. Aj pri meraní parametru eliptického kolektívneho toku sme previedli dve merania. Jedno publikované pre Au+Au ukazuje, že tento parameter má nulovú hodnotu. To znamená, že J/ψ je doposiaľ jediný meraný hadrón, ktorý netečie. Avšak aj predbežné výsledky zo zrážok U+U pri podobnej energii ukazujú, že aj v tomto zrážkovom systéme je hodnota parametru v_2 nulová. Z dôvodu farebného tienenia

dikvarkového väzbového potenciálu, je produkcia viazaného stavu J/ψ potlačená v centrálnych Au+Au zrážkach pri energii 200 GeV. Podobné potlačenie sme pozorovali aj pri nižších energiách, avšak z dôvodu relatívne väčšieho vplyvu efektov studenej jadrovej hmoty. V tejto chvíli nemáme k dispozícii potrebné experimentálne údaje zo zrážok p+Au pri nižších energiách, aby sme tieto efekty studenej hmoty mohli experimentálne overiť.

Autor vybudoval na FJFI ČVUT experimentálnu skupinu experimentu STAR, ktorá sa nad rámec prezentovanej problematiky zaoberá tiež výskumom mezónu Υ, viazaného stavu $b\bar{b}$, korelačnou femtoskopiou a tiež vývojom a aplikáciou nových analyzačných metód pre spracovanie experimentálnych údajov. Podielali sme sa na príprave simulácií a návrhu detektora HFT, na jeho testovaní a príprave softvéru pre simuláciu jeho odozvy. Práve tento detektor výrazne posunul experimentálne možnosti experimentu STAR vo výzkume ťažkých kvarkov. Autor sa tiež čiastočne podieľa na experimente ALICE, kde prispel ku skúmaniu produkcie výtryskov častíc v protón-protónových zrážkach a štúdiom výtryskov obsahujúcich ťažký kvark. Experimentálne dáta z LHC, ktoré sa očakávajú z meraní po plánovanej odstávke v roku 2019, vďaka novému dráhovému detektoru v experimente ALICE umožnia podrobné štúdium výtryskov obsahujúcich ťažký kvark.

Experimentálny program kolaborácie STAR je naplánovaný minimálne až do roku 2022. Po publikovaní výsledkov, ktoré získame ešte analýzou signálov spojených s ťažkými kvarkami z dát z rokov 2014 až 2016 pomocou nových metód strojového učenia a pomocou tzv. KFParticle metódy, sa zameriame na hľadanie hraničných prejavov existencie QGP a kritického bodu fázového diagramu jadrovej hmoty. V rokoch 2019 a 2020 experiment STAR prevedie niekoľko dedikovaných meraní pri nižších energiách zameraných práve na hľadanie kritického bodu. V súvislosti s prípravou nového urýchľovača EIC (Electron-Ion Collider), ktorý bude zrážať elektróny s jadrami, zahájime v blízkej budúcnosti prípravu analýz zameraných na hlbšie pochopenie gluónovej a kvarkovej štruktúry protónu.

Slovník

Z dôvodu, že v slovenskom jazyku nie sú ustálené všetky odborné termíny použité v tejto práci, uvádzam v tejto kapitole niektoré použité odborné slová spolu s ich anglickým ekvivalentom.

slovensky	**anglicky**
centralita	centrality
dopredná rapidita	forward rapidity
dozadná rapidita	backward rapidity
farebné uväznenie	color confinement
fotónový elektrón	photonic electron
krásny kvark	beauty quark
kvarkovo-gluónová plazma	quark-gluon plasma
najmenšie zaujatie	minimum bias
nefotónový elektrón	non-photonic electron
početnosť	multiplicity
pôvabný kvark	charm quark
rovina zrážky	reaction plane
semileptónový	semileptonic
spúšťač	trigger
spúšťací systém	trigger system
stredná rapidita	midrapidity
účastník	participant
údaje, dáta	data
udalosť	event
vôňa kvarku	quark flavor
vrchol	vertex
vymrznutie	freeze-out
výtrysk	jet
tok	flow
zarovnanie spinu	spin alignment
zhášanie výtryskov častíc	jet quenching
zrážkový parameter	impact parameter

Zoznam autorových publikácií, vedených prác a citovanej literatúry

Zoznam autorových publikácií k 2.3. 2018:

[1] J. Mrazek *et al.*, Acta Phys. Pol. B **29**, 433 (1998).
[2] A. Lindroth *et al.*, Phys. Rev. Lett **82**, 4783 (1999).
[3] J. Mrazek *et al.*, Eur. Phys. J. A **5**, 399 (1999).
[4] J. Mrazek *et al.*, Czech. J. Phys. **50**, 331 (2000).
[5] J. Adams *et al.* [STAR Collaboration], Phys. Lett. B **616**, 8 (2005).
[6] A. Kugler *et al.*, Acta Phys. Slov. **54**, 375 (2004).
[7] C. Muntz *et al.* [HADES-MDC Collaboration], Nucl. Instrum. Meth. A **535**, 242 (2004).
[8] P. Salabura *et al.* [HADES Collaboration], Acta Phys. Polon. B **35**, 1119 (2004).
[9] A. Kugler *et al.* [HADES Collaboration], Nucl. Phys. A **734**, 78 (2004).
[10] P. Salabura *et al.* [HADES Collaboration], Prog. Part. Nucl. Phys. **53**, 49 (2004).
[11] J. Adams *et al.* [STAR Collaboration], Phys. Rev. C **72**, 014904 (2005).
[12] J. Adams *et al.* [STAR Collaboration], Phys. Rev. C **73**, 064907 (2006).
[13] J. Adams *et al.* [STAR Collaboration], Nucl. Phys. A **757**, 102 (2005).
[14] J. Adams *et al.* [STAR Collaboration], Phys. Rev. Lett. **95**, 062301 (2005).
[15] P. Salabura *et al.* [HADES Collaboration], Nucl. Phys. A **749**, 150 (2005).
[16] J. Adams *et al.* [STAR Collaboration], Phys. Rev. Lett. **95**, 122301 (2005).
[17] J. Bielcik *et al.*, J. Phys. G **31**, S231 (2005).
[18] J. Adams *et al.* [STAR Collaboration], Phys. Rev. C **72**, 044902 (2005).
[19] J. Otwinowski *et al.* [HADES Collaboration], Int. J. Mod. Phys. A **20**, 602 (2005).
[20] T. Eberl *et al.*, Nucl. Phys. A **752**, 433 (2005).
[21] J. Adams *et al.* [STAR Collaboration], J. Phys. G **32**, L37 (2006)
[22] J. Adams *et al.* [STAR Collaboration], Phys. Rev. C **73**, 034903 (2006).
[23] J. Adams *et al.* [STAR Collaboration], Phys. Rev. C **74**, 064906 (2006).
[24] J. Bielcik [STAR Collaboration], Nucl. Phys. A **774**, 697 (2006).
[25] J. Adams *et al.* [STAR Collaboration], Phys. Rev. C **73**, 034906 (2006).
[26] B. I. Abelev *et al.* [STAR Collaboration], Phys. Rev. C **76**, 011901 (2007).
[27] M. Calderon de la Barca Sanchez *et al.* [STAR Collaboration], Eur. Phys. J. C **43**, 187 (2005).

[28] A. A. P. Suaide *et al.* [STAR Collaboration], Eur. Phys. J. C **43**, 193 (2005).
[29] C. A. Gagliardi *et al.* [STAR Collaboration], Eur. Phys. J. C **43**, 263 (2005).
[30] J. Adams *et al.* [STAR Collaboration], Phys. Lett. B **637**, 161 (2006).
[31] J. Adams *et al.* [STAR Collaboration], Phys. Rev. Lett. **97**, 152302 (2006).
[32] W. Przygoda *et al.* [HADES Collaboration], Acta Phys. Polon. B **37**, 139 (2006).
[33] J. Adams *et al.* [STAR Collaboration], Phys. Rev. Lett. **97**, 162301 (2006).?
[34] B. I. Abelev *et al.* [STAR Collaboration], Phys. Rev. Lett. **97**, 132301 (2006).
[35] J. Adams *et al.* [STAR Collaboration], J. Phys. G **34**, 451 (2007).
[36] B. I. Abelev *et al.* [STAR Collaboration], Phys. Rev. Lett. **97**, 152301 (2006).
[37] J. Bielcik [STAR Collaboration], Proceedings, 41st Rencontres de Moriond, 2006 QCD and High Energy Hadronic Interactions : La Thuile, Val d'Aoste, Italy, Mar 18-25, p.249 (2006).
[38] J. Adams *et al.* [STAR Collaboration], Phys. Rev. Lett. **98**, 062301 (2007).
[39] J. Adams *et al.* [STAR Collaboration], Phys. Rev. D **74**, 032006 (2006).
[40] J. Adams *et al.* [STAR Collaboration], Phys. Rev. C **75**, 034901 (2007).
[41] B. I. Abelev *et al.* [STAR Collaboration], Phys. Rev. Lett. **98**, 192301 (2007) Erratum: [Phys. Rev. Lett. **106**, 159902 (2011)]
[42] B. I. Abelev *et al.* [STAR Collaboration], Phys. Rev. C **75**, 064901 (2007).
[43] B. I. Abelev *et al.* [STAR Collaboration], Phys. Rev. C **74**, 054902 (2006).
[44] B. I. Abelev *et al.* [STAR Collaboration], Phys. Rev. Lett. **97**, 252001 (2006).
[45] G. Agakichiev *et al.* [HADES Collaboration], Phys. Rev. Lett. **98**, 052302 (2007).
[46] B. I. Abelev *et al.* [STAR Collaboration], Phys. Rev. C **76**, 054903 (2007).
[47] B. I. Abelev *et al.* [STAR Collaboration], Phys. Rev. C **75**, 054906 (2007).
[48] B. I. Abelev *et al.* [STAR Collaboration], Phys. Rev. Lett. **99**, 112301 (2007).
[49] B. I. Abelev *et al.* [STAR Collaboration], Phys. Lett. B **655**, 104 (2007).
[50] J. Bielcik [STAR Collaboration], Nucl. Phys. A **783**, 539 (2007).
[51] B. I. Abelev *et al.* [STAR Collaboration], Phys. Rev. C **76**, 024915 (2007).
[52] B. I. Abelev *et al.* [STAR Collaboration], Phys. Rev. C **77**, 044908 (2008).
[53] J. Bielcik, Eur. Phys. J. C **49**, 375 (2007).
[54] B. I. Abelev *et al.* [STAR Collaboration], Phys. Rev. Lett. **99**, 142003 (2007).
[55] B. I. Abelev *et al.* [STAR Collaboration], Phys. Rev. C **76**, 064904 (2007).
[56] B. I. Abelev *et al.* [STAR Collaboration], Phys. Rev. Lett. **100**, 232003 (2008).
[57] B. I. Abelev *et al.* [STAR Collaboration], Phys. Rev. C **77**, 034910 (2008).
[58] A. Kugler *et al.* [HADES Collaboration], AIP Conf. Proc. **947**, 436 (2007).
[59] B. I. Abelev *et al.* [STAR Collaboration], Phys. Rev. C **78**, 044906 (2008).
[60] B. I. Abelev *et al.* [STAR Collaboration], Phys. Rev. C **77**, 061902 (2008).
[61] B. I. Abelev *et al.* [STAR Collaboration], Phys. Rev. Lett. **101**, 222001 (2008).
[62] B. I. Abelev *et al.* [STAR Collaboration], Phys. Rev. C **77**, 054901 (2008).
[63] B. I. Abelev *et al.* [STAR Collaboration], Phys. Rev. Lett. **102**, 052302 (2009).
[64] B. I. Abelev *et al.* [STAR Collaboration], Phys. Rev. Lett. **101**, 252301 (2008).
[65] B. I. Abelev *et al.* [STAR Collaboration], Phys. Rev. C **79**, 024906 (2009).
[66] B. I. Abelev *et al.* [STAR Collaboration], Phys. Rev. C **79**, 034909 (2009).

[67] P. Cortese *et al.* [ALICE Collaboration], CERN-LHCC-2008-014, CERN-ALICE-TDR-014.
[68] K. Aamodt *et al.* [ALICE Collaboration], JINST **3**, S08002 (2008).
[69] J. Bielcik, J. Phys. Conf. Ser. **110**, 032002 (2008).
[70] B. I. Abelev *et al.* [STAR Collaboration], Phys. Rev. C **79**, 064903 (2009).
[71] B. I. Abelev *et al.* [STAR Collaboration], Phys. Lett. B **673**, 183 (2009).
[72] J. Bielcik [STAR Collaboration], "Proceedings, 34th International Conference on High Energy Physics (ICHEP 2008) : Philadelphia, Pennsylvania, July 30-August 5, (2008)."
[73] B. I. Abelev *et al.* [STAR Collaboration], Phys. Rev. Lett. **102**, 112301 (2009).
[74] M. Sudol *et al.* [HADES Collaboration], Eur. Phys. J. C **62**, 81 (2009).
[75] B. I. Abelev *et al.* [STAR Collaboration], Phys. Rev. D **79**, 112006 (2009).
[76] B. I. Abelev *et al.* [STAR Collaboration], Phys. Rev. Lett. **103**, 092301 (2009).
[77] G. Agakishiev *et al.* [HADES Collaboration], Eur. Phys. J. A **41**, 243 (2009).
[78] G. Agakishiev *et al.* [HADES Collaboration], Eur. Phys. J. A **40**, 45 (2009).
[79] B. I. Abelev *et al.* [STAR Collaboration], Phys. Rev. C **80**, 024905 (2009).
[80] B. I. Abelev *et al.* [STAR Collaboration], Phys. Rev. C **80**, 041902 (2009).
[81] B. I. Abelev *et al.* [STAR Collaboration], Phys. Lett. B **683**, 123 (2010).
[82] B. I. Abelev *et al.* [STAR Collaboration], Phys. Rev. Lett. **103**, 172301 (2009).
[83] B. I. Abelev *et al.* [STAR Collaboration], Nucl. Phys. A **832**, 134 (2010)
[84] B. I. Abelev *et al.* [STAR Collaboration], Phys. Rev. C **80**, 044905 (2009).
[85] J. Bielcik [STAR Collaboration], "Proceedings, 17th International Workshop on Deep-Inelastic Scattering and Related Subjects (DIS 2009) : Madrid, Spain, April 26-30, 2009"
[86] B. I. Abelev *et al.* [STAR Collaboration], Phys. Rev. C **80**, 064912 (2009).
[87] B. I. Abelev *et al.* [STAR Collaboration], Phys. Rev. C **81**, 054908 (2010).
[88] B. I. Abelev *et al.* [STAR Collaboration], Phys. Rev. Lett. **103**, 251601 (2009).
[89] B. I. Abelev *et al.* [STAR Collaboration], Phys. Rev. C **81**, 024911 (2010).
[90] B. I. Abelev *et al.* [STAR Collaboration], Phys. Rev. D **80**, 111102 (2009).
[91] B. I. Abelev *et al.* [STAR Collaboration], Phys. Rev. D **80**, 111108 (2009).
[92] B. I. Abelev *et al.* [STAR Collaboration], Phys. Rev. C **81**, 054907 (2010).
[93] K. Aamodt *et al.* [ALICE Collaboration], Eur. Phys. J. C **65**, 111 (2010).
[94] B. I. Abelev *et al.* [STAR Collaboration], Phys. Rev. C **81**, 044901 (2010).
[95] B. I. Abelev *et al.* [STAR Collaboration], Phys. Rev. C **82**, 034909 (2010).
[96] B. I. Abelev *et al.* [STAR Collaboration], Phys. Rev. C **81**, 064904 (2010).
[97] B. I. Abelev *et al.* [STAR Collaboration], Phys. Rev. Lett. **105**, 022301 (2010).
[98] K. Aamodt *et al.* [ALICE Collaboration], JINST **5**, P03003 (2010).
[99] B. I. Abelev *et al.* [STAR Collaboration], Phys. Rev. D **82**, 012004 (2010).
[100] B. I. Abelev *et al.* [STAR Collaboration], Phys. Rev. C **81**, 044902 (2010).
[101] B. I. Abelev *et al.* [STAR Collaboration], Phys. Lett. B **690**, 239 (2010).
[102] B. I. Abelev *et al.* [STAR Collaboration], Science **328**, 58 (2010).
[103] M. M. Aggarwal *et al.* [STAR Collaboration], Phys. Rev. C **83**, 064905 (2011).

[104] M. M. Aggarwal *et al.* [STAR Collaboration], Phys. Rev. C **82**, 024912 (2010).
[105] K. Aamodt *et al.* [ALICE Collaboration], Eur. Phys. J. C **68**, 345 (2010).
[106] K. Aamodt *et al.* [ALICE Collaboration], Eur. Phys. J. C **68**, 89 (2010).
[107] M. M. Aggarwal *et al.* [STAR Collaboration], Phys. Rev. Lett. **105**, 022302 (2010).
[108] M. M. Aggarwal *et al.* [STAR Collaboration], Phys. Rev. C **82**, 024905 (2010).
[109] M. M. Aggarwal *et al.* [STAR Collaboration], Phys. Rev. C **84**, 034909 (2011).
[110] K. Aamodt *et al.* [ALICE Collaboration], Phys. Rev. Lett. **105**, 072002 (2010).
[111] K. Aamodt *et al.* [ALICE Collaboration], Phys. Rev. D **82**, 052001 (2010).
[112] M. M. Aggarwal *et al.* [STAR Collaboration], Phys. Rev. Lett. **105**, 202301 (2010).
[113] M. M. Aggarwal *et al.* [STAR Collaboration], Phys. Rev. C **83**, 034910 (2011).
[114] M. M. Aggarwal *et al.* [STAR Collaboration], Phys. Rev. Lett. **106**, 062002 (2011).
[115] M. M. Aggarwal *et al.* [STAR Collaboration], Phys. Rev. C **83**, 024901 (2011).
[116] K. Aamodt *et al.* [ALICE Collaboration], Phys. Rev. Lett. **105**, 252301 (2010).
[117] K. Aamodt *et al.* [ALICE Collaboration], Phys. Rev. Lett. **105**, 252302 (2010).
[118] K. Aamodt *et al.* [ALICE Collaboration], Phys. Lett. B **696**, 30 (2011).
[119] K. Aamodt *et al.* [ALICE Collaboration], Phys. Rev. Lett. **106**, 032301 (2011).
[120] K. Aamodt *et al.* [ALICE Collaboration], Eur. Phys. J. C **71**, 1594 (2011).
[121] K. Aamodt *et al.* [ALICE Collaboration], Phys. Lett. B **696**, 328 (2011).
[122] J. Bielcik, Acta Phys. Polon. Supp. **3**, 1003 (2010).
[123] K. Aamodt *et al.* [ALICE Collaboration], Phys. Rev. D **84**, 112004 (2011).
[124] K. Aamodt *et al.* [ALICE Collaboration], Eur. Phys. J. C **71**, 1655 (2011).
[125] H. Agakishiev *et al.* [STAR Collaboration], Phys. Rev. C **83**, 061901 (2011).
[126] H. Agakishiev *et al.* [STAR Collaboration], Phys. Rev. D **83**, 052006 (2011).
[127] H. Agakishiev *et al.* [STAR Collaboration], Nature **473**, 353 (2011). Erratum: [Nature **475**, 412 (2011)]
[128] K. Aamodt *et al.* [ALICE Collaboration], Phys. Lett. B **704**, 442 (2011). Erratum: [Phys. Lett. B **718**, 692 (2012).]
[129] K. Aamodt *et al.* [ALICE Collaboration], Phys. Rev. Lett. **107**, 032301 (2011).
[130] H. Agakishiev *et al.* [STAR Collaboration], Phys. Lett. B **704**, 467 (2011).
[131] G. Agakishiev *et al.* [STAR Collaboration], Phys. Rev. Lett. **108**, 072301 (2012).
[132] G. Agakishiev *et al.* [STAR Collaboration], Phys. Rev. C **85**, 014910 (2012).
[133] J. Bielcik, J. Bielcikova, V. Petracek and M. Pachr, "Jets in proton-proton and heavy-ion collisions. Proceedings, International Workshop, Prague, Czech Republic, August 12-14, 2010," Int. J. Mod. Phys. E **20** pp.1533 (2011).
[134] K. Aamodt *et al.* [ALICE Collaboration], Phys. Lett. B **708**, 249 (2012).
[135] G. Agakishiev *et al.* [STAR Collaboration], Phys. Rev. C **86**, 064902 (2012).
[136] G. Agakishiev *et al.* [STAR Collaboration], Phys. Rev. C **85**, 014901 (2012).
[137] K. Aamodt *et al.* [ALICE Collaboration], Phys. Rev. Lett. **108**, 092301 (2012).
[138] G. Agakishiev *et al.* [STAR Collaboration], Phys. Rev. Lett. **108**, 072302 (2012).

[139] G. Agakishiev *et al.* [STAR Collaboration], Phys. Rev. C **85**, 014903 (2012).
[140] B. Abelev *et al.* [ALICE Collaboration], Phys. Rev. Lett. **108**, 082001 (2012).
[141] B. Abelev *et al.* [ALICE Collaboration], JHEP **1201**, 128 (2012).
[142] G. Agakishiev *et al.* [STAR Collaboration], Phys. Rev. C **86**, 014904 (2012).
[143] B. Abelev *et al.* [ALICE Collaboration], JHEP **1207**, 116 (2012).
[144] B. Abelev *et al.* [ALICE Collaboration], Phys. Lett. B **710**, 557 (2012).
[145] L. Adamczyk *et al.* [STAR Collaboration], Phys. Rev. D **85**, 092010 (2012).
[146] L. Adamczyk *et al.* [STAR Collaboration], Phys. Rev. Lett. **108**, 202301 (2012).
[147] B. Abelev *et al.* [ALICE Collaboration], JHEP **1203**, 053 (2012).
[148] B. Abelev *et al.* [ALICE Collaboration], Phys. Lett. B **708**, 265 (2012).
[149] B. Abelev *et al.* [ALICE Collaboration], Phys. Rev. Lett. **109**, 072301 (2012).
[150] B. Abelev *et al.* [ALICE Collaboration], Phys. Lett. B **712**, 165 (2012).
[151] B. Abelev *et al.* [ALICE Collaboration], JHEP **1209**, 112 (2012).
[152] B. Abelev *et al.* [ALICE Collaboration], Phys. Rev. Lett. **109**, 252302 (2012).
[153] B. Abelev *et al.* [ALICE Collaboration], Phys. Lett. B **718**, 295 (2012). Erratum: [Phys. Lett. B **748**, 472 (2015)]
[154] B. Abelev *et al.* [ALICE Collaboration], Phys. Lett. B **712**, 309 (2012).
[155] L. Adamczyk *et al.* [STAR Collaboration], Phys. Rev. C **86**, 024906 (2012).
[156] L. Adamczyk *et al.* [STAR Collaboration], Phys. Rev. D **86**, 072013 (2012).
[157] L. Adamczyk *et al.* [STAR Collaboration], Phys. Rev. D **86**, 032006 (2012).
[158] B. Abelev *et al.* [ALICE Collaboration], Eur. Phys. J. C **72**, 2124 (2012).
[159] B. Abelev *et al.* [ALICE Collaboration], JHEP **1207**, 191 (2012).
[160] B. Abelev *et al.* [ALICE Collaboration], Phys. Rev. D **86**, 112007 (2012).
[161] B. Abelev *et al.* [ALICE Collaboration], Phys. Lett. B **717**, 162 (2012).
[162] B. Abelev *et al.* [ALICE Collaboration], Phys. Lett. B **719**, 18 (2013).
[163] B. Abelev *et al.* [ALICE Collaboration], JHEP **1211**, 065 (2012).
[164] B. Abelev *et al.* [ALICE Collaboration], Phys. Rev. Lett. **109**, 112301 (2012).
[165] L. Adamczyk *et al.* [STAR Collaboration], Phys. Rev. D **86**, 051101 (2012).
[166] L. Adamczyk *et al.* [STAR Collaboration], Phys. Lett. B **719**, 62 (2013).
[167] B. Abelev *et al.* [ALICE Collaboration], Phys. Lett. B **717**, 151 (2012).
[168] L. Adamczyk *et al.* [STAR Collaboration], Phys. Rev. C **86**, 054908 (2012).
[169] B. Abelev *et al.* [ALICE Collaboration], Phys. Rev. Lett. **110**, no. 1, 012301 (2013).
[170] B. Abelev *et al.* [ALICE Collaboration], Phys. Rev. Lett. **110**, no. 15, 152301 (2013).
[171] B. Abelev *et al.* [ALICE Collaboration], Phys. Lett. B **721**, 13 (2013).
[172] B. Abelev *et al.* [ALICE Collaboration], Phys. Lett. B **718**, 279 (2012).
[173] B. Abelev *et al.* [ALICE Collaboration], Phys. Rev. Lett. **109**, 252301 (2012).
[174] B. Abelev *et al.* [ALICE Collaboration], Phys. Lett. B **720**, 52 (2013).
[175] L. Adamczyk *et al.* [STAR Collaboration], Phys. Lett. B **722**, 55 (2013).
[176] B. Abelev *et al.* [ALICE Collaboration], Eur. Phys. J. C **73**, no. 6, 2456 (2013).
[177] B. Abelev *et al.* [ALICE Collaboration], Eur. Phys. J. C **72**, 2183 (2012).

[178] B. Abelev *et al.* [ALICE Collaboration], Phys. Lett. B **718**, 1273 (2013).
[179] J. Bielcik [STAR Collaboration], 'Proceedings, 21st Lake Louise Winter Institute on Fundamental Interactions : Lake Louise, Canada, February 17-23, 2006.
[180] B. Abelev *et al.* [ALICE Collaboration], Phys. Rev. Lett. **110**, no. 3, 032301 (2013).
[181] B. Abelev *et al.* [ALICE Collaboration], Phys. Rev. Lett. **110**, no. 8, 082302 (2013).
[182] L. Adamczyk *et al.* [STAR Collaboration], Phys. Rev. C **87**, no. 4, 044903 (2013).
[183] B. Abelev *et al.* [ALICE Collaboration], Phys. Lett. B **719**, 29 (2013).
[184] L. Adamczyk *et al.* [STAR Collaboration], Phys. Rev. Lett. **111**, no. 5, 052301 (2013).
[185] B. Abelev *et al.* [ALICE Collaboration], Phys. Rev. D **87**, no. 5, 052016 (2013).
[186] L. Adamczyk *et al.* [STAR Collaboration], Phys. Rev. C **88**, no. 1, 014904 (2013).
[187] L. Adamczyk *et al.* [STAR Collaboration], Phys. Rev. Lett. **110**, no. 14, 142301 (2013).
[188] L. Adamczyk *et al.* [STAR Collaboration], Phys. Rev. C **88**, 014902 (2013).
[189] B. Abelev *et al.* [ALICE Collaboration], Phys. Lett. B **722**, 262 (2013).
[190] B. Abelev *et al.* [ALICE Collaboration], Phys. Lett. B **723**, 267 (2013).
[191] B. Abelev *et al.* [ALICE Collaboration], Phys. Rev. C **88**, no. 4, 044909 (2013).
[192] L. Adamczyk *et al.* [STAR Collaboration], Phys. Rev. C **87**, no. 6, 064902 (2013).
[193] L. Adamczyk *et al.* [STAR Collaboration], Phys. Rev. C **88**, no. 3, 034906 (2013).
[194] L. Adamczyk *et al.* [STAR Collaboration], Phys. Rev. C **88**, no. 6, 064911 (2013).
[195] L. Adamczyk *et al.* [STAR Collaboration], Phys. Rev. Lett. **112**, no. 12, 122301 (2014).
[196] B. Abelev *et al.* [ALICE Collaboration], Phys. Rev. C **88**, 044910 (2013).
[197] L. Adamczyk *et al.* [STAR Collaboration], Phys. Rev. C **89**, no. 4, 044908 (2014).
[198] E. Abbas *et al.* [ALICE Collaboration], Phys. Rev. Lett. **111**, 162301 (2013).
[199] E. Abbas *et al.* [ALICE Collaboration], Phys. Lett. B **726**, 610 (2013).
[200] E. Abbas *et al.* [ALICE Collaboration], Eur. Phys. J. C **73**, no. 11, 2617 (2013).
[201] E. Abbas *et al.* [ALICE Collaboration], Eur. Phys. J. C **73**, 2496 (2013).
[202] B. Abelev *et al.* [ALICE Collaboration], Phys. Rev. Lett. **111**, 102301 (2013).
[203] E. Abbas *et al.* [ALICE Collaboration], JINST **8**, P10016 (2013).
[204] B. Abelev *et al.* [ALICE Collaboration], Phys. Rev. Lett. **111**, no. 23, 232302 (2013).
[205] B. B. Abelev *et al.* [ALICE Collaboration], Eur. Phys. J. C **73**, no. 12, 2662 (2013).
[206] B. B. Abelev *et al.* [ALICE Collaboration], Phys. Lett. B **727**, 371 (2013).
[207] B. Abelev *et al.* [ALICE Collaboration], JHEP **1309**, 049 (2013).
[208] B. B. Abelev *et al.* [ALICE Collaboration], Phys. Lett. B **726**, 164 (2013).
[209] B. B. Abelev *et al.* [ALICE Collaboration], Phys. Rev. Lett. **111**, 222301 (2013).
[210] B. B. Abelev *et al.* [ALICE Collaboration], Phys. Lett. B **728**, 216 (2014). Erratum: [Phys. Lett. B **734**, 409 (2014)]

[211] B. B. Abelev *et al.* [ALICE Collaboration], Phys. Lett. B **728**, 25 (2014).
[212] B. B. Abelev *et al.* [ALICE Collaboration], JHEP **1402**, 073 (2014).
[213] L. Adamczyk *et al.* [STAR Collaboration], Phys. Rev. D **89**, no. 1, 012001 (2014).
[214] L. Adamczyk *et al.* [STAR Collaboration], Phys. Rev. Lett. **112**, 032302 (2014).
[215] L. Adamczyk *et al.* [STAR Collaboration], Phys. Rev. C **90**, no. 2, 024906 (2014).
[216] B. B. Abelev *et al.* [ALICE Collaboration], Phys. Rev. C **89**, no. 2, 024911 (2014).
[217] B. B. Abelev *et al.* [ALICE Collaboration], Phys. Lett. B **734**, 314 (2014).
[218] B. Abelev *et al.* [ALICE Collaboration], JHEP **1403**, 013 (2014).
[219] L. Adamczyk *et al.* [STAR Collaboration], Phys. Lett. B **739**, 180 (2014).
[220] J. Bielcik [STAR Collaboration], Proceedings, 48th Rencontres de Moriond on QCD and High Energy Interactions : La Thuile, Italy, March 9-16, 2013.
[221] L. Adamczyk *et al.* [STAR Collaboration], Phys. Lett. B **735**, 127 (2014). Erratum: [Phys. Lett. B **743**, 537 (2015)]
[222] L. Adamczyk *et al.* [STAR Collaboration], Phys. Rev. Lett. **113**, no. 2, 022301 (2014). Addendum: [Phys. Rev. Lett. **113**, no. 4, 049903 (2014)]
[223] B. B. Abelev *et al.* [ALICE Collaboration], Phys. Lett. B **736**, 196 (2014).
[224] L. Adamczyk *et al.* [STAR Collaboration], Phys. Rev. Lett. **112**, no. 16, 162301 (2014).
[225] J. Bielcik [STAR Collaboration], PoS DIS **2013**, 198 (2013).
[226] L. Adamczyk *et al.* [STAR Collaboration], Phys. Rev. Lett. **113**, 092301 (2014).
[227] L. Adamczyk *et al.* [STAR Collaboration], Phys. Rev. C **90**, no. 6, 064904 (2014).
[228] B. B. Abelev *et al.* [ALICE Collaboration], Int. J. Mod. Phys. A **29**, 1430044 (2014).
[229] B. B. Abelev *et al.* [ALICE Collaboration], Eur. Phys. J. C **74**, no. 8, 2974 (2014).
[230] L. Adamczyk *et al.* [STAR Collaboration], Phys. Rev. C **92**, no. 1, 014904 (2015).
[231] B. B. Abelev *et al.* [ALICE Collaboration], Phys. Rev. C **91**, 024609 (2015).
[232] H. Agakishiev *et al.* [STAR Collaboration], Phys. Rev. C **89**, no. 4, 041901 (2014).
[233] B. B. Abelev *et al.* [ALICE Collaboration], Phys. Lett. B **739**, 139 (2014).
[234] L. Adamczyk *et al.* [STAR Collaboration], Phys. Rev. Lett. **113**, 052302 (2014).
[235] L. Adamczyk *et al.* [STAR Collaboration], Phys. Rev. Lett. **113**, no. 14, 142301 (2014).
[236] J. Bielcik, EPJ Web Conf. **70**, 00057 (2014).
[237] L. Adamczyk *et al.* [STAR Collaboration], Phys. Rev. Lett. **113**, 072301 (2014).
[238] B. B. Abelev *et al.* [ALICE Collaboration], JINST **9**, no. 11, P11003 (2014).
[239] B. B. Abelev *et al.* [ALICE Collaboration], Phys. Rev. C **90**, no. 3, 034904 (2014).
[240] B. B. Abelev *et al.* [ALICE Collaboration], Eur. Phys. J. C **74**, no. 9, 3054 (2014).
[241] B. B. Abelev *et al.* [ALICE Collaboration], Phys. Rev. Lett. **113**, no. 23, 232301 (2014).
[242] B. B. Abelev *et al.* [ALICE Collaboration], Eur. Phys. J. C **74**, no. 10, 3108 (2014).
[243] B. B. Abelev *et al.* [ALICE Collaboration], JHEP **1412**, 073 (2014).
[244] B. B. Abelev *et al.* [ALICE Collaboration], Phys. Rev. D **91**, no. 1, 012001 (2015).

[245] B. B. Abelev *et al.* [ALICE Collaboration], Phys. Lett. B **738**, 97 (2014).
[246] B. B. Abelev *et al.* [ALICE Collaboration], Phys. Lett. B **738**, 361 (2014).
[247] B. B. Abelev *et al.* [ALICE Collaboration], JHEP **1506**, 190 (2015).
[248] L. Adamczyk *et al.* [STAR Collaboration], Phys. Rev. Lett. **115**, no. 9, 092002 (2015).
[249] L. Adamczyk *et al.* [STAR Collaboration], Phys. Rev. C **95**, no. 3, 034907 (2017).
[250] B. B. Abelev *et al.* [ALICE Collaboration], Phys. Rev. C **90**, no. 5, 054901 (2014).
[251] B. B. Abelev *et al.* [ALICE Collaboration], Eur. Phys. J. C **75**, no. 1, 1 (2015).
[252] B. B. Abelev *et al.* [ALICE Collaboration], Phys. Lett. B **741**, 38 (2015).
[253] B. B. Abelev *et al.* [ALICE Collaboration], Phys. Rev. Lett. **113**, no. 23, 232504 (2014).
[254] B. Abelev *et al.* [ALICE Collaboration], J. Phys. G **41**, 087001 (2014).
[255] B. Abelev *et al.* [ALICE Collaboration], J. Phys. G **41**, 087002 (2014).
[256] B. B. Abelev *et al.* [ALICE Collaboration], Eur. Phys. J. C **74**, no. 10, 3077 (2014).
[257] L. Adamczyk *et al.* [STAR Collaboration], Phys. Rev. Lett. **114**, no. 2, 022301 (2015).
[258] L. Adamczyk *et al.* [STAR Collaboration], Phys. Rev. C **91**, no. 3, 034905 (2015).
[259] N. M. Abdelwahab *et al.* [STAR Collaboration], Phys. Lett. B **745**, 40 (2015).
[260] B. B. Abelev *et al.* [ALICE Collaboration], Phys. Lett. B **740**, 105 (2015).
[261] L. Adamczyk *et al.* [STAR Collaboration], Phys. Lett. B **751**, 233 (2015).
[262] N. M. Abdelwahab *et al.* [STAR Collaboration], Phys. Rev. C **92**, no. 2, 021901 (2015).
[263] B. B. Abelev *et al.* [ALICE Collaboration], Phys. Rev. D **91**, no. 11, 112012 (2015).
[264] B. B. Abelev *et al.* [ALICE Collaboration], Eur. Phys. J. C **75**, no. 4, 146 (2015).
[265] J. Adam *et al.* [ALICE Collaboration], Phys. Rev. C **91**, no. 6, 064905 (2015).
[266] L. Adamczyk *et al.* [STAR Collaboration], Phys. Lett. B **743**, 333 (2015).
[267] L. Adamczyk *et al.* [STAR Collaboration], Phys. Lett. B **750**, 64 (2015).
[268] J. Adam *et al.* [ALICE Collaboration], JHEP **1505**, 097 (2015).
[269] J. Adam *et al.* [ALICE Collaboration], Phys. Rev. C **91**, 034906 (2015).
[270] J. Adam *et al.* [ALICE Collaboration], Phys. Lett. B **746**, 1 (2015).
[271] L. Adamczyk *et al.* [STAR Collaboration], Phys. Lett. B **747**, 265 (2015).
[272] J. Adam *et al.* [ALICE Collaboration], Phys. Lett. B **749**, 68 (2015).
[273] J. Adam *et al.* [ALICE Collaboration], Phys. Lett. B **746**, 385 (2015).
[274] J. Adam *et al.* [ALICE Collaboration], JHEP **1506**, 055 (2015).
[275] J. Adam *et al.* [ALICE Collaboration], JHEP **1509**, 095 (2015).
[276] J. Adam *et al.* [ALICE Collaboration], Eur. Phys. J. C **75**, no. 5, 226 (2015).
[277] L. Adamczyk *et al.* [STAR Collaboration], Phys. Rev. Lett. **115**, 242501 (2015).
[278] L. Adamczyk *et al.* [STAR Collaboration], Phys. Rev. C **92**, no. 2, 024912 (2015).
[279] L. Adamczyk *et al.* [STAR Collaboration], Phys. Rev. Lett. **114**, no. 25, 252302 (2015).

[280] J. Adam *et al.* [ALICE Collaboration], JHEP **1507**, 051 (2015).
[281] J. Adam *et al.* [ALICE Collaboration], JHEP **1509**, 148 (2015).
[282] L. Adamczyk *et al.* [STAR Collaboration], Phys. Rev. Lett. **115**, no. 22, 222301 (2015).
[283] J. Adam *et al.* [ALICE Collaboration], JHEP **1509**, 170 (2015).
[284] J. Adam *et al.* [ALICE Collaboration], JHEP **1511**, 205 (2015).
[285] J. Adam *et al.* [ALICE Collaboration], Phys. Rev. C **93**, no. 3, 034913 (2016).
[286] J. Adam *et al.* [ALICE Collaboration], Phys. Lett. B **752**, 267 (2016).
[287] L. Adamczyk *et al.* [STAR Collaboration], Phys. Rev. C **93**, no. 2, 021903 (2016).
[288] J. Adam *et al.* [ALICE Collaboration], Phys. Rev. C **92**, no. 5, 054908 (2015).
[289] J. Adam *et al.* [ALICE Collaboration], Phys. Lett. B **753**, 126 (2016).
[290] J. Adam *et al.* [ALICE Collaboration], JHEP **1605**, 179 (2016).
[291] J. Adam *et al.* [ALICE Collaboration], JHEP **1511**, 127 (2015).
[292] J. Adam *et al.* [ALICE Collaboration], Phys. Lett. B **754**, 360 (2016).
[293] J. Adam *et al.* [ALICE Collaboration], Phys. Lett. B **768**, 203 (2017).
[294] J. Adam *et al.* [ALICE Collaboration], Phys. Rev. C **93**, no. 2, 024917 (2016).
[295] J. Adam *et al.* [ALICE Collaboration], Phys. Lett. B **753**, 41 (2016).
[296] L. Adamczyk *et al.* [STAR Collaboration], Phys. Rev. C **94**, no. 2, 024909 (2016).
[297] L. Adamczyk *et al.* [STAR Collaboration], Phys. Rev. Lett. **116**, no. 6, 062301 (2016).
[298] J. Adam *et al.* [ALICE Collaboration], Phys. Rev. C **93**, no. 3, 034916 (2016).
[299] J. Adam *et al.* [ALICE Collaboration], Phys. Rev. C **93**, no. 2, 024905 (2016).
[300] L. Adamczyk *et al.* [STAR Collaboration], Nature **527**, 345 (2015).
[301] J. Adam *et al.* [ALICE Collaboration], JCAP **1601**, no. 01, 032 (2016).
[302] J. Adam *et al.* [ALICE Collaboration], Nature Phys. **11**, no. 10, 811 (2015).
[303] J. Adam *et al.* [ALICE Collaboration], Phys. Lett. B **751**, 358 (2015).
[304] J. Adam *et al.* [ALICE Collaboration], JHEP **1603**, 081 (2016).
[305] J. Adam *et al.* [ALICE Collaboration], Eur. Phys. J. C **76**, no. 2, 86 (2016).
[306] J. Adam *et al.* [ALICE Collaboration], JHEP **1603**, 082 (2016).
[307] J. Adam *et al.* [ALICE Collaboration], Phys. Lett. B **754**, 373 (2016).
[308] J. Adam *et al.* [ALICE Collaboration], Phys. Lett. B **754**, 235 (2016).
[309] J. Adam *et al.* [ALICE Collaboration], Phys. Lett. B **753**, 511 (2016).
[310] J. Adam *et al.* [ALICE Collaboration], Phys. Lett. B **754**, 81 (2016).
[311] J. Adam *et al.* [ALICE Collaboration], Eur. Phys. J. C **77**, no. 1, 33 (2017).
[312] J. Adam *et al.* [ALICE Collaboration], Eur. Phys. J. C **76**, no. 4, 184 (2016).
[313] L. Adamczyk *et al.* [STAR Collaboration], Phys. Rev. C **93**, no. 1, 014907 (2016).
[314] J. Adam *et al.* [ALICE Collaboration], Phys. Lett. B **753**, 319 (2016).
[315] J. Adam *et al.* [ALICE Collaboration], Phys. Rev. Lett. **116**, no. 22, 222301 (2016).
[316] J. Bielcik [STAR Collaboration], Nucl. Phys. A **932**, 516 (2014).
[317] L. Adamczyk *et al.* [STAR Collaboration], Phys. Rev. Lett. **116**, no. 13, 132301 (2016).

[318] J. Adam *et al.* [ALICE Collaboration], Phys. Rev. C **93**, no. 4, 044903 (2016).
[319] J. Adam *et al.* [ALICE Collaboration], Phys. Rev. Lett. **116**, no. 22, 222302 (2016).
[320] J. Adam *et al.* [ALICE Collaboration], Phys. Lett. B **758**, 389 (2016).
[321] J. Adam *et al.* [ALICE Collaboration], Phys. Rev. C **93**, no. 5, 054908 (2016).
[322] L. Adamczyk *et al.* [STAR Collaboration], Phys. Rev. Lett. **116**, no. 11, 112302 (2016).
[323] J. Adam *et al.* [ALICE Collaboration], Phys. Lett. B **760**, 720 (2016).
[324] L. Adamczyk *et al.* [STAR Collaboration], Phys. Rev. C **94**, no. 3, 034908 (2016).
[325] J. Adam *et al.* [ALICE Collaboration], Eur. Phys. J. C **76**, no. 5, 245 (2016).
[326] J. Adam *et al.* [ALICE Collaboration], Phys. Rev. Lett. **116**, no. 13, 132302 (2016).
[327] J. Adam *et al.* [ALICE Collaboration], Eur. Phys. J. Plus **131**, no. 5, 168 (2016).
[328] L. Adamczyk *et al.* [STAR Collaboration], Phys. Rev. C **93**, no. 6, 064904 (2016).
[329] J. Adam *et al.* [ALICE Collaboration], JHEP **1608**, 078 (2016).
[330] J. Adam *et al.* [ALICE Collaboration], JHEP **1606**, 050 (2016).
[331] J. Adam *et al.* [ALICE Collaboration], Eur. Phys. J. C **76**, no. 5, 271 (2016).
[332] J. Adam *et al.* [ALICE Collaboration], Phys. Rev. C **94**, no. 3, 034903 (2016).
[333] B. Abelev *et al.* [STAR Collaboration], Phys. Rev. C **94**, no. 1, 014910 (2016).
[334] J. Crkovska, J. Bielcík, L. Bravina, G. Eyyubova and E. Zabrodin, PoS EPS **-HEP2015**, 201 (2015).
[335] J. Crkovska *et al.*, Phys. Rev. C **95** no.1, 014910 (2017).
[336] L. Adamczyk *et al.* [STAR Collaboration], Phys. Lett. B **760**, 689 (2016).
[337] J. Adam *et al.* [ALICE Collaboration], Phys. Rev. Lett. **117**, 182301 (2016).
[338] J. Adam *et al.* [ALICE Collaboration], Phys. Lett. B **762**, 376 (2016).
[339] J. Adam *et al.* [ALICE Collaboration], Eur. Phys. J. C **77**, no. 4, 245 (2017).
[340] J. Adam *et al.* [ALICE Collaboration], Phys. Rev. C **94**, no. 5, 054908 (2016).
[341] J. Adam *et al.* [ALICE Collaboration], JHEP **1609**, 028 (2016).
[342] J. Adam *et al.* [ALICE Collaboration], JHEP **1609**, 164 (2016).
[343] J. Adam *et al.* [ALICE Collaboration], Nature Phys. **13**, 535 (2017).
[344] J. Adam *et al.* [ALICE Collaboration], Phys. Lett. B **766**, 212 (2017).
[345] L. Adamczyk *et al.* [STAR Collaboration], Phys. Lett. B **770**, 451 (2017).
[346] L. Adamczyk *et al.* [STAR Collaboration], Phys. Lett. B **771**, 13 (2017).
[347] L. Adamczyk *et al.* [STAR Collaboration], Phys. Rev. Lett. **118**, no. 1, 012301 (2017).
[348] L. Adamczyk *et al.* [STAR Collaboration], Phys. Rev. C **94**, no. 6, 064904 (2016).
[349] J. Adam *et al.* [ALICE Collaboration], Phys. Lett. B **763**, 238 (2016).
[350] J. Adam *et al.* [ALICE Collaboration], JHEP **1707** 052 (2017).
[351] L. Adamczyk *et al.* [STAR Collaboration], Phys. Rev. Lett. **119** 062301 (2017).
[352] J. Adam *et al.* [ALICE Collaboration], Phys. Rev. Lett. **119** no.10, 102301 (2017).
[353] J. Adam *et al.* [ALICE Collaboration], Phys. Rev. C **96** no.3, 034904 (2017).
[354] J. Adam *et al.* [ALICE Collaboration], Phys. Lett. B **771** 467 (2017).

[355] J. Adam *et al.* [ALICE Collaboration], Eur. Phys. J. Plus **132** no.2, 99 (2017).
[356] L. Adamczyk *et al.* [STAR Collaboration], Phys. Rev. D **95** no.7, 071103 (2017).
[357] J. Adam *et al.* [ALICE Collaboration], JHEP **1702** 077 (2017).
[358] J. Adam *et al.* [ALICE Collaboration], Phys. Lett. B **772** 567 (2017).
[359] J. Adam *et al.* [ALICE Collaboration], Eur. Phys. J. C **77** no.8, 569 (2017).
[360] L. Adamczyk *et al.* [STAR Collaboration], Phys. Rev. Lett. **118** no.21, 212301 (2017).
[361] L. Adamczyk *et al.* [STAR Collaboration], Nature **548** 62 (2017).
[362] L. Adamczyk *et al.* [STAR Collaboration], Phys. Rev. C **96** no.4, 044904 (2017).
[363] D. Adamova *et al.* [ALICE Collaboration], Eur. Phys. J. C **77** no.6, 389 (2017).
[364] J. Adam *et al.* [ALICE Collaboration], Phys. Rev. C **95** no.6, 064606 (2017).
[365] S. Acharya *et al.* [ALICE Collaboration], Eur. Phys. J. C **77** no.6, 392 (2017).
[366] S. Acharya *et al.* [ALICE Collaboration], Eur. Phys. J. C **77** no.8, 550 (2017).
[367] S. Acharya *et al.* [ALICE Collaboration], Phys. Lett. B **776** 249 (2018).
[368] S. Acharya *et al.* [ALICE Collaboration], Eur. Phys. J. C **77** no.5, 339 (2017).
[369] L. Adamczyk *et al.* [STAR Collaboration], Phys. Rev. C **96** no.2, 024905 (2017).
[370] S. Acharya *et al.* [ALICE Collaboration], Phys. Lett. B **770** 459 (2017).
[371] D. Adamova *et al.* [ALICE Collaboration], Phys. Rev. Lett. **118** no.22, 222301 (2017).
[372] J. Adam *et al.* [ALICE Collaboration], Phys. Rev. Lett. **118** no.16, 162302 (2017).
[373] L. Adamczyk *et al.* [STAR Collaboration], Phys. Rev. C **96** no.5, 054904 (2017).
[374] D. Adamová *et al.* [ALICE Collaboration], Phys. Lett. B **776** 91 (2018).
[375] S. Acharya *et al.* [ALICE Collaboration], Phys. Lett. B **773** 68 (2017).
[376] S. Acharya *et al.* [ALICE Collaboration], Phys. Lett. B **774** 64 (2017).
[377] S. Acharya *et al.* [ALICE Collaboration], JHEP **1709** 032 (2017).
[378] S. Acharya *et al.* [ALICE Collaboration], Eur. Phys. J. C **77** no.10, 658 (2017).
[379] S. Acharya *et al.* [ALICE Collaboration], Eur. Phys. J. C **77** no.12, 852 (2017).
[380] L. Adamczyk *et al.* [STAR Collaboration], Phys. Rev. D **97** no.3, 032004 (2018).
[381] L. Adamczyk *et al.* [STAR Collaboration], Phys. Rev. Lett. **120** no.6, 062301 (2018).
[382] S. Acharya *et al.* [ALICE Collaboration], Phys. Rev. C **97** no.2, 024906 (2018).
[383] S. Acharya *et al.* [ALICE Collaboration], Phys. Rev. C **96** no.6, 064613 (2017).
[384] S. Acharya *et al.* [ALICE Collaboration], Nucl. Instrum. Meth. A **881** 88 (2018).
[385] S. Acharya *et al.* [ALICE Collaboration], Phys. Lett. B **777** 151 (2018).
[386] S. Acharya *et al.* [ALICE Collaboration], Phys. Rev. Lett. **119** no.24, 242301 (2017).
[387] S. Acharya *et al.* [ALICE Collaboration], Phys. Rev. C **97** no.2, 024615 (2018).
[388] S. Acharya *et al.* [ALICE Collaboration], Nucl. Phys. A **971** 1 (2018).

Zoznam bakalárskych, diplomových a dizertačných prác vypracovaných pod autorovým vedením:

[B1] M. Tesař. *STAR Heavy Flavor Tracker detektor.* Praha, 2008. Bakalářská práce. České vysoké učení technické v Praze. Fakulta jaderná a fyzikálně inženýrská.

[B2] M. Vajzer. *Study of Identification of Jets Containing Heavy Quarks.* Praha, 2008. Bakalářská práce. České vysoké učení technické v Praze. Fakulta jaderná a fyzikálně inženýrská.

[B3] M. Sloboda. *Energy loss of partons in quark-gluon plasma.* Praha, 2008. Bakalářská práce. České vysoké učení technické v Praze. Fakulta jaderná a fyzikálně inženýrská.

[B4] O. Hájková. *Quarkonia production in heavy-ion collision at RHIC and LHC.* Praha, 2009. Bakalářská práce. České vysoké učení technické v Praze. Fakulta jaderná a fyzikálně inženýrská.

[B5] J. Brabcová. *Charm quark production.* Praha, 2010. Bakalářská práce. České vysoké učení technické v Praze. Fakulta jaderná a fyzikálně inženýrská.

[B6] J. Crkovská. *Antimatter production in nucleus-nucleus collisions.* Praha, 2012. Bakalářská práce. České vysoké učení technické v Praze. Fakulta jaderná a fyzikálně inženýrská.

[B7] O. Kukral. *Heavy Flavor Physics at STAR Experiment.* Praha, 2012. Bakalářská práce. České vysoké učení technické v Praze. Fakulta jaderná a fyzikálně inženýrská.

[B8] K. Šramková. *Nucleus-nucleus collisions.* Praha, 2013. Bakalářská práce. České vysoké učení technické v Praze. Fakulta jaderná a fyzikálně inženýrská.

[B9] K. Gajdošová. *Charmed mesons in nucleus-nucleus collisions.* Praha, 2013. Bakalářská práce. České vysoké učení technické v Praze. Fakulta jaderná a fyzikálně inženýrská.

[B10] V. Pacík. *Study of properties of nuclear matter by heavy flavour quarks.* Praha, 2014. Bakalářská práce. České vysoké učení technické v Praze. Fakulta jaderná a fyzikálně inženýrská.

[B11] L. Kramárik. *Studium jetů těžkých kvarků v jádro-jaderných srážkách.* Praha, 2014. Bakalářská práce. České vysoké učení technické v Praze. Fakulta jaderná a fyzikálně inženýrská.

[B12] M. Šaur. *Hard probes production in heavy ion collisions.* Praha, 2015. Bakalářská práce. České vysoké učení technické v Praze. Fakulta jaderná a fyzikálně inženýrská.

[B13] J. Kvapil. *Heavy Flavor Tracker detector.* Praha, 2015. Bakalářská práce. České vysoké učení technické v Praze. Fakulta jaderná a fyzikálně inženýrská.

[B14] J. Vaněk. *Study of nuclear matter at the LHC.* Praha, 2015. Bakalářská práce. České vysoké učení technické v Praze. Fakulta jaderná a fyzikálně inženýrská.

[B15] Z. Moravcová. *Methods of optimalization of charm hadrons reconstruction.* Praha, 2017. Bakalářská práce. České vysoké učení technické v Praze. Fakulta jaderná a fyzikálně inženýrská.

[D1] M. Krůs. *Study of Interaction of Heavy Quarks with Nuclear Matter in Cu+Cu at 200 GeV.* Praha, 2008. Diplomová práce. České vysoké učení technické v Praze. Fakulta jaderná a fyzikálně inženýrská.

[D2] M. Tesař. *Vertex detectors for heavy flavor physics.* Praha, 2010. Diplomová práce. České vysoké učení technické v Praze. Fakulta jaderná a fyzikálně inženýrská.

[D3] M. Vajzer. *Study of Properties of b-tagged Jets.* Praha, 2010. Diplomová práce. České vysoké učení technické v Praze. Fakulta jaderná a fyzikálně inženýrská.

[D4] O. Hájková. *Study of J/ψ in STAR experiment.* Praha, 2010. Diplomová práce. České vysoké učení technické v Praze. Fakulta jaderná a fyzikálně inženýrská.

[D5] J. Crkovská. *Triangular particle flow in HYDJET++.* Praha, 2015. Diplomová práce. České vysoké učení technické v Praze. Fakulta jaderná a fyzikálně inženýrská.

[D6] K. Gajdošová. *Production of non-photonic electrons in U+U collisions at 193 GeV in STAR experiment.* Praha, 2015. Diplomová práce. České vysoké učení technické v Praze. Fakulta jaderná a fyzikálně inženýrská.

[D7] L. Kramárik. *Analysis of b-Jets in p+Pb collisions at 5 TeV.* Praha, 2016. Diplomová práce. České vysoké učení technické v Praze. Fakulta jaderná a fyzikálně inženýrská.

[D8] J. Vaněk. *Non-photonic reconstruction in heavy-ion collisions.* Praha, 2017. Diplomová práce. České vysoké učení technické v Praze. Fakulta jaderná a fyzikálně inženýrská.

[D9] J. Kvapil. *Charged charm mesons in Au+Au collisions.* Praha, 2017. Diplomová práce. České vysoké učení technické v Praze. Fakulta jaderná a fyzikálně inženýrská.

[T1] D. Tlustý. *A study of open charm production in p+p collisions at STAR.* Praha, 2014. Disertační práce. České vysoké učení technické v Praze. Fakulta jaderná a fyzikálně inženýrská.

[T2] O. Rusňáková. *Heavy flavor physics in the STAR experiment.* Praha, 2015. Disertační práce. České vysoké učení technické v Praze. Fakulta jaderná a fyzikálně inženýrská.

[T3] M. Vajzer. *Study of hard processes in the ALICE experiment.* Praha, 2015. Disertační práce. České vysoké učení technické v Praze. Fakulta jaderná a fyzikálně inženýrská.

Použitá literatúra:

[R1] C. Patrignani *et al.* [Particle Data Group], Chin. Phys. C **40**, no. 10, 100001 (2016) and 2017 update.

[R2] R. Aaij *et al.* [LHCb Collaboration], Phys. Rev. Lett. **115**, 072001 (2015).

[R3] S. Chatrchyan *et al.* [CMS Collaboration], Phys. Lett. B **716**, 30 (2012).

[R4] G. Aad *et al.* [ATLAS Collaboration], Phys. Lett. B **716**, 1 (2012).

[R5] H. Caines, J. Phys. G **31**, S101 (2005).

[R6] U. W. Heinz and M. Jacob, nucl-th/0002042.

[R7] M. Connors, C. Nattrass, R. Reed and S. Salur, arXiv:1705.01974

[R8] K. Adcox *et al.* [PHENIX Collaboration], Nucl. Phys. A **757**, 184 (2005).

[R9] I. Arsene *et al.* [BRAHMS Collaboration], Nucl. Phys. A **757**, 1 (2005).

[R10] B. B. Back *et al.*, Nucl. Phys. A **757**, 28 (2005).

[R11] B. Alver and G. Roland, Phys. Rev. C **81** (2010) 054905 Erratum: [Phys. Rev. C **82** (2010) 039903]

[R12] I. P. Lokhtin, L. V. Malinina, S. V. Petrushanko, A. M. Snigirev, I. Arsene and K. Tywoniuk, Comput. Phys. Commun. **180** 779 (2009).

[R13] I. P. Lokhtin and A. M. Snigirev, Eur. Phys. J. C **45**, 211 (2006). [hep-ph/0506189].

[R14] T. Sjostrand, S. Mrenna and P. Z. Skands, JHEP **0605**, 026 (2006)

[R15] J. Adams *et al.* [STAR Collaboration], Phys. Rev. Lett. **92**, 052302 (2004).

[R16] S. Chatrchyan *et al.* [CMS Collaboration], Phys. Lett. B **718**, 795 (2013).

[R17] V. Khachatryan *et al.* [CMS Collaboration], Phys. Rev. Lett. **115**, no. 1, 012301 (2015).

[R18] P. Huo, K. Gajdošová, J. Jia and Y. Zhou, Phys. Lett. B **777**, 201 (2018).

[R19] H. Song, Y. Zhou and K. Gajdosova, Nucl. Sci. Tech. **28**, no. 7, 99 (2017).

[R20] Z. Lin and M. Gyulassy, Phys. Rev. Lett. **77**, 1222 (1996).

[R21] J. Adams *et al.* [STAR Collaboration], Phys. Rev. Lett. **94**, 062301 (2005).

[R22] M. Cacciari, P. Nason and R. Vogt, Phys. Rev. Lett. **95**, 122001 (2005).

[R23] Z. Ye [STAR Collaboration], Nucl. Phys. A **931**, 520 (2014).

[R24] A. Adare *et al.* [PHENIX Collaboration], Phys. Rev. Lett. **97**, 252002 (2006)

[R25] T. Sjostrand, P. Eden, C. Friberg, L. Lonnblad, G. Miu, S. Mrenna and E. Norrbin, Comput. Phys. Commun. **135**, 238 (2001).

[R26] M. Djordjevic, M. Gyulassy and S. Wicks, Phys. Rev. Lett. **94**, 112301 (2005).

[R27] Y. L. Dokshitzer and D. E. Kharzeev, Phys. Lett. B **519**, 199 (2001).

[R28] M. Djordjevic, M. Gyulassy, R. Vogt and S. Wicks, Phys. Lett. B **632**, 81 (2006)

[R29] A. Andronic *et al.*, Eur. Phys. J. C **76**, no. 3, 107 (2016).

[R30] R. Rapp *et al.*, arXiv:1803.03824 [nucl-th].

[R31] S. S. Adler *et al.* [PHENIX Collaboration], Phys. Rev. Lett. **94**, 082301 (2005).

[R32] S. S. Adler *et al.* [PHENIX Collaboration], Phys. Rev. Lett. **96**, 032301 (2006)

[R33] A. Adare *et al.* [PHENIX Collaboration], Phys. Rev. Lett. **98**, 172301 (2007)

[R34] K. Gajdosova [STAR Collaboration], EPJ Web Conf. **126**, 04018 (2016).

[R35] R. Sharma, I. Vitev and B. W. Zhang, Phys. Rev. C **80**, 054902 (2009).
[R36] R. Sharma and I. Vitev, Phys. Rev. C **87**, no. 4, 044905 (2013).
[R37] A. M. Sirunyan *et al.* [CMS Collaboration], Phys. Rev. Lett. **119**, no. 15, 152301 (2017).
[R38] T. W. Wang [CMS Collaboration], Nucl. Part. Phys. Proc. **289-290**, 229 (2017).
[R39] E. Braaten, S. Fleming and T. C. Yuan, Ann. Rev. Nucl. Part. Sci. **46**, 197 (1996).
[R40] T. Todoroki [STAR Collaboration], Nucl. Phys. A **967**, 572 (2017).
[R41] Y. Q. Ma and R. Venugopalan, Phys. Rev. Lett. **113**, no. 19, 192301 (2014).
[R42] H. S. Shao, H. Han, Y. Q. Ma, C. Meng, Y. J. Zhang and K. T. Chao, JHEP **1505**, 103 (2015).
[R43] Y. Q. Ma and R. Vogt, Phys. Rev. D **94**, no. 11, 114029 (2016).
[R44] A. Abulencia *et al.* [CDF Collaboration], Phys. Rev. Lett. **99**, 132001 (2007).
[R45] S. Chatrchyan *et al.* [CMS Collaboration], Phys. Lett. B **727**, 381 (2013).
[R46] R. Aaij *et al.* [LHCb Collaboration], Eur. Phys. J. C **73**, no. 11, 2631 (2013).
[R47] H. S. Chung, C. Yu, S. Kim and J. Lee, Phys. Rev. D **81**, 014020 (2010).
[R48] J. P. Lansberg, Phys. Lett. B **695**, 149 (2011).
[R49] T. Matsui and H. Satz, Phys. Lett. B **178**, 416 (1986).
[R50] M. C. Abreu *et al.*, Z. Phys. C **38**, 117 (1988).
[R51] W. Zha *et al.*, Phys. Rev. C **93**, no. 2, 024919 (2016).
[R52] X. Zhao and R. Rapp, Phys. Rev. C **82**, 064905 (2010).